Copyright

by

Babar Masood Koraishy

2010

The Dissertation Committee for Babar Masood Koraishy Certifies that this is the approved version of the following dissertation:

Continuous Manufacturing of Direct Methanol Fuel Cell Membrane Electrode Assemblies

Committee:

Jeremy P. Meyers, Supervisor

Kristin L. Wood, Co-Supervisor

Arumugam Manthiram

David L. Bourell

Daniel Jensen

Continuous Manufacturing of Direct Methanol Fuel Cell Membrane Electrode Assemblies

by

Babar Masood Koraishy, B.S.M.E.; M.S.

Dissertation

Presented to the Faculty of the Graduate School of

The University of Texas at Austin

in Partial Fulfillment

of the Requirements

for the Degree of

Doctor of Philosophy

The University of Texas at Austin

December, 2010

Dedication

To my mother, Kishwar Koraishy

Acknowledgements

I would like to thank my son Ibrahim, for the joy he has brought in my life, my mother, my brothers, my aunts, the rest of family, and friends for their steadfast support and encouragement over these past five and a half years.

I would like to thank Dr Kris Wood, for his support, guidance and mentorship throughout my association with him, also for always inviting and appreciating innovation and creativity.

I would like to thank Dr Jeremy Meyers, for his keen insights and the fruitful discussions I have had with him over the years, and his generous guidance.

I would like to thank Dr Manthiram, Dr Bourell, and Dr Jensen for being on my committee, also for always offering their time and much valued opinions whenever I have sought them.

I would like to thank Dr Crawford who I was associated with, when I was a teaching assistant.

I would like to appreciate the hard work of the undergraduate students who have worked with me over the years: Ryan Phillips, Chelsea Lawson, Douglas Morter, Sam Solomon, Marcus Minchew and Brian McDonald.

I would like to thank my fellow students in the MADlab and the Meyers research group for their company and opinions.

I would also like to thank the guys in the machine shop: Curtis Johnston, Danny Jares, Michael Slotboom; the administrative staff: Rosalie Foster, Cindy Raman, Becky Harrison; and the graduate coordinators: Ruth Schwab and David Justh.

Continuous Manufacturing of Direct Methanol Fuel Cell Membrane Electrode Assemblies

Publication No._____

Babar Masood Koraishy, PhD

The University of Texas at Austin, 2010

Supervisor: Jeremy P. Meyers

Co-Supervisor: Kristin L. Wood

Direct Methanol Fuel Cells (DMFC) provide an exciting alternative to current energy storage technologies for powering small portable electronic devices. For applications with sufficiently long durations of continuous operation, DMFC's offer higher energy density, the ability to be refueled instead of recharged, and easier fuel handling and storage than devices that operate with hydrogen. At present, materials and manufacturing challenges impede performance and have prevented the entry of these devices to the marketplace. Higher-performing, cost-effective materials and efficient manufacturing processes are needed to enable the commercialization of DMFC.

In a DMFC, the methanol-rich fuel stream and the oxidant are isolated from one another by a proton-conducting and electrically insulating membrane. Catalysts in the electrodes on either side of the Membrane Electrode Assembly (MEA) promote the two

simultaneous half-reactions which allow the chemical energy carried in the fuel and oxidant to be converted directly into electricity. The goal of this research effort is to develop a continuous manufacturing process for the fabrication of effective DMFC MEAs.

Based on the geometry of the electrode and materials used in the MEA, we propose a roll-to-roll process in which electrodes are coated onto a suitable substrate and subsequently assembled to form a MEA. Appropriate coating methods for electrode fabrication were identified by evaluating the requirements of continuous manufacturing processes; an appropriate set of these processes was then reduced to practice on a custom-designed flexible test bed designed explicitly for this project. After establishing baseline capabilities for several candidate methods, a spraying process was selected and a continuous manufacturing process concept was proposed. Finally, key control parameters of the spraying process were identified and their influence tested on actual MEAs to define optimal operating conditions.

Table of Contents

List of Tables

List of Figures

1. Introduction

Fuel cells are electrochemical devices that produce energy by reacting a fuel and oxidant [1]. The original invention of a fuel cell, dating back more than 160 years, is attributed to Sir William Grove [2]. It was not until the work of Sir Francis Bacon, beginning in 1933, that fuel cells became a practical reality, and were eventually used in the U.S Apollo space program [3]. The Bacon Cell utilized an alkaline electrolyte (KOH), and is more commonly referred to as the alkaline fuel cell (AFC). Around the same time period, other major types of fuel cells were conceived, including phosphoric acid fuel cell (PAFC), solid polymer fuel cell (SPFC, aka the polymer electrolyte membrane fuel cell, PEMFC), molten carbonate fuel cell (MCFC), solid oxide fuel cell (SOFC) and the direct methanol fuel cell (DMFC) [4].

Of the different types of fuel cells available, low temperature fuel cells such as DMFC and PEMFC have the potential of supplying energy for portable electronics and small systems [2, 5]. They can offer an excellent alternative to batteries, which being energy storage devices are limited by their storage capacity (~350WhL^{-1}), whereas fuel cells generate electricity during operation from fuel stored within them. This fuel, liquid methanol in the case of DMFC and compressed hydrogen in the case of PEMFC offers much higher specific energy density (~4900WhL^{-1} for MeOh)[6], which if utilized can offer up to 10x improvement in the overall system energy density [5]. Additionally fuel cell systems can be instantly recharged when their fuel supply is replenished.

The conversion of chemical energy stored in the fuel to usable electricity is achieved by reactions happening on catalyst sites in the fuel cell. These reactions are enabled by a host of supporting physical processes, such as mass transport, proton and electron conduction which occur with the help of a few key components of a fuel cell, namely the two electrodes, the proton conducting membrane and diffusion media, which is fed with reactants by channels inside bipolar plates.

The electrode is one of the most important components of a fuel cell, as a pair of electrode, the anode and cathode enables the chemical reactions, which produce electricity. These electrodes, along with the membrane are assembled to form a 'membrane electrode assembly' (MEA). The goal of this research effort is to develop a continuous manufacturing process for the fabrication of effective DMFC MEAs. For this purpose existing manufacturing processes are examined, prototyped and tested, on the basis of which an overall concept for a continuous manufacturing process is conceived and detailed.

1.1 BASIC ARCHITECTURE OF DIRECT METHANOL FUEL CELLS

Fuel cells convert the free energy of a chemical reaction directly into electrical energy. A typical DMFC using a polymer electrolyte is shown in Figure 1. On the anode, methanol and water react to produce carbon dioxide, protons and electrons. The protons produced migrate from the anode through the polymer electrolyte membrane to the cathode side where they react with oxygen to produce water. The electrons are free to flow through the external electrical circuit where they can drive an electrical load [7].

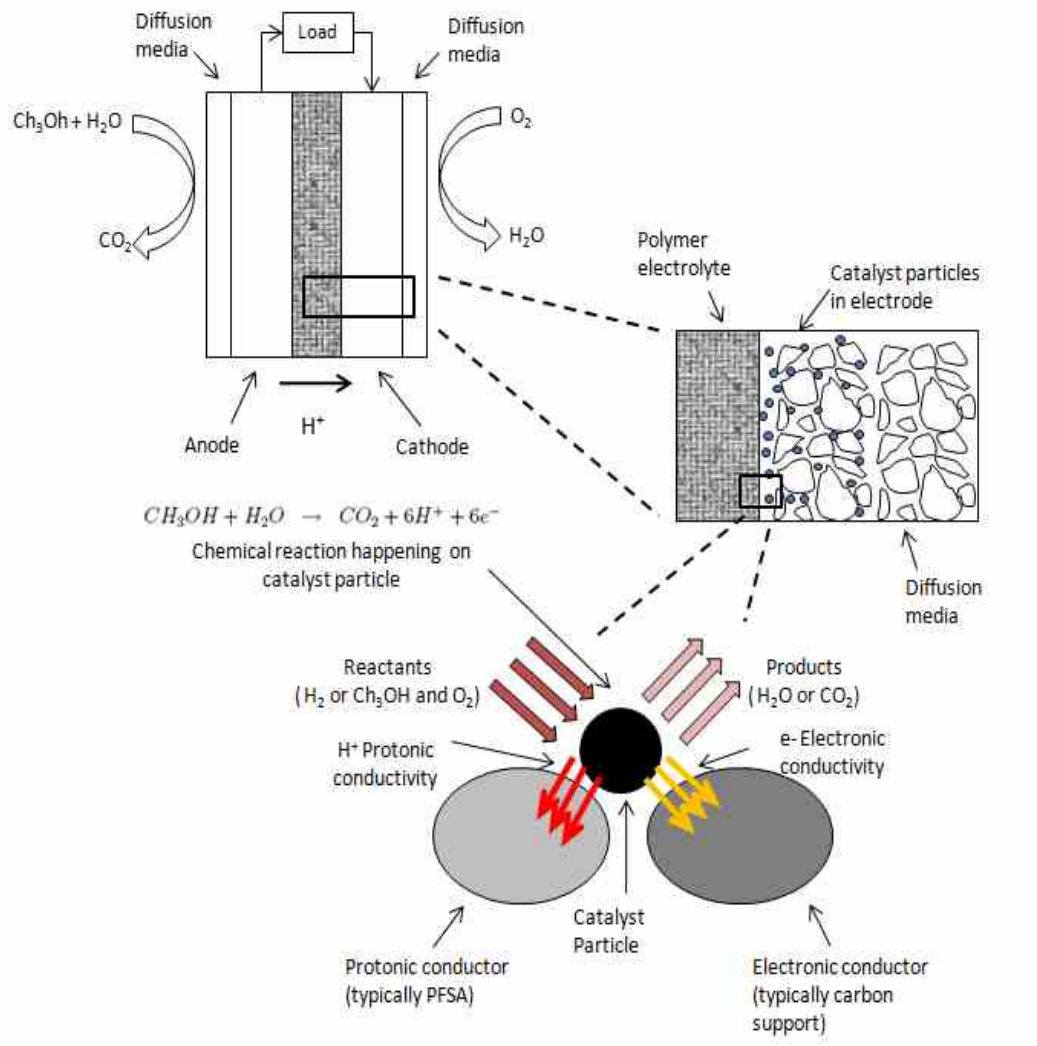

Figure 1: Chemical reactions in a DMFC.

A PEMFC works in very similar fashion: on the anode side, humidified hydrogen gas is supplied, where it breaks down into protons and electrons. The electrons travel through the external circuit driving the load, while the protons permeate through the polymer electrolyte, and combine with oxygen on the cathode to form water.

Figure 2 shows an exploded view of a single fuel cell, revealing the key components that are: the membrane electrode assemble (MEA), diffusion media, bipolar plates and gaskets for sealing. Two bipolar plates, one on either side of the MEA, provide reactants to the electrodes (through the diffusion media), and channel the reaction products out of the cell. The sealing media is to ensure against leakage of the pressurized reactants in fuel cell. Additionally the plates physically contain the entire assembly and along with the diffusion media form a conductive path for the electrons to flow to the external circuit. Multiples of such cells are assembled together to form a fuel cell 'stack'. More detail about the individual components and their function is provided in the proceeding paragraphs.

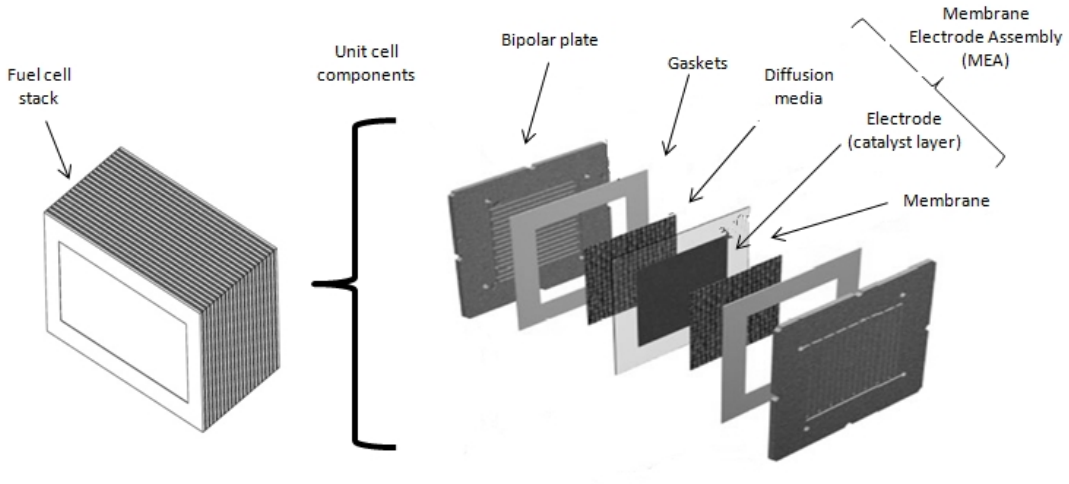

Figure 2: Key components of a fuel cell.

1.1.1 Bipolar plates

In a fuel cell stack, individual cells are connected in series, and the stack voltage is the sum of the voltages of individual cells. For this serial connection, two electrodes of different polarities have to be electrically connected to each other [2], which is achieved by using a 'bipolar' plate in between the electrodes. Additionally the bipolar plates provide paths for the fuel and oxidant to reach the membrane electrode assembly and for the reaction products to be removed. This is achieved by the presence of channels in the bipolar plate surface called 'flow fields', as shown in Figure 3. The reactants are generally fed from the periphery of the plate, and are channeled through the flow fields. Excess reactant and reaction products are removed through these same channels. The entire area of the diffusion media is pressed against these flow fields, to ensure electrical conductivity as well as mass transport.

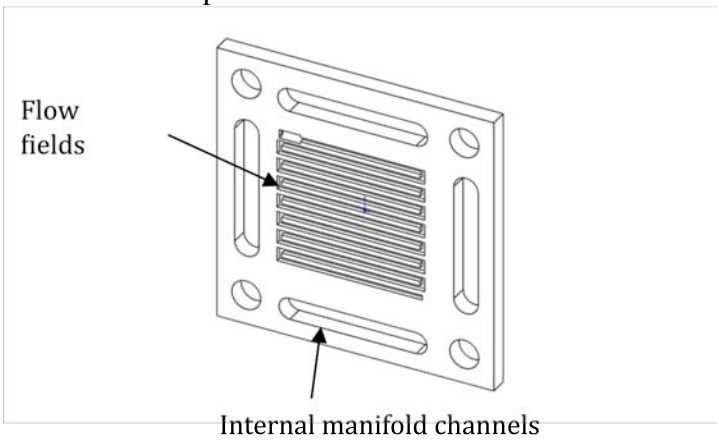

Figure 3: Bipolar plate.

1.1.2 Sealing media

Sealing media is sandwiched between the MEA and the bipolar plates so as to prevent any exchange of fuel or oxidant between the cell and the environment. Additionally in some stack designs an internal manifold configuration is used, as shown in Figure 3 where reactants supply channels and cooling channels are also present on the bipolar plates, which have to be sealed.

1.1.3 Membrane electrode assembly

The membrane electrode assembly (MEA) provides sites for chemical reactions occurring inside a fuel cell to take place, to convert the fuel into usable electrical power. MEA's are commonly referred to as a three-layer or a five-layer MEA. A three layer MEA is composed of the proton conducting membrane and two electrodes (anode and cathode), whereas a five-layer assembly refers to the instance where two diffusion layers have been affixed to a three layer MEA, one on each electrode [8, 9].

1.2 MEA COMPONENTS

The membrane electrode assembly (MEA), shown in Figure 4, is essentially the heart of a DMFC. As the name implies, an MEA consists of a proton-conducting membrane sandwiched between anode and cathode electrode layers, with a gas diffusion layer (GDL) on either side. A brief discussion of each component of a MEA follows.

1.2.1 Ionomer membrane

The ionomer (polymer which contains ions) membrane has two major functions in a fuel cell: the first is to separate the fuel and the oxidant, and the second is to allow for the transport of protons from the anode to the cathode to complete the redox reaction. It must provide strong mechanical, chemical, and electrochemical stability in a harsh chemical rich environment over a range of operating conditions, while at the same time offering a long life, low reactant permeability, and high proton conductivity, and serving as an effective electrical insulator.

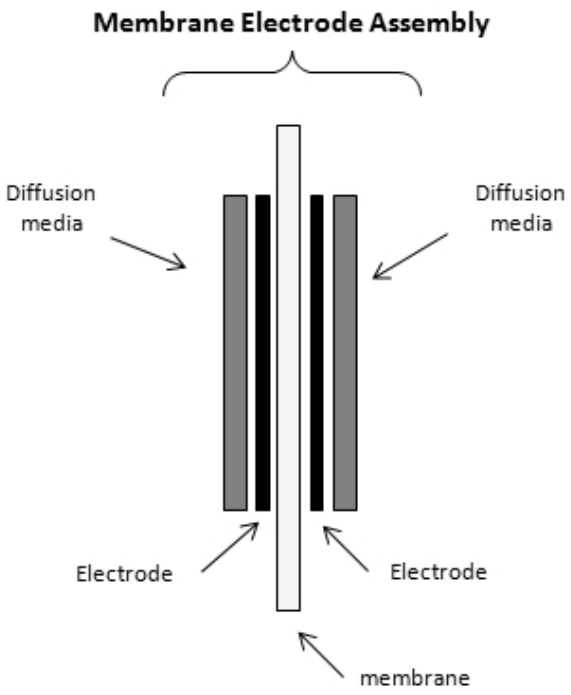

Figure 4: Cross section of a typical MEA.

1.2.2 Gas diffusion layer

The diffusion layer is a porous media, which allows for the transport of reactant from the bipolar plate flow field and evenly disperses the reactant over the catalyst sites. Besides this key role, a diffusion layer serves as a conducting path to the external circuit via the bipolar plates. It should thus have low electronic resistivity. Carbon cloth or paper, being conductive and stable in the fuel cell environment, are typical choices for the diffusion, and have been widely employed as the diffusion media [10, 11].

1.2.3 Electrodes

The electrodes are typically porous structures of nanometer-sized catalyst particles dispersed in a suitable binder medium [12]. Catalysts can be supported on carbon media to promote dispersion and lower catalyst loading. It is important to allow adequate pathways for diffusion of the reactant media to the catalyst site, removal of reaction products, as well as good electrical and protonic conductivity. The electrons

generated during the reaction have to be transported to the external circuit, whereas the protons have to cross the electrolyte to complete the reaction at the counter electrode, as shown in Figure 1. Electrical conductivity in an electrode is either provided by the carbon support, in the case of supported catalyst, or the catalyst particles themselves in case of unsupported ones [2]. Protonic conductivity is provided by the addition of ionomer material into the catalyst layer, which also acts as a binder for the catalyst particles. The extent of the three-phase boundary, which is where the reactant, the catalyst and the ionomer interact, contributes to the performance of the fuel cell.

1.3 RESEARCH OPPORTUNITIES IN MEMBRANE ELECTRODE ASSEMBLY (MEA) MANUFACTURING

Fuel cell technology is at the cusp of commercialization, the impediments being cost and performance. A significant amount of fundamental research has been conducted over the past two decades, with the main thrust being on reducing the cost barriers and improving performance. These research efforts have mostly been focused towards identifying better materials, some which can alleviate existing performance and durability problems, and others that can replace or reduce the expensive noble metal content. These efforts are necessary to enable fuel cell technology to effectively compete with other energy generation and storage technologies for mainstream applications [2].

Considering the costs involved in the technology, the material cost of the catalyst and the ion exchange membrane are key contributors to the overall system cost. The labor-intensive nature of the membrane electrode assembly processing contributes a major portion of the manufacturing costs. Performance issues, which range from overall system energy density, to long term performance and stability, are also tied directly to the materials and the manufacturing process choices.

The major thrust of the research effort by the scientific community has been on developing better catalysts and membranes for DFMC fuel cells [1, 13]. A two-pronged approach has been undertaken: firstly to develop alternative materials, which perform

better and/or are less expensive than current technology, and, in parallel, improving performance from the existing materials by utilizing them differently. Most of the research is focused around small-scale laboratory experimentation, and there is very little data available in the literature on how the manufacturing processes can be scaled up for volume production, or on how the choice of manufacturing process of critical fuel cell components, such as the membrane electrode assembly (MEA) will dictate performance improvements and cost benefits at the component, sub-system, and system level.

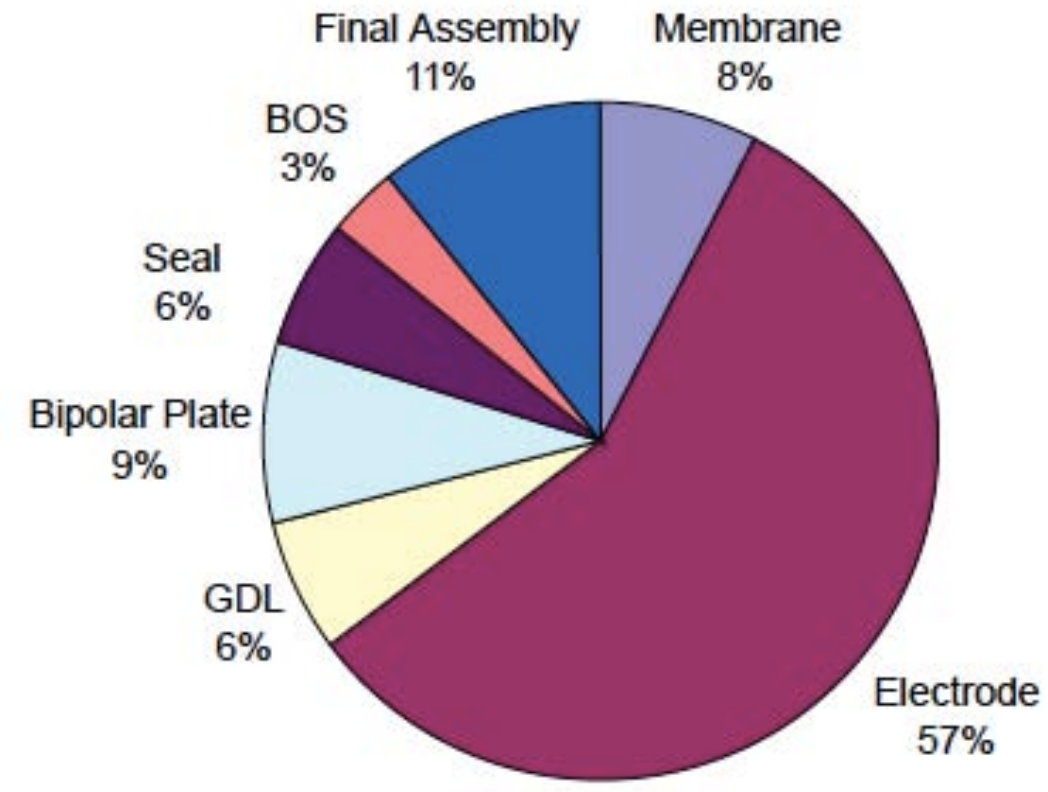

Figure 5: Component contribution to overall stack cost (PEMFC) [14].

The membrane electrode assembly is a key component of a PEMFC and DMFC fuel cell system. Of the three MEA components, electrode, diffusion media and the membrane, the electrode represents a 57% share in overall stack cost as shown in Figure 5. This cost model assumes a production volume of 500000 stack per year, with a power

output of 80 KW and total platinum loading of 0.3 mg/cm^2 on the PEMFC electrodes. Catalyst material costs contribute to 91% of the cost of the electrode [14].

There is an urgent need to identify and develop automated, continuous manufacturing processes for MEA fabrication, from both an economic and a performance standpoint [9]. From a performance standpoint it is important to study continuous manufacturing process choices and process parameters in detail, and understand how they can be related to easily quantifiable and measurable fuel cell performance metrics. From an economic point of view, it is important to develop a continuous manufacturing process for the fabrication of fuel cell MEAs to harness cost benefits and allow for volume production.

Off the MEA components identified earlier, the ionomer membrane and diffusion media already exist in a continuous roll form and are available from OEM suppliers [15]. The problem essentially reduces to developing a continuous electrode fabrication process. In subsequent processing steps these electrodes have to be attached on either side of the ionomer membrane to form an MEA.

A continuous electrode fabrication process would involve the identification and selection of a suitable coating process, with which relevant experiments can be conducted to gauge its suitability for electrode fabrication. Subsequently process parameters that impact the electrode/MEA performance can be identified and tuned to deliver optimal performance.

Precursors for the electrode (catalyst, binder, additives) are typically formulated into liquid ink, which is then applied onto a relevant substrate by a coating process. In this research effort, it is hypothesized that *"the design and fabrication of the electrode is influenced by the material composition of the catalyst ink, and the method of catalyst ink deposition"*. The material composition and ink application method will affect the microstructure of the electrode produced, which can be studied by microscopy techniques and the performance of the electrode can be measured by electrochemical methods. The

performance of the coating process used to apply the ink can be measured by the consistency of the coating thickness produced.

1.4 SCOPE OF DISSERTATION

The scope of this research effort gravitates around the design of a continuous manufacturing process for the fabrication of effective electrodes and membrane electrode assemblies for Direct Methanol Fuel Cells. Such an undertaking requires an in-depth knowledge of pertinent coating processes, electrode precursors, and continuous web processing. For this purpose, electrode and MEA fabrication processes are first studied, candidate processes for continuous manufacturing are identified, prototyped and tested, and an advanced process is proposed. MEAs produced by this process are optimized, and the results are presented in this dissertation.

1.5 RESEARCH APPROACH

In this section, the research methodology that has been followed to fulfill the aforementioned research scope is presented. As shown in Figure 6, the overall research objective is broken down in to smaller tasks, beginning with an understanding of the literature and state-of-the-art in fuel cell technology, and ending with a process concept for DMFC MEA fabrication.

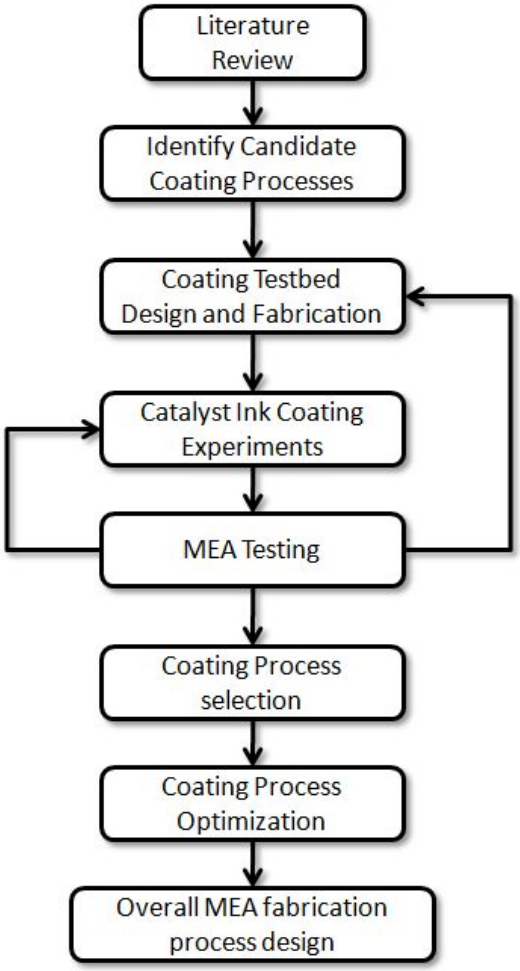

Figure 6: Research Methodology.

1.5.1 Literature review

The first task undertaken for this research has been a thorough literature review. The purpose of the literature review was to identify the state-of-the-art of PEMFC and DMFC fuel cell research, and on the basis of this information future research avenues were identified.

1.5.2 Candidate coating processes

In this task, several different coating processes were examined and compared. Processes that could potentially be compatible with the requirements for the PEMFC and DMFC electrode were selected and studied in detail. On the basis of a feasibility study, a

few coating processes that could be prototyped were identified. Coating processes that were examined were:

- Flexography
- Gravure coating
- Slot Die Extrusion
- Mayer bar coating
- Rotary Screen Printing
- Tape Casting
- Spraying

1.5.3 Modular coating test bed design and construction

The need for a flexible and modular coating test platform was realized where candidate coating processes could be prototyped and different ink formulations studied. Based on these requirements, an initial concept for a test bed for continuous electrode fabrication was conceived and is shown in Figure 7. The concept has modules for web management: web unwinder, rewinder and the tensioning module. The catalyst ink is applied via the ink application or coating module and solidified in the dryer module. These key modules would be common to most of the coating processes that will be studied with this platform. Such a flexible approach allows for the test bed to accept multiple coating heads, fabricate multiple membranes, and adjust and tune web parameters, such as tension and feed, to suit the particular web material and drying conditions. On the basis of this concept an actual machine was designed and constructed.

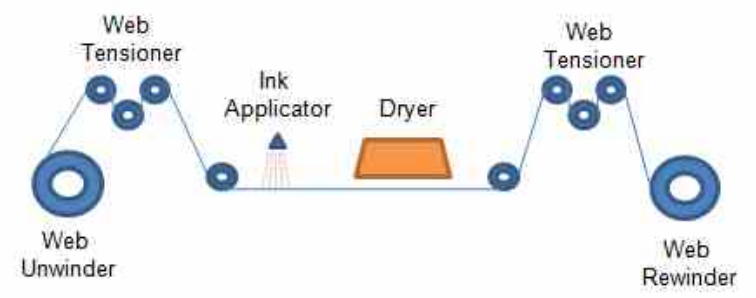

Figure 7: Coating test bed concept.

1.5.4 MEA testing

In the MEA testing stage, a new MEA break-in procedure and testing protocol was developed which was the used to test MEAs fabricated by the various coating methods on a fuel cell test station.

1.5.5 Coating process selection

Of the seven coating processes identified in the initial stages of the project, three were prototyped in order to apply a coating on a continuous substrate mounted on the coating test bed. Of the two processes that were successfully deployed, a final was selected on the ability of the process two deposit a uniform layer as needed for an electrode and of the desired thickness to achieve the necessary catalyst loading.

1.5.6 Process optimization

After the selection of a suitable coating process, key process parameters were identified and their influence on the electrochemical processes in an electrode studied. Additionally catalyst ink composition was also examined to identify the effect of its components on MEA performance. On the basis of this knowledge optimal operating conditions for the coating process were defined.

1.5.7 Overall process design

In the last stage of this research effort, the studies done on individual elements of the MEA fabrication process were assimilated together and an overall process for the continuous manufacturing of DMFC electrodes has been proposed.

1.6 ORGANIZATION

The first chapter of this dissertation provides an overview of DMFC operation and its components; describes the research opportunity and details the methodology that was followed in the due course of this investigation.

Chapter 2 provides a detailed discussion of the current state-of-the-art of DMFC and PEMFC MEA fabrication, and that of other supporting components in a fuel cell.

Chapter 3 ventures into different coating processes and examines them on their merit, identifying processes that can be used to apply a coating onto a continuous substrate that meet the requirements of fabricating DMFC electrodes.

Chapter 4 discusses the design and fabrication of a modular coating test bed that is built to accept different coating modules, which are used to deposit catalyst ink onto a continuous substrate. This allows for a thorough examination of coating process capability. The chapter concludes with the selection of a final coating process, spraying that will be used for DMFC electrode fabrication

Chapter 5 offers a brief examination of the spraying process and equipment used to produce an atomized spray. Then discusses a droplet sizing apparatus that was used to characterize the spraying process at different operating conditions. On the basis of these results an empirical relation was proposed to predict the mean drop size of the spray produced.

Chapter 6 uses the knowledge gained in the previous chapter regarding drop sizes and applies that into the fabrication of actual MEAs, which results in the identification of

optimal operating conditions. The testing and fabrication procedure for DMFC MEAs is also presented in great detail.

Chapter 7 Reviews the contributions made by this research effort, discusses important observations, limitations and identifies opportunities for future work that can be pursued in the area of continuous MEA fabrication process.

2. Materials and manufacturing of DMFC

2.1 INTRODUCTION

The first goal of this research effort is to identify the current status of materials and manufacturing of critical DMFC components, the bipolar plates and the MEA. In order to do so, a thorough literature review has been conducted, the information gathered is presented in this chapter.

Besides providing a deeper understanding into the workings of a DMFC, the relevance of this review is that, firstly it will provide a snapshot of DMFC manufacturing technology as it stands today. The performance of fuel cell systems is dependent on its constituent components, which in turn depend on the materials, and the associated manufacturing processes. Not only does this interaction between materials and manufacturing dictate performance, but they also define the cost of the technology. It is fundamentally important to understand these materials and manufacturing choices, their underlying relationship, and the identification of the most appropriate avenues for innovation.

Secondly, once an understanding of the state-of-the art of DMFC MEA manufacturing is developed, it will be possible to identify areas where research efforts should be focused. The aim is to identify the future course of this research.

An overarching observation can be immediately made upon the examination of research literature available, that is in general there is a great abundance of research charting the progress of certain materials used in a fuel cell, specifically electrocatalysts and membranes, but fewer sources of information exist which focus on how these materials will be utilized in manufacturing processes to create components such as the MEA for PEMFC and DMFC. Both of these types of fuel cells share key components and are manufactured using similar processes.

This chapter begins with a detailed look at MEA components: the membrane, diffusion media and the electrodes. The different types of MEAs are identified, and the associated MEA assembly process discussed. From the information gleaned it is clearly obvious that the most critical step in MEA manufacture is electrode fabrication, therefore a major portion of this chapter is spent on reviewing the different types of electrodes and the associated manufacturing processes, as relevant to a DMFC.

Subsequently diffusion media and bipolar plate materials and manufacturing are briefly discussed as well, to present a well-rounded picture of the state of the art of DMFC component manufacture.

2.2 MEMBRANE ELECTRODE ASSEMBLY

The membrane electrode assembly (MEA), Figure 8, is essentially the heart of a DMFC. It is where the two half-reactions, oxidation of fuel and reduction of oxygen, take place to create usable electrical power. As the name implies, an MEA consists of a proton-conducting membrane sandwiched between anode and cathode electrode layers, with a gas diffusion layer (GDL) on either side. Note that the term GDL is slightly misleading in the case of the DMFC anode, as the fuel stream consists primarily of liquid fuel, so they are also referred to as diffusion media. The following paragraphs briefly discuss the function of each element of the MEA.

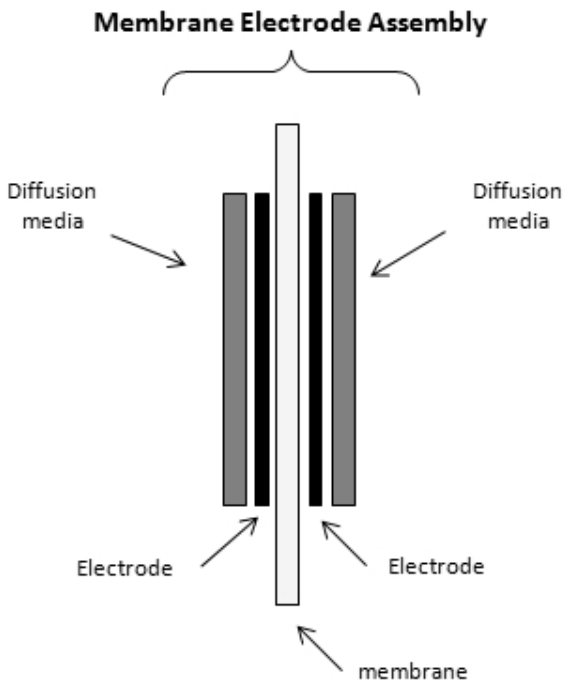

Figure 8: Cross section of a typical membrane electrode assembly.

2.2.1 Polymer electrolyte membranes

The membrane has two major functions in a fuel cell; the first is to separate the fuel and the oxidant, and the second is to transport protons across from the anode to the cathode to complete the redox reaction. The membrane must provide strong mechanical, chemical, and electrochemical stability in a harsh chemical environment over a range of operating conditions, while at the same time offer a long life, low reactant permeability and high proton conductivity.

The first significant use of proton-exchange membrane (PEM) was reported by GE in 1955; a polystyrene sulfonic acid (PSSA) membrane was used with an application in the NASA Gemini program [13]. The membrane offered a limited life. It was not until the 1960's when DuPont introduced the per fluorinated ionomer membrane Nafion that

PEMs truly made a difference and more than 60,000 hrs of stable operation of a hydrogen PEMFC was demonstrated [16].

Nafion is a copolymer of polytetrafluoroethylene (PTFE, Teflon) and vinyl ether, which, upon treatment, is converted into a highly conducting (-SO_3H form) ionomer membrane. The PTFE backbone is hydrophobic in nature and provides a strong mechanical and chemical backbone, whereas the sulfonic acid group is strongly hydrophilic, affects the water uptake, and hence, the proton conductivity. When exposed to water, the sulfonic acid group, provides a counterbalancing charge that enables effective proton transport across the membrane. These properties make it attractive for use in PEMFCs and DMFCs. With regards to DMFCs methanol, which is supplied as a fuel on the anode side, permeates across to the cathode and decreases cell performance. This is commonly referred to as 'methanol crossover'

Besides the brief discussion above, it is beyond the scope of this document to describe and chart the large quantity of research that has been carried out in developing new membranes for PEMFC and DMFC fuel cells. The motivators for this research are membrane durability and longevity for PEMFC and DMFC fuel cells and membranes with reduced methanol crossover for DMFC fuel cells. Methanol crossover is briefly discussed below.

2.2.2 Methanol crossover

Methanol permeates through the membrane and reacts at the cathode, resulting in a loss of fuel, and a decrease of the cathode potential. There have been extensive studies on methanol crossover by many researchers. Ravikumar et al. [17, 18] tested a liquid feed DMFC, and reported a loss in performance beyond methanol concentrations of 2M. Ren et al. [18, 19] have studied the uptake of water and methanol across Nafion membranes of different equivalent weights and their affect on cathode performance. They report a decrease in crossover as the equivalent weight increases, but this effect is accompanied

by an overall reduction in cell performance. Heinzel et al. [20] provide an excellent review on methanol crossover, its effects and how it varies across different fuel concentrations, membrane thickness, catalyst morphologies, temperatures and pressures. Zhao et al. [6] discuss how the overall system energy suffers when running a DMFC system at low methanol concentrations to alleviate problems caused by methanol crossover, and reviews the use of higher methanol concentrations in passive DMFC systems.

What can be summarized from these research efforts is that researchers have explored different strategies to deal with the crossover problem, the most effective being to use diluted methanol concentrations as fuel. While this addresses the crossover problem, it significantly affects the overall system energy density, which is the key advantage DMFC technology offers to begin with [6, 18].

2.2.3 Diffusion layer

The gas diffusion layer (GDL) as it is called for a PEMFC, or simply the diffusion layer or diffusion media for DMFC (liquid diffusion), provides a medium for reactant distribution onto the electrode [11]. On one side of each GDL are flow fields as part of the bipolar plates; the other side is in contact with the electrode itself. As shown in Figure 9, the reactants are distributed in bulk by the channels in the flow field and then diffuse through the GDL to the electrode. The by-products produced in the electrode on the active sites of the catalyst permeate back through the GDL to the flow field to be vented out of the system. So, essentially, the GDL assists in mass transfer, and acts as a current collector to provide a conductive path for the electrons generated at the electrode to reach the bipolar plates and then on to the external circuit.

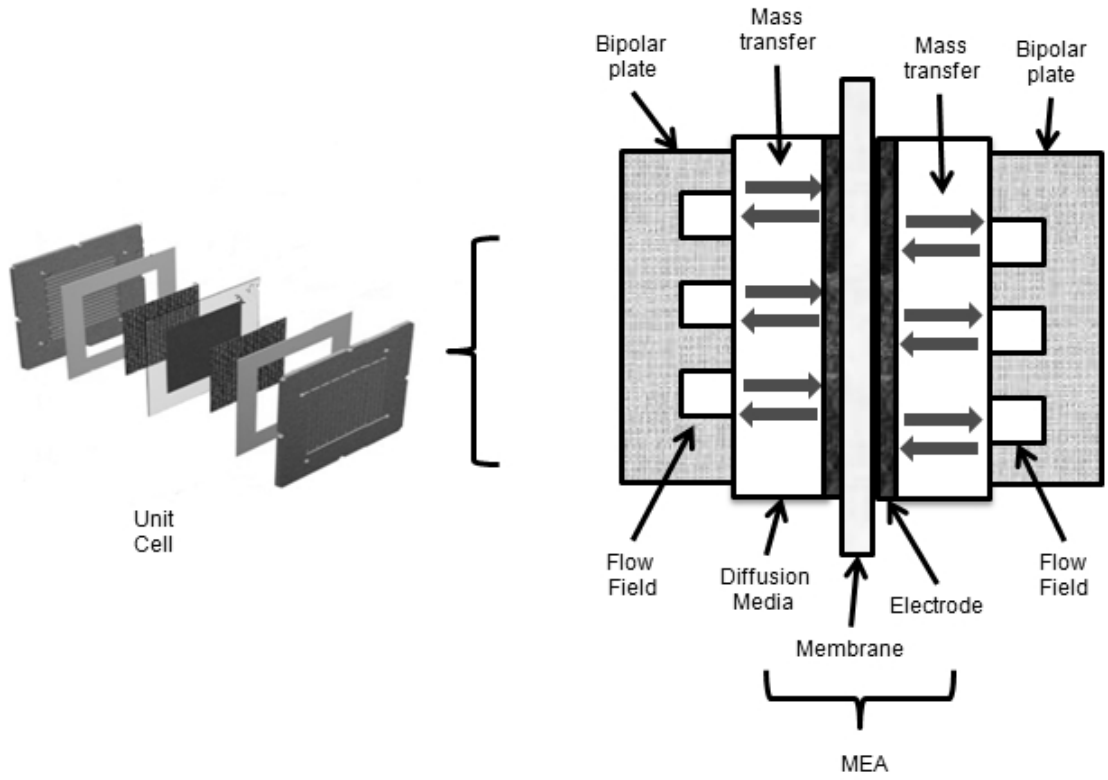

Figure 9: Mass transfer in diffusion layer.

Electrical conductivity, thermal conductivity and chemical stability are key requirements for the diffusion media. Predominantly macroporous carbon media such as carbon cloth or carbon paper have been used. This media is treated with PTFE to boost its hydrophobicity; additionally a microporous layer composed of carbon black with PTFE can be deposited on to the macroporous carbon substrate. Passalacqua et al.[21] report improved performance of the electrodes due to the presence of this microporous layer and explore different carbon blacks for this purpose. PTFE content in both layers is also very important, as it directly affects the porosity of the diffusion media which in turn affects the mass transport of react media to the catalyst layers [22].

The amount of compression applied onto the diffusion media in a fuel cell can also affect its performance. The tradeoff's involved in GDL compression are that as the compressive loads are increased, contact resistance decreases, but so does the pore

volume, which can potentially limit mass transfer. Compressive loads are applied in a fuel cell to prevent reactant/product leakage. Gee et al.[23] discuss how increasing the compression decreases the contact resistance and improves cell performance in the high current density region. The performance initially increases with increasing compression but then begins to deteriorate after reaching an optimal compression ratio.

Sung-Dae [24] has studied the effect of GDL compression in a fuel cell stack, rather than a single cell as done in most studies, using commercially available GDL material at two different compression levels (15% and 30% compression) and conclude that the higher level of compression, 30% produces better performance, owing to lower contact resistance.

Cinderella et al. [10] provide an excellent review of the different properties of a gas diffusion layer for PEM fuel cells.

2.2.4 Electrodes / Catalyst layers

The electrodes are typically porous structures of nanometer-sized catalyst particles dispersed in a suitable binder medium. Additionally, catalysts can be supported on carbon media to promote dispersion and lower catalyst loading. It is important to allow adequate pathways for diffusion of the reactant media to the catalyst site, removal of reaction products, as well as good electrical and protonic conductivity. The electrons generated during the reaction have to be transported to the external circuit, whereas the protons have to cross the electrolyte to complete the reaction at the counter electrode [12]. Electrical conductivity in an electrode is either provided by the carbon support, in case of supported catalyst, or the catalyst particles themselves in case of unsupported ones. The interfaces between the electrode, the membrane, the diffusion layer and the three-phase boundary between the reactant, the catalyst and the ionomer dictate the performance of the fuel cell.

Electrode fabrication has received considerable attention and over the past few years there have been a number of improvements. Significant research has been done on PEMFC electrodes and due to the similarly nature of DMFC electrodes the same results have been applied to DMFC's with good effect. The following paragraphs discuss the types and electrode fabrication methods applicable to low temperature (PEMFC and DMFC) fuel cells.

2.3 TYPES OF MEA

There are two types of MEAs used in PEMFC and DMFCs, the first type is called catalyst coated substrate (CCS) and the second type is referred to as the catalyst coated membrane (CCM). The difference between these two types is the substrate onto which the electrode is fabricated and how the overall MEA is assembled.

2.3.1 Catalyst coated substrate (CCS)

If catalyst particles are deposited onto a diffusion media, which is typically carbon paper or carbon cloth, then the electrode formed is called a gas diffusion electrode, as shown in Figure 10. The steps in preparing a gas diffusion electrode as shown in Figure 13 are as follows. The gas diffusion layer is first prepared by treating porous carbon media (cloth or paper) with Teflon to hydrophobize it, after which a mixture of carbon black and Teflon is applied onto it to form the microporous layer. A catalyst layer is then deposited onto this microporous layer to form an electrode [25]. Depending on the deposition process multiple layers might have to be applied to reach the desired catalyst loading. Two such gas diffusion electrodes (GDE) with suitable dimensions can be affixed onto either side of an ionomer membrane by the action of heat and pressure to form a catalyst coated substrate (CCS) type MEA.

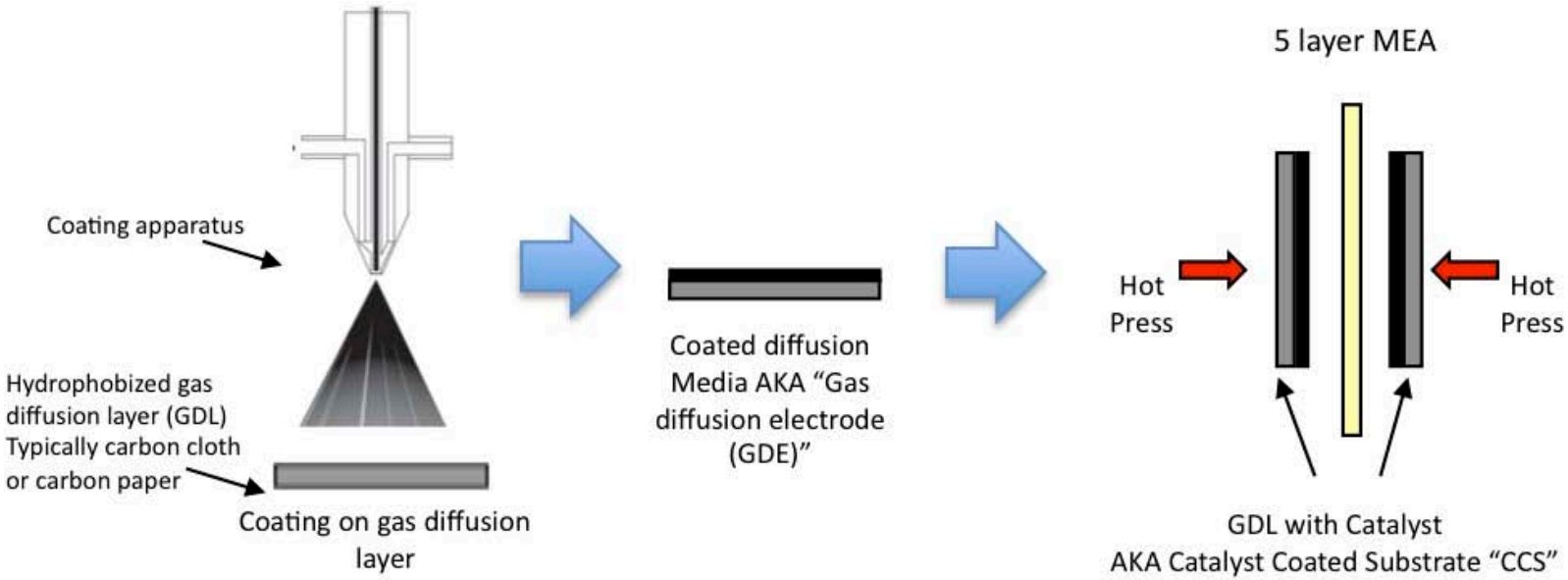

Figure 10: Catalyst Coated Substrate (CCS) type of MEA.

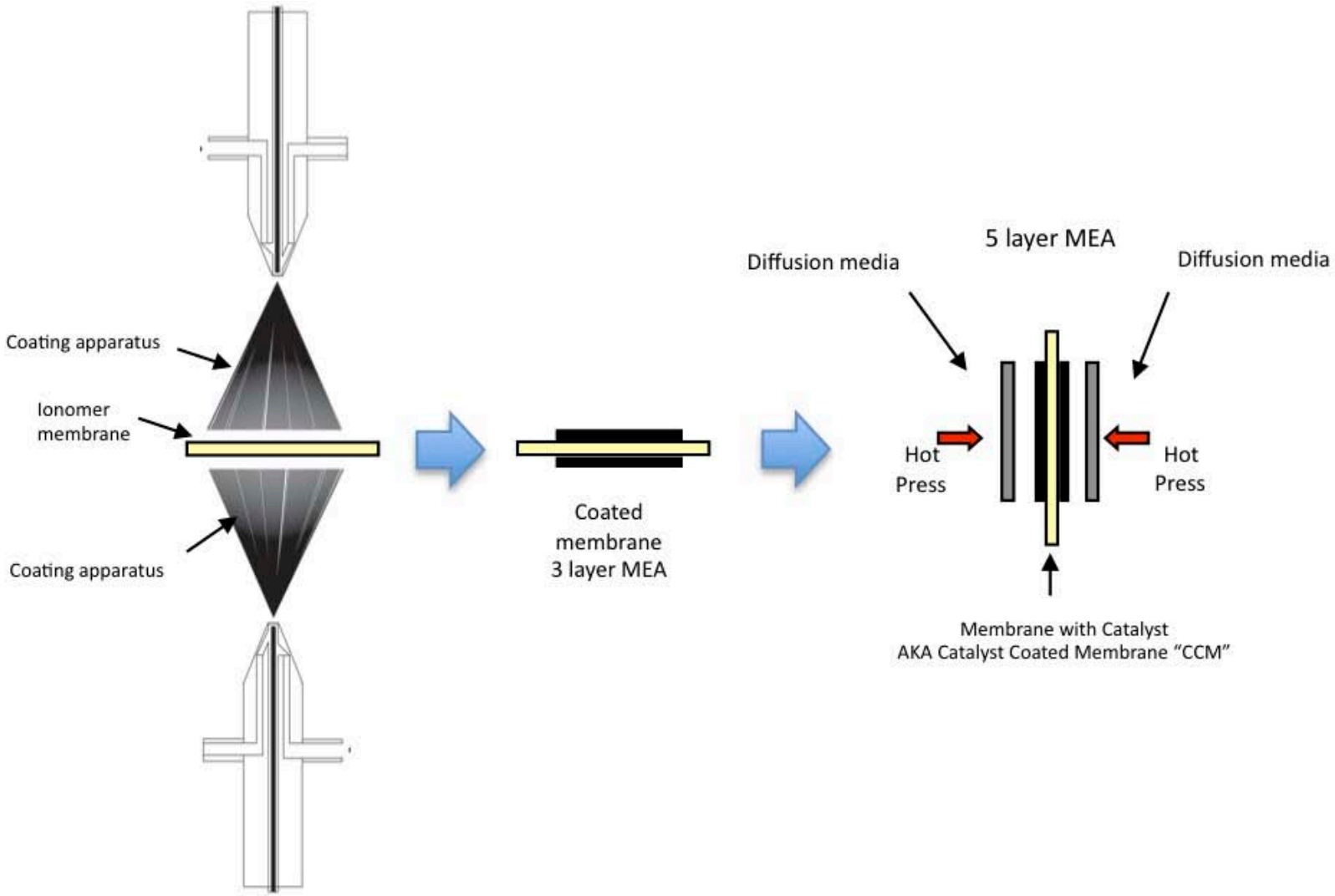

Figure 11: Catalyst coated membrane (CCM) type of MEA.

2.3.2 Catalyst coated membrane (CCM)

A CCM type MEA is fabricated by directly depositing catalyst particles onto the ionomer membrane[26, 27]. The processing steps for such an MEA are shown in Figure 11 and with more detail in Figure 13. Catalyst is deposited directly onto both sides of an ionomer membrane by any suitable process. Depending on the loading, multiple layers might have to be deposited to achieve the desired catalyst loading of the electrode. In this fashion a 3 layer MEA is fabricated. Diffusion media is typically attached in subsequent steps by the application of heat and pressure.

The direct application of catalyst onto the ionomer membrane allows for intimate contact of the electrode with the membrane at their interface, which may lead to performance benefits [26]. Typically the catalyst is in the form of nanometer-sized particles, which are suspended into solvents to form an ink. A suitable amount of ionomer is added to act as a binder[28]. The ionomer membrane used in a direct methanol fuel cell, such as Nafion, absorbs water and solvents and swells. This behavior is favorable for the protonic conductivity of the membrane but poses a significant challenge during ink application and drying [9, 29].

2.3.3 Decal Transfer Method (DTM)

To avoid this problem an alternate path for manufacturing CCM type MEAs is often used [28]. The electrodes are cast onto a temporary decal transfer substrate, such as Teflon or Kapton film, two suitably sized tokens of which are then hot-pressed on to the ionomer membrane after which the transfer substrate is peeled off. This method, as shown in Figure 12 is called the "decal transfer method" (DTM).

The decal transfer method adds additional processing steps as compared to the direct CCM method, the first being a hot pressing step where the electrodes are transferred to the membrane, and the second is a 'peeling' step in which the decal transfer substrate has to be peeled of the electrode. However the DTM method helps avoid the problem of ionomer membrane swelling, as the ink is applied and dried on a separate transfer substrate, and the membrane never encounters any solvents that it can absorb, which is the key concern in coating and drying of the electrode directly onto the membrane.

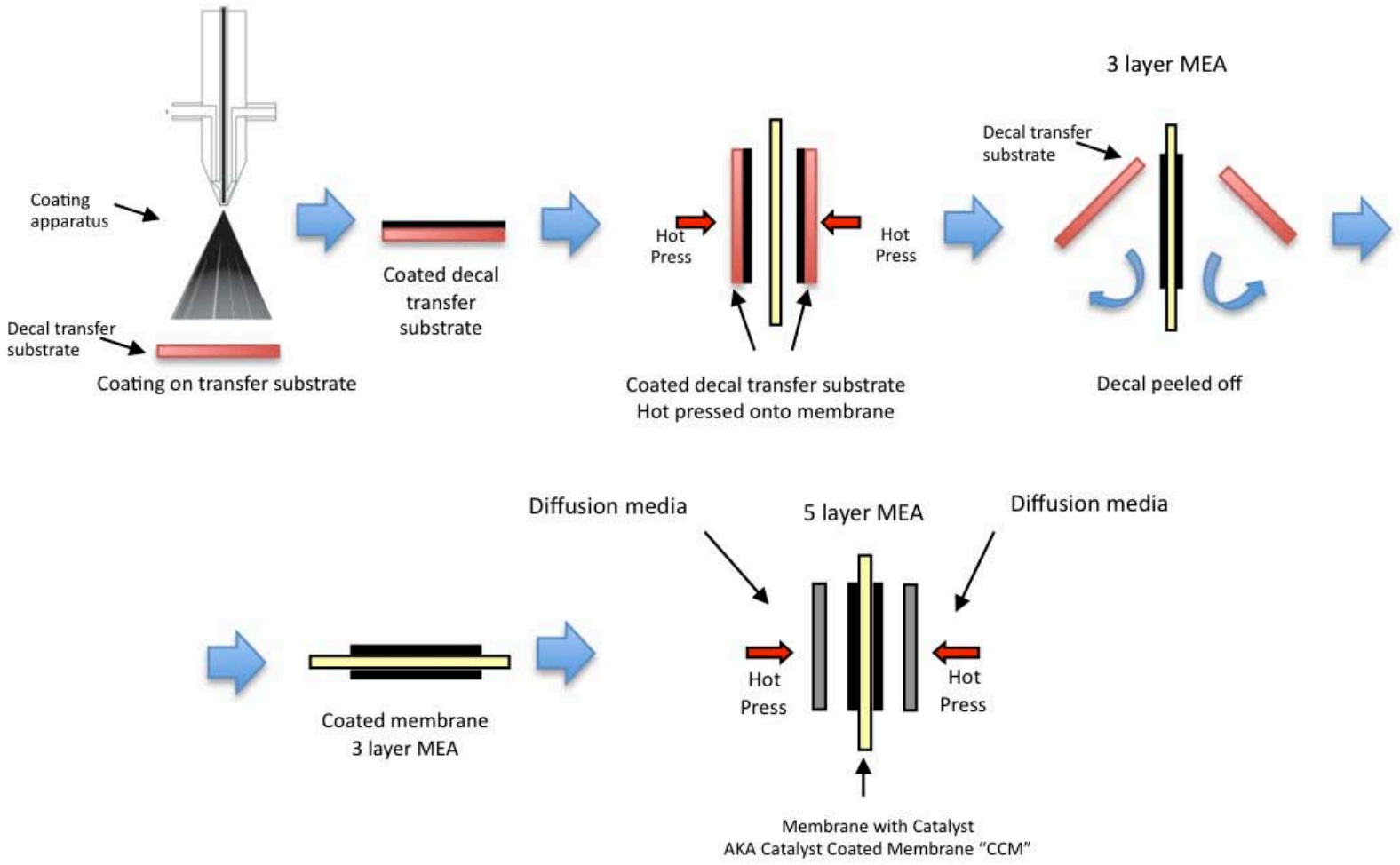

Figure 12: Decal Transfer Method (DTM) of making CCM MEAs.

2.4 TYPES OF ELECTRODES

Irrespective of the type of MEA used, all MEA's comprise of two electrodes, an anode and a cathode. It is imperative to identify the evolution and current status of fuel cell electrode technology. This will assist in identifying manufacturing processes that can be utilized to fabricate them.

2.4.1 Teflon-bonded electrodes

Although PTFE electrode technology is no longer used, it is important to mention it to chart the evolution of electrodes used in PEMFC and DMFC. In the early 1960's when solid polymer electrolyte technology was emerging and liquid electrolytes were dominant, Teflon bonded electrodes comprised a major breakthrough. The key role played by Teflon was that not only was it a good binder for the catalysts, the inherent hydrophobicity prevented the electrolyte from flooding the electrode, a film of Teflon deposited on Teflon bound catalyst would be porous enough to allow gas to pass through, but the pore walls due to hydrophobicity would not wet and prevent electrolyte from entering the electrode excessively, and impede reactants from reaching the catalyst sites. PTFE bound electrode preparation details can be found in patents by Niedrach and Alford et al. from GE [30, 31].

As solid polymer electrolytes began to be used, PTFE bound electrodes were deposited directly onto the electrolyte membrane. Much of this pioneering work on electrodes and solid polymer electrolyte (SPE) membranes by GE was embodied by the use of solid polymer fuel cells (SPFC) by NASA for the Gemini space missions.

Chun et al. [32] fabricated PTFE electrodes and compared them with thin film MEA's and concluded that thin film MEA's performed significantly better than conventional PTFE ones.

2.4.2 PFSA impregnated electrodes

Research into polymer electrolyte membrane electrodes remained dormant for a better part of the period between the 1960's and 1980's. Fuel cells (PEMFC) used in the Gemini program had high catalysts loadings (up to 4mg/cm^2) and it wasn't until the late 1980's that some fundamental breakthroughs were made at LANL by Raistrick and Srinivasan [33-35]. They were able to achieve a tenfold reduction in catalyst loading by coating a layer of the proton conducting ionomer (Nafion) on the surface of the electrode while maintaining the performance levels. By impregnating Nafion in the porous electrode structure the three-phase boundary is essentially extended and the electrochemically active area of the electrodes is increased, enabling low catalyst loading electrodes to perform as well as high catalyst loading electrodes. These electrodes were made by waterproofing carbon cloth with Teflon, applying a microporous layer on the surface (mixture of Teflon and carbon black) and then a layer of carbon-supported catalyst bound in Teflon. Sputtering a thin layer of Pt on the catalyst layer was also examined [36]. These porous electrodes are then coated by a thin layer of recast Nafion solution and then hot pressed on either side of the proton-conducting membrane, typically Nafion. Much of these concepts were borrowed from phosphoric acid fuel cells, and applied to PEMFC and DMFC [28].

2.4.3 Thin film electrodes

Wilson et al.[28] Noted that the presence of PTFE in the catalyst layer had little function, discrete clumps of Teflon can form and the application of ionomer film on the catalyst layer can lead to areas where the catalyst layer is not fully impregnated or areas where the ionomer extends through the catalyst layer to the diffusion layer acting as a transport barrier. Sites that are totally enveloped by Teflon are denied proton access and do not participate in the electrochemical

process. On the other hand, the presence of Teflon in the diffusion layer is welcome since it provides hydrophobicity and prevents clogging of pores with water.

To address these concerns, a new electrode structure was proposed in which the catalyst and ionomer are blended together to form an “ink" and cast to form the catalyst layer, with no PTFE content. The gas diffusion layer is fabricated separately by coating carbon cloth with a mixture of Teflon and carbon black, which is then pressed onto the electrodes. Such electrodes are called the “Thin Film" electrodes.

The use of Nafion as a binder poses a few challenges. Electrodes formed lack the mechanical properties of PTFE bound electrodes; additionally, it is not melt processable as PTFE is, therefore catalyst layers have reduced structural integrity. Elevated drying temperatures can improve these properties. With thin-film electrodes the catalyst loading was further reduced to 0.15 mg/cm^2 (PEMFC). Subsequent work by the same authors [37] detailed the casting of catalyst layers directly onto the membrane without the intermediate decal step, although it requires the use of a vacuum table to hold the membrane as it is being dried to prevent defects and distortion. Improved performance is achieved by this direct method as compared to the decal method and is attributed to the improved continuity between the catalyst-ionomer /ionomer interface. In order to alleviate the defects associated with Nafion as a binder, Wilson [38] employed the use of a thermoplastic form of Nafion, formed by ion exchange with tetrabutylammonium(TBA^+)which is moderately melt processable and gives better long-term performance, but generally most literature use the Na^+ form.

The thin film method has been used to fabricate electrodes for CCM and DTM type MEAs [29] . Paganin et al. [25] followed the same steps as described earlier by Wilson and co workers [28, 37] to prepare CCS type MEAs and studied the effects of diffusion layer thickness, PTFE content, Nafion content and catalyst loading. They report that the best performance achieved was with 20 wt % Pt-C, 0.4 mg/cm^2 and

1.1 mg/cm^2 Nafion in the catalyst layer and 15% PTFE in a diffusion layer of 50 μm thickness, for both the cathode and the anode.

2.4.4 Thin film electrodes: CCM vs. CCS

There is no clear winner between the CCM and CCS type of MEA's. From a performance stand point, for CCM type MEA's have been reported to give better performances, but from a mass production standpoint, CCS type MEA's have a clear advantage as it is easier to deposit catalyst layers on the carbon substrate (diffusion media) as compared to direct deposition on a Nafion membrane. The mechanical behavior and handling of the membrane being a concern in continuous production [29].

Chun et al.[32] compared the performance of CCM type, thin film electrodes prepared by two methods, by decal transfer, and direct application. These CCM type MEA's are compared with conventional CCS electrodes (PTFE Bound). Results reported show that CCM type MEA's prepared with direct application of ink on the membrane, performed better. This is attributed to the fact that the direct application of ink on the membrane produces a more intimate contact between the catalyst layer and the membrane extending the three-phase region.

Thin-film electrodes have also been applied on DMFC's. Ren[39] prepared and tested thin film MEA's made by the decal transfer method using unsupported catalyst and found their performance to be equal or better than conventional wet proofed electrodes configurations. With regards to DMFC, CCM type MEA's as compared to CCS type MEA's have a much denser structure, whereas the latter has a continuation of the porous structure of the diffusion layer [40]. This dense structure is attributed to pose a strong resistance to CO_2 bubbles whereas in a CCS catalyst layer CO_2 penetration and holdup is increased, which deteriorates mass transport.

2.5 ELECTRODE FABRICATION METHODS

From the discussion presented so far on MEA types, components and manufacturing it can be identified that electrode fabrication is the most important step in the overall MEA manufacturing process. The other two components of an MEA, membrane and diffusion media are already manufactured in a continuous roll form and are available from OEM suppliers [15, 41].

Off the types of electrodes discussed, thin film electrodes represent the state of the art of PEMFC and DMFC electrode technology. Figure 13 summarizes the steps required to fabricate thin film electrodes, for both types of MEAs. Due to the sequential nature of processing steps, thin film electrodes lend themselves well to a continuous manufacturing process.

The key step in the electrode fabrication process is the manner in which the ink is applied onto the substrate, which can be a decal transfer substrate, the membrane itself or the diffusion layer. The electrode is created by the ink deposition process, its microstructure, catalyst loading, geometry, morphology all being defined at this stage. The other processing stages shown, support the ink application step.

This section of the literature review examines the different catalyst ink deposition methods onto a substrate, These methods follow the same general thin film electrode fabrication method as developed by Wilson et al.[28].

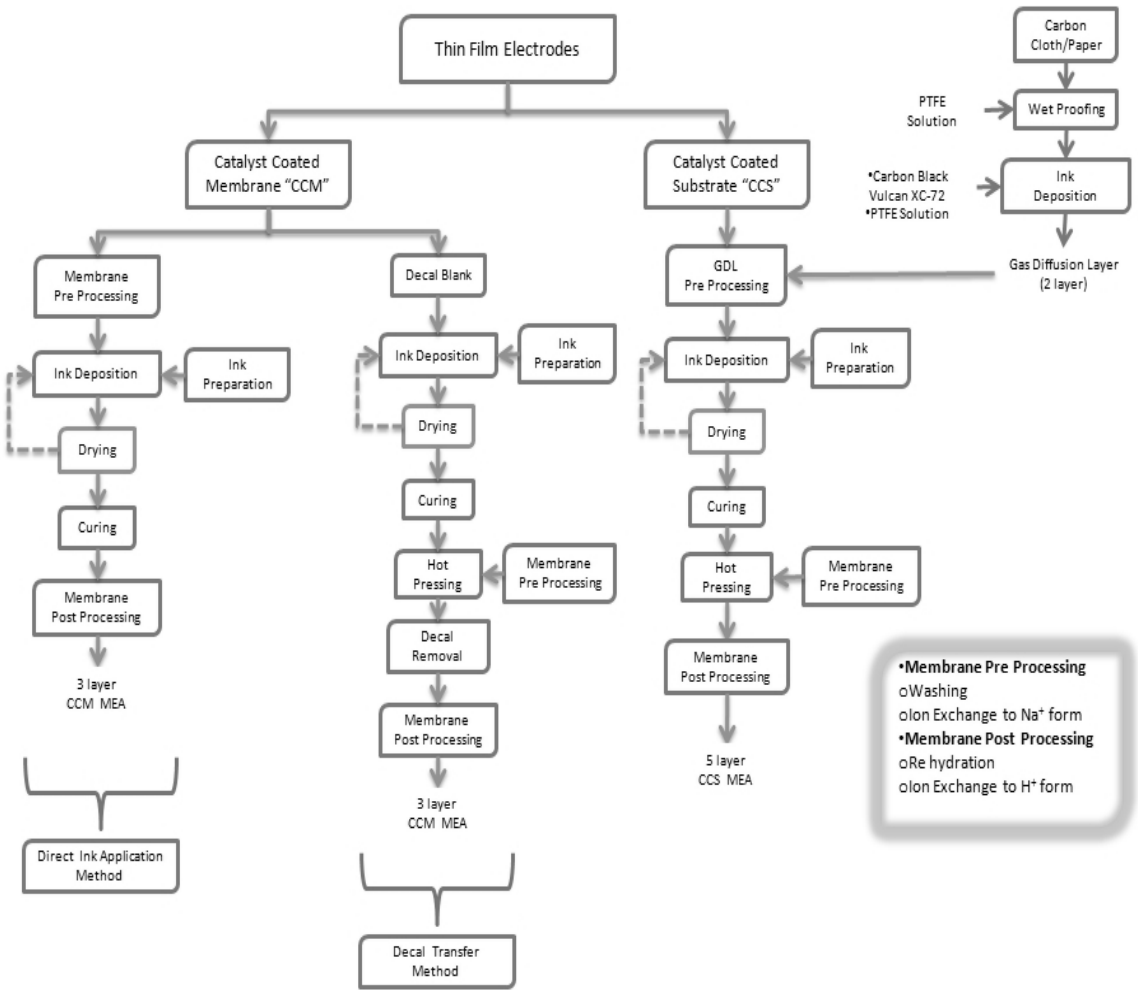

Figure 13: Thin film electrodes.

2.5.1 Brush painting method

The brush painting method, as described by Wilson et al. [28, 37] and by Zelenay et al.[42] involves mounting the membrane on a vacuum table, heated to between 20 and 80^{o}c, a piece of Teflon the size of the active area is placed between the membrane and vacuum table, and a sheet of silicon rubber, with a window cut in it of the size of the area to be painted. Catalyst ink is applied using a brush of an appropriate size; the layers are applied sequentially, which generally implies that a layer must be allowed to dry before a new layer is painted.

Depending on ink viscosity and catalyst loading, up to 30 coatings have been applied. The brush painting method can be used to apply a layer of ink onto a decal,

the membrane or onto the gas diffusion layer. It is widely used method for lab experimentation [39, 43-45] and small batch preparation, scale up of the process for mass production seems unlikely because of the manual nature of the application process, the uneven consistency of catalyst loading and the intermittent drying cycles.

2.5.2 Spraying

Spraying (Figure 14) is another common method used for catalyst ink deposition onto substrate. Typically in a laboratory setup spraying is done by a handheld airbrush or spray gun, but the process has been automated and scaled up for mass production. A variety of wet spraying machines are available for automated spraying of catalyst onto substrate [40].

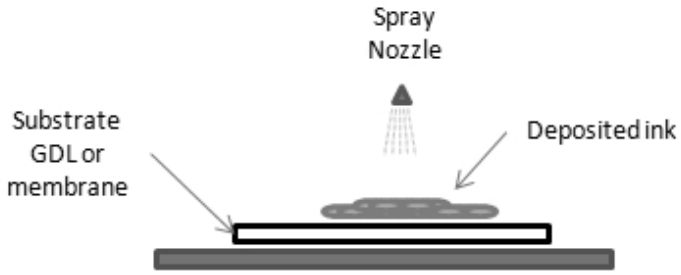

Figure 14: Spraying of catalyst ink onto a substrate.

2.5.3 Doctor blade technique/Tape casting

Tape casting, also known as doctor blading, is a widely used process for producing thin layers of a substance onto a moving substrate, as shown in Figure 15. Originally conceived for producing ceramics the process has evolved and been adapted to a wide variety of materials. Bender et al. [46] describe an automated process to coat transfer decals for MEA production. They utilize a motor-driven doctor blade mechanism; in order to reduce the time required to individually hand paint each layer onto the Teflon decal, which can be in excess of 6hrs. Ink viscosity and composition were appropriately modified to suit the apparatus. Lim et al. [47]

describes the use of a doctor blade to produce microporous layers on wet proofed carbon paper by evenly spreading a mixture of Vulcan XC-72R carbon black dispersed in a water alcohol mixture containing 40% PTFE, which is dried and subsequently sintered. The same process is applied to spread a slurry of Nafion, unsupported Pt-Ru black and organic solvent on the macroporous layer to form the anode of a DMFC, and a mixture of Nafion and carbon supported Pt black to form the cathode. Tape casting is also widely employed to produce Solid Oxide Fuel Cells, (SOFC) electrode supports.

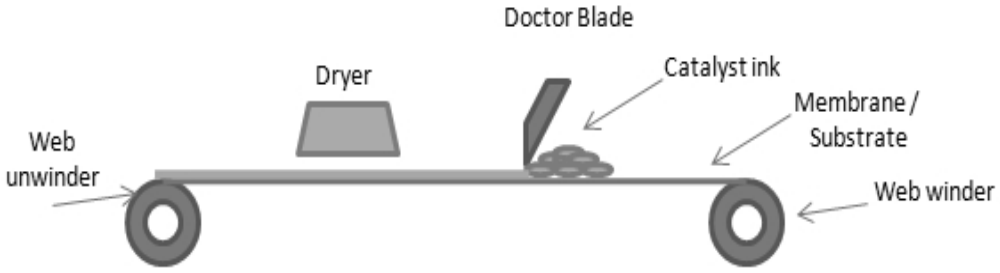

Figure 15: Tape casting process for MEA fabrication.

2.5.4 Dry spraying method

Gulzow et al.[48] describe a new production technique, based on an adaptation of a rolling process. Dry powder electrode material is mixed in a mill, atomized and sprayed in nitrogen through a nozzle onto the membrane or backing, resulting in a thin uniformly distributed layer. This layer is affixed to the substrate by passing through calendar rolls. The advantages of the process are, that it is a dry process, which results in simpler processing and removes the need for further drying steps. The performance of the PEMFC MEA's produced is comparable to those produced by other processes. In another article, [49] the authors discuss the production of DMFC electrodes by the same process. CCM or CCS MEA's can be produced with this process, as well as the macroporous layer on the GDL.

2.5.5 Screen printing

Chun et al.[32] Describe the fabrication of thin film electrodes for PEMFC by screen-printing (Figure 16) catalyst slurry directly onto Nafion membrane as well as onto a Kapton polyimide film, which was used as a decal. The thin film MEA's prepared showed superior performance as compared to conventional CCS type MEA's. Manco et al.[50] Describes the use of screen printing to produce electrodes in a single pass as compared to other processes, which require multiple iterations. Schonert et al. [51]discussed the use of additives which provide dimensional stability and gel forming polymers which adjust the viscosity of inks and act as binders for catalyst inks used in tape casting or screen printing.

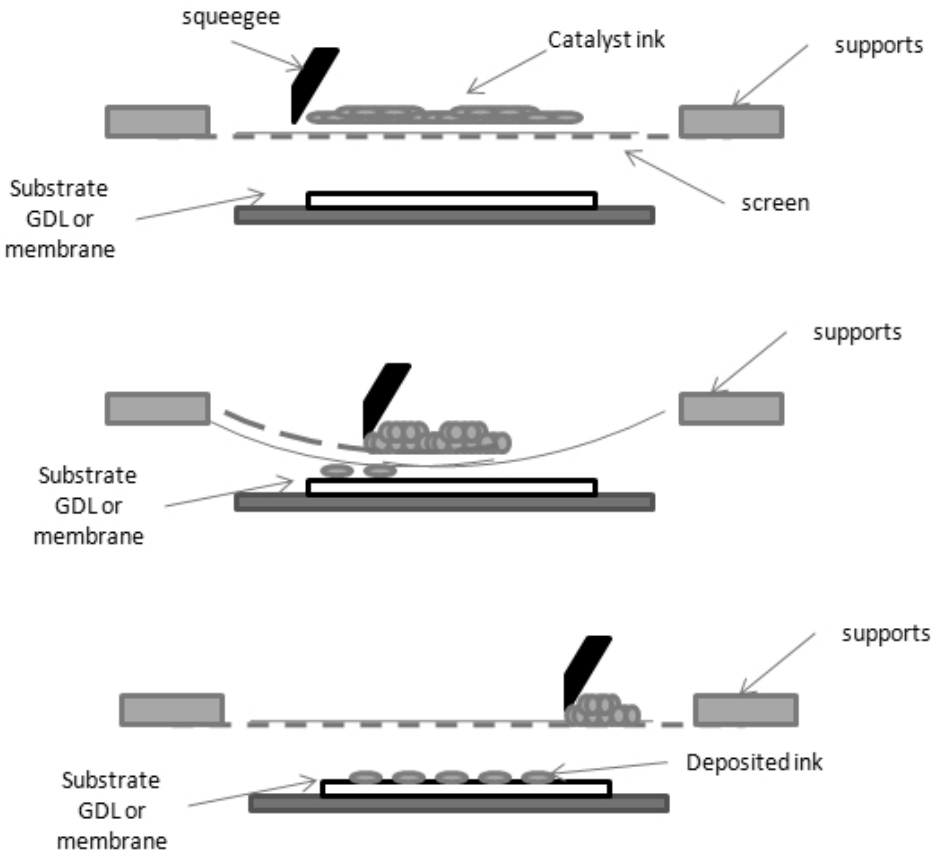

Figure 16: Screen printing process for MEA fabrication.

2.5.6 Vapor deposition electrodes

Vapor deposition processes refers to those techniques in which the catalyst is vaporized and deposited onto a substrate, which can be the gas diffusion layer or the membrane itself to form a thin uniform catalyst layer which is the electrode. Such techniques have been applied to form electrodes for both PEMFC and DMFC. The exact deposition mechanism can be due to condensation or chemical reaction, and the entire process is carried out in a vacuum chamber. The following paragraphs discuss the different vapor deposition techniques applied to form gas diffusion electrodes for PEMFC and DMFC.

2.5.7 Sputtering

Sputtering is a type of a physical vapor deposition (PVD) technique in which atoms are extracted form the target material (catalyst) by bombardment with an ion source such as plasma, and condensed on a substrate. It is purely a physical process and no chemical interactions assist the deposition of the thin film. Figure 17 shows the general apparatus used to create argon plasma in a vacuum chamber. It has been employed to produce catalyst layers with extremely low loadings. These thin layers do not require the use of a proton conducting ionomer and can potentially simplify production [12].

Sputtering has been used to manufacture electrodes for use in a DMFC. Witham et al.[52] Prepared sputter deposited catalyst layers for DMFC from Pt-Ru (52:48) targets and DMFC testing achieved a maximum power density of 104 mW/cm^2 with a catalyst loading of $1mg/cm^2$ (90^oc, O_2). An interesting observation was that on the use of ex-situ Nafion as a proton-conducting path on the MEA had some detrimental effects, the authors argue that the Nafion sprayed onto sputter deposited catalyst layers tends to electrically isolate the catalyst sites. MEA's with

catalyst loading of 0.03mg/cm^2 with no Nafion spray, performed as well as MEA's with 3 times more loading, and showed much higher catalyst utilization.

Sputter deposited electrodes were fabricated for use in micro-fuel cells by O'Hayre et al.[53]. The performance of the cells was tested with non-humidified reactant gases and was found to be sensitive to the layer thickness, with peak performance achieved with 5 nm thick films. A sputtered MEA with Pt loading of 0.04 mg/cm^2 was compared to a conventional MEA 0.4 mg/cm^2, which produced a peak power of 50 mW/cm^2 as compared to 33 mW/cm^2 with the sputtered one, 3/5 of peak power performance achieved with 1/10 the catalyst loading.

An important contribution by Haug et al. [54] was to compare sputter deposited CCS and CCM MEAs with electrodes prepared by ink based methods. Multilayered MEA's were also prepared by alternating layers of Nafion carbon ink and sputtered catalyst layers. They found that CCS performed better than CCM MEA's, with the performance equaling that of similarly loaded conventional electrodes. Adding multiple layers for CCS type did not increase performance even though high catalyst activities were achieved. The authors conclude that simultaneous sputtering of Pt and spray deposition of Nafion ink would generate a continuous three-phase interface.

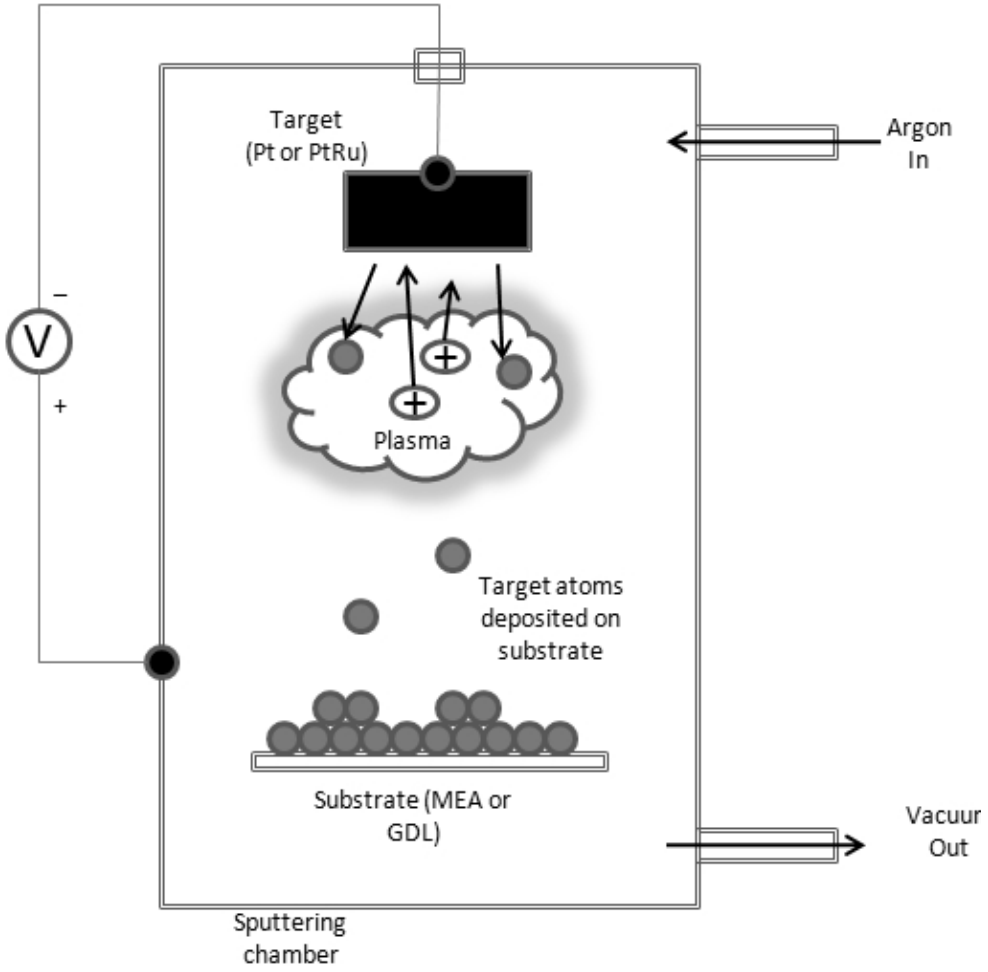

Figure 17: Sputtering [12].

2.5.8 Novel composite MEA processes

In addition to conventional MEA fabrication processes, there has been research conducted on more novel approaches. Frey et al.[55] describe a layer upon-layer based preparation method in which the complete MEA is fabricated onto a suitable substrate by spraying one functional layer onto another. The critical electrolyte layer is deposited using an airbrush, alcohol-free Nafion solution is used and several layers are formed with vacuum drying steps in between. Promising power densities were delivered by such MEA's upon testing.

Wan et al.[56] fabricated a titanium sheet substrate, with pores and micro channels made by etching. An expanded PTFE (e-PTFE) substrate was sandwiched

between two such titanium sheets and impregnated with electrolyte ionomer. Further the catalyst layers were deposited on either side to crease an integrated composite MEA (IC-MEA). A MPL was added on top of the catalyst layers and carbon paper used as the GDL. The performance results are promising, warranting further research.

2.5.9 Commercially used MEA fabrication processes

Electrode fabrication processes identified so far are predominantly used in a laboratory environment on discrete pieces of substrate. A key research question posed for this literature review was the identification of electrode fabrication processes that can be scaled up for mass production of MEA's onto a continuous web of substrate.

Unfortunately there is little information available on the actual MEA fabrication processes used in the industry for PEMFC and DMFC. Since exact processes used in the industry are of proprietary nature, a patent search was done to identify coating processes that are being actively considered in the industry. Table 1 lists these processes along with the year the patent was awarded, and company name.

Table 1: Commercial MEA Fabrication processes.

Component Type	MEA Fabrication Process	Company	Year	US Patent Reference
CCM	Spray Coating	Samsung SDI	2007	[57]
CCM	Flexographic printing	DuPont	2007	[58]
MEGA, CCS	Spraying	Hyundai	2007	[59]
CCM	Magnetron DC Sputtering	Samsung	2004	[60]
CCS, CCM	Electron Beam PVD	Gore	2007	[61]
GDL, CCM	Extrusion, Calendaring	3M	2002	[62, 63]
CCM	Tri Layer CO-Extrusion	Ballard	2001	[64]
CCM+CCS	Screen Printing	Japan Gore-Tex	2004	[65]
CCM	Screen Printing	Honda	2007	[66]
CCM	Bar Coater	Asahi Glass	2007	[67]
CCM	Die Coater	Matsushita	2005	[68]
CCM+CCS	Screen Printing	Umicore	2006	[69]

The processes represented here are used to fabricate MEA's for both PEMFC and DMFC type fuel cells, and both types CCM and CCS have been explored. As can be seen a variety of web coating processes are employed, such as extrusion, bar and die coating etc. These coating processes are generally not found considered in academia, because of the cost associated with the equipment, and the volume of material required for a reasonable production run are not feasible for academic pursuit.

Another observation that can be made from this data is that all processes considered are used to deposit a coating onto a continuous web of substrate, i.e. they are all roll-to-roll MEA manufacturing processes. No discrete manufacturing process for MEA fabrication is being considered in industry.

2.6 MEA OPTIMIZATION

In this section results are presented of a brief survey conducted in literature to identify material choices and processing conditions that can positively influence MEA performance.

2.6.1 Membrane thickness

Membrane thickness can have a significant effect on cell performance. As membrane thickness increases, cell resistance increases and subsequently cell performance decreases. Furthermore in a DMFC, methanol crossover is also affected by membrane thickness. Paganin et al.[25] shows the decreasing ohmic resistance as membrane thickness is decreased, 50μm for N112 to 175μm for N117. Ren et al.[39] show that for a 1M feed of methanol at 90ºC the permeation rate is three times greater for Nafion 112 membrane relative to Nafion 117. In another study [18], the same authors conclude that the methanol crossover rate through a 1200 EW membrane is only half of that through an 1100 EW membrane.

2.6.2 Ionomer content

A soluble form of Ionomer (typically Nafion) is added to the catalyst ink and acts as a binder, as per the thin film electrode fabrication method. A few studies which have explored the effect of ionomer content on DMFC electrode performance are summarized.

Thomas [70] studied the effect of ionomer content in the catalyst layers of a DMFC, and found that in the anode, which has Pt-Ru catalyst, the presence of hydrous RuOx actually assists in proton conductivity and the ionomer content can be reduced or even eliminated, whereas on the cathode, the ionomer is necessary to provide an adequate three-phase boundary. In a recent study, Sister et al.[71] found that in the anodic catalytic layer of a DMFC, the optimal content of the ionomer is around 25 vol%, and that compacting the catalyst layers reduces the ohmic losses in the system. It must be noted that a 40% Pt-Ru supported catalyst was used for this study. In other studies where Pt-Ru and Pt Blacks have been used, the ionomer content is significantly lower. Reshetenko et al. [40] uses a Nafion-to-catalyst ratio of 0.12 for the anode and 0.26 for the cathode of a DMFC fuel cell.

2.6.3 Hot-Pressing conditions

Hot pressing is used to assemble the electrodes to the membrane in the CCS process and transfer electrodes in the DTM process of MEA manufacture. Hot pressing conditions, such as the applied pressure and temperature can affect the structure, porosity and performance of the cell. Typically the temperature is kept above the glass transition temperature of Nafion, at 130ºC with the pressures ranging from 20 to 350 kg/cm^2, and the pressing time ranging from 30 to 300s [72]. The effects of hot pressing conditions are more obvious on DMFC as compared to PEMFC. Song et al.[73] finds that catalyst coated carbon fiber electrodes (CCS) do not require hot pressing. Elevated temperature (130ºC) and higher pressures exacerbate these performance losses, which are attributed to the collapsing of pores within the catalyst layers. Chen et al.[74] focused on improving

the DMFC performance of an air breathing stack (passive DMFC) via catalyst loading and hot pressing conditions in MEA fabrication. Results indicate that the specific power density of the cell is doubled by increasing porosity of the cathode from 57% to 76%. The hot-pressing conditions do not affect the catalyst nanostructure but a network of macro fissures exist on the catalyst surface. By hot pressing at lower pressure, larger macroporous fissures are formed, which aid in mass transport at the cathode. Zhang et al.[72] argue that, although increased pressure reduces the thickness of the GDL, thereby reducing the mass transport path, the accompanying decrease in porosity adversely affects the cell performance, with optimal results achieved at around 80 kg/cm^2 at 90 ^oc for 90 s.

Tucker et al.[75] studied the pore structure of DMFC electrodes which were CCS type, with both unsupported and supported catalyst. The authors find that the pore size distribution of the microporous and catalyst layers is defined by the pore size distribution of the catalyst or binder powders used to make the ink. The deposition process does not significantly alter the pore sizes. Figure 18 shows the range of pore sizes found in a DMFC MEA and the transport process that take place in them.

For DTM electrode transfer, generally temperatures ranging from 130 ^oc to 210 ^oc are employed in the transfer process with pressures ranging from 250-3500 psi and transfer time ranging from 180 s to 720 s [29, 76-82].

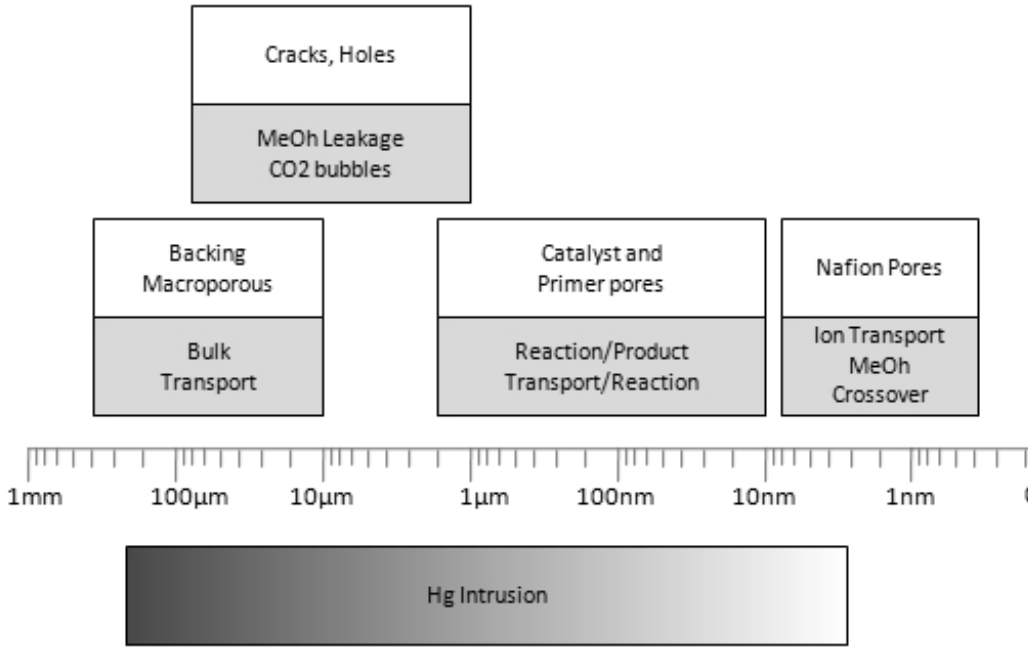

Figure 18: Pore sizes and mass transport processes [75].

2.6.4 MEA defects

As commercialization and mass production of PEMFC and DMFC technology becomes inevitable, it is becoming even more important to understand and control the defects introduced in manufacturing. Although MEA degradation mechanisms (chemical degradation) have been the focus of recent studies, but there is little literature available on manufacturing defects. Such defects will deteriorate performance and operating life of MEA components, which even now have a target of 4000 hr for automobile applications.

Table 2, shows typical defects in MEA, introduced during manufacturing, their probable causes and the possible effects they can have on MEA performance.

Table 2: Typical MEA defects.

Defect	Description	Causes	Effects	Reference
Cracking	Breaking of electrode	Drying rate, Handling	Pinhole, tear formation, Increased resistance, Flooding	[83]
Orientation	Macroscopic features on surface	Manufacturing process	Variable contact resistance, Stress variations	[83]
Delamination	Catalyst layer separates from membrane	Processing conditions, swelling and thermal expansion behavior	Flooded areas, Increased resistance, Pinholes, Loss of activity	[83],[40]
Electrolyte clusters	Ionomer clusters in catalyst layer	Excess ionomer, incomplete mixing	Increased resistance, Loss of activity	[83],[64], [84]
Catalyst Clusters	Catalyst agglomerates	Insufficient mixing	Reduced Activity, thickness variations	[83]
Thickness Variations		Processing conditions	Variable resistance, Pinholes, Mechanical Weakness	[83],[40], [72]
Crushing	Electrode, diffusion layer crushed	Stack assembly, hot pressing	Mass transport, cell performance, cathode degradation	[47],[75], [72],[72, 73]

From a mass production standpoint, substrate web management will be a key concern in a continuous process, even more so if CCM type MEA's are to be fabricated. This is due to the swelling behavior of Nafion, which complicates web control. For both CCM and CCS type MEA's cracking, and delamination will be a major concern, the other defects being more easily corrected by proper mixing and ink application.

2.7 BIPOLAR PLATES

Bipolar Plates (BPP), Figure 19 are a critical component of a fuel cell stack; their performance, durability, and cost have to be optimized if PEMFC and DMFC are to become a commercial reality [85]. The most important functions of a bipolar plate are to provide a path for the reactants to reach the gas diffusion layer and for the reaction products to be removed from the gas diffusion layer, as well as to provide a conducting path between adjacent cells. A bipolar plate on one side has the anode flow field for one cell and on the other side the cathode flow field for the next cell. Bipolar plates account for about 80% of total weight. There is some ambiguity on the cost contribution of

bipolar plates. Tsuchiya et al. [86] report that bipolar plates contribute up to 45% of the stack cost whereas Lasher et al. [14] report that bipolar plates contribute up to 9% of the stack cost. This difference is because of the material costs the authors have assumed in their costing models. Tsuchiya assumes a cost of $\$1650/m^2$, whereas Lasher assumes a cost of $\$18/m^2$. Graphite, sheet metal and polymer composites are the main materials explored for fabricating bipolar plates

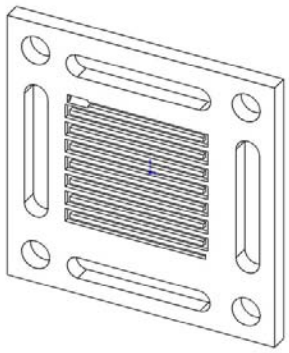

Figure 19: Bipolar plate.

2.7.1 BPP requirements

Key requirements of a BPP are summed up in Table 3. Key material requirement such as corrosion rate and contact resistance have a direct impact on the performance and life of a BPP. It is desired that the plate material not 'dissolve' or chemically react and participate in the reactions happening in a fuel cell, while contact resistance introduces ohmic losses. The mechanical properties are important from a stack perspective, so that the plates can endure the mechanical loads they will be exposed to.

Table 3: Bipolar plate requirement,[85, 87-89].

Requirement	Target
Corrosion Rate	< 0.016 ma/cm^2
Electrical Conductivity	> 100 S/cm
Compressive Strength	> 22 psi
Tensile Strength	> 41 MPa
Flexural Strength	> 59 MPa
Impact Strength	> 40.5 JM^{-1}
Crush Strength	> 4200 kPa
Gas Permeability	16x10^{-6} cm^3/s/cm^2
Surface Finish	50 μm
Tolerance	> 0.05 mm
Thermal Conductivity	> W m^{-1}K^{-1}

2.8 BIPOLAR PLATE MATERIALS AND PROCESSES

Graphite has been the most predominantly used material for bipolar plates because it offers excellent chemical stability and high electrical conductivity, however the cost, manufacturability, inherent brittleness and low mechanical strength has prompted the search for alternative low cost materials. Figure 20 shows a classification of materials that have been explored for use in bipolar plates. The following paragraphs will discuss alternative materials and processes that have been explored by researchers around the world to come up with a suitable alternative for graphite. Table 4 shows the key properties of graphite versus 316L stainless steel.

Table 4: Graphite and 316L properties [89].

Property	Graphite	SS316L
Cost (US$ kg^{-1})	75	15
Density (gm cm^{-3})	2.25	8.02
Thickness of bipolar plate (mm)	2.54	1.2
Modulus of Elasticity (GPa)	10	193
Tensile Strength (MPa)	15.85	515
Corrosion Current (MA m^{-2})	< 0.1	< 0.1
Electrical Resistivity (Ω cm 10^{-6})	6000	73
Thermal Conductivity (Wm^{-1}K^{-1})	23.9	16.3
Permeability (cm s^{-1})	10^{-2} to 10^{-6}	< 10^{-12}

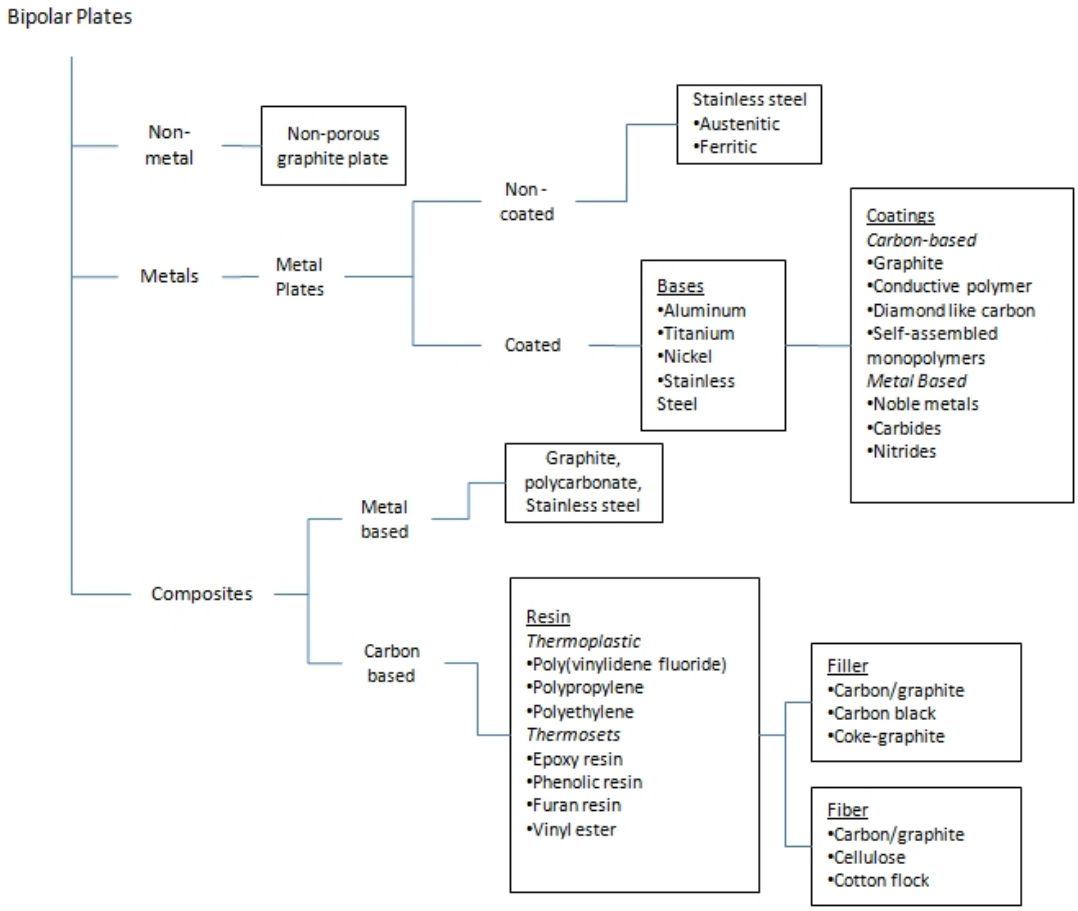

Figure 20: Bipolar plate materials [90].

2.8.1 Composites

Bipolar plates made of composites offer a worthy alternative to graphite or metal-based bipolar plates. Lower cost can be achieved through mass manufacturing and simpler processing, as compared to graphite plates, and over the years the aim has been to tailor the properties so that thinner plates can be formed, thereby increasing volumetric and mass power density of the entire system. Key ingredients of composite materials are a resin or binder to provide a matrix in which conducting particles are embedded such as carbon, graphite, conductive fibers, metals or metal oxides, carbides etc. Additionally, fiber elements are added to increase strength and conductivity.

Commonly used polymeric resins can be either thermoplastic or thermosetting. A patent by GE from 1980 [91], describes the use of a thermoplastic material PVDF as a binder with graphite particles for conductivity, and a subsequent patent [92], describes the addition of carbon fibers to reinforce the plate and enhance mechanical and electrical properties [93].

Thermoplastic resins are typically used in dry mixtures with carbon or graphite powder and are suitable for compression molding, must be allowed to cool before removal from the mold, whereas thermosetting resins (e.g., phenolics, epoxies and vinyl esters) can be removed immediately offering faster processing times [94, 95].

Besmann et al.[96] at Oak Ridge National Laboratory prepared carbon-carbon composite bipolar plates by slurry molding chopped carbon fiber in a phenolic resin. Vacuum molding was used to prepare the green part and additional application of phenolic and chemical vapor infiltration (CVI) was used to reduce surface porosity. The CVI process coats additional carbon and pyrolyzes the remaining phenolic resin giving the plates very high conductivity. In lab tests the flow fields were machined on, but embossing the preform is envisaged for mass production. Although excellent corrosion resistance and high mechanical strength were measured, the process, especially the CVI step, is not cost effective.

Busick and Wilson et al.[95, 97] created low-cost composite graphite plates by using a vinyl ester resin and graphite powder and compression molding them into thin plates. The graphite content is high in order to ensure adequate conductivity.

The main processes for molding composite plates are [98] compression molding and injection molding. Compression molding methods typically start with a powder blend fed in to a heated mold. Depending on the binder, if thermo-set the part has to cool down first with typical cycle times of 15-20 min. Injection molding offers faster cycle times, automated production but has drawbacks such as excessive mold wear, limited size to thickness ratio

and poor conductivity [98]. Table 5, summarizes different materials and processes that have been tried to produce composite BPP

Table 5: Composite bipolar plate materials.

Resin	Filler	Fiber	Process	Post Processing	Year	Ref
PVDF	Graphite		Compression molding		1980	[91]
PVDF	Graphite	Carbon fiber	Compression molding		1982	[92]
Phenolic	Graphite	Carbon fiber	Slurry molding, Vacuum drying, CVI	FF Machining, Embossing	2000	[96]
Vinyl Ester	Graphite powered		BMC, Injection molding		2004	[99]
Nylon6	Graphite powder	S316L	Injection molding	4 h Drying	2006	[89]
Phenol	Graphite flake and EG		Preform molding, preheat, Stamping		2007	[100]
Vinyl Ester	Graphite	Cotton fiber	Compression molding		2001	[101]
PVDF	80% wt Ti_3SiC_2		Compression molding 10 MPa, 200°c, 10 min		2006	[102]
Epoxy	20% v/o Expanded graphite		Compression molding 155°c, 20 min		2006	[103]
Aluminate cement	60 wt% graphite		Compression molding		2006	[104]
PVDF	60 wt% graphite	PPS wet-lay	Wet lay material rolling	Blank preheat and molding	2007	[105, 106]
Epoxy	50 wt% Carbon black	Expanded Graphite	Blending, Vacuum drying, Compression molding	Curing	2007	[107]
Epoxy	Polypropylene, Graphite, Carbon black		Solution blending, Vacuum drying, Compression molding	Curing	2007	[108]

2.8.2 Metals

Metals in sheet form offer an attractive alternative as they posses the necessary characteristics: low cost, well established sheet metal mass manufacturing processes, good mechanical properties, chemical stability, and high electrical and thermal conductivities, but the exposure to an acid environment of pH of 2.3 and temperatures ranging from 60 to 80°C promotes corrosion and dissolution. The dissolved metal species

can potentially poison the catalyst and/or the electrolyte membrane, reducing the overall performance of the fuel cell [90]. Metals form a passive layer on the surface, due to corrosion which, although protects against further chemical attack, it increases the contact resistance, which increase the ohmic losses of the fuel cell. In order to address these shortcomings, researchers have tested various types of metals, alloys and protective coatings.

2.8.3 Uncoated metals

In non-coated metals, stainless steels, aluminum, titanium and nickel among others have been explored. Stainless steel is an attractive material because of its inherent corrosion resistance, and extremely thin plates can be fabricated from it. Davies et al. [109] tested three different grades of stainless steel alloys for over 3000h and observed increased polarization in the following order 904L<310< 316. Interfacial contact resistance was also measured before and after passivation in the fuel cell environment, and a relation between the thickness of the passive film and resistivity was observed; increased film thickness led to higher resistivity. In another study by the same authors [110], the passivation film thickness was measured for some alloys and the thickness decreased in the following order:

321 > 304 > 316 > 347 > 310 > 904 > Incoloy 800 > Inconel 601

with the trend verified by the interfacial resistance which decreased in the order:

321 > 304 > 347 > 316 > Ti > 310 > 904 > Incoloy 800 > Inconel 601 >Poco graphite

Wind et al. [111, 112] tested coated and uncoated metals, and found that for uncoated 316L the losses were significant, but with a gold coating the performance was

equal to that of graphite plates. Other proprietary low cost coatings were tried, and stable operation was achieved for over 1000 h.

Wang and Turner et al.[112] tested different stainless steel alloys and found that Cr content plays an important part. Interfacial contact resistance decreases with increasing Cr content, among the tested alloys the contact resistance followed the order 349<904L<317L<316L, which agrees with previous results [109, 110]. The passivation film thickness formed in air, grows in usage and then stabilizes.

In a subsequent study [113] thermal nitriding of 349 was done but instead of a continuous film of CrN/Cr_2N discrete particles were formed which although reduced the interfacial contact resistance significantly, significantly higher corrosion currents were observed. More stainless steel alloys were studied [114]and corrosion resistance was in the order

AISI446 >AISI444 > AISI436 > AISI434 > AISI441

Whereas contact resistance performance was in the order:

AISI444 > AISI436 > AISI441 > AISI434 > AISI446

From these results AISI446 showed to be a most promising candidate and further in [115], AISI446 was nitrided to obtain good corrosion and order of magnitude lower contact resistance as compared to untreated alloy.

Lee et al.[116], modified the passive layer on 316 by an electrochemical surface treatment. The Cr content on the surface was doubled after treatment, the corrosion rate was improved by 66% and the improved surface properties reduced surface resistance as well making it a possible candidate for bipolar plate application. In a subsequent study [117], although performance is greatly improved over untreated 316 alloy but still lags behind that of graphite plates.

Padhy et al.[118] tested a DMFC with 316 bipolar plates for over 100h and stable operation was demonstrated although no comparison was offered with graphite or other materials. Fleury et al.[119] prepared amorphous Fe alloys, which exhibited comparable contact resistance to SS316 but much higher corrosion resistances, which makes them a potential candidate for use in bipolar plates. A bulk amorphous alloy of $Zr_{75}Ti_{25}$ was tested and compared with 316L stainless steel [120] and it showed marginally better performance in simulated environments.

2.8.4 Coated metals

Different coatings have been tried on base metals such as aluminum, stainless steels, titanium and nickel to further improve their corrosion resistance and decrease the interfacial contact resistance. Table 6 summarizes base metals and coatings that have been tried out.

Chung et al.[121] prepared carbon film coated stainless steel CFCSS by a chemical vapor deposition process. A thin nickel layer was sputtered on to 304SS and then the CVD process was carried out. It was found that the surface morphologies were highly dependent on the concentration of carbonaceous species during the CVD process, with a C_2H_2 ratio of 0.45 providing the optimal morphology. Testing revealed that the CFCSS had superior corrosion resistance and reduced contact resistance and performed significantly better than uncoated 304ss and equal or better performance to that of Poco graphite plates.

Feng[122] ion implanted nickel on a SS316L substrate and conducted potentiostatic, potentiodynamic and contact resistance studies to determine the effects and found that a Ni-rich surface layer formed improved the corrosion resistance and significantly lowered the contact resistance. A micro-arc alloying process was used to

deposit a thin TiC film on 304SS substrate [123]. the TiC increased the corrosion resistance in the simulated environment, and exhibited high stability during a 30-day immersion in cathode conditions. The authors conclude that the promising results warrant further testing. Carbon coated SS304 samples were prepared by plasma assisted CVD by Fukutsuka et al.[124], showing good potential for bipolar plate application. El-Enin et al.[125] electroplated different nickel alloys on an aluminum substrate, studied the properties and found that a Ni-Mo-Fe-Cr film showed excellent corrosion resistance, high conductivity and good mechanical properties making it a viable candidate for further testing in a fuel cell. Optimal pretreatment steps were also detailed. TiN coating was sprayed onto Al6061 and tested in a DMFC [126]. Testing with uncoated Al showed a high amount of Al dissolution and presence in the MEA, whereas with the coated sample after 100 hrs of testing no evidence of metal dissolution was found.

Metal nitrides exhibit good corrosion resistance and conductivity and have been the subject of interest as a coating on stainless steel base materials. Fu et al.[127] used pulsed bias arc ion plating (PBAIP) to deposit different Cr_xN films on a SS316L substrate. $Cr_{0.49}N_{0.51}$ to $Cr_{0.43}N_{0.57}$ exhibited high interfacial conductivity, good corrosion resistance and high surface energy as compared to the base metal. Brady et al.[128] developed Cr_xN layers on a Ni-50Cr material using a preferential nitriding process and the coated material showed excellent corrosion resistance and very low contact resistance.

Pyrrole monomers have demonstrated good corrosion resistance ability on stainless steel and aluminum allows. Utilizing these properties, Garcia et al.[129] electrochemically deposited polypyrrole on SS304 samples and characterized their performance in simulated fuel cell environments. Initially the coatings perform up to four orders of magnitude better but over time the protective properties decay and corrosion

protection properties are lost. The authors conclude that better coating compositions need to be researched but the potential has been demonstrated. A similar study was done by [130], where polypyrrole coated Al6061 samples were prepared by electrochemical deposition and polyanailine coated Al6061 samples were prepared by painting the polymer on the metal substrate. On corrosion testing and characterization it was shown that polypyrrole coating did little to improve the base metals characteristics while polyanalynine coated Al6061 showed much better corrosion resistance than the base metal albeit a slightly higher contact resistance. It was speculated that in actual fuel cell environment the conductivity of polyanailine would increase due longer exposure and oxidation in the acidic medium. Wang and Northwood et al.[131] prepared polypyrrole coatings on 316L with promise for application in bipolar plates.

Table 6: Base metal and coatings.

Metal	Alloy	Carbon	Ni-Mo-Fe-Cr	Nickel	CrxN	Polypyrrole	Polyanailine	TiN	TiC	IrO2	Pt	Gold	SnO2
Stainless Steel	304	[121, 124]			[132]	[129]			[123]				
	316L			[122]	[127]	[131]-[133]		[134]				[111]	[135]
	317L												[135]
	349												[135]
	AISI441												[136]
	AISI444												[136]
	AISI446				[115]								[136]
Aluminum	1050		[125]										
	6061					[130]	[130]	[126]					
Titanium										[137]	[137]		
Ni-Cr					[128]								

2.9 INSIGHTS FROM LITERATURE SURVEY

The goal of this literature study was to outline the state of the art of materials and manufacturing processes used in the manufacture of key components of a direct methanol fuel cell, the MEA and the bipolar plates. The purpose being that from this study, information would be extracted that will be used to identify a clear research path for the development of a continuous MEA fabrication process for DMFC, during the subsequent stages of this research effort. Key observations regarding the MEA and its components are identified as follows.

2.9.1 MEA type

Of the two main types of MEAs, CCS and CCM, literature examined identified the CCM type as having better performance as compared to a CCS MEA, but CCM manufacturing is complicated due to the behavior of the ionomer membrane upon direct coating. The DTM method, although has a few extra processing steps, offers a viable alternative for CCM type MEA manufacturing. If a DTM process is to be used, PTFE film, Kapton and PTFE coated fiberglass could be potential candidates for the decal transfer substrate.

2.9.2 Electrode type

Of the different electrode types discussed, thin film electrodes clearly offers the best performance and lower catalyst loadings. The choice of thin film electrode is significant for further efforts in the continuous manufacturing process development. This is because thin film electrodes are fabricated by the application of catalyst ink onto a relevant substrate. This confines the continuous manufacturing process to be built around a coating method that is capable of applying the necessary thickness of catalyst ink onto a substrate.

2.9.3 Electrode fabrication methods

Thin film electrode fabrication methods have been found to differ mainly in the method in which the catalyst ink is applied. For this purpose a few processes that are used for manual electrode fabrication were identified and discussed. Of these methods, spraying, tape casting and screen printing could potentially be scaled up and used in a continuous manufacturing environment to deposit a coating on a continuous web of substrate. Along with the processes that are used in the industry which were identified by a patent search, the following candidate coating processes are suitable for further consideration

- Flexography
- Slot die extrusion
- Screen printing
- Mayer bar coating
- Spraying
- Tape casting

2.9.4 Membrane and catalyst

Although the ionomer membrane and electrocatalysts used in the DMFC electrode were not a subject of discussion in this literature review, almost every source suggested Pt:Ru as the catalyst of choice for the DMFC anode, Pt for the cathode and Nafion as the ionomer membrane. Substantial research is being done to identify alternatives, but as of yet the materials mentioned are predominantly used in DMFC MEA manufacturing.

2.10 FUTURE RESEARCH OPPURTUNITIES IN MEA MANUFACTURE

Of the components of a MEA, the electrodes play the most important part. In recent years thin film electrodes have greatly reduced the catalyst loading in PEMFC and DMFC, and the processes used to prepare such electrodes have been discussed. At this stage of fuel cell research and development, there is room for opportunity in the following areas of electrode/MEA fabrication.

Further reduction in noble metal usage while maintaining or improving performance levels, would reduce the material cost of fuel cells. This would greatly enable PEMFC and DMFC to compete with other energy technologies, which are in use today. From a processing stand point it would be of much interest to do a direct comparison of how the choice of ink application process effects the electrode microstructure and performance; and to explore the possibility of achieving more performance out of existing noble metal loadings by creating unique electrode structures through a bulk manufacturing process that could offer higher catalyst utilization and dispersion.

From a purely coating standpoint, as compared to PEMFC, DMFC electrodes pose a much bigger challenge. The reason being that DMFC noble metal loadings are almost twenty five times higher than a PEMFC electrode. This results in a much thicker electrode, which is difficult to coat and also difficult to dry. The number of coating processes that can deposit such a thick 'wet layer' is limited and these electrodes are prone to mud cracking upon drying due to internal stresses being developed in the layers. Additionally unsupported Pt:Ru and Pt catalyst are prone to agglomeration during the ink formulation phase, steadily decay, as in the catalyst particles settle down from the suspension when stored and exposed to the environment. This requires the development of new catalyst inks with binders that can withstand these internal forces upon

solidification, additives that minimize agglomeration and stabilize the suspension while maintaining performance and not interfering with the electrochemical activity in any way.

Continuous roll-to-roll coating processes need to be developed/evolved to suit the unique requirements of PEMFC and DMFC fuel cells. The geometry of the electrode and associated membrane requires that discrete patches of electrode be coated onto a substrate. This 'picture frame' geometry is required to save the wastage of catalyst in areas that would be covered by seals and not contribute to the electrochemical processes occurring in the fuel cell.

Besides geometry, of supreme importance is the substrate onto which the electrode is to be coated. As discussed in the preceding sections, there are three types of MEA's. From a performance standpoint, CCMs offer the most advantage, but such is difficult to realize due the manufacturing challenges. Nafion readily absorbs water, and/or other solvents and swells considerably. This impedes the coating and the subsequent drying steps. Strategies to control or avoid this effect need to be developed so that CCM type MEA's can be produced en masse.

2.11 CHAPTER SUMMARY

This chapter outlines the materials and processes used in the fabrication of two key fuel cell components, the membrane electrode assembly and the bipolar plate. Due to the similar nature of these components between a direct methanol fuel cell (DMFC) and a proton exchange membrane fuel cell (PEMFC), most of the processes used are the same.

The types of MEAs and its components most specifically the electrode, and the associated manufacturing processes are presented and discussed in elaborate detail. Key observations that are relevant to the continuous manufacturing process being developed

are identified. Additionally a few research avenues are discussed that can be pursued to improve the performance and manufacture of DMFC MEAs.

3. Coating process selection for electrode fabrication

The electrode is the heart of a membrane electrode assembly (MEA). It is a porous structure, where the fuel and the oxidants react to produce usable electrical energy from the ensuing chemical reaction. For fuel cells to be successfully commercialized it is essential to develop cost-effective manufacturing processes for fuel cell components.

3.1 INTRODUCTION

The literature review, presented in the previous chapter, discussed MEA types, and their components. The electrode is the most crucial part of an MEA, and it is evident that any MEA fabrication process would have to be designed around the electrode fabrication step. Further information was presented on electrode types, and thin-film electrodes developed by Wilson et al. [28].

Thin film electrodes are fabricated by formulating an ink out of catalyst and using soluble ionomer as a binder. This method of catalyst delivery immediately confines electrode manufacturing to a coating process, which is actually advantageous as coating processes lend themselves well to continuous manufacture with the substrate being in the form of a web. Furthermore insights gathered from the review suggest the DTM method of CCM type MEA manufacture to be a viable processing choice.

This chapter builds on these insights and examines coating processes that can be used for the continuous manufacture of DMFC electrodes. A few candidate processes are briefly described and a critical assessment is done on their capability to meet the coating requirements for a DMFC electrode. The chapter concludes with the selection of a few processes for actual prototyping.

3.2 KEY REQUIREMENTS OF A CONTINUOUS ELECTRODE COATING PROCESS

Thin film electrode fabrication involves the application of suitably formulated catalyst ink onto a flat substrate to form an electrode, an action readily performed by a multitude of coating processes. As a continuous manufacturing process is to be developed, coating processes that can accept a continuous web of substrate have to be identified and examined as per the requirements of a DMFC electrode.

The primary requirement is the wet layer thickness that can be deposited onto a substrate by a particular process, which in effect translates to the catalyst loading that can be deposited by the process. The second factor to be considered while examining the feasibility of a coating process is the coating geometries that the process can deposit onto the substrate. These requirements are examined in further detail in the following paragraphs.

3.2.1 Electrode thickness requirement

Every coating process can deposit a certain range of volume of ink onto the substrate surface. This volume of ink is spread onto the substrate by the coating mechanisms and a certain thickness of coating is achieved. This thickness is typically referred to as the wet layer thickness or the wet film thickness.

Every ink or coating contains a certain mass of solids, which, in the case of DMFC, can be catalyst, binder, and additives. Liquid components, typically solvents, make up the remainder of the composition. The solid content (*SC*) is the mass percentage of solids in the ink. Once the solvents in a coating evaporate, the remaining thickness is known as the dry layer thickness.

$$SC = \frac{Mass\ of\ Solids}{Total\ Mass\ of\ Ink}$$

With regards to a PEMFC and DMFC electrode, the catalyst ink is composed of unsupported or supported catalyst particles, a soluble form of ionomer, which also acts as a binder, additives, such as pore formers and release agents, and solvents, such as water and isopropyl alcohol (IPA). The 'wet layer thickness' is important because it controls the amount of catalyst that is dispersed onto the surface of a substrate, also known as the "loading" (mass/area, mg/cm^2). Typical catalyst loadings for a PEM fuel cell are 0.1 to 0.4 mg/cm^2 and for a direct methanol fuel cell the loading is approximately 2.5 mg/cm^2 [28, 29, 37].

PEM fuel cells use supported catalysts, which consist of nanometer sized (~2nm) catalyst particles, which are supported on carbon black particles[28]. The noble metal content in supported catalysts typically ranges from 20-80%. Nafion content is usually approximately 30 wt% of the noble metal loading. DMFC fuel cells use unsupported catalysts, Pt-Ru for the anode and Pt black for the cathode, with the Nafion content ranging from 10-15% [43]. The catalyst and ionomer are mixed with solvents to form an ink. From a coating process point of view, the ink viscosity is of fundamental importance. Different processes operate with certain viscosity ranges. Inks used for flexography and gravure coatings are low viscosity inks, whereas inks used in roll coating or screen printing have a higher viscosity, such as the consistency of a paste.

It is important to theoretically calculate the wet layer thickness of a coating, and also to identify how it changes with different solid contents. This would represent a case where an ink is being formulated for a coating process; the solid content of the ink can be increased to reduce the wet layer thickness, while delivering the same catalyst loading onto the substrate.

Figure 21 shows the relation between wet layer thickness and ink solid content. These results are computed by keeping the required loading from the coating constant at 3mg/cm^2. It identifies the coating thickness that would be needed to achieve the required loading by an ink of a given SC. The four plots represent different supported catalysts (10-40%). The dashed lines represent the final dry layer thickness for those particular ink combinations, once all the solvents have dried.

What can be gathered is that for a dilute ink (low SC) a much thicker layer must be deposited to achieve the same loading. As the ink SC increases, applying thinner layers onto the substrate can provide the required loading. Also, as the percentage of noble metal increases in a supported catalyst, thinner layers are required to achieve the same loading.

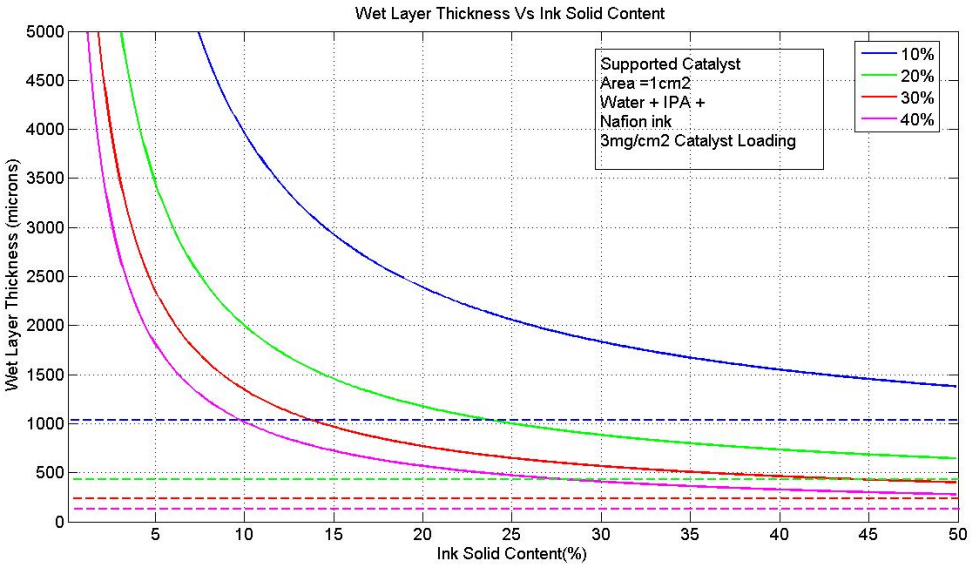

Figure 21: Wet layer thickness Vs ink solid content.

Similarly, Figure 22 shows how the wet layer thickness would change if the ink solid content was fixed and the loading was allowed to vary. As shown in the figure, a higher loading requires a thicker wet layer.

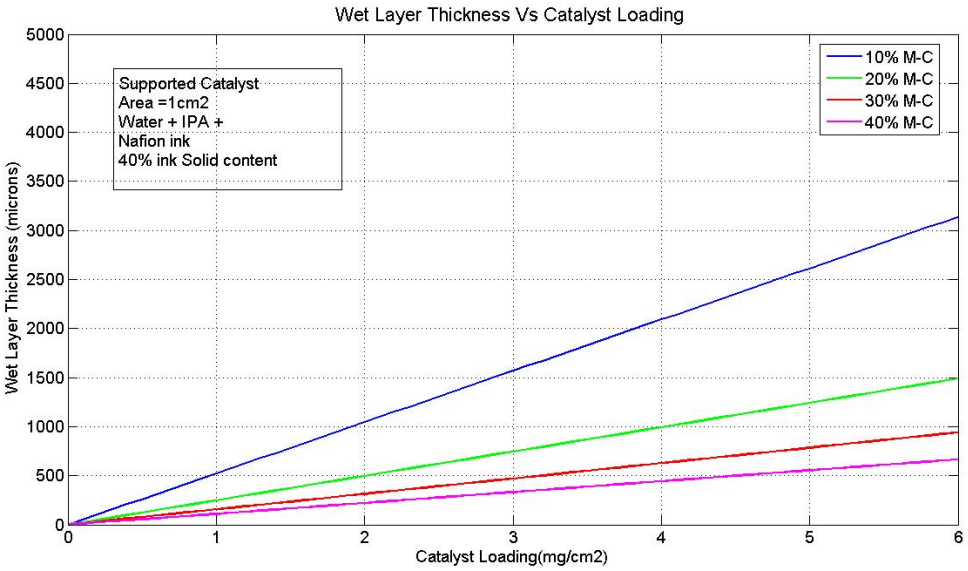

Figure 22: Wet layer thickness Vs catalyst loading.

The relevance of all this information is that the first and foremost parameter by which the suitability of a coating process will be examined is whether or not it can deposit the required wet layer thickness. PEMFC electrodes are very thin and a multitude of processes can be used to fabricate PEMFC electrodes in a continuous web process, but a DMFC electrode has 25 to 40 times more catalyst, making it thicker by comparison.

A DMFC fuel cell uses unsupported catalyst (100% catalyst content, also called 'blacks'). Inks of different solid contents can be made by these catalysts to match the viscosity requirement of a particular coating process. Once this solid content is defined using a calculation similar to the ones shown in Figure 21 and Figure 22, the wet layer thickness can be calculated. This value can then be compared with the wet layer

thicknesses that process can deposit, and it can be determined whether the process is feasible for DMFC electrode fabrication or not. Not every process can satisfy the wet layer thickness requirement for a direct methanol fuel cell.

3.2.2 Possible electrode geometries with relation to MEA type

It is important to pay due consideration to the type of geometries that are possible by the particular coating process under examination, as the coating geometry required varies with the type of MEA being fabricated.

If the roll-to-roll manufacturing of the three different types of MEAs (CCS,CCM, CCM-DTM) is considered, then there can be three different substrates. For CCS, a roll of diffusion media would have to be coated with catalyst ink, for DTM, the transfer substrate and for CCM, the actual ionomer membrane would have to be coated on both sides.

The geometry of the coating applied will be dependent upon which type of MEA is being fabricated. Figure 23 shows exemplar coating geometries. For a CCS type electrode, the coating should preferably be edge to edge, as in band coating so that no diffusion media is wasted. Once a continuous electrode has been coated on the diffusion media, it can cut into discrete shapes and subsequently hot pressed onto a membrane.

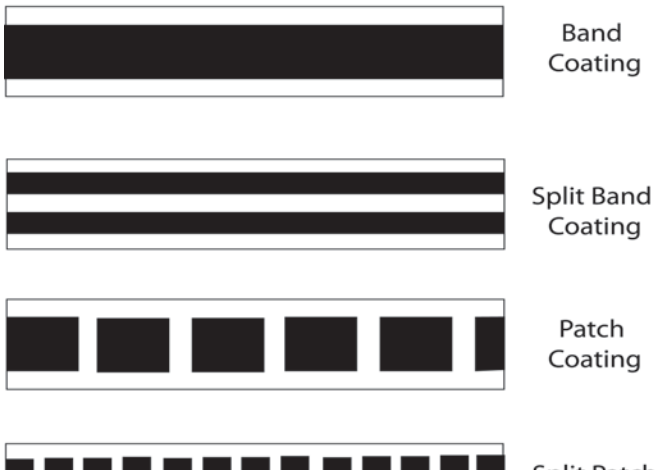

Figure 23: Types of coating geometries.

For a DTM type MEA, all four types of coatings shown in Figure 23 can potentially be utilized. The coating geometry would dictate how the electrode is cut from the roll and transferred onto a membrane. For CCM, double-sided patch coating is the most suitable coating geometry, as no catalyst will be wasted in the area occupied by the seal. The continuous roll of MEA can then be cut into individual MEA's.

As discussed above, an MEA consists of a proton conducting membrane, sandwiched between electrodes and diffusion media. When a MEA is assembled in a unit cell or a stack, on each side of an MEA a seal is installed to prevent leakage of reactants and reaction products from the flow field channels. Similarly, a bipolar plate has a flat border, or picture frame area around it, which constitutes the seal 'seat.' The flow fields do not extend to the edge of the plate, but are centered in the plate, leaving room for this sealing surface and space for holes, manifolds etc.

Figure 24 shows the geometry of a MEA. If the electrodes were to extend all the way to the edge of the membrane, the portion that extends beyond the flow field area

would not be fed by reactants nor could reaction products exit. This portion of the electrode would essentially be wasted, thereby wasting catalyst [9]. This is why a border is left around the electrode where the membrane is not covered by the electrode or the diffusion media. This is where the seal interfaces with the membrane.

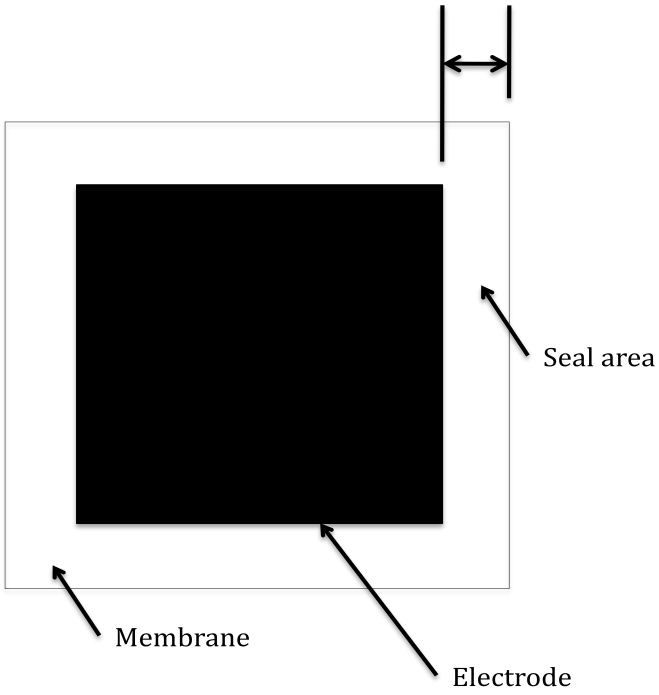

Figure 24: MEA geometry.

3.3 CANDIDATE COATING PROCESSES

The literature review detailed the state-of-the-art of DMFC manufacturing, and identified a few coating processes that can be used to deposit catalyst inks onto the relevant substrate for the fabrication of DMFC electrodes. This section provides details about the capabilities and operation of these processes.

3.3.1 Flexography

Flexography, also known as "aniline printing" [138], is a printing process dating back to the mid-nineteenth century. It involves the usage of printing plates that have

raised areas, and is quite similar to the letterpress process. These raised areas are used to transfer low viscosity inks onto a relevant substrate. It is used extensively in roll-to-roll processes to print onto paper and polymer substrates used in the food and packaging industries [139].

The first step in the flexography, or "flexo", process is the plate making process. The geometry of the areas that have to be printed must be raised above the rest of the surface. This can be achieved by using a mask to selectively expose light sensitive polymers, and then washing away the unexposed polymer. Other methods to achieve the same results are to either use a laser to etch away the unwanted material on a roll, or alternatively a molding process can be used to produce the plate.

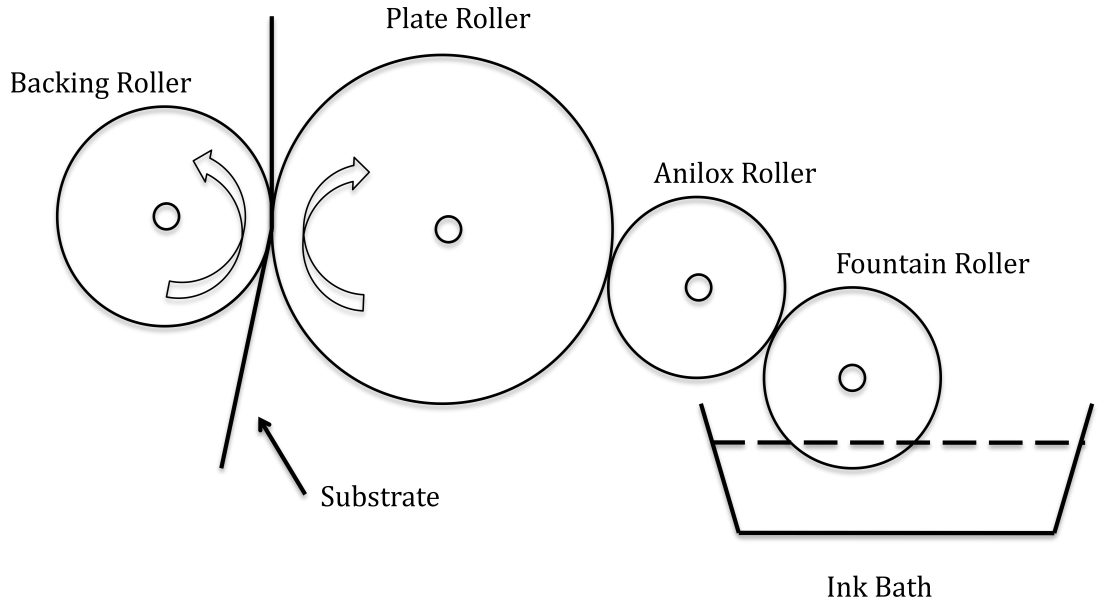

Figure 25: Flexographic coating process.

The actual printing process involves delivering a metered dose of ink to the raised portions of a flexo plate, as shown in Figure **25**. This is achieved by using an "anilox roller." An anilox roller is a roller whose surface is completely covered by millions of

small cups, or cells. The size of these cups allows a certain volume of ink to be held by the roller, which can then be transferred to the roller onto which the plate is mounted, i.e., the printing cylinder.

The anilox roller can be fed ink in two ways: the first is to use another roller called a fountain roller, which is immersed in a bath of ink and applies a metered amount of ink onto the anilox roller; alternatively, the anilox roller itself can be immersed directly in an ink bath and the excess ink is 'wiped' away using a doctor blade system. Once the anilox roll has been 'charged' with ink, it transfers this ink onto the plate roller when it comes into contact with it.

The raised areas of the plate roller apply this ink volume onto the coating substrate, which is supported by a backing roller to maintain adequate pressure. In this way millions of small dots are transferred onto the coating substrate, which make up the image or text or whatever figure is to be printed onto the coating substrate. For a multicolor image, one color is applied at a time and a multitude of flexo stations apply different colors on top of the prior image, which then combine to form the final image.

O'Brien [58]details the use of flexography to produce CCM type MEAs, and reports that the process can be used to deposit wet films with thickness ranging from 1 to 20 μm. Thicker layers can also be produced by applying multiple coats onto the same, previously coated area on the substrate, which could be used to produce electrodes with higher catalyst loadings, such as those used in DMFC.

3.3.2 Gravure coating

Rotogravure or gravure coating is a type of a coating process in which the shape or image that has to be applied onto a surface is first cut into the surface of a plate or a cylinder. Gravure cylinders can be made by chemically etching, embossing or laser

etching sunken cells or 'cups' onto the cylinder in the shape of the graphic to be printed or coated. These cells are not interconnected and the final print consists of millions of small, discrete dots [139].

As with the flexographic process, the gravure process uses ink with very low viscosities. This is because the ink is transferred form the cells on the gravure cylinder to the substrate by capillary action.

The first step in the gravure process is the application of ink to the gravure cylinder, which contains millions of small, discrete cells. A typical way of ink application is to partially immerse the gravure cylinder in an ink bath, where the individual cells are filled up with ink. In this fashion, ink is uniformly applied across that plate/cylinder, and the excess ink is removed by a doctor blade, as shown in Figure 26. This cylinder then rotates and makes contact with the substrate, which is typically in the form of a continuous web. As contact is made between the gravure cylinder and substrate, which is being supported by the impact roller, ink transfers by capillary action onto the substrate, and subsequently dries. The maximum wet layer thickness a gravure coating process can deposit is dependent on the volume of the cells that are engraved on the gravure roll's surface. One manufacturer reports that the maximum wet layer thickness that can be deposited by the process ranges between 50-80μm [140].

The theoretical wet layer thickness requirements for a DMFC electrode can be identified by examining Figure 22. From the plot, it can be ascertained that in order to fabricate a DMFC cathode with a loading of 4 mg/cm^2 using a 40-wt% supported Pt catalyst, a wet layer thickness of around 400 μm will be needed. It is important to understand that this calculation was done using an ideal ink with a 40% SC, and this calculation does not account for the porosity in an electrode. Typically, ink with less than 20% SC are used in flexography and gravure coating [58].

Multiple coatings would be needed to achieve the catalyst loading requirements of DMFC electrodes. In comparison to a DMFC, PEMFC electrodes require loadings in the range of 0.1 mg/cm^2 to 0.4 mg/cm^2, which translates into a substantially lower wet layer thickness. Gravure coating process has been reported to manufacture PEMFC electrodes [141, 142].

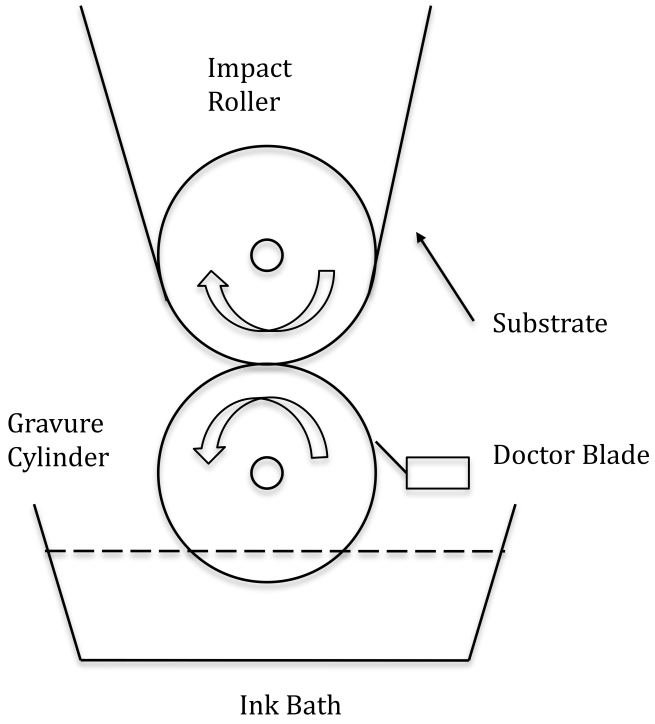

Figure 26: Gravure coating process.

3.3.3 Mayer bar coating

A Mayer bar is a solid metal rod onto which a wire has been tightly wound, as shown in Figure 27. It is used to meter and apply a consistent layer of coating material/ink onto a suitable substrate. The diameter of the wire wound on the rod is varied to control the wet layer thickness of the coated layer. Varying the diameter changes the size of the gaps between the individual coils in a Mayer bar thereby

controlling the volume of ink that can ‘squeeze‘ between the coating substrate and the wire surfaces, as shown in the inset in Figure 27.

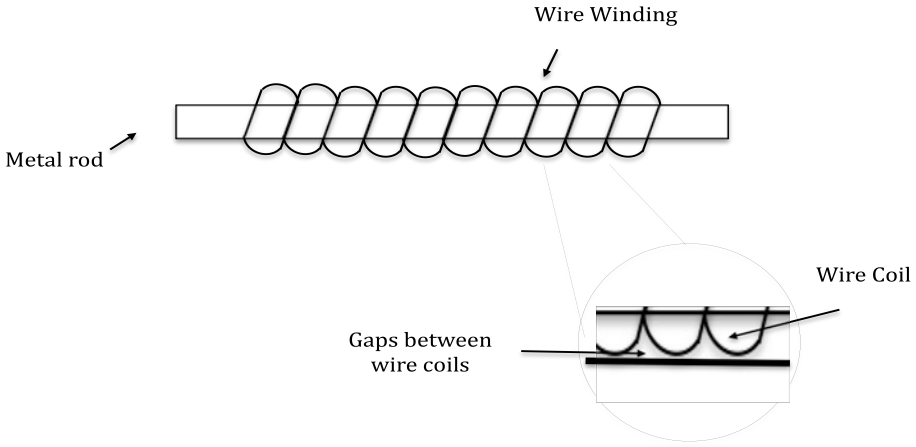

Figure 27: Mayer bar.

The wet layer thickness is approximately 0.1 times the wire diameter, whereas the dry layer thickness is dependent on the solid content of the coating material/ink [143]. A maximum wire thickness of 9 mils, which would result in a coating wet layer thickness of 228 μm, has been reported [138].

Mayer bars are extensively used in continuous roll-to-roll coating processes, where a typical arrangement is shown Figure 28. Excess ink/coating is applied by an inking or fountain cylinder, which is immersed in an ink bath. As the inking cylinder rotates, it picks up ink, some of which is applied onto a substrate, which is moving along one side of the cylinder. In this fashion, ink is transferred onto the coating substrate. Further downstream, a Mayer bar is used to meter the amount of ink on the substrate and also remove the excess ink.

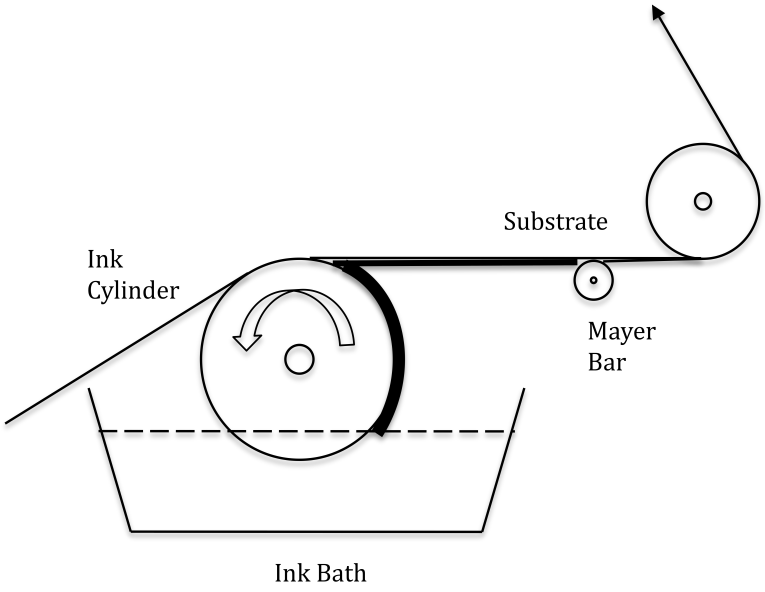

Figure 28: Continuous roll-to-roll Mayer bar coating.

3.3.4 Slot die coating

The slot die coating process involves forcing a pressurized fluid out of slot-shaped orifice. The dimensions of the slot dictate the width and the cross sectional thickness of the coating, which is then transferred onto a moving web.

There are two main parts of a die, the manifold area and the lip. The purpose of the manifold area is to ensure sufficient flow to the ends of the die [138], whereas the lip participates in controlling the thickness of the coating. There are many variations of slot die coating, which are mainly due to the position of the die with respect to the web and the distance between the die and the web. For example, in curtain coating there is a vertical gap between the die and substrate web, while in slot die coating the die is against the web, separated only by the coating ink [144]. Loadings as high as 20mg/cm^2 can be applied onto a substrate by the slot die coating method [145], with wet layer thickness ranging from 4 to 100 mils [142].

One of the attractive features of the slot die coating process is that the liquid delivery channels are completely sealed; hence, the ink is never exposed to the environment until it is applied onto the substrate. This process can be of importance for PEMFC and DMFC catalyst inks, which have volatile content in them. If exposed to the environment, solvents can evaporate, thus affecting the ink solid content.

The thickness of the coating in a slot die system is controlled mostly by the line speed, i.e. the speed at which the web is moving. If the web speed is slow, a thicker coating will result; faster speeds will yield thinner coatings. Another important feature of slot die coating is that the flow of the liquid can be made to be intermittent, resulting in regular gaps between the coated layers. This type of coating is also knows as patch coating, as shown in Figure 29.

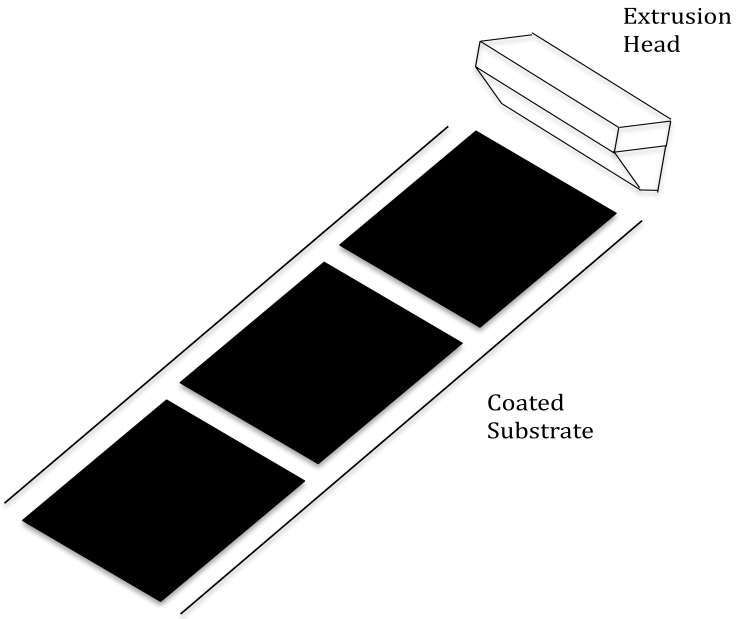

Figure 29: Slot die coating: Patch coating.

3.3.5 Rotary screen printing

In rotary screen-printing a squeegee forces ink from out of a mesh onto a substrate. The mesh, or screen, is in the form of a cylinder and the squeegee is placed inside it, as shown in Figure 30. Paste is dispensed into the cylinder and the squeegee forces the paste out of the screen onto the substrate. The advantage of this rotary screen is that it allows for the substrate to be in the form of a continuous web rather than discrete sheets in screen-printing.

The wet layer thickness of coatings applied by rotary screen-printing is controlled by the number of perforations in the screen (its mesh number), the pressure on the squeegee, and the viscosity of the coating paste. Loadings as high as 30 mg/cm^2 can be applied onto a substrate [138]. Screen printing has been used in the lab-scale manufacture of PEMFC electrodes [141].

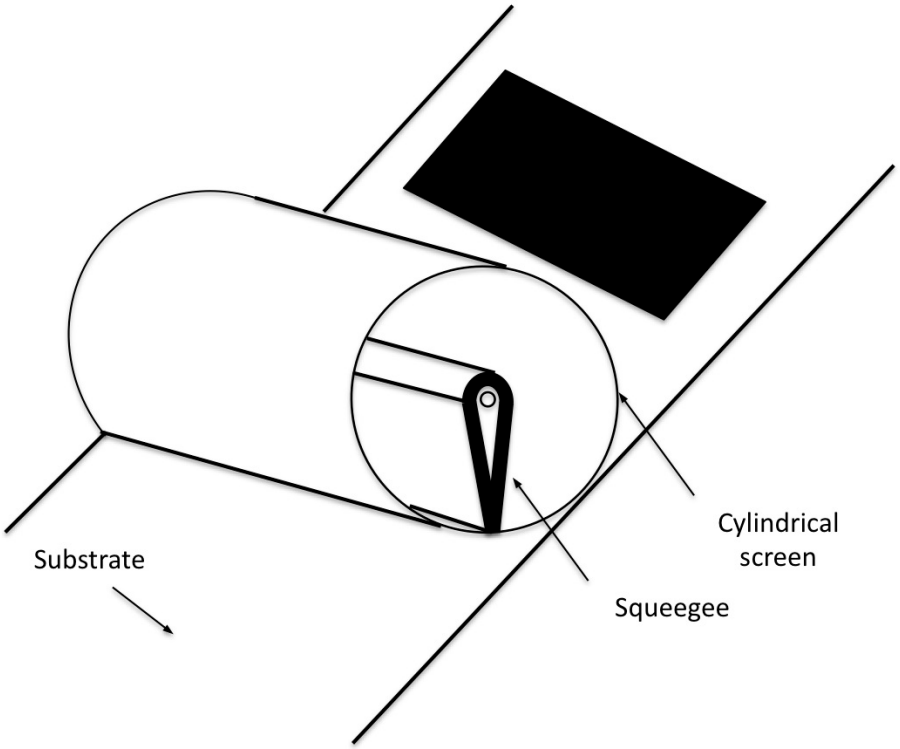

Figure 30: Rotary screen printing.

3.3.6 Spraying

Spraying, or atomization, is the breakup of one fluid into drops upon entering and interacting with another fluid. The device used to produce the atomized droplets is called a nozzle or an atomizer, as shown in Figure 31.

Spraying is used extensively to apply coatings onto various surfaces and substrates [146], and there are many different forms of spraying [147]. Low volume-low pressure (LVLP) twin fluid nozzles can be used to apply a coating onto a moving web. In a twin fluid configuration, one fluid is to be atomized and the other fluid provides the atomizing energy. Twin fluid nozzles come in various configurations, nozzle orifice sizes, spray patterns, etc. The ink can be siphon fed, gravity fed, or pressure fed to the nozzle depending on the configuration. The nozzle geometry can allow for internal mixing where the ink and atomizing fluid mix within the nozzle or it can be an external mix nozzle where the atomization process happens at the mouth of the nozzle.

Ultrasonic nozzles are also capable of producing very fine droplets and can potentially be used to apply coatings onto a web substrate. In an ultrasonic nozzle, the high frequency oscillations of the tip of the nozzle energizes and atomizes the fluid into a spray [148].

Another method of producing small, discrete droplets that can coat a substrate is to use a solenoid valve coupled with a nozzle. Pressurized ink is supplied to this arrangement and a driver circuit rapidly actuates the valve at frequencies less than 1 kHz. This causes a steady stream of drops to emerge form the nozzle, which can be utilized to apply a coating onto a substrate. There must be relative motion between the nozzle and the substrate to uniformly distribute these drops.

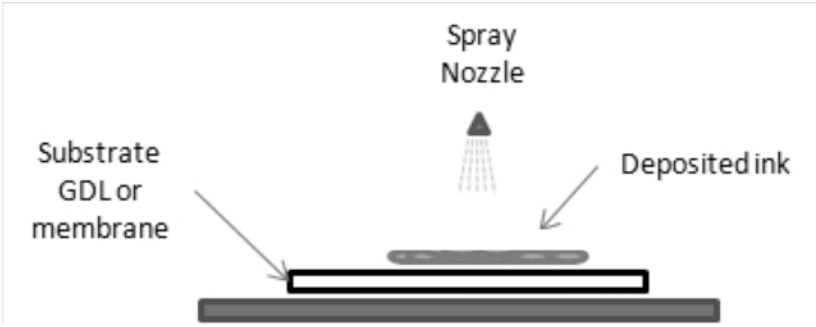

Figure 31: Spraying.

3.3.7 Tape casting / Doctor blading

In the tape casting process, ink is deposited onto a moving substrate, which is then metered by a blade. The height of the blade can be adjusted to control the wet layer thickness of the coating, as shown in Figure 32. Tape casting is a well established process, used to fabricate PEMFC and DMFC electrodes manually [46], where the relative motion between the substrate and blade can be automated. This automation, when combined with a continuous substrate, can form the basis of a roll-to-roll electrode fabrication process.

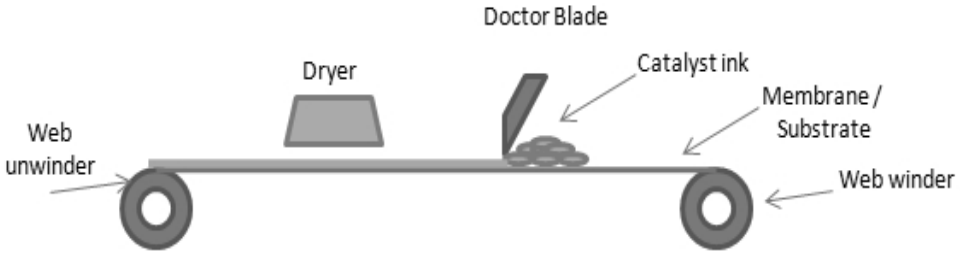

Figure 32: Tape casting process.

3.4 PROCESS DOWN SELECTION

In the previous sections, seven coating processes are introduced, all of which are well established roll-to-roll coating processes that are used on a multitude of substrates to deposit a variety of inks, adhesives, and coatings. Each process is capable of operating at

certain speeds, has limits on the wet layer thickness it can deposit and the coating geometries possible etc.

In this section, the pros and cons of these processes will be discussed to determine their feasibility for the continuous manufacturing of PEMFC and DMFC electrodes. On the basis of this analysis, a subset of these processes will be identified for actual prototyping. The salient points of each process are listed in Table 7 and a detailed discussion of each process follows.

Table 7: Pros and Cons of coating processes being considered.

Process	Pros	Cons
Flexography	• Fast line speed • Patch coating	• Multiple passes required to achieve catalyst loading • Discrete dots of coating on substrate • Ink exposed to environment • Low viscosity, fast drying inks required
Gravure coating	• Fast line speed • Patch coating	• Multiple passes required to achieve catalyst loading • Discrete dots of coating on substrate • Ink exposed to environment • Low viscosity, fast drying inks required
Mayer bar coating	• Fast line speed • High loading possible • Simple process • Low Cost	• Grooves in coating • Ink exposed to environment • Patch coating not possible • Low viscosity inks needed
Slot die coating	• Ink path completely sealed • Patch coating possible • Fast line speed • High loading possible • Possible to do double sided coating without	• Low viscosity inks needed • Thicker coatings require viscous ink

Table 7, cont.

	backup roller contact	
Rotary screen printing	• Screen cylinder, cheaper than engraved rolls • Extremely high loadings possible • Fast line speed • Patch coating possible	• High viscosity inks or Catalyst paste needed • Ink exposed to environment
Spraying	• Low to medium viscosity inks • Fast line speed • Simple apparatus needed • Ink path completely sealed • Patch coating possible	• Multiple passes required for higher loadings • Loss of coating material due to over spray at edges
Tape casting	• Fast line speed • Simple coating apparatus • High loading possible	• Ink exposed to environment • Patch coating not possible

Flexography is a high speed printing process, which is extremely popular in the packaging industry[149]. It is able to print high-resolution graphics on a wide variety of substrates. Low-viscosity (10-100cP), fast drying inks are typically used [150], but it is interesting to note that O'Brien reports the use of highly viscous catalyst inks (5000-20000 cP) with 18 wt% SC that have been successfully used to fabricate DMFC electrodes for CCM type MEAs. It can be reasoned that for printing graphics, a higher resolution is needed to accurately reproduce colors and sharp edges, therefore anilox rolls with very small cells are used, necessitating the use of thinner inks. For printing electrode geometry, there is no such requirement, therefore anilox rolls with a coarser and deeper cell structure can be used to produce thicker films. Gravure coating offers very similar advantages: extremely high line speeds, and requires very low viscosity inks (10-50 cP)[150]. Both processes can easily deposit catalyst inks in the form of discrete patches,

the importance of which was discussed earlier. Gravure cylinders are more expensive to change as compared to flexography plates.

With regard to coating a substrate with catalyst inks for use in PEMFC and DMFC, there are two major concerns when it comes to the flexography and the gravure coating processes. The first is that the wet layer thickness that can be deposited by these processes is low; therefore multiple coat and dry cycles are required to build up the catalyst loading in the electrode. The second concern is that, upon careful examination of a flexographic or gravure coating, discrete dots are evident, as depicted in Figure 33, These are present due to the 'cups' on the anilox roller and cells/grooves on the gravure cylinder [151, 152]. In the printing and packaging industry, these dots are of no consequence, as they are not visible without magnification; however, for a fuel cell electrode, their presence can potentially have a negative impact, as it would break the continuity of the electrode, exposing the membrane to the reactants and reaction products, and effecting a loss in active area. O'Brien [58] reasons that multiple passes smooth out these non-uniformities. Additionally, deposition of a higher volume of inks that 'flow' upon application to the substrate, due to surface tension forces, may cause these discrete dots to blend into each other.

Both flexography and gravure coating machines require significant capital investment, and are suitable for applications requiring high throughput, which, over time, balances out the initial capital expenses.

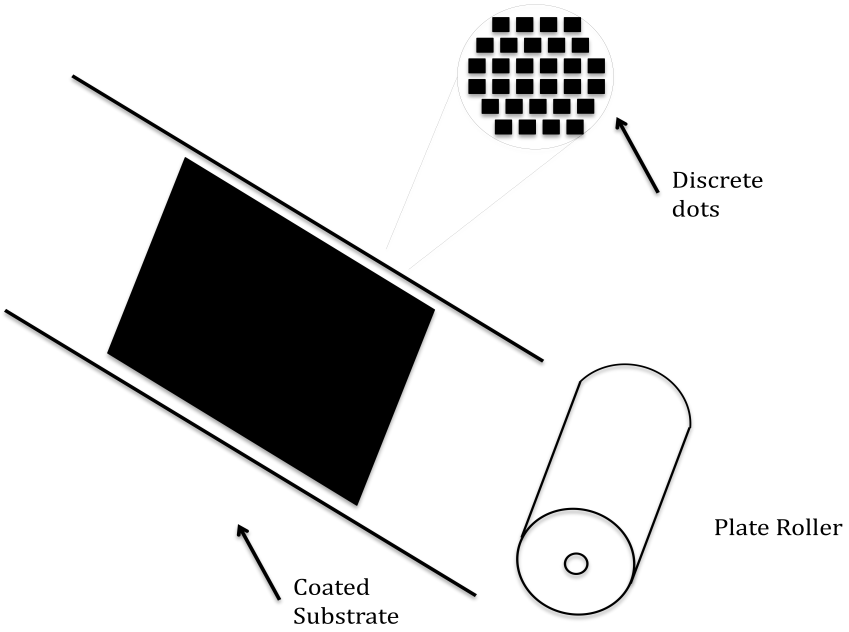

Figure 33: Presence of discrete dots on flexographic and gravure coatings.

Mayer bar coating offers several advantages: low cost, ease of use, simplicity, fast changeover times, and accurate control of coating weights. The concern with Mayer bar coating is the surface morphology of the coating. The ink is metered by the gaps between the wires, and the coating layer tends to adopt this shape, which could potentially create hills and valleys on the surface. However, this problem can potentially be resolved by experimentation with the coating material viscosity, as surface tension forces persuade the coating to flow and distribute more evenly [138]. The other concern with Mayer bar coating is coating geometry. It can only produce band coating, by which the coated film extends from edge to edge of the substrate.

Slot die coating offers several advantages, including: fast line speeds (up to 10m/min), completely sealed ink path, ability to perform patch coating, and the ability to do double sided coating, as no back up roll is needed. The tension in the substrate ensures adequate contact and pressure between the substrate and the slot die lip.

In slot die coating, all the ink supplied to the die is transferred to the substrate, so there is no loss of catalyst material. Ink viscosities typically range from 1-100cp. A concern with slot die coating is that the ink viscosity has to be carefully tuned to the line speed of the substrate. For a given ink composition there is a range of speeds in which coating is possible [153], and the web speed is one of the key factors that controls the wet layer thickness. Extensive experimentation is involved in deciding the gap thickness in the die, the line speed of the web, and the ink composition.

Rotary screen-printing is a versatile process, with which a wide variety of coating geometries are possible. Patch coating required for DMFC electrodes can be easily performed and thick coatings with extremely high loadings can be deposited, but this requires the development of highly viscous inks.

A concern with depositing a thick layer in a single pass with processes like Mayer bar coating, screen printing, and slot die coating is that this layer has to be dried slowly. The choice of drying process and the rate at which drying is performed is dependent on the ink chemistry [138]. The drying process dictates the line speed of the overall process.

Spraying is a simple, flexible, low cost coating process, which can accept a range of ink viscosities, and can apply the required patch coating geometry on a substrate as required for DMFC electrodes.

With regard to spraying catalyst ink, the spraying process also poses a challenge when it comes to the amount of material that can be deposited in a single pass. Higher flow rates and viscosities require higher pressures that, although it would deposit more material per pass, could cause material wastage, as the catalyst particles would disperse into the environment. This can be addressed by applying multiple coats at lower spraying pressures, until the desired mass loading is achieved. As with other processes, ink

chemistry dictates the line speed, but with low viscosity, fast drying inks, the drying process is instantaneous.

Tape casting, also referred to as doctor blading, requires a very simple apparatus to coat ink onto a substrate. Thick coatings with high viscosity inks (>50cp inks required) are possible, but the line speed is dependent on the drying rate, which will be dictated by the ink chemistry. A concern with tape casting is that it can only produce band coating.

3.4.1 Selection criteria

In order to select from the above seven processes, the necessary performance criteria are identified. These are: catalyst loading, coating geometry, ink exposure, coating morphology, process complexity, and cost. The first criterion is loading. It is of foremost importance that the coating process is able to deposit the required amount of catalyst loading for a DMFC electrode. PEMFC electrodes are not mentioned because all processes will be able to fulfill the low loading requirements for PEMFCs, most in a single coating pass. It can be reasonably argued that if a process cannot deposit the desired wet layer thickness in one pass, then multiple passes can be used. This approach is entirely possible but would potentially add to the cost, complexity, and the overall process duration; therefore, an advantage is given to a process that can deposit the required thickness in a single pass.

The second criterion is the coat geometries that the coating process can apply onto the substrate. The goal is to identify processes that can perform patch coating, as opposed to edge-to-edge band coating. Wheeler et al. [9] reports that 15% of electrode area is lost if patch coating is not used. In the selection process, an advantage is given to processes that can apply patch coating.

Process cost is an entirely qualitative criterion in which an attempt is made to represent the capital expenditure involved in deploying a particular coating method to fabricate DMFC electrodes. Processes such as flexography, screen-printing, and gravure require highly specialized machinery, which would require significant investment. On the other hand, processes like tape casting, slot die extrusion, Mayer bar coating, and spraying are available in the form of simpler coating modules around which a coating process can be built.

Like process cost, complexity is another qualitative criterion, which aims to capture the effort involved in successfully fabricating electrodes from a process, so that this information can be used in coating process selection. It can be argued that all of the mentioned coating processes can eventually be optimized to fabricate DMFC electrodes by designing inks to suit that particular coating process, and evolving the coating line design to accommodate for multiple coating modules if required. Additionally the drying process would have to be designed with respect to the ink chemistry. This assertion is supported by the fact that upon examination of patent literature relevant to DMFC electrodes and MEA fabrication, almost every patent claims that the catalyst ink can be deposited by a multitude of coating processes, most of which have been discussed in this chapter.

For example, in the rotary screen printing process, ink design and testing would involve the development of highly viscous paste inks, which would require the identification of the appropriate solvents and additives that do not interfere with the electrochemical process in the electrode.

Coating morphology refers to the uniformity of the coated surface, in this case the electrode. Some processes leave their characteristic features on the coating, which might not be feasible for an electrode.

Although line speed is a critical parameter, it is not included in the selection criteria because such data is available only for generic inks used in the coating and printing industry. Ink chemistry designed to suit DMFC electrodes would dictate entirely different requirements on the ink application and drying process. A determination of process line speed would only be possible after such prototyping.

On the basis of these criteria, a Pugh chart has been created, as shown in Table 8. The tape casting process was used as a reference and every other process was compared to it. Spraying is identified as the best candidate for future prototyping, followed by slot die coating. Tape casting, rotary screen-printing and Mayer bar coating are found to be equal, while flexography and gravure coating rank the lowest among the seven processes.

Table 8: Coating process selection Pugh chart.

	Tape casting	Flexography	Gravure Coating	Mayer bar coating	Slot die coating	Rotary screen printing	Spraying
Loading	0	-	-	+	+	+	-
Geometry	0	+	+	-	+	+	+
Complexity	0	-	-	+	-	-	+
Ink Exposure	0	-	-	-	+	-	+
Cost	0	-	-	+	-	-	+
Coating morphology	0	-	-	-	+	+	+
Σ +	0	1	1	3	4	3	5
Σ -	0	5	5	3	2	3	1
Σ	**0**	-4	-4	0	**2**	0	**4**

In terms of prototyping complexity, slot die extrusion, Mayer bar coating, and rotary screen-printing will offer a significant challenge. Tape casting, on the other hand, requires a much simpler apparatus. Another important consideration here is that slot die extrusion and tape casting are very similar processes, as they both force the ink out of an opening by mechanical action. The deposited wet layer will undergo similar shear forces and will have the same drying requirements. After due consideration, spraying, tape casting, and slot die extrusion were selected as the processes that will be prototyped.

3.5 CHAPTER SUMMARY

This chapter begins with the examination of seven coating processes, which were identified in the literature review done in the previous chapter. The workings of these processes are briefly discussed with a focus on the catalyst loading that can be achieved by a particular process and the coating geometries possible. The pros and cons of each process are discussed and selection criteria are identified. On the basis of this knowledge, spraying, slot die coating and tape casting are selected for further experimentation and prototyping.

4. Modular Coating Test Bed

Spraying, slot die coating, and tape casting have been selected as processes that warrant further examination. Ink chemistry to suit each process will have to be identified. For actual coating on a web substrate in order to study the selected coating processes, a modular coating test bed apparatus is needed, upon which each coating module can be installed and tested. In this chapter, the requirements for such an apparatus are identified, concepts are generated, and a final design is detailed and constructed, after which coating tests are performed on web substrates. Based on the results of these coating tests, a final candidate is selected for the development of a continuous manufacturing process for DMFC MEAs.

4.1 INTRODUCTION

Since a continuous manufacturing process is being pursued, a platform that provides a continuous web of a suitable substrate moving at controlled line speeds is needed. Additionally, this apparatus would need to provide a function to dry the coatings, and must also have access points to install different coating modules.

Then this apparatus would be used to produce electrodes with the shortlisted coating processes, which can then be further studied and tested. From these tests, a refined coating process would emerge as the most feasible. The entire MEA fabrication process would be designed around this final electrode fabrication step.

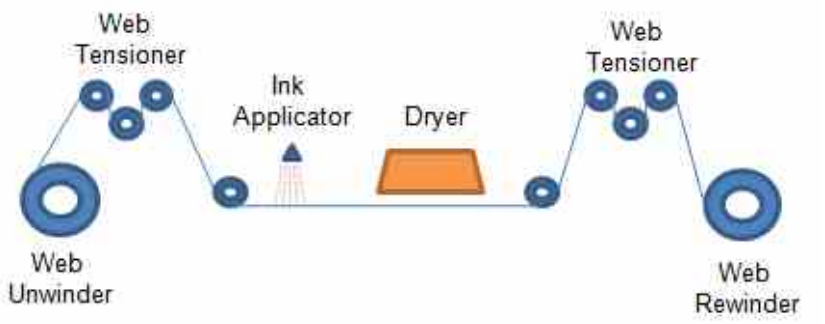

Figure 34: Electrode fabrication process concept.

With this intent in mind an initial concept for a test bed for continuous electrode fabrication was developed, as shown in Figure 34. The concept, as shown, has modules for web management: web unwinder, rewinder, and the tensioning module. The catalyst ink is applied via the ink application or coating module and solidified by the dryer. These key modules would be common to most of the coating processes to be tested on this platform. Such a versatile approach allows the test bed to accept multiple coating heads, and the web parameters such as tension and feed can be modified to suit the particular web material and drying conditions.

4.2 MODULAR COATING TEST BED DESIGN

4.2.1 Modular coating test bed requirements

The first stage of the design process was to identify key requirements and constraints, as given in Table 9. A few of these requirements that significantly influenced the design of the test bed are discussed in the following paragraphs.

DMFC electrodes have high catalyst loading, resulting in thick coatings, which take longer to dry. This constraint lead to requirements of a very low web line speed and a dryer power capacity of 3kW.

Roller width was constrained at 6.5", as the maximum width of web substrate that could be used was fixed at 6". This was chosen because it was calculated that with a 6" web, an electrode of maximum 4" width could be comfortably fabricated. This would translate into a maximum electrode (square) size of $100cm^2$, which is more than adequate for DMFC testing in an academic environment.

Two coating positions were required for the ink application modules. Spraying, tape casting, and slot die extrusion methods coat the top surface of a web. Other processes like gravure and Mayer bar, apply a coating on the bottom surface of a web. Thus, it was decided to design the layout such that both types of modules could be attached if necessary.

Table 9: Modular coating test bed requirements.

Key Requirements	Target Value
Minimum line speed	< 1 ft/min
Web direction reversible	No
Roller width	> 6.5”
Roller Material	Stainless Steel
Roller position adjustment	1” along traverse direction
Core size	3”
Web Width	6 ”
Under web coating module position	1
Over web coating module position	1
Dryer Type	Convective and Infrared
Single bank or multi bank dryer	Multi bank dryer
Drier position	Vertical and Horizontal
Dryer power capacity	3KW
Web tension	Adjustable

4.2.2 Black box model and functional structure

On the basis of the design requirements, a black box model and a function structure was created. In a black box model, an abstract representation of a product is depicted, with three different types of inputs and outputs entering and leaving the ‘system’ boundary. These three types of ‘flows’ are energy, signal and material. Such a representation of a design problem or product allows one to identify and focus on the most important design needs and requirements [154].

A black box model for the modular coating test bed was created, as shown in Figure 35. The main function of the entire apparatus is to coat the web, which is achieved by the different energy, material and signal inputs and outputs of the system.

Figure 35: Modular coating test bed black box diagram.

A function structure allows a designer to decompose a problem into functions and sub-functions, which describe 'what' needs to be done rather than 'how', or in other words, a function structure focuses the designers attention on function rather than form [154, 155]. These functions and sub functions are linked to each other through the same three types of 'flows': energy, material, and signal. A function structure describes how the inputs of a black box model are converted into outputs.

Figure 36 shows the function structure of the modular coating test bed. As an illustration, one of the material flows is described in detail. In order to accept the material input, 'web', an import web function is defined. This identifies the need to design suitable features in the design where a web substrate can be introduced into the system. The next two functions should happen in parallel, in which the web is moved and guided. ('move web' and 'guide web' functions). A 'tension web' function identifies the

important functional need of applying adequate tension on the web. The next two functions ('position web', 'coat web') are defined so that features are designed which allow for the web to be brought into a position where it can be subsequently coated. The last function is the 'dry coated web' function, which necessitates the construction of an adequate apparatus to dry the coating that has been applied onto the web. In this fashion, a function structure identifies what action is needed. How that action or need will be fulfilled is postponed until the concept generation stage, during which a variety of potential solutions are conceived to execute key functions.

On the basis of this function structure, key functions have been identified, and concepts generated in order to perform those functions. Web handling and coating are well-established industries and most coating and converting systems are modular, hence a multitude of suppliers exists that can supply modules that can be combined to build an entire system. For some of the functions, the design activity was to identify a source for a part, whereas some functions like the 'move web' function and 'guide web' function required more effort. Table 10 shows key functions and proposed solutions for these functions.

Table 10: Key functions and proposed solutions.

Key Function	Proposed Solution
Import web	Core holder chuck system
Move web	AC motor, Drive and reduction gear
Tension web	Disk brake system
Guide web	Rollers and Over all layout
Coat web	Spraying, Tape casting and Slot die coating modules
Dry coated web	IR heater banks and Hot air blower

It was readily evident that the layout of the machine would depend on the design choices for the ‘move web’ function and ‘guide web’ function. The subsequent paragraphs delve into more detail about these important design choices.

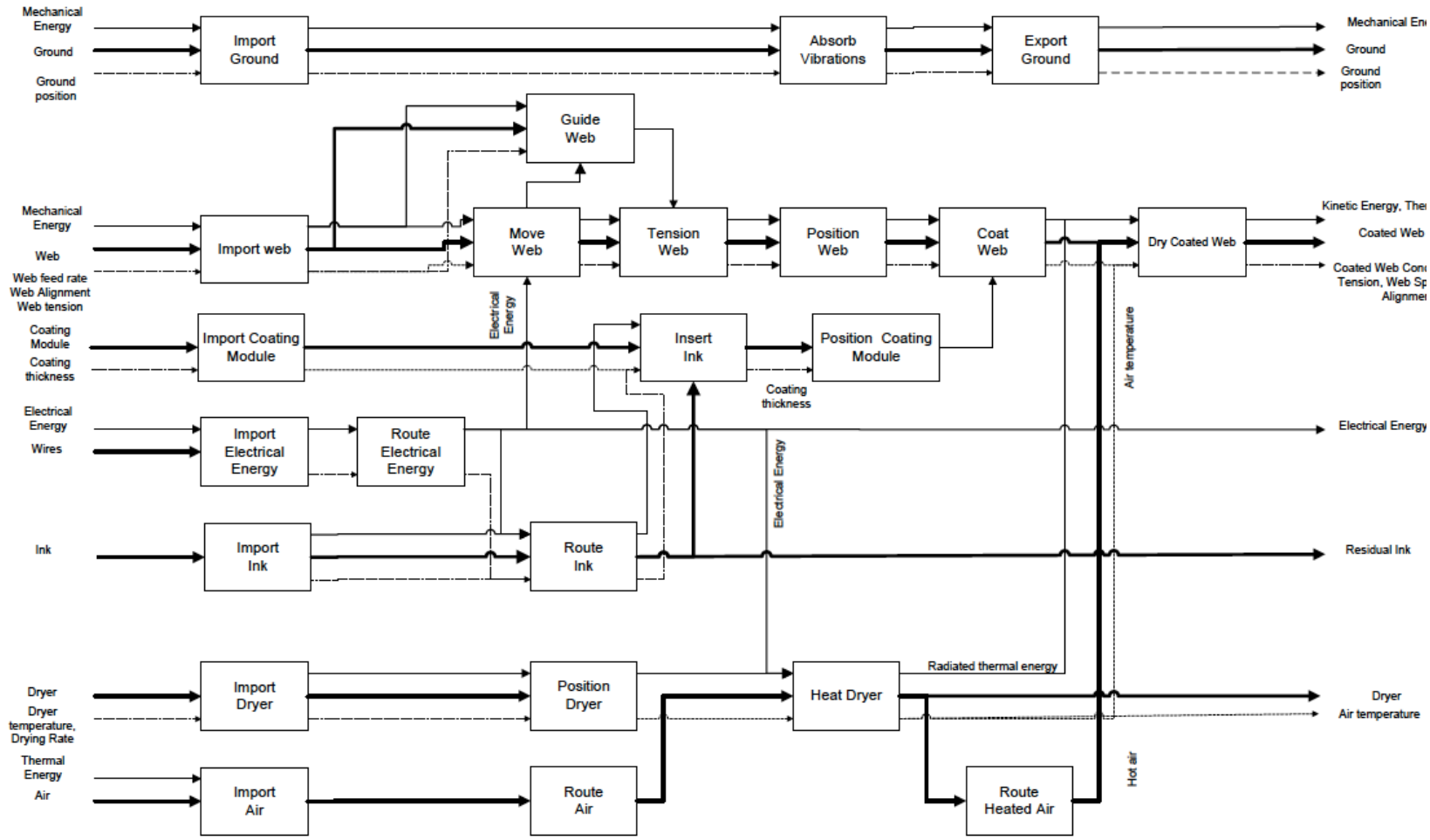

Figure 36: Function structure of modular coating test bed.

4.2.3 Drive system

A simple, unidirectional drive system was selected for the test bed. It is comprised of an AC, variable frequency drive unit for motor speed control (GS2-10p5) and a 0.5 horsepower, three-phase AC motor (Marathon MicroMAX Y360). The motor has a maximum speed of 1800 RPM. The motor is connected to a worm gearbox, which has a speed reduction ratio of 60:1. The output of this reducer gearbox is then connected to a belt drive, which further reduces speed by a factor of 10. The belt drive connects to a core holder chuck, or the 'rewind roller'. When the system is powered on, the rewind roller rotates at the set RPM, which is controlled via the interface knobs and buttons in the drive unit or it may be controlled through a computer.

The unwind roller is where the spool of fresh, unused substrate is mounted. The unwind roller is connected via a shaft to a disk brake. When the brake is engaged, it resists the rotary motion of the shaft and the substrate spool. The web handling system facilitates the following sequence: the web is unwound from the spool, guided over the idler rollers, through the coating stations and dryers, and onto the rewind roller. When activated, the rewind roller starts to pull the web, and the brake on the unwind roller resists this motion, thereby creating the required tension in the web. This implements the 'tension web' function.

A six-inch-wide web can be mounted onto the machine using core holders, which allow for rapid mounting and removal of a new web. At this stage the design intent was to have the ability to very closely monitor the deposition process and the drying process, therefore the machine was designed to be able to operate at a web feed as low as 0.2 ft/min, and as high as 12ft/min. The entire drive train is modular and, if need be, can be easily upgraded.

Other design choices, which would have worked just as well or even better, were to use either servomotors, or stepper motors. They were not considering due to the fact that they were substantially more expensive than a simple, variable frequency, AC drive system.

4.2.4 Web path and test bed layout

The next step in the design process was to examine the 'guide web' function and generate concepts for it. 'Guide web' refers to the means by which the degrees of freedom of the web of substrate were constrained so that it follows the desired path through the machine. This motion would be enabled by the 'move web' function, implemented through the drive system described earlier, through a powered winder roll. 'Tension web' function is implemented through a disk brake attached to the unwind roll.

This path should be such that it exposes the web substrate to the other key functions, 'coat web' and 'dry coated web', which would be fulfilled by a coating module and dryer of adequate design. In essence, the four key functions have been reduced to four physical modules, through which the substrate must pass to fulfill the design requirements. The 'guide web' function will physically be implemented by using rollers, which meet the design requirements defined earlier.

Concepts for the web path layout were generated and are shown in Figure 37. Concept 1 is a very basic inline design, which implements the four key modules such that the web follows a straight line. Longer webs suffer from sagging once coated, which theoretically could be addressed by increasing tension, but that would endanger the mechanical integrity of the web substrate itself. Concept 2 solved the tension problem by introducing a roller in the web path, but the resulting orientation might cause the liquid coating to slide down before it has dried. Concept 3 had a space saving design, as it is of value to reduce the overall path length, and in general the footprint of the machine. The

final concept was selected after evolving the prior concepts, orienting the coating head and dryer banks such that they met the design requirements. The final layout of the test bed showing its different parts is shown in Figure 38, a CAD model is shown in Figure 39, and the actual machine that has been built is shown in Figure 40.

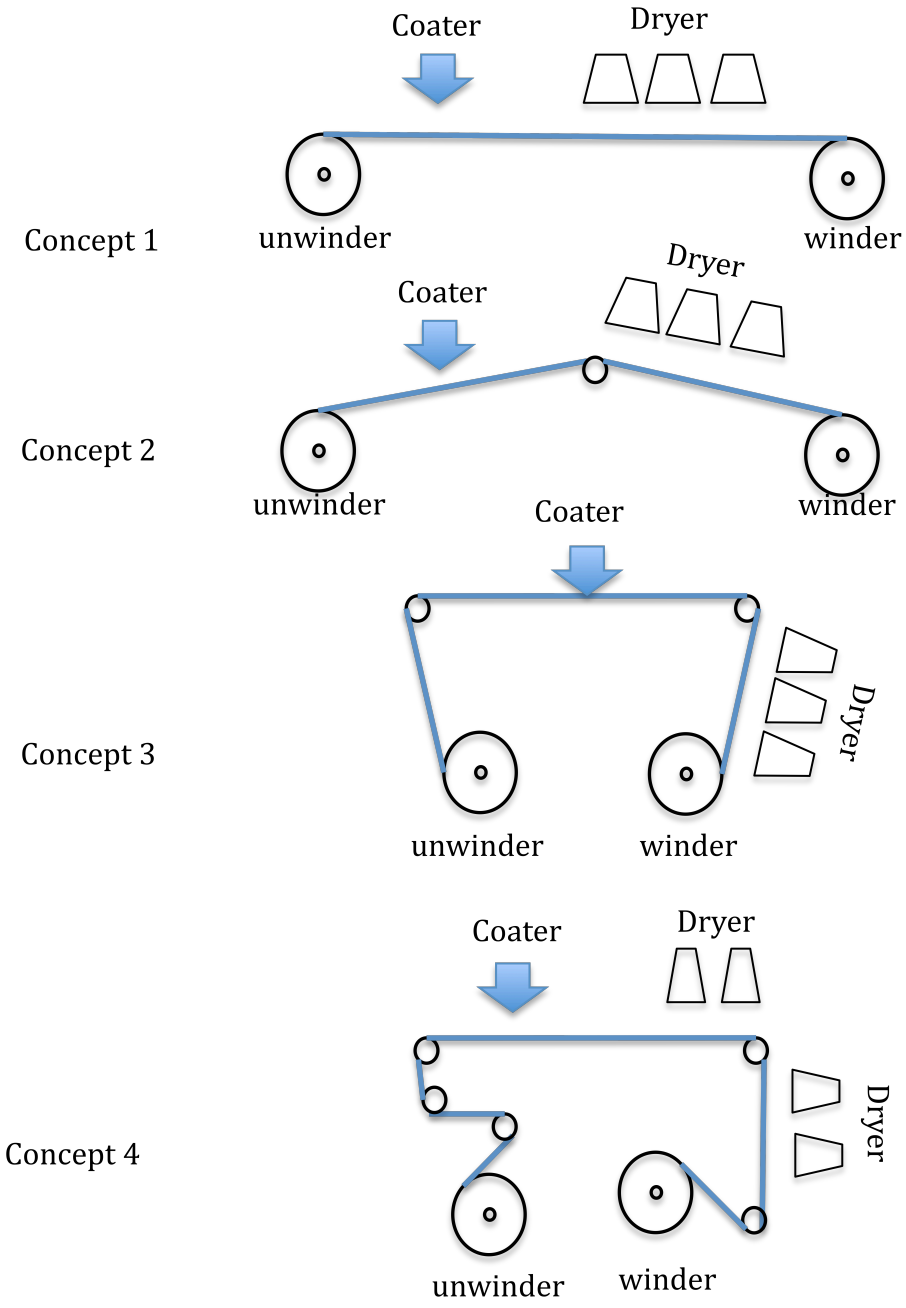

Figure 37: Machine layout concepts.

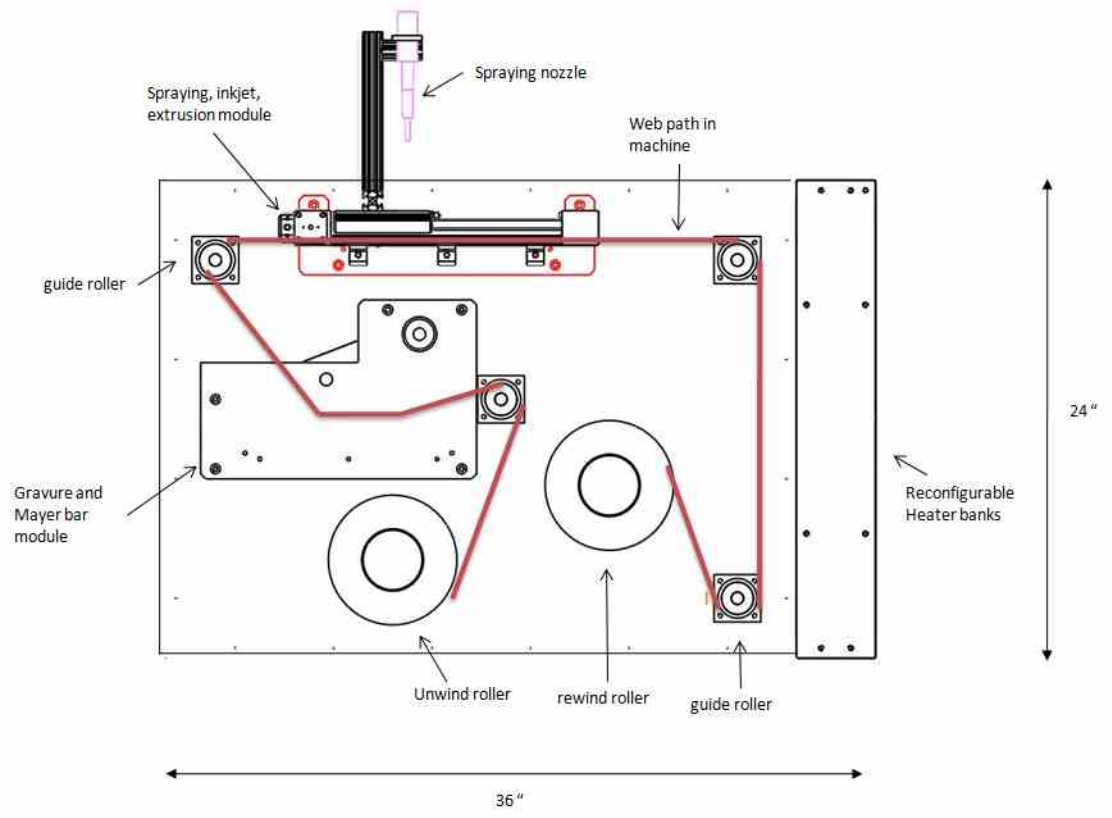

Figure 38: Different parts of the modular coating test bed.

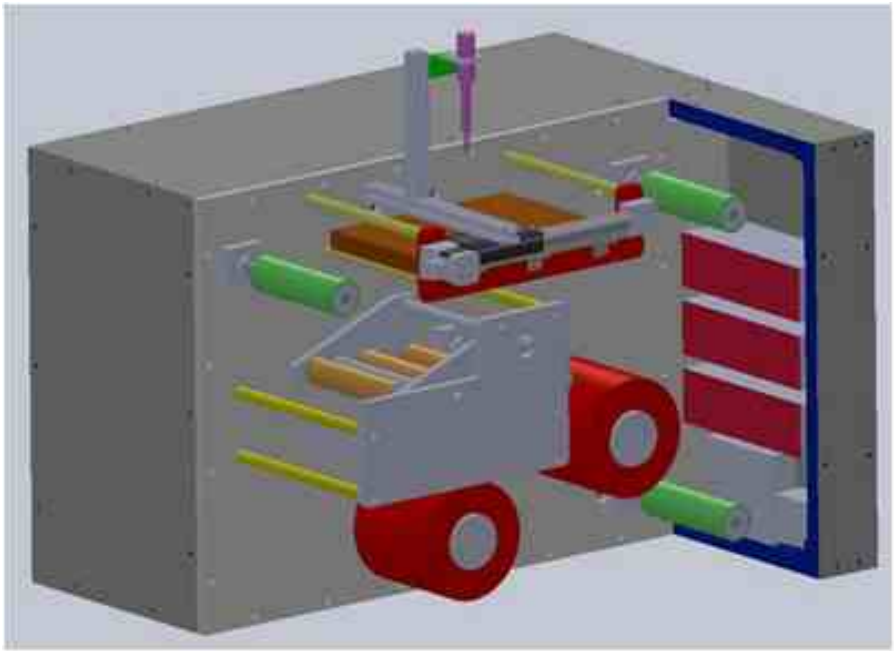

Figure 39: CAD model of modular coating test bed.

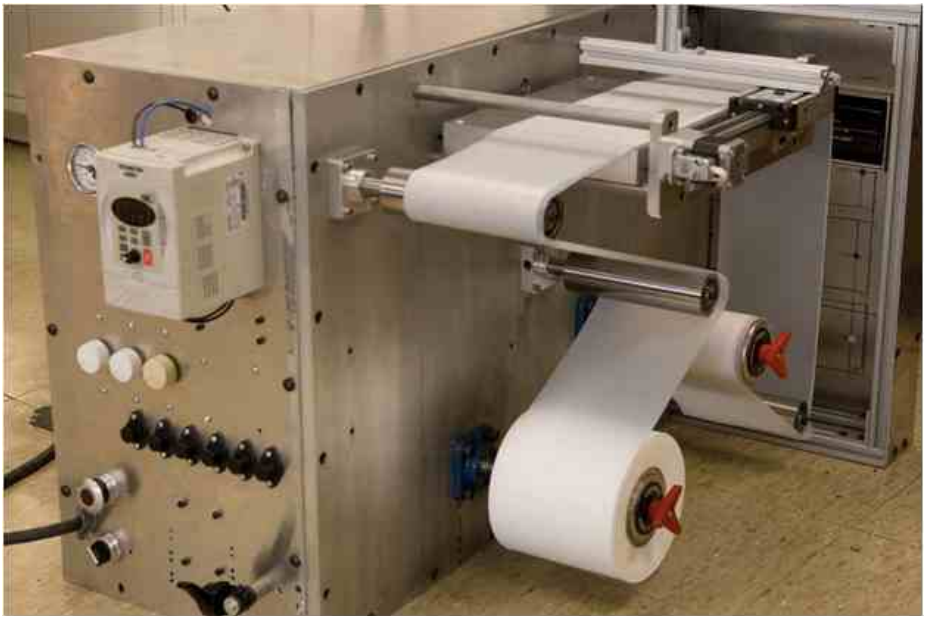

Figure 40: Modular coating test bed.

4.3 INK APPLICATION MODULES

As discussed earlier, three different coating processes were selected for prototyping: spraying, tape casting, and slot die coating. The following paragraphs discuss the modules that employ these coating processes.

4.3.1 Spraying module

The spraying module, allows for the movement of the spray head in the web feed direction. Rapid traversal of the spray head, in combination with the web feed, will allow for multiple spray passes on the substrate. A vacuum table is mounted under the web surface so that, in addition to continuous web handling, even discrete samples of substrate can be mounted in the test bed and coated.

Three different types of nozzles were considered for the spraying module. The first nozzle that was installed was a 'pressure less' ultrasonic nozzle. Two problems were immediately revealed: the ultrasonic nozzle could only atomize very low viscosity fluids and, it atomised the fluid to such fine particles that the spray became a mist that was nearly impossible to direct and very sensitive to even slight air drafts.

The second spraying head tested was actually a nozzle that delivered a discrete stream of droplets, which were produced by a fast acting solenoid, allowing a pressurised fluid to flow through an orifice. This is quite similar to ink jet printing, albeit this nozzle dispensed a greater droplet volume than that of an ink jet droplet. This nozzle also had a readily evident flaw: it was prone to clogging, which occurred so frequently that it was deemed unsuitable for operation.

The third nozzle that was tried was a twin fluid external mixing nozzle, where pressurized air was used to atomise the catalyst ink. The nozzle used was a Nordson EFD 781S series spray valve with a 46mil diameter nozzle. The nozzle provided for adjustable fluid flow rates, adjustable air pressures and, in combination with the Nordson EFD

ValveMate 8040 controller, provided computerised control over the spray cycle. This nozzle performed flawlessly, although it does require periodic cleaning to prevent clogging, but that is fundamentally an ink problem rather than a nozzle problem, and it is believed that it will be eliminated with ink filtration.

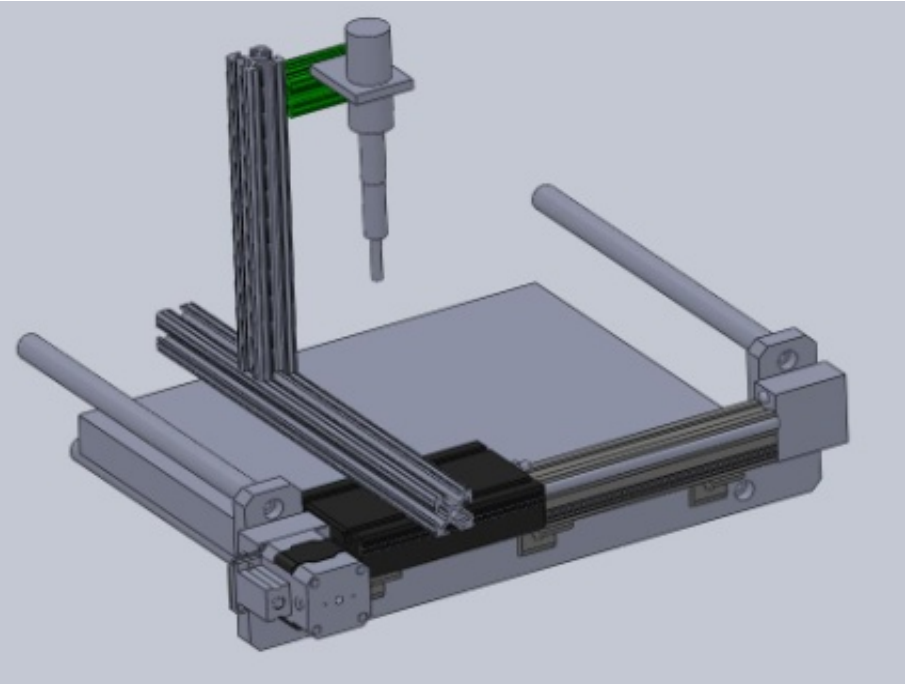

Figure 41: Spray head and ultrasonic spray nozzle.

4.3.2 Slot die coating module

An attempt was made to design and build a slot die coating head, as shown in Figure 42. The die consists of two halves, as shown in the figure, which are assembled together. A spacer (shim stock) is placed in between to create the desired gap at the lip of the die. Fluid enters the die through the inlet port, is channeled through the die where it is ejected out of the die through the lip. The machining finish at the lip dictates the uniformity of the fluid film that is extruded from the lip. The finish required at the lip of

the die was beyond the capabilities of in-house facilities. Commercial die manufacturers were contacted and quotes obtained, but it was decided to abandon this particular coating module due to the cost, complexity of the die, and the inking system involved. Also, as previously mentioned, there are certain similarities between tape casting and extrusion. Since a tape casting module was being pursued and was operational, pursuing the slot die coating module was not made a priority.

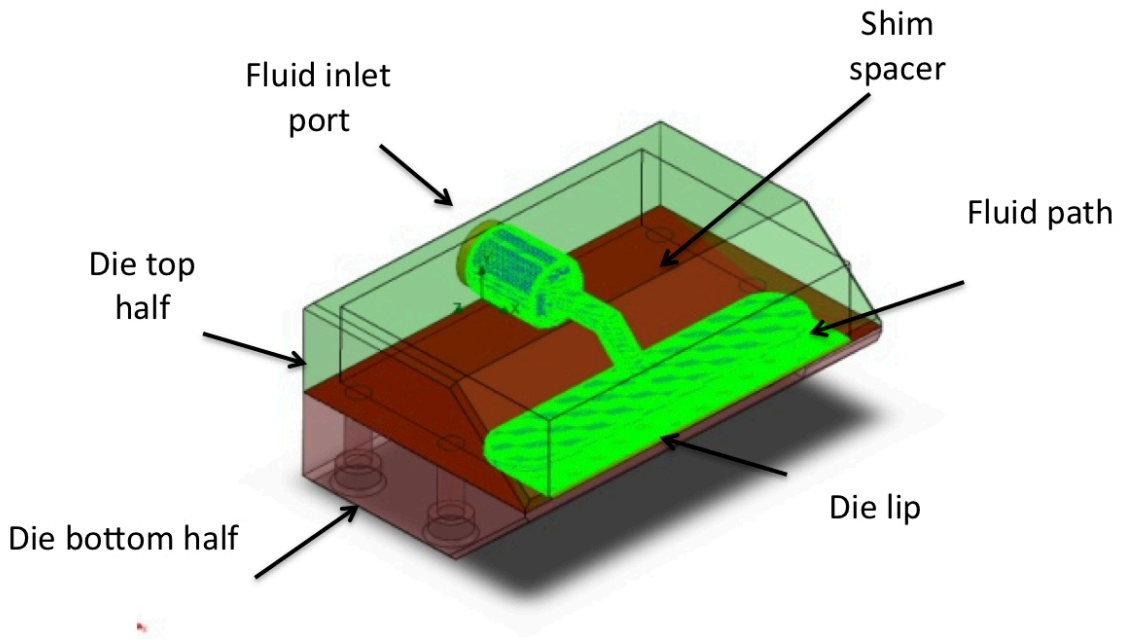

Figure 42: Slot die coating head.

4.3.3 Tape casting/Doctor blade module

Developing a tape casting module required creating a flat surface onto which the tape casting head could be installed. The tape casting head has an ink reservoir, through which a metered quantity of ink is mechanically released by an adjustable doctor blade, as depicted in Figure 43.

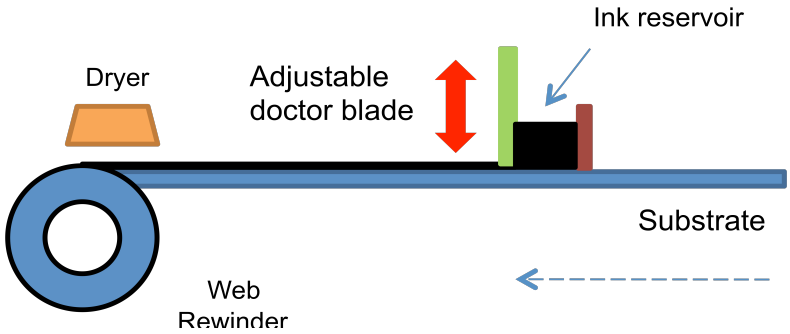

Figure 43: Tape casting process.

In Figure 44, the design of a tape casting head is shown. The doctor blade is held in place by micrometers, which can be used to adjust the gap. This controls the wet layer thickness of the ink being deposited onto the substrate. In Figure 45, the actual catalyst ink layer deposition is shown.

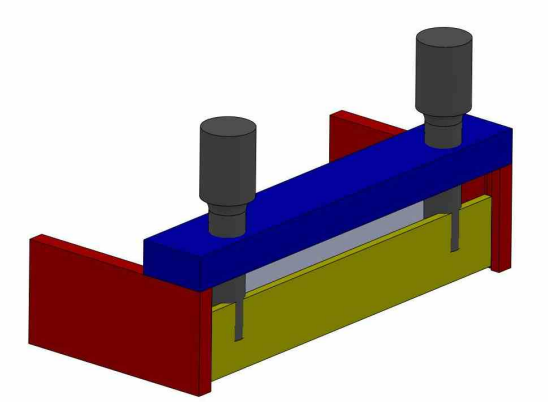

Figure 44: CAD model of tape casting head.

Figure 45: Actual tape casting head during operation.

4.4 COATING PROCESS SELECTION

The goal of this research effort has been to identify a single process that can be used to fabricate effective PEMFC and DMFC electrodes. This was done by first examining seven coating processes, from which three were selected for prototyping. Two of these three processes warranted designing the coating modules, and were subsequently constructed and installed on the test bed. In order to select a final coating process, the two coating processes were compared on their ability to successfully deposit the desired wet layer thickness, and the uniformity of the electrode produced.

4.4.1 Electrode uniformity and surface morphology

It is of considerable importance to examine the surface of the coatings produced by both spraying and tape casting. This information is needed in order to identify any anomalies in the coating process. Ideally the surface should be spatially uniform, i.e. have

uniform thickness in both the web feed direction and the traverse direction. If there is more catalyst in one part of the electrode as compared to the other (due to non uniform coating) this would to lead to variable resistance through the MEAs, as thicker areas would have a higher resistance. [83].

Another important quality that must be addressed is whether or not there is a difference between the microstructures of electrodes produced by these two processes? On might anticipate differences in the microstructures as tape casting deposits a thick single layer of catalyst ink, which is slowly dried, and spraying builds the electrode in progressive layers, until the desired loading is reached.

To study the uniformity of the surface, small samples of coatings by both methods were taken and examined using a scanning white light interferometry apparatus. The coatings were made on a woven substrate, a PTFE coated fiberglass tape. The surface of the tape-casting sample is shown in Figure 46. The weave pattern of the substrate is clearly visible, but is otherwise a fairly uniform surface, as shown in the three dimensional image. Figure 47, shows the interferometry results of a coating made by spraying, again the weave pattern of the PTFE coated fiber glass substrate is visible, but the overall surface is uniform.

The dashed line represents an imaginary surface, relative to which the height of the substrate is measured. The peaks that are observed coincide with the weave pattern and should be neglected. As shown in the first figure, the line represents the plane from which the data in the bottom graph is extracted. The two peaks are clearly identifiable on that line as shown by the red dots.

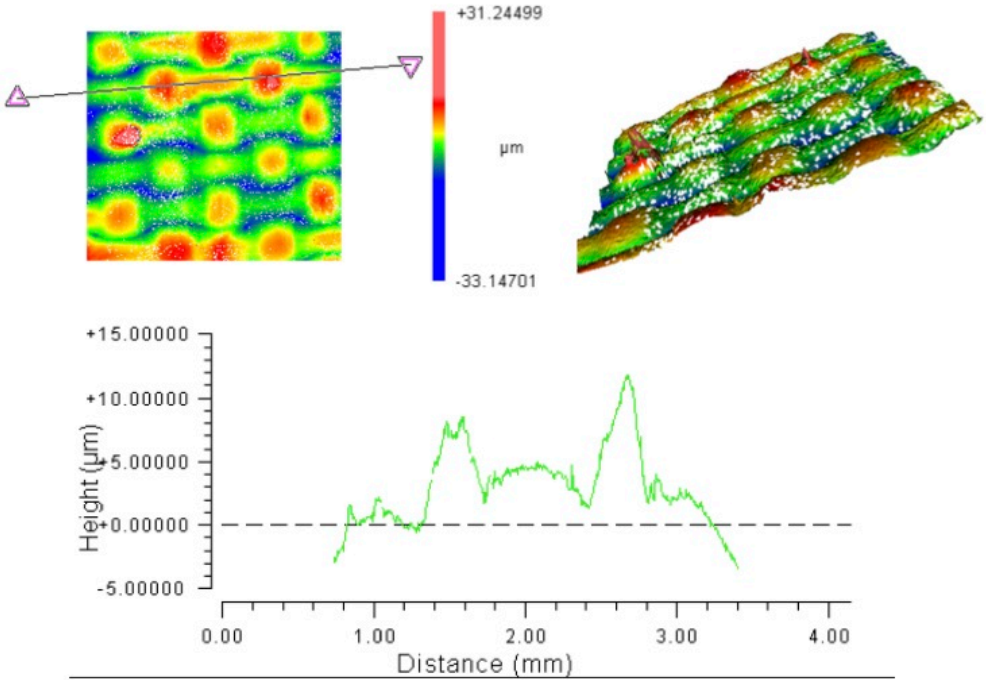

Figure 46: Surface interferometry results for tape casting.

In the results from the sample made by spraying, the peaks are not as obvious as that on the tape casting sample, but they are still identifiable. Neglecting this interference caused by the substrate morphology, it can be concluded that both processes perform equally well in terms of the spatial uniformity of the coating, as identified by the interferometry results.

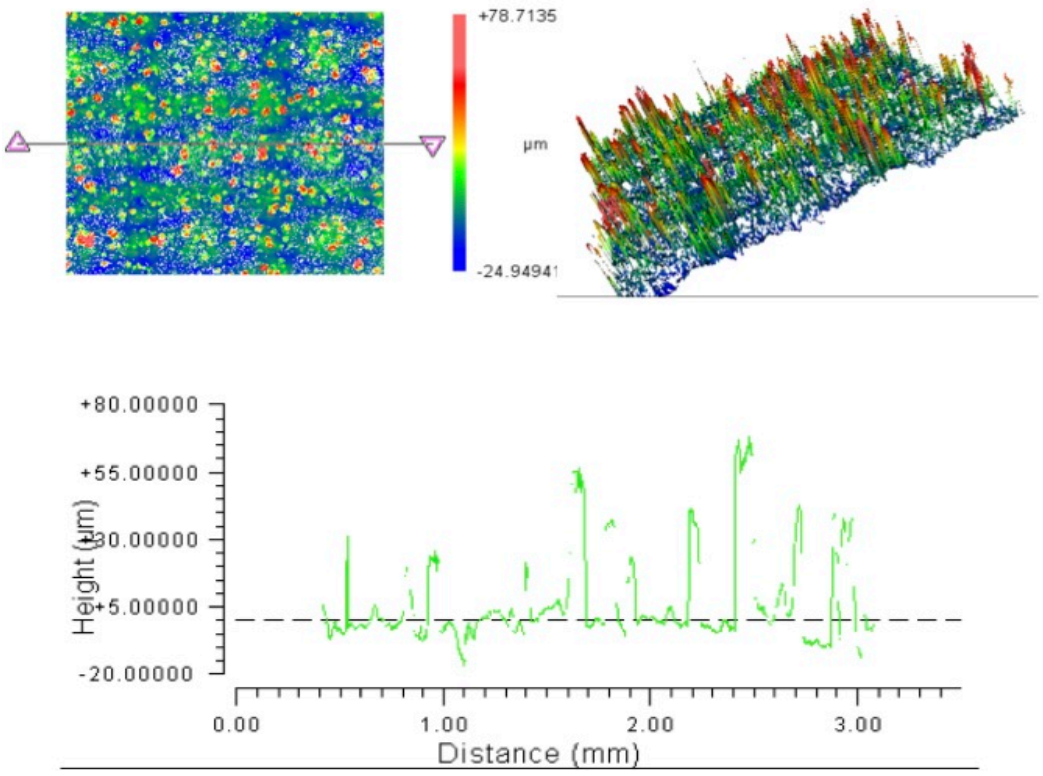

Figure 47: Surface interferometry results for spraying.

Coating samples made by both processes were studied in a scanning electron microscope to examine the coating microstructure. This was done to address the question posed earlier, "is there a difference between electrodes formed in a single layer, versus multiple layers?" As can be seen from the SEM results in Figure 48, at lower magnifications, the surface of the sprayed coating is grainy, but at higher magnifications (5000x), where the real microstructure is revealed, there seems to be no difference, and pore sizes appear to be similar in both coatings.

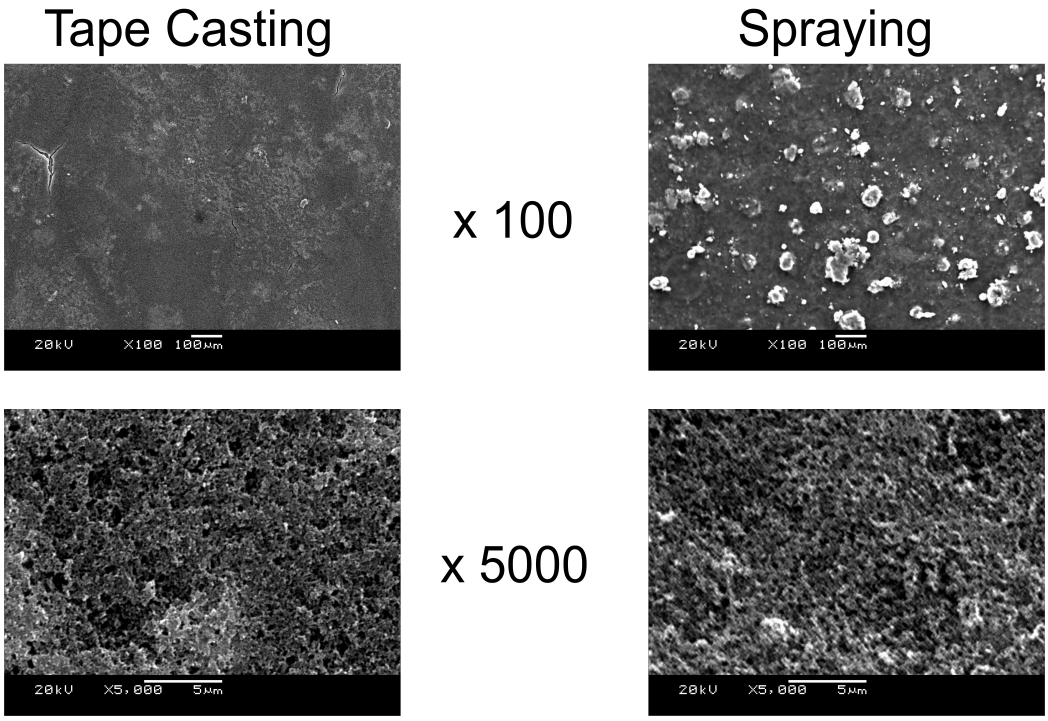

Figure 48: Microstructure of coatings made by tape casting and spraying.

From the interferometry results and SEM imagery it is concluded that there is no difference between the two processes, as far as coating uniformity and morphological features are concerned.

4.4.2 Loading control

The second criterion by which to compare the two processes is loading control. What that means is that the processes will be examined on the basis of their ability to accurately deposit the required loading on the substrate. One way to measure the loading of material on a substrate for a continuous coating process is to measure the coating thickness and from that compute the loading. Alternatively, discrete samples of a given area can be cut from the substrate, their mass measured and loading calculated. It must also be ascertained whether or not the processes can achieve the desired loading for a DMFC fuel cell, which can be as high as 4 mg/cm^2.

It is extremely important that the mass loading on a continuous substrate remain consistent during coating deposition. Variations in the catalyst loading of a fuel cell can produce significantly different electrochemical results. Loading control tests for both tape casting and spraying were conducted using a carbon black ink, rather than actual catalyst ink, to save on costs.

For spraying, the loading control was done in a very simple, but accurate, manner. A token was cut from a suitable substrate, and its mass was recorded. The desired number of layers was deposited on a known area, using a mask. The token was weighed after the coating and the mass difference divided by the area, which gives the loading. Figure 49 shows how the loading of coating samples increases with the number of layers deposited by the spraying nozzle. A maximum loading of almost 5 mg/cm^2 is achieved, showing that the spraying process can deposit the required mass loading for a DMFC electrode (typically 2.5 mg/cm^2), additionally the linearity of the relation between loading and number of layers demonstrates that the amount of mass deposited per layer is constant; the process is stable and does not drift. In the results shown, a 3% solid content ink was used. Thicker inks will reduce the amount of layers required to achieve the desired loading.

It must be pointed out that around 25 layers are required to achieve a loading of $2.5mg/cm^2$, but these are results with a carbon ink with 3% SC. In actuality Pt:Ru or Pt black would require fewer layers as they are much more dense as compared to carbon black. Additionally inks with SC greater than 3% can be explored.

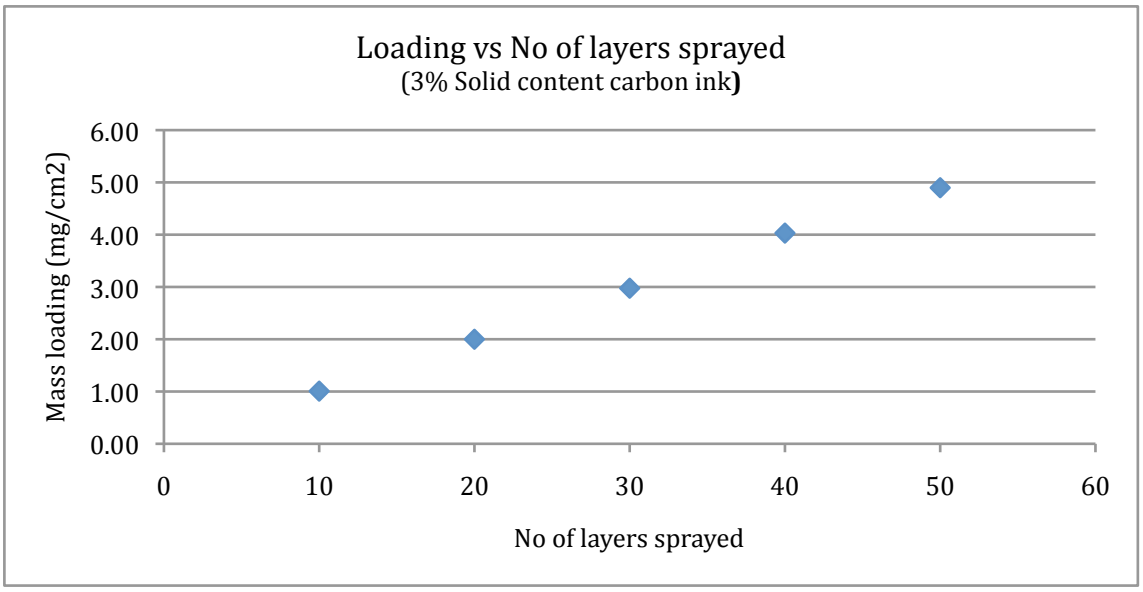

Figure 49: Loading control results for spraying.

The entire exercise of first showing that the process can repeatedly produce the same loading, and then that it can produce the overall desired loading on a substrate as required for a DMFC electrode was repeated for the tape casting process. Figure 50 shows the loading of samples that were taken 1 ft apart, along the web feed direction for three different wet layer thicknesses. Samples were cut out from the coated substrate similar to what is shown in Figure 51, the difference being that they were further apart, and then their masses were measured. The coating was washed off the substrate, which was then dried and weighed. In this fashion an initial and final mass for a known area of substrate was measured and loading was calculated by dividing the amount of coating mass deposited by the area.

As can be seen that the process produces highly repeatable results, and that loading can be effectively controlled.

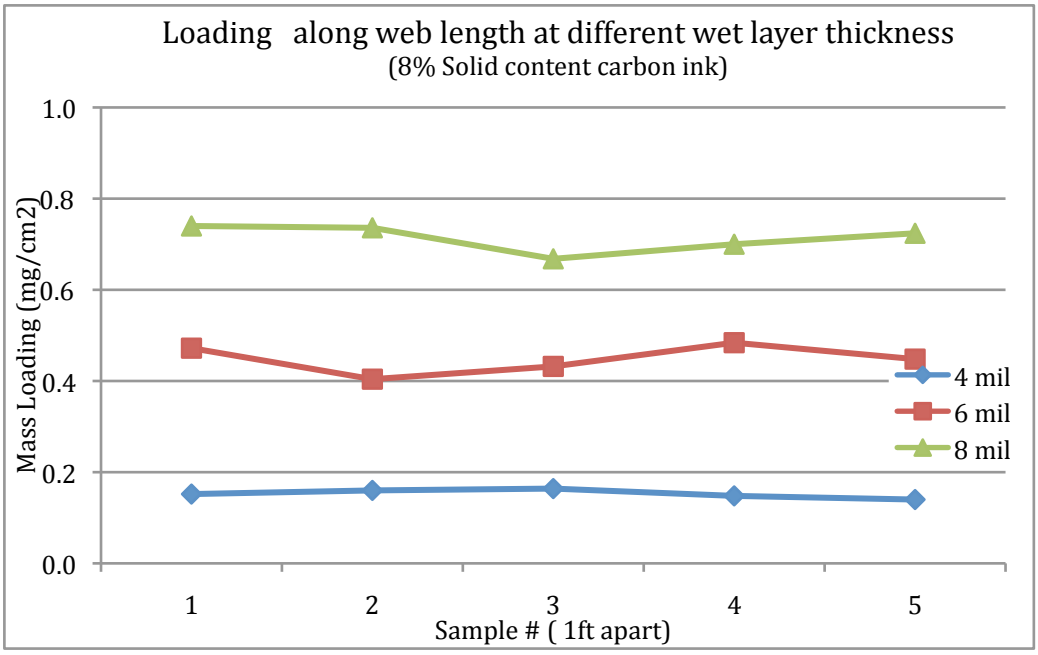

Figure 50: Tape casting loading repeatability.

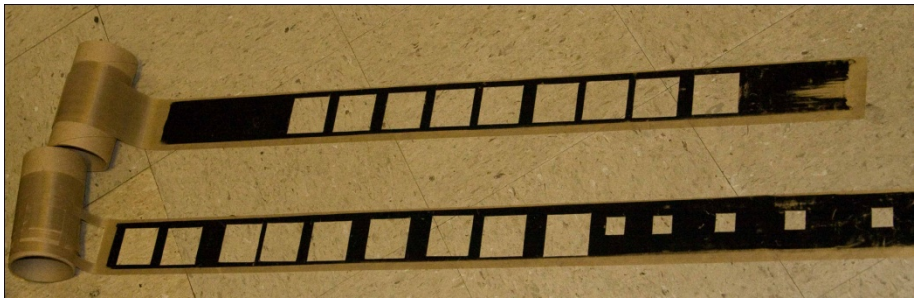

Figure 51: Tape casting of PEMFC electrodes on modular coating test bed.

Figure 52, shows how the mass loading achieved by the tape casting process varies with different wet layer thicknesses. The ink used was an 8% solid content ink. Inks with higher solid contents were fabricated and coated onto the substrate in order to achieve higher catalyst loadings (2.5 mg/cm^2 required for DMFC).

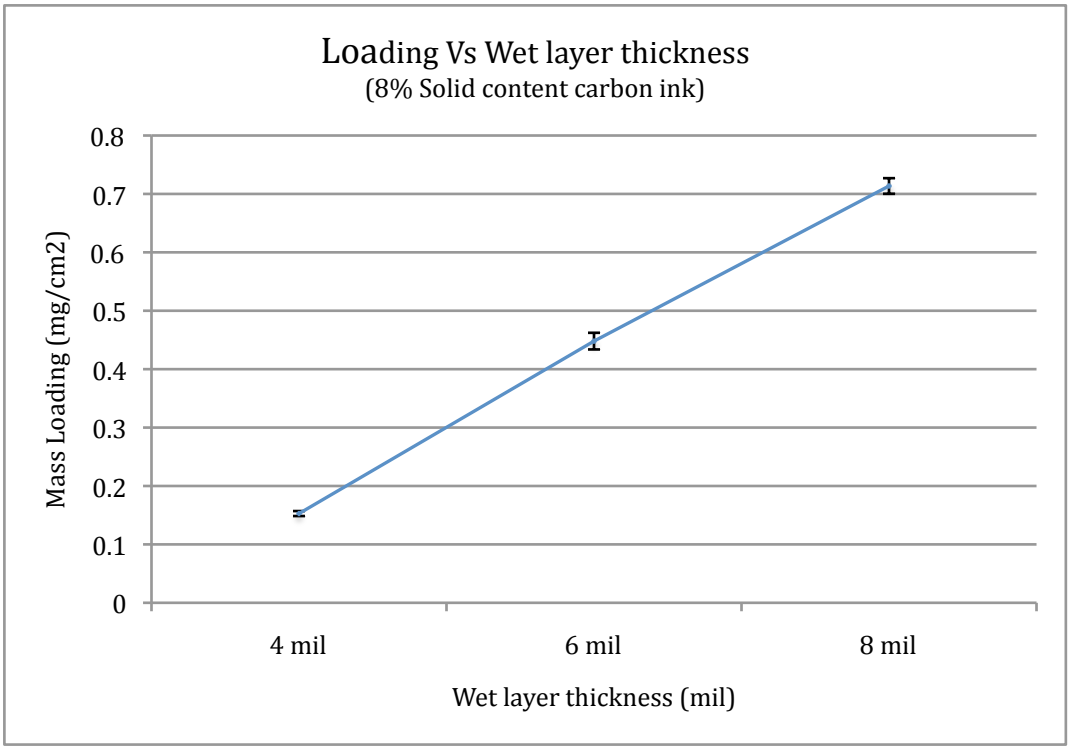

Figure 52: Loading vs. Wet layer thickness.

There were no issues in applying the coating, but during drying, a completely new problem was encountered. During and after drying the coated layer developed cracks and peeled, as shown in Figure 53. Thicker layers of high solid-content inks are necessary to achieve the high catalyst loading for a DMFC electrode (typically 2.5 mg/cm^2). Upon drying, internal stresses develop between the top layers of the coating, and the bottom layers, which are adjacent to the substrate. These stresses are caused by the different amounts of shrinkage of the top and bottom layers; the bottom layers shrink less due to their adhesion to the substrate surface, which constrains their movement.

For industrial coatings, the inks can be tuned to the particular coating process by increasing the binder content, which would eliminate this problem. But for inks used in PEMFC and DMFC electrodes, the binder used has a dual role. It provides for proton conducting paths, and acts as a binder as well. Increasing the binder content significantly

affects the overall electrochemical performance of the electrode and the MEA.

Considering these results, tape casting was deemed unfeasible for producing coatings suitable to make DMFC electrodes.

Figure 53: Cracking and peeling.

4.5 CHAPTER SUMMARY

In the previous chapter, seven coating processes were examined, out of which four were ruled out on the basis of a feasibility study. The remaining three processes, tape casting, spraying, and slot die coating, were selected for further experimentation and prototyping. In order to study them, a modular coating test bed was designed and fabricated where coating modules, which implemented these processes were installed.

Slot die coating was found to be too complex during the prototyping stage, and was abandoned. The remaining two processes, spraying and tape casting, were selected for further optimization, as depicted in Figure 54.

In the optimization stage, the processes were compared on the basis of the uniformity of the electrode they produced, the control they offered on the mass loading of the coating, and the maximum loading that could be achieved with inks that mimic the performance of catalyst inks used for PEMFC and DMFC fabrication. In these final tests, a severe limitation was identified in the tape casting process: when thicker coatings were attempted, the coating would develop cracks and peel upon drying. Based on these results, spraying was selected for further research, testing, and evaluation.

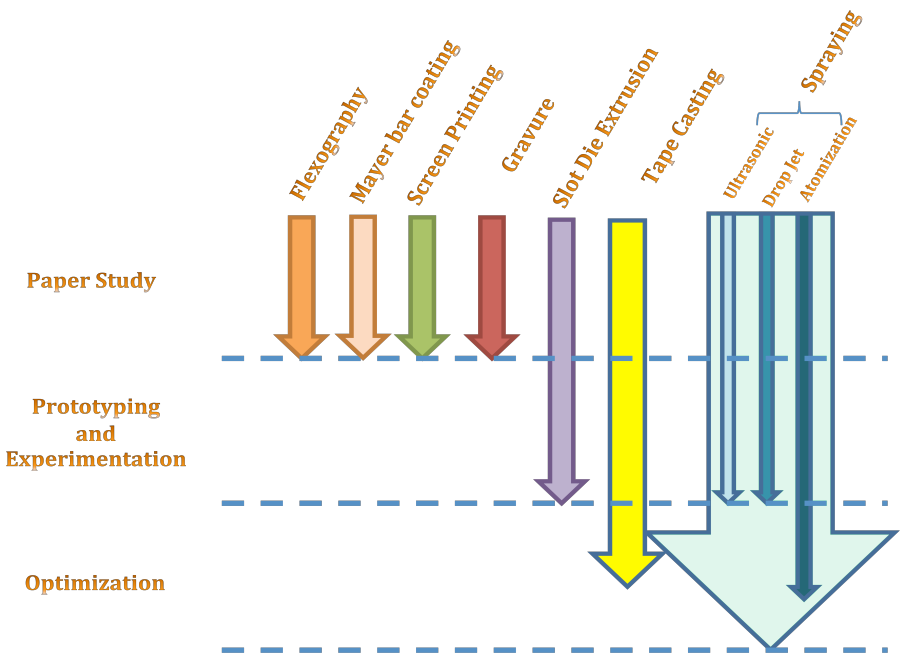

Figure 54: Coating process selection study.

5. Spraying

Spraying is a well-established coating process used for the fabrication of electrodes for both PEMFC and DMFC, and for the fabrication of micro porous layers (MPL) on gas-diffusion media (GDM) used in fuel cells[40]. In a laboratory environment, it is common practice for airbrushes and small spray guns to be used to atomize catalyst inks, of which multiple coats are applied onto discrete pieces of the relevant substrates.

Despite its popularity as a process, there is little basic research on how spray parameters and nozzle characteristics affect the droplet sizes of catalyst inks, and how these droplet sizes affect the electrode structure and overall MEA performance.

The feasibility study conducted in Chapter 4 identifies spraying as the coating process of choice for the continuous fabrication of DMFC electrodes. A two-fluid, air-assist, external mixing configuration was selected as the best candidate for development. In this process, pressurized air atomizes the catalyst ink, the nozzle provides adjustable fluid flow rates by controlling the coating fluid pressure and cross sectional area of the nozzle exit, and the flow can be metered by a plunger needle. In order to develop a better understanding of the influence of these control parameters on spray characteristics, a study conducted on the spraying process is presented.

5.1 INTRODUCTION AND PROCESS FEATURE REQUIREMENTS

In the context of catalyst ink spraying, the atomization process involves the decomposition of the catalyst ink suspension into droplets upon entering, mixing and interacting with air at the nozzle orifice. The catalyst ink is provided sufficient energy to penetrate the ambient fluid and facilitate subsequent dispersion, by a separate stream of

high-pressure air. This energy can be provided by the kinetic energy of the liquid that is to be atomized, by the action of high velocity gas, or by mechanical energy applied through an external device [147]. Such devices, which are used to produce the atomized droplets, are called atomizers. We surveyed the various methods by which the catalyst ink might be atomized and transferred to a substrate. Ultimately, a two-fluid, air-assisted, low volume, low-pressure (LVLP) pneumatic nozzle was selected but, in this section, we present the other types of atomizers available and a comparison of their properties, in order to justify the selection that we made.

For the application under consideration, we require the ability to handle a high-viscosity suspension, a high degree of atomization, a fairly narrow spray to ensure uniform distribution on the two-dimensional plane of the substrate, and reasonably high throughput. The ability to constrain overspray is also critical, as the catalyst ink is very expensive due to its platinum content, and recovering catalyst from outside the designated area would be a potential source of loss and process cost.

5.2 TYPES OF ATOMIZERS

Atomization process selection is a critical part of the overall design of the coating process. Process control parameters and spray characteristics, which depend entirely on the atomization process, will dictate other design variables such as substrate width, nozzle height, and line speed. We classify atomizers by the type of energy employed to produce perturbations and instability in a fluid. These instabilities lead to the detachment of smaller volumes from the bulk fluid, resulting in droplet formation. A nozzle is an atomizing device that ejects a liquid through an orifice. Other types of atomizers are centrifugal devices that spin and thereby create droplets, electrostatic atomizers, and ultrasonic vibrators. Table 11 provides a brief summary of the different types of

atomizers. From these characteristics, we can evaluate the atomization techniques and their appropriateness for the electrode deposition process.

Table 11: Types of Atomizers [147, 148, 156].

Energy	Type		Droplet Size(μm)	Application	Advantage	Limitation
Liquid Energy	Pressure Atomization	Plain Orifice	25-250	Diesel, jet engines, afterburners, ramjets	Simple, rugged cheap	High pressure, Narrow spray angle, solid spray cone
		Simplex	20-200	Gas turbines, Industrial Furnaces	Simple, Cheap, Wide spray angle	High pressure, varying spray angle
		Duplex	20-200	Gas turbine combustors	Simple, cheap, wide spray angle, good atomization	High pressure, Narrow spraying angle
		Dual-Orifice	20-200	Aircraft, Industrial Turbines	Good atomization, constant spray angle	High pressure, Complex design, susceptible to blockage
		Spill Return	20-200	Combustors	Simple, good atomization, low risk of blockage	High pressure, varying spray angle, high power requirements
		Fan Spray	100-1000	High pressure painting/coating, combustors	Good atomization, narrow elliptical spray pattern	High supply pressure
Mechanical Energy	Rotary Atomization	Spinning Disk	10-200	Spray drying, pesticide distribution	Good mono-dispersity of droplets	360^{o} spray pattern
		Rotary Cup	10-320	Spray drying, spray cooling	Capable of handling slurries	360^{o} spray pattern, may require air blast around periphery
Pneumatic Energy	Two-Fluid Air-Assist	Internal Mixing	50-500	Industrial furnaces, gas turbines, paint spraying/coating	Good atomization, low risk of clogging, capable of atomizing high-viscosity fluids, low volume, low pressure nozzles	Possible liquid backup into air line, requirement for external source of pressure

Table 11, cont.

		External Mixing	20-140	Industrial furnaces, gas turbines, paint spraying/coating	Good atomization, Low risk of clogging, capable of atomizing high-viscosity fluids, low volume, low pressure nozzles	Requirement for external source of pressurized air
	Two-Fluid Air-Blast	Plain-Jet	15-130	Industrial gas turbines	Simple, cheap, good atomization	Narrow spray angle, Atomizing performance inferior to prefilming air blast
		Pre-filming	25-140	Aircraft and industrial gas turbines	Good atomization at high ambient pressures	Poor atomization at low air velocities
Electrical Energy	Electrostatic Atomization		0.1-1000	Paint spraying, Printing, Oil burner	Fine and uniform droplets	Very low flow rates, Strongly dependent on liquid electrical properties
	Ultrasonic Atomization		1-200	Medical spray, humidification, Spray drying, Acid etching, Printing	Very fine and uniform droplets, Low spray rates	Incapable of handling high liquid flow rates

5.2.1 Electrostatic atomization

In electrostatic atomization, also referred to as electrospraying, the energy required to break-up a fluid is provided by the accumulation of like charges on the surface of a fluid. These charges impart mutually repulsive forces, acting to distend the surface, which are reciprocally opposed by surface tension forces. When the repulsive forces exceed the opposing surface tension forces, droplets begin to form. Martin et al. [157] describe the use of this process for the deposition of catalyst layers with ultra-low noble metal loadings for use in PEM fuel cells. Jaworek et al.[158] provide an excellent review of the capabilities of electrostatic atomization. The synopsis of these reports indicates that electrostatic atomization operates at very low liquid flow rates (0.3 ml/hr) [157]. If electrostatic atomization were to be used to fabricate DMFC electrodes, an inordinate amount of time would be required for spraying, due to the higher catalyst loadings in a DMFC electrode. This technique was therefore excluded from further consideration.

5.2.2 Ultrasonic atomization

Droplet formation via ultrasonic atomizers is induced by the dispersal of a liquid on a vibrating surface, which causes the formation of waves in the fluid. Increasing the amplitude of the vibrating surface causes the ejection of droplets from the fluid film. The spray produced by ultrasonic atomization has very low velocity, and often requires the use of an external stream of gas to control it [147]. As with electrostatic atomization, the low flow rate capabilities and the consequent long times required for fabrication preclude this method from further consideration.

5.2.3 Rotary atomization

In rotary atomizers, atomization is achieved by introducing a liquid onto a rotating surface, where it is uniformly spread by the action of centrifugal force. Drops form at, or near, the edge of the rotating surface[156]. Rotary atomization produces a 360º spray pattern, as the drops produced are on the periphery of a disk or cup. This spray geometry makes rotary atomization incompatible with the geometry requirements of a continuous coating process. Such atomizers can be eliminated from further consideration because of the 360° spray pattern, as it is incompatible with directing a spray onto a two-dimensional substrate.

After considering and rejecting rotary, electrostatic, and ultrasonic atomization, based upon flowrate and spray pattern characteristics we turn our attention to the processes that induce atomization through pressure differences.

5.2.4 Pressure atomization

In pressure atomization, the pressure of a fluid is converted into kinetic energy in the atomizer, and a high velocity liquid jet is ejected, which disintegrates into an atomized spray. There are many subtypes of pressure atomizers, which vary in key spray characteristics such as spray angle [156]. Pressure atomization processes are dependent on the kinetic energy of the fluid for droplet formation. The liquid stream exits the nozzle as a jet, which disintegrates to form a spray[147]. The high velocity and pressure involved render pressure atomization to be entirely infeasible for the application of catalyst ink.

5.2.5 Two-fluid air blast atomization

Air blast atomizers work on the same principle as air-assist atomizers, the difference being the velocity of the atomizing air and its volume. They require large air

volumes at low velocity and pressures[147]. Air-blast atomization involves exceedingly high airflow rates, which could cause wastage of catalyst ink.

5.2.6 Two-fluid air-assist atomization

In an air-assist atomizer, the atomization occurs due to the kinetic energy of a flowing air stream, which causes the liquid stream to break-up into fine droplets. Air-assist atomizers operate at low airflow rates, but there are no restrictions on air pressure and air velocity. They are well suited for atomizing highly viscous fluids [147]. Air-assist atomization is compatible with viscous fluids and can easily produce solid cone, hollow cone, and flat fan spray patterns, which are attractive characteristics. Air-assist nozzles generally require high air pressures to effectively atomize fluids; however, low volume, low pressure atomizers such as the Nordson EFD 781S do exist, and are used for the application of paints and coatings [146].

5.2.7 Atomization process feasibility for spraying catalyst ink

Table 12 summarizes the evaluation of the various techniques. These characteristics are summarized in the context of the current application, which requires spraying viscous ink onto a moving substrate at close proximity. Based on these considerations it was concluded that the two-fluid, external mixing, air-assist type nozzle (Nordson EFD781S) used in the feasibility study is a suitable choice for the overall continuous manufacturing process. Multiples of these nozzles could potentially be used in tandem, applying high viscosity inks onto the substrate.

Table 12: Feasibility of atomization processes with respect to spraying catalyst inks on a substrate.

Atomizer	Pros	Cons
Pressure Atomization		• High pressure • High flow rate • Narrow spray angle
Rotary Atomization		• Spray geometry
Two-fluid Air-assist Atomization	• Low airflow rates • Low pressure • High viscosity fluids • Low cost	• High velocity
Two-fluid Air Blast Atomization	• Low velocity • Low pressure	• High airflow rates
Electrostatic Atomization	• Minimal pressure • Minimal velocity • Drop size	• Complexity • Cost • Low flow rates
Ultrasonic Atomization	• Minimal pressure • Minimal velocity • Drop size	• Cost • Low flow rates • Low viscosity • Spray control

A spray can be characterized by three factors: shape, patternation and droplet size. The shape refers to the region through which the droplets are dispersed. Shape is defined by the width of the spray W and the spray angle θ, as shown in Figure 55. The spray angle is defined as the angle between two tangents made by the spray at the point where its velocity is maximum, which is typically at the orifice. A spray with $\theta<30^0$ is classified as a narrow spray, a medium-angle spray is defined by $30^0<\theta<70^0$, and a wide angle spray is classified as having $\theta\geq70^0$ [146].

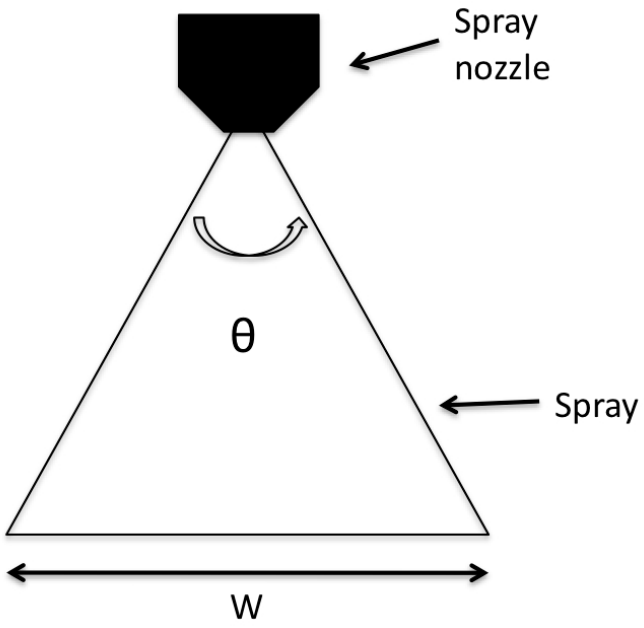

Figure 55: Spray shape.

Patternation is the flux of droplets across a plane in the spray pattern; it is the spatial distribution of droplets within the spray. It refers to both the distribution and the shape of the spray. Three common types of spray shapes are cone spray, hollow cone spray, and flat fan spray, as shown in Figure 56. Internal geometry and the shape of the orifice determine the shape of the spray. In order to study and characterize a spray, it is important to measure drop size and distribution.

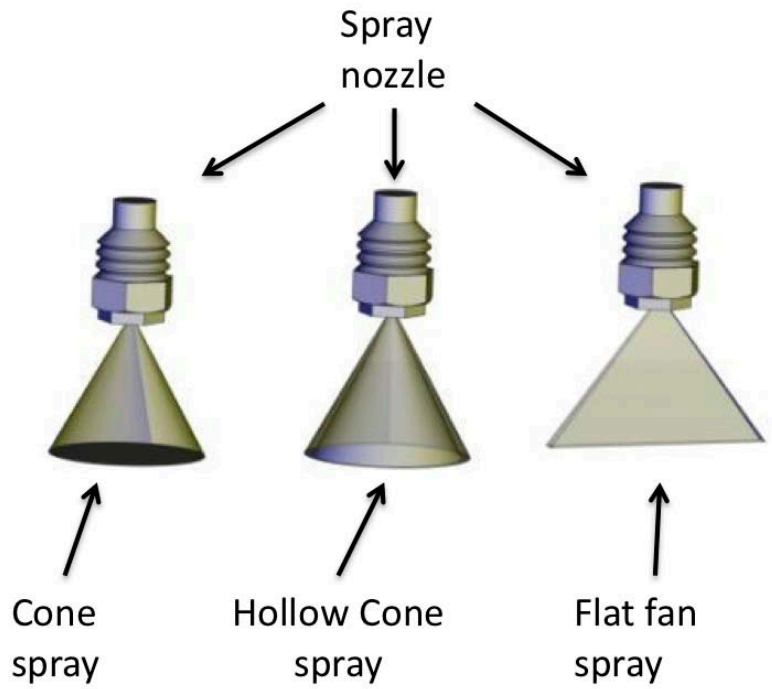

Figure 56: Types of spray patterns.

5.3 DROPLET SIZE MEASUREMENT

A spray is characterized on the basis of its shape, patternation, and droplet size. For the nozzle under consideration, the nozzle orifice controls the shape and patternation of the spray. A narrow, solid cone spray was chosen with consideration to the geometry of the electrodes to be fabricated. The other property of interest was the droplet size produced by this nozzle. The next few paragraphs discuss the significance of droplet size, the apparatus used to perform these measurements, and the results of using a custom built high-speed photography apparatus.

Need for droplet size measurement

The controllable parameters of the spray nozzle (Nordson EFD 781S) are the air pressure, the fluid pressure, and the effective nozzle area, as controlled by the needle plunger setting. Figure 57 shows a general schematic of the nozzle. An additional port

(not pictured) exists in the nozzle. Its function is to lift the needle plunger from its seat, facilitating fluid flow, but does not participate in the atomization process.

Other parameters that could potentially affect the mean droplet size of the spray are the nozzle orifice diameter and ink viscosity, both of which are kept constant. The reason for keeping the nozzle orifice diameter constant is that the 46 mil diameter orifice offers a 0.25" spot size when the nozzle sprays from a distance of 1" from the surface [159]. Catalyst ink viscosity is dependent on the ink solid content, which is kept fixed at 4%. Higher solid contents have been attempted, but they resulted in frequent clogging. Air pressure settings can range from 0 to 30 psi, fluid pressure settings range from 0 to 15 psi, and the adjustable plunger has 20 settings.

It was observed that different combinations of these parameters produced sprays with different characteristics, which, from visual inspection, could be identified as ranging from 'coarse' to 'fine'.

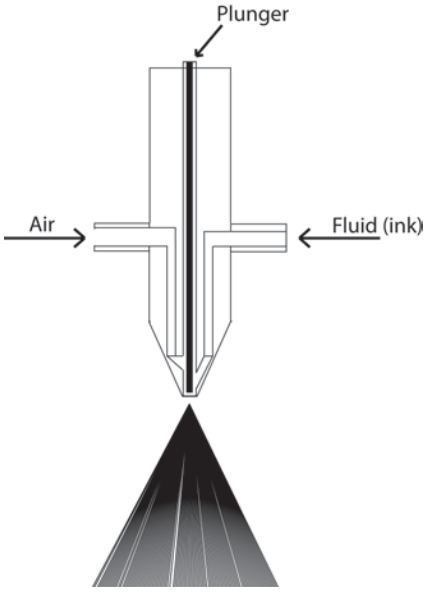

Figure 57: Two-fluid air-assist external mixing nozzle.

These observations led to the following, basic questions that needed to be addressed:

- What are the optimal settings at which to operate this nozzle?
- How can the spray produced at different settings be characterized and compared?
- What effect do these different sprays have on the microstructure of the electrode produced?
- How do these different microstructures affect the electrochemical performance of the electrode?

It was therefore imperative to characterize the different sprays that can be produced by this nozzle, with particular emphasis on the mean droplet size. This led to an effort to identify a suitable apparatus for measuring droplet sizes of different sprays, and then the characterization of the Nordson EFD 781S nozzle. The subsequent sections detail the techniques that are available for these measurements.

5.3.1 Droplet size measurement techniques

Measuring droplet size is a challenging task due to the vast number of droplets in a spray and the wide range of velocities and sizes. Ideally, non-intrusive or minimally intrusive processes are preferred to prevent altering or disturbing the atomization process or spray. Additionally, it is important to obtain a large sample size to accurately represent the droplet size distribution within a spray[147]. Numerous drop size measurement techniques are available, and can be grouped into a four broad categories: mechanical, electrical, optical, or acoustic techniques, as summarized in Table 13.

Mechanical methods involve the physical capture of droplets on a media such as a slide, after which the drops are individually measured and counted. Concerns with this method are that the drops flatten upon impact and correction factors must be used.

Furthermore, very small droplets are susceptible to effects of evaporation, which would produce erroneous results [147].

In electrical methods, both charged wire and hot wire techniques measure the impact of a droplet on a wire. In the charged wire technique, a change in the charge is measured. In the hot wire technique, local cooling of the wire causes a change in resistivity, which is measured. Both electrical methods are intrusive. The charged wire method performs well only with high conductivity fluids, and the hot wire method is limited to fluids that will not leave a residue on the wire [156].

High-speed photography is considered to be one of the least expensive and most accurate droplet sizing methods available. Associated challenges are accurately focusing the optics and counting the droplets that are captured in an image.[147]. Based on accuracy, ease of use, cost, and availability, high-speed photography and the hot wire technique warranted further review.

Table 13: Measurement techniques for droplet size[156].

Categories	Methods	Size Range (μm)
Mechanical	Collection of droplets on slides	≥~3
	Cascade impactor	≥~3
	Molten-Wax, frozen drop techniques	
	Mechanical sieving of metal powder	
Electrical	Pulse counting technique	
	Charged wire technique	
	Hot wire technique	1-600
Optical	Imaging Photography	>~5
	Videography	
	Holography	5-1000
	Non-imaging Light-scattering interferometry	5-3000
	Phase-Doppler anemometry	0.5-3000
	Light intensity deconvolution technique	0.2-200
	Light scattering technique	10-250
	Malvern particle analyzer	1-500
	Polarization ratio particle sizer	
	Intensity ratio method	
	Phase optical-microwave method	
	Dual-cylindrical wave laser technique	
Acoustical		5-30

5.3.2 Hot wire technique

In the hot wire technique, a hot wire anemometer is used to measure the velocity and droplet size distribution of a spray. It is an intrusive technique in which a heated, 5 μm diameter platinum wire is introduced into the spray. When a droplet impinges on this heated wire, it reduces the resistance of the wire upon evaporation. This change in resistance is in proportion to the size of the droplet. Each individual measurement takes a few milliseconds; therefore the overall data sampling time is longer in order to collect more sample points for an accurate representation of the size distribution in the spray. From this data, the mean droplet size and spray velocity is calculated.

A KLD labs DC-III hot wire droplet analyzer was used in the drop size and velocity experiments. Operation of the device is a fairly simple procedure: the analyzer module is connected to a computer, the accompanying software initiates a self-test and calibration procedure, sampling time interval and fluid type are selected, and the probe is positioned in the spray. Upon completion of the data collection, a distribution and spray statistics are presented.

It would be pertinent to mention few key limitations of the hot wire technique with respect to the measurement of catalyst ink spray droplet sizes. The hot wire method relies on the evaporation of the drop on the wire, and catalyst inks contain solids and particulate matter. If catalyst inks were to be used, upon evaporation of the solvents, a solid residue would remain. Accumulation of this residue on the wire prevents subsequent droplets from directly contacting the wire surface. Also, it would disrupt the calibration of the instrument, as the algorithms for calculating the sizes are specific to the fluid used, which in the case of the DC-III analyzer, were limited to water and mineral oils.

Another complication of using a hot wire anemometer is the delicate nature of the probe used in the measurement. The probe contains a fine, platinum wire 5 μm in diameter, which must be placed in the spray. This wire is extremely delicate and prone to breakage due to the impact of droplets and handling. It also has to be carefully cleaned in solvents prior to each use, to remove any residue that might have accumulated on the wire surface.

Due to the reasons mentioned, it was very difficult to use the hot wire technique directly with catalyst inks. Instead, it was used for two very important purposes. The first was that the DC-III droplet analyzer was used to probe and identify the velocity of the droplets at different distances from the nozzle. This data was needed in order to identify

the height at which the high-speed camera should be placed for the in-house, high-speed photography based droplet size measurement system. Additionally, it was used to compare results of an atomized water spray with the photography method, details of which are described in the following sections.

Figure 58 shows how the velocity of drops produced by the Nordson EFD 781S nozzle change with the distance at which the probe is placed from the nozzle. Initially the drop velocity is very high, but the drops decelerate due to aerodynamic drag and reach their terminal velocity, as shown in measurements taken at longer distances from the nozzle. Since water was used to measure the velocity, the calibrations in the instrument were not disturbed. The water velocity data was used as a guide to determine the camera distance for the ink experiments.

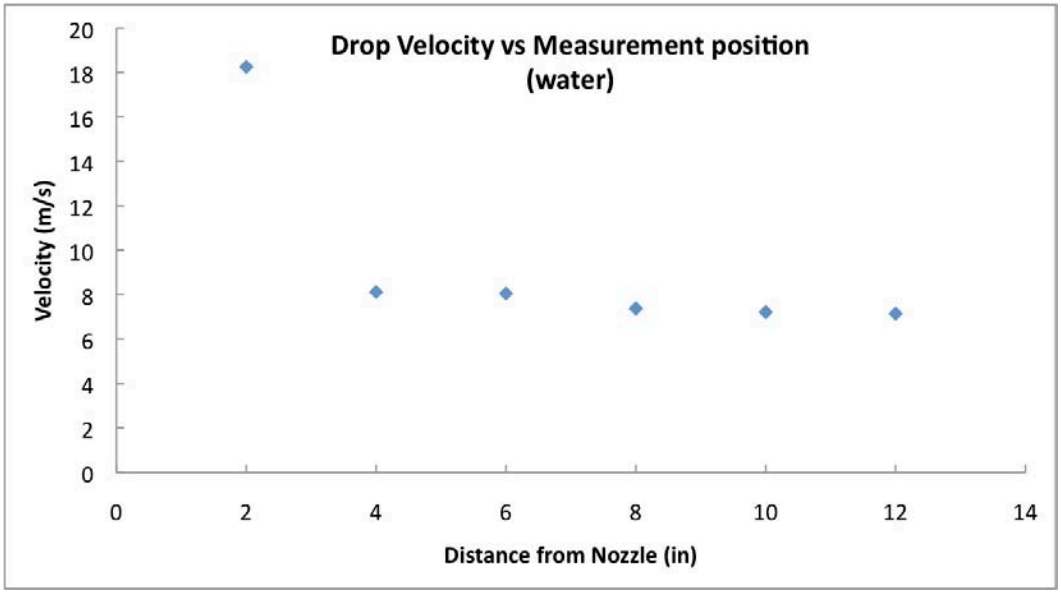

Figure 58: Drop velocity measurements.

The assumption that the catalyst ink would follow similar deceleration as a water drop were proved correct, as there was no evidence of streaking in the catalyst ink photographs. These streaks would have been present if the drop was moving to fast.

5.3.3 Optical method: High-speed photography

There exists a multitude of droplet size measurement technologies based on optical recognition of a droplet. Two main categories are imaging and non-imaging methods. As the name implies, imaging methods involve photography, videography and holography. Other types are identified in Table 13. Of the three imaging methods, high-speed photography offers a significant cost advantage and is considered to be a very accurate method for droplet size measurements.

The goal in high-speed photography is to 'freeze' the motion of a fast-moving object, a droplet in this case, and capture it on a suitable media. In the past, photographic film was used, but as imaging technology has evolved, images are predominantly captured, stored, and analyzed in digital form. Two kinds of techniques can be used to capture such images; the first utilizes a fast light source, which permits the use of a camera with a slower shutter speed. The second method requires the use of a camera with a very high shutter speed and a constant light source. Traditionally, high-speed photography of droplets was done with the first method, by creating a high-intensity light source for an extremely short duration (~1 μs).

The way the first method works is that the photography is conducted in a darkened environment, with the high-speed flash being the only light source. The shutter is kept open (or it can be synced with the flash unit), and the flash is triggered. This momentarily illuminates the spray, and the image is recorded on the capturing media in the camera, after which the shutter is closed. Since the environment is dark, no other image is recorded on the light sensitive image recording media.

The second method utilizes a camera, which exposes the recording media for extremely short durations of time (~1 μs). With modern CCD and CMOS cameras, this is easily achieved by using an electronic shutter, where individual pixels in a camera sensor are electronically triggered, instead of a moving mechanical one. Constant back lighting is required, so that the drops appear as dark objects against a plain background [160].

For the purpose of photographing the atomized spray of catalyst inks used in the manufacture of PEMFC and DMFC fuel cells, we selected the latter method, as it was cheaper to source a camera with a fast shutter than to procure a high-speed flash. As shown in Figure 59, the overall imaging system consists of a constant light source, a camera with an extremely fast shutter, and the necessary optics to magnify the droplets so that they can be successfully measured.

The first step in the measurement process is to capture an image. This is achieved by the optical system, comprised of a high-speed CCD camera (AMAZON IMB-7015G 1/3 CCD 1296x964 pixels), and a 5W LED spot light (Advanced Illumination SL-073). The maximum frame rate of the camera is 30FPS, but the more important parameter is the minimum shutter speed it can achieve: 1 μs, an appropriate shutter speed to photograph the relatively low velocity droplets (~8 m/s) being studied. The camera communicates with a host computer using a gigabit Ethernet connection to ensure fast data transfer and maximum compatibility.

Two interchangeable lens systems were mounted on the camera. The first was for large droplet sizes: a 12.5-75mm Navitar TV zoom lens was used in conjunction with 35mm spacers. The second setup, as shown in Figure 60, involved using a 10X long working distance Mitiyoto microscope objective mounted on a lens tube with 35mm spacers. This setup provided for higher resolution to capture smaller droplet sizes.

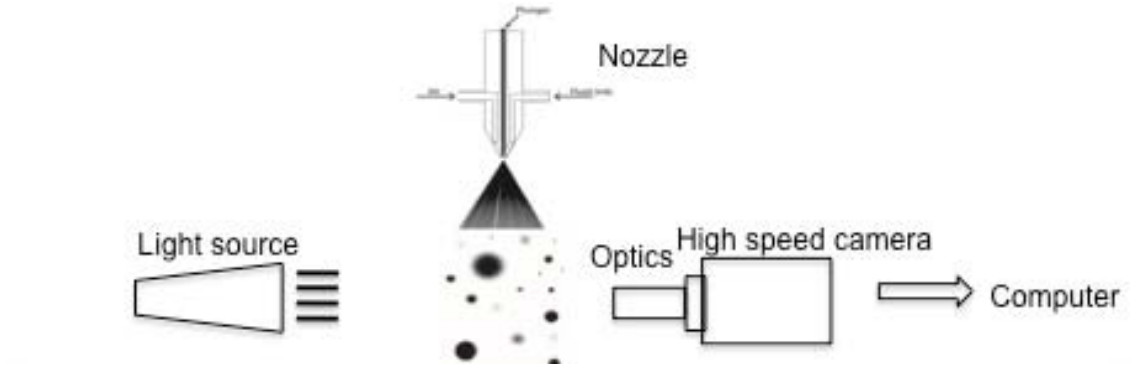

Figure 59: Droplet size measurement system layout.

Once the image was captured, the second step in the droplet sizing process was to analyze the data. Digital image capture and advanced digital image processing algorithms allow image processing to be completed automatically by software[147, 160]. Irrespective of the sizing method used, the net result is a distribution of droplet sizes, from which further calculation produced the length mean diameter (LMD). This number is the arithmetic mean of the droplet size distribution and is useful in droplet size comparison of two sprays. Other 'diameters', such as the surface mean, volume mean, and Sauter mean diameter (SMD), represent the mean surface area, mean volume and volume to surface area ratio of sprays[148]. The choice of this diameter is dependent upon which spray characteristic is of interest. In the case of catalyst ink sprays, the size of different particles is being studied, so the length mean diameter was most relevant.

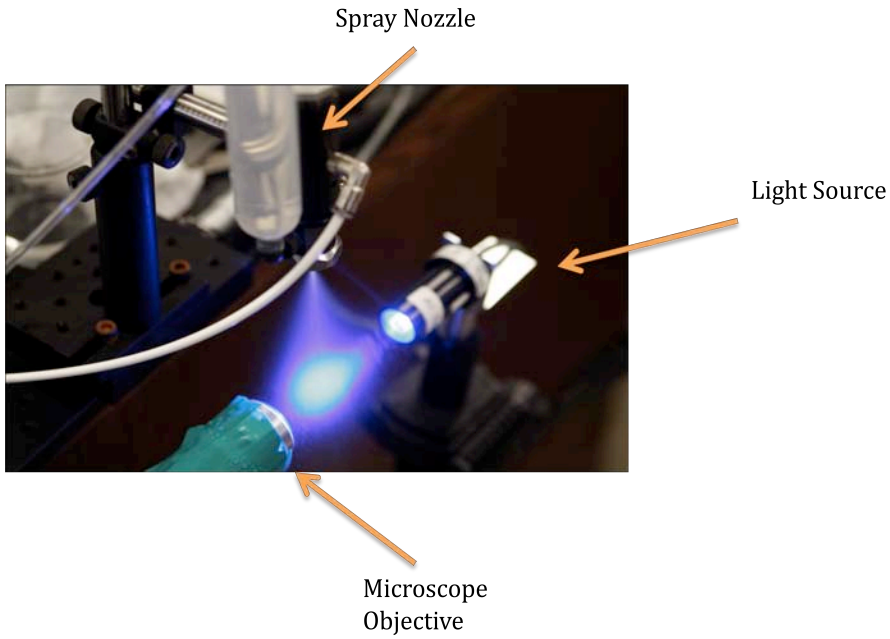

Figure 60: Optical droplet sizing system.

In order to process the image data, *ImageWarp*, an image-processing program from ab-soft.com, aided in automating the process. *ImageWarp* contained prebuilt image processing functions that were pieced together to create a script that detected the edges of droplets within the captured images, processed them, and output the size of each droplet measured.

The first step in processing the image was to apply a median filter on the image, which is a popular technique in digital image processing to remove noise from an image. This was done to remove any artifacts present in the original image. The second step was to perform edge detection on the image, as shown in Figure 61. This is done by identifying closed contours in the image, which are in the general shape of a circle, and then separate them from the background. The *ImageWarp* software came with prebuilt functions that performed these actions. Once these edges are isolated, they are filled with an area and then classified according to their size. The final step was to display the

detected drops as an overlay on the original image and output a distribution of the diameter of drops detected in the image.

Hundreds of images were processed to produce a droplet size distribution, which consist of at least 5000 data points. This is required for an adequate representation of the spray.

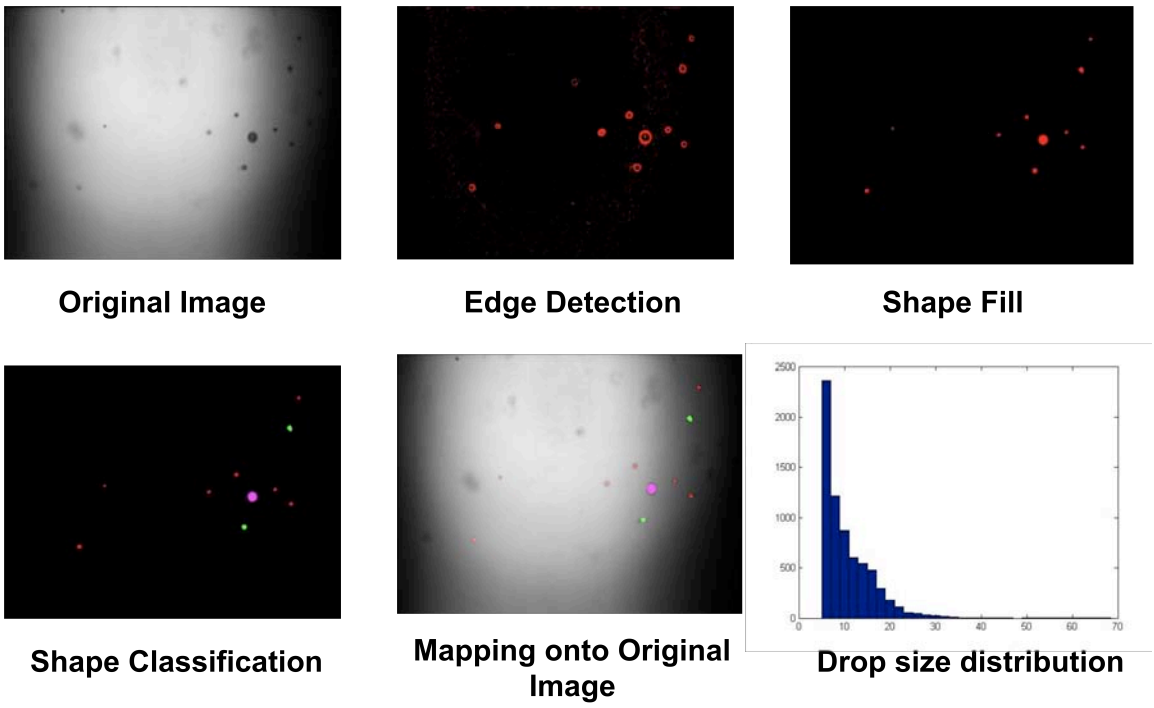

Figure 61: Image processing steps.

5.3.4 Comparison of results obtained by hot wire method and optical method

As described earlier, the hot wire method's applicability was extremely limited due to the fact that it was incompatible with catalyst inks, due to their solid content depositing on the platinum wire, and thereby corrupting data measurements. This method does contribute to the ability to corroborate the results of the high-speed photography apparatus by comparing results of each method, using water as the medium.

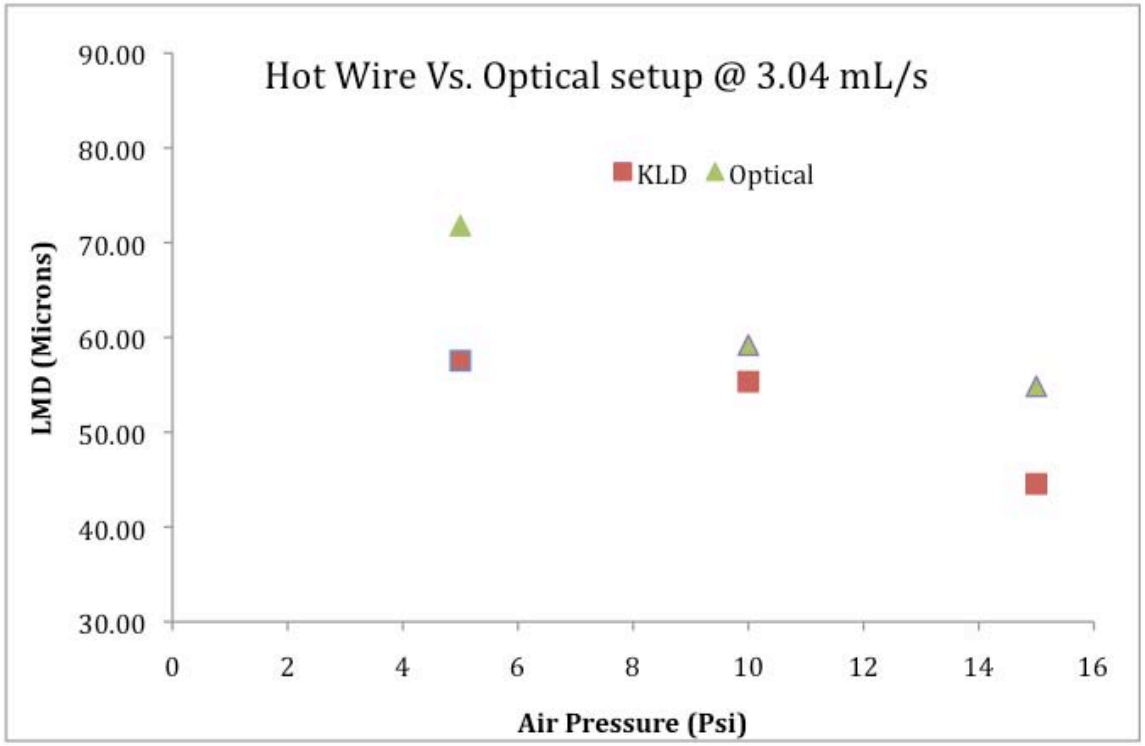

Figure 62: Comparison of results produced by hot wire method and high-speed photography method.

Figure 62 shows the length mean diameter (LMD) results of a spray produced by the Nordson EFD-781S nozzle at various pressures, measured by both apparatuses, using water as the fluid. The figure indicates that there is good correlation between the data. The results produced by the hot wire anemometer are consistently lower than that of the high-speed photography setup, an observation that has also been noted in prior studies comparing different droplet-sizing instruments [161].

5.4 NOZZLE CHARACTERIZATION

The result of this experimental development is to create and validate the tools that will allow us to study and characterize the effects of changing the control parameters of

the nozzle. To this end, a high-speed photography setup has been devised and calibrated to measure the droplet diameters of the spray produced.

As mentioned in the initial description of the spray technique, there are three control parameters of interest: the atomizing air pressure, fluid pressure, and plunger setting. In order to characterize the nozzle, the first step is to control the flow rate of the fluid that is being atomized. One would infer that, ideally, the flow rate would be a function of the nozzle orifice area through which the fluid is discharged, as controlled by the plunger setting, and the fluid pressure; however, this an external mixing nozzle, and the fluid exits the nozzle orifice in the midst of a stream of pressurized air. Therefore, there might exist interactions between the fluid flow rate and the atomizing air pressure, which could influence the flow rate of the ink. The first section of this chapter studies this interaction and presents an empirical model for the flow rate of this nozzle.

Subsequent sections discuss the formulation and key characteristics of surrogate inks, which are used instead of the actual catalyst ink to save on the expensive noble metal catalyst used. The final section presents empirical models for three different fluids used as media for the nozzle in question. These models facilitate identification of the different droplet sizes possible at different control parameter settings.

5.4.1 Flow rate model

In the context of spraying catalyst inks onto a substrate, the flow rate and the velocity of the spray nozzle relative to the substrate (moving substrate, stationary nozzle or moving nozzle, stationary substrate) determines the wet layer thickness, which defines the catalyst loading on the electrode. Also, the amount of ink that is deposited onto the substrate must be subsequently dried; therefore it is of considerable value to accurately control the fluid flow rate.

A design of experiments (DOE) approach was taken to identify possible coupled effects between the different control variables and the response. There were three control parameters: air pressure, fluid pressure, and plunger setting. An experiment was designed in which these parameters were varied systematically to determine the response, *i.e.* the flow rate. A 2^k factorial design was selected, where k factors were run at 2 levels. The experimental design used is shown in Table 14.

Table 14: Experimental design for 2^3 flow rate model.

Run	Fluid Pressure	Area	Air Pressure
1	-	-	-
2	+	-	-
3	-	+	-
4	+	+	-
5	-	-	+
6	+	-	+
7	-	+	+
8	+	+	+

In the present case, k=3, as there are three factors. The general linear regression model used to fit this data was:

$$y = \beta_0 + \beta_1 x_1 + \beta_2 x_2 + \beta_3 x_3 + \beta_4 x_1 x_2 + \beta_5 x_1 x_3 + \beta_6 x_2 x_3 + \beta_7 x_1 x_2 x_3$$

x_1, x_2, x_3, represent the model variables and $\beta_o \ldots \beta_7$ represent the regression coefficients that were calculated during model fitting. Four replicates were run for each setting for a total of 32 observations, actual data from the experiment is attached in Appendix A. Analysis of variance (ANOVA) is a collection of statistical techniques used to determine the significance of factors and interactions in a DOE study. Table 15 shows the ANOVA table for the flow rate empirical model fit to the linear regression model described above. F_o and p-statistics are shown. The F-test is a statistical test used to compare the variances of two populations [154]. If a model is being fit with the least

squares method, the F-test is used in the ANOVA study to determine the significance of the factor under study to the overall model. The F_o value of a factor is computed and compared against tabulated values of critical $F_{a-1,N-a}$(for a given significance level α, and DOFs, a-1 is the degree of freedom of the numerator, N-a is the degree of freedom of the denominator or the error).

$$F_o = \frac{MS_R}{MS_E}$$

Where:

MS_R = Mean square of regression

MS_E = Mean square of error

If the values of $F_o > F_{a-1,N-a}$ then that factor has a significant contribution to the model, otherwise it can be neglected. For the factors in this model, $F_{7,24} = 2.423$ (α=0.05). The *p*-test is a statistical test, which determines the probability of the value being tested to occur (at the given confidence level). In the ANOVA table, *p*-values are also calculated for the different factors and their interactions, and were compared against p=0.05, which represents a 5% significance level in the data. After comparison it was observed that the F_o and *p* values that 'fluid pressure', 'area' and their interaction 'fluid pressure*area' were the only variables that contribute to the model, and that the tests are significant at α=0.05. The other variables were rejected from the model. As observed air pressure does not contribute to the flow rate, which is explained by the fact that nozzle used is an external mixing nozzle,

Table 15 ANOVA table for flow rate model.

Source	Degrees of Freedom	Sum of Squares	Mean Square	F_o	P
Fluid Pressure	1	0.83044	0.83044	27681.333	0.000
Area	1	2.84829	2.84829	94943	0.000
Air Pressure	1	0.000034	0.000034	1.133	0.298
Fluid Pressure*Area	1	0.14298	0.14298	4766	0.000
Fluid Pressure*Air Pressure	1	0.00002	0.00002	0.667	0.422
Area*Air Pressure	1	0.00004	0.00004	1.333	0.259
Fluid Pressure*Area*Air Pressure	1	0.00002	0.00002	0.667	0.422
Error	24	0.00078	0.00003		
Total	31	3.82291			

On the basis of the results the following model was generated:

$$\dot{V} = -0.140 - 0.0193\, P_f + 0.0352\, N + 0.0110\, P_f N$$

Where

P_f= Pressure of fluid

N = Plunger setting (effective area of nozzle orifice)

5.4.2 Model Adequacy Checking

It is important to inspect the fitted empirical model to ensure that it provides an accurate representation of the actual system, also that any assumptions of the least square regression process used to fit the model are not violated [162].

5.4.2.1 Residual Analysis

Residuals play an important part in evaluating the adequacy of a model fit by the least squares method. A residual is defined as:

$$e_i = y_i - \hat{y}_i, \quad i = 1,2,...n,$$

where:

y_i = *actual response*

$\hat{y}_i$ = *model response*

Fundamental assumptions made in the least squares method used in the regression analysis are that the errors in the observations are independent, normally distributed and have equal variance at each value of the independent variable. A normal probability plot as shown in Figure 63 can check the normality assumption. It is calculated by arranging the residuals data in ascending order, and calculating the *z*-scores for each residual and plotting it. If the residuals lie in an approximate straight line, as can be seen from the normal probability plot of the model in question, this assumption is clearly satisfied.

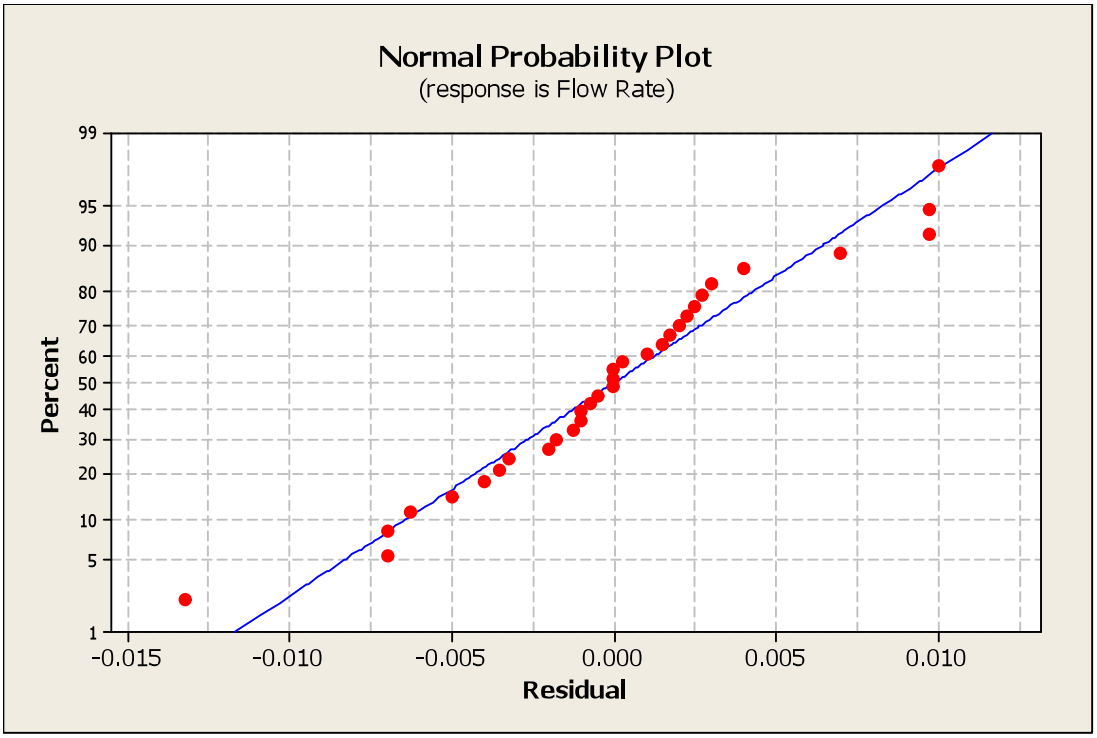

Figure 63: Normal probability plot, flow rate model.

A plot of residuals versus the response shows the variance of the error in the original response. To apply the least squares method, it was assumed that this variance is constant. A horizontal band like pattern would show constant variance, whereas increasing or decreasing variance would disprove the original assumption. For the flow rate model, Figure 64 shows that the residuals lie in an approximate horizontal band shape; hence this model satisfies the assumption of constant variation.

A plot of residuals vs. run order identifies correlation between residuals, which would violate the independence assumption. Figure 65 shows the residual vs. observation order plot for the flow rate model. No patter was identified, implying that no correlation exists between the residuals and they are independent of each other.

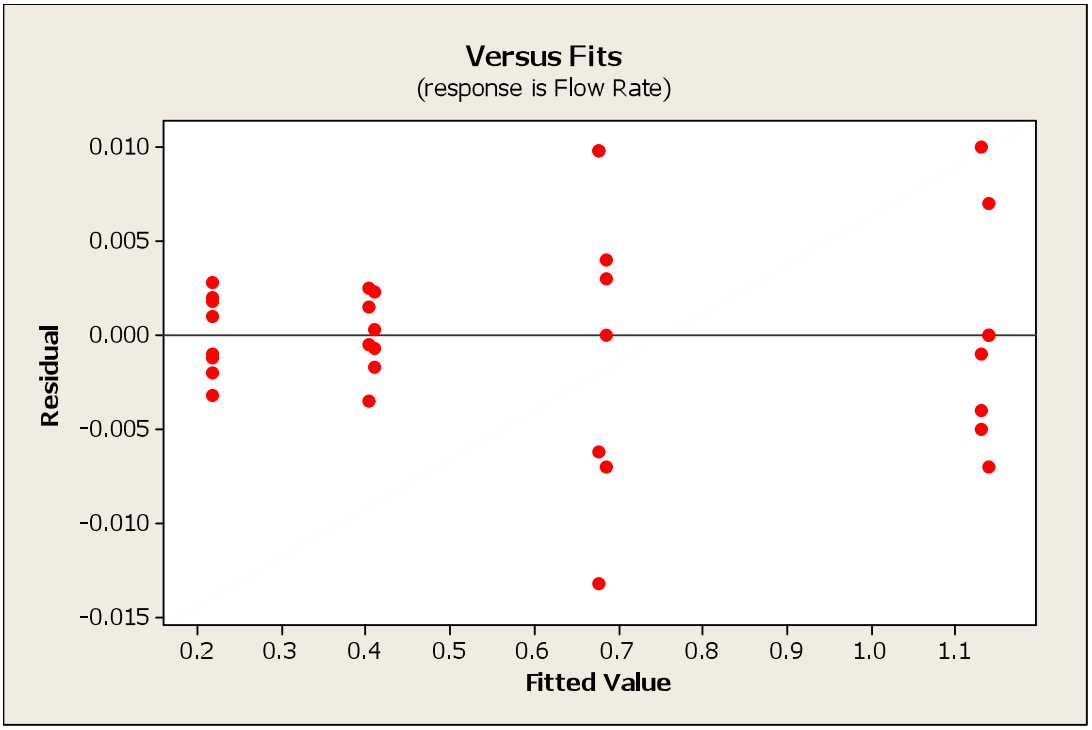

Figure 64: Residual vs. response, flow rate model.

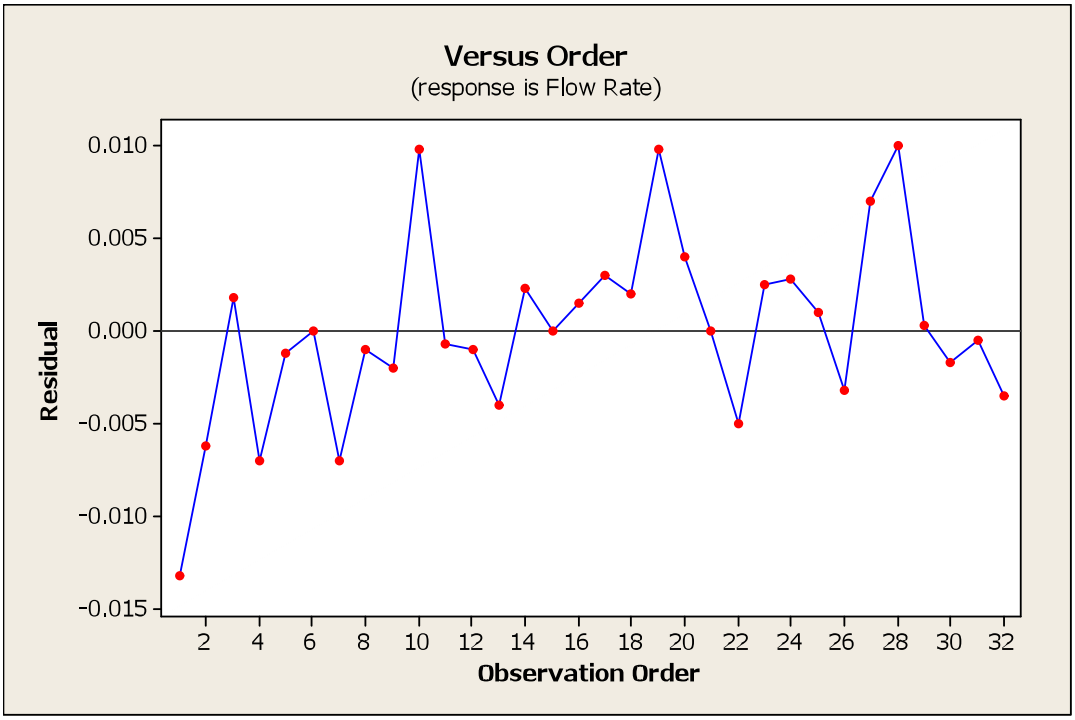

Figure 65: Residual vs. observation order, flow rate model.

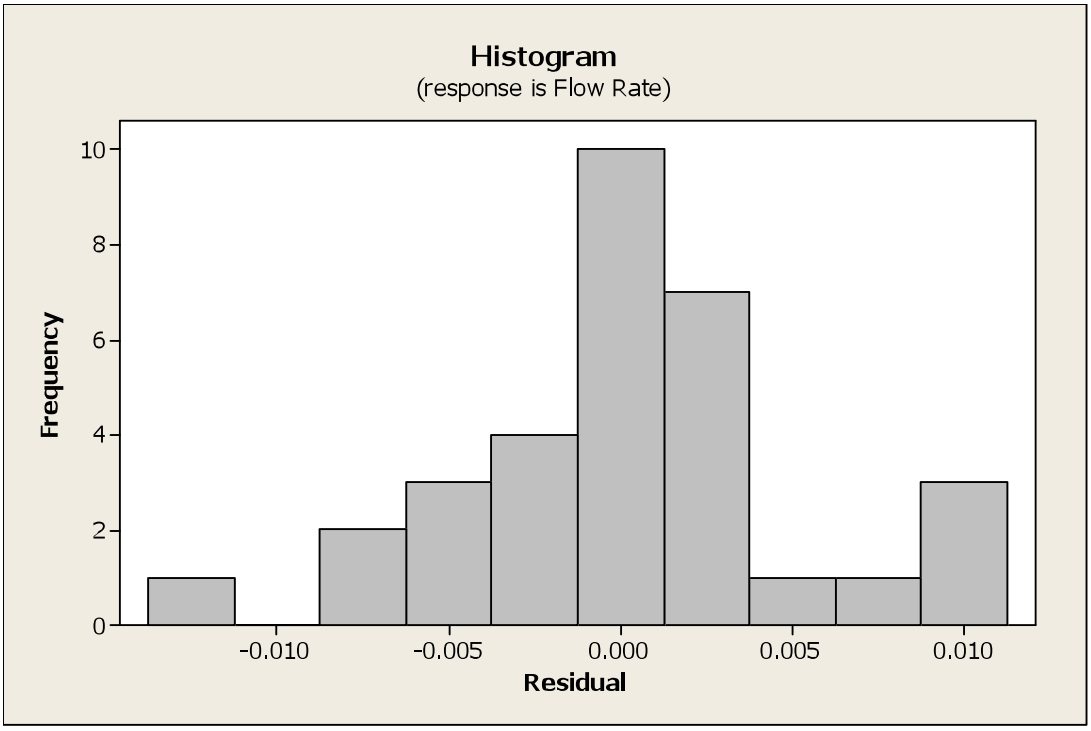

Figure 66: Histogram of residuals plot of flow rate model.

A histogram of residuals is a frequency plot, which shows the distribution of the residuals; ideally it should approximate a normal distribution. As shown in Figure 66, the flow rate model residuals did resemble a normal distribution. This showed that the variance was normally distributed.

Results of the linear regression model for the flow rate data are visually presented in Figure 67. Volumetric flow rate of water was calculated for three different pressure settings and three different plunger settings, which represents the open area of the nozzle orifice. The flow rate increases with increasing fluid pressure and increasing plunger setting value.

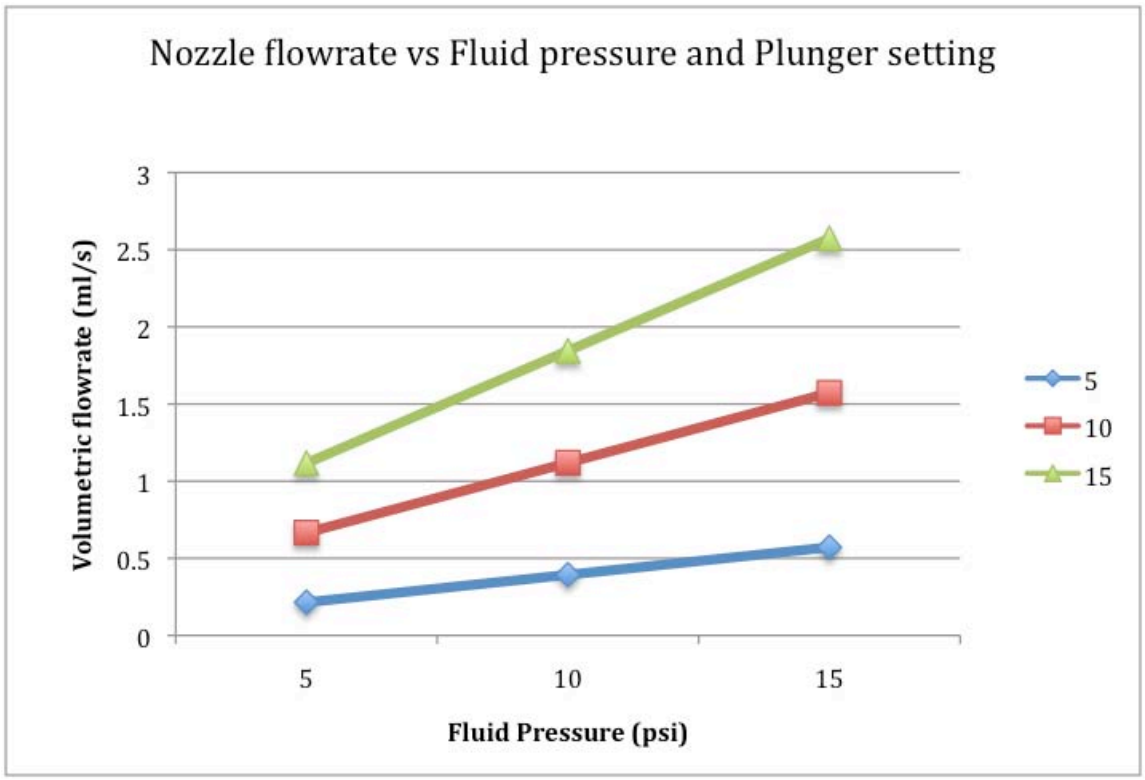

Figure 67: Nozzle flow rate model (Water).

5.4.3 Surrogate inks for spraying experiments

After identifying the relationship between flow rate and plunger setting, the next stage in the nozzle characterization process was to study the spray characteristics of the nozzle with various fluids: water and catalyst inks of various solid contents. The aim behind these experiments was to identify the relationship between drop sizes, air pressure and flow rate. Fluids of different viscosities were studied so that the impact of changing viscosity on the drop size could also be identified.

The volume of catalyst ink required to perform these experiments would be substantial and an enormous amount of platinum catalyst would have to be used to produce these inks, which would go to waste once it had been sprayed from the nozzle. In

order to save on the catalyst costs, it was decided to design surrogate inks, which would emulate the performance of catalyst inks.

Catalyst inks used in PEMFC and DMFC manufacture, can contain supported or unsupported nanometer-sized noble metal particles[12, 43]. Supported catalysts are essentially larger carbon particles onto which the catalyst particles are attached. This allows for better dispersion and utilization of catalyst in the electrode layers. They range from 20% to 80% noble metal loading, where 0% is carbon black and 100% is pure catalyst black. Other constituents of the catalyst inks are a suitable amount of ionomer, and solvents (typically water and IPA). Bearing this information in mind, it was considered that ink made purely of carbon black, along with the necessary ionomer and solvents, would closely represent the characteristics of catalyst inks used in PEMFC and DMFC, and could be used to emulate its behavior during spraying.

A variety of carbon inks were created, containing between 2% and 10% suspended carbon and Nafion solid content, and the viscosities of these inks were studied. The purpose of the carbon ink viscosity experiment is to determine a correlation between the ink solid content and its viscosity. The viscosity instrument used was a Brookfield DV-E Viscosity Meter with the number 18 spindle. A constant temperature of 22°C was maintained since viscosity is a strong function of temperature [163].

.

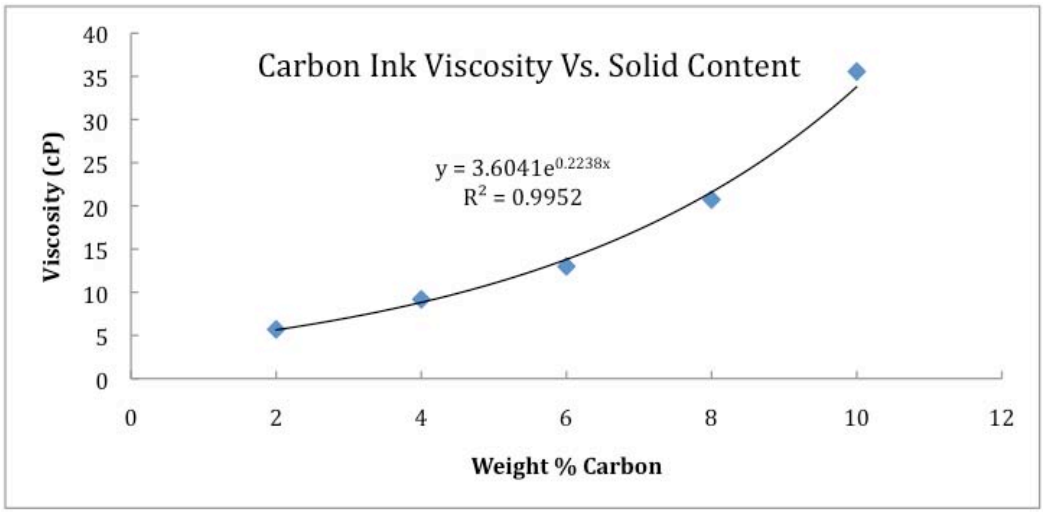

Figure 68: Carbon ink viscosity vs. Ink solid content.

Figure 68 shows how the ink viscosity increases nonlinearly as the overall solid content of the ink solution is increased. These results are as expected, and the trend can be attributed to the increasing polymer (Nafion) content. This data will contribute to developing an understanding as to how the nozzle spray characteristics change with varying solid content of the inks. Understanding of this relationship would be critical to tailor the manufacturing process for inks of various solid contents. Controlling the spray characteristics is necessary to regulate the amount of catalyst per sprayed layer, potentially to reduce the requisite number of layers to achieve a specific electrode loading.

5.4.4 Droplet size models

Having reduced the three control parameters of the nozzle into two variables, namely the flow rate and atomizing air pressure, a study was conducted to ascertain how the spray characteristics changed with these variables. The length mean diameter (LMD) is used to reduce the droplet size distribution obtained into a single number, so that a

spray produced at one setting can be compared with another produced at a different setting.

Figure 69 depicts such a scenario, in which three different sprays of water are produced, by increasing the atomizing air pressure at from 10 psi, to 20psi and then 30 psi. The larger droplet sizes of the 10psi spray are clearly identifiable in the first picture, whereas the last picture, which shows a spray produced at 30psi, appears to have a much finer spray. The image I the upper right corner shows an actual spray exiting from the nozzle orifice.

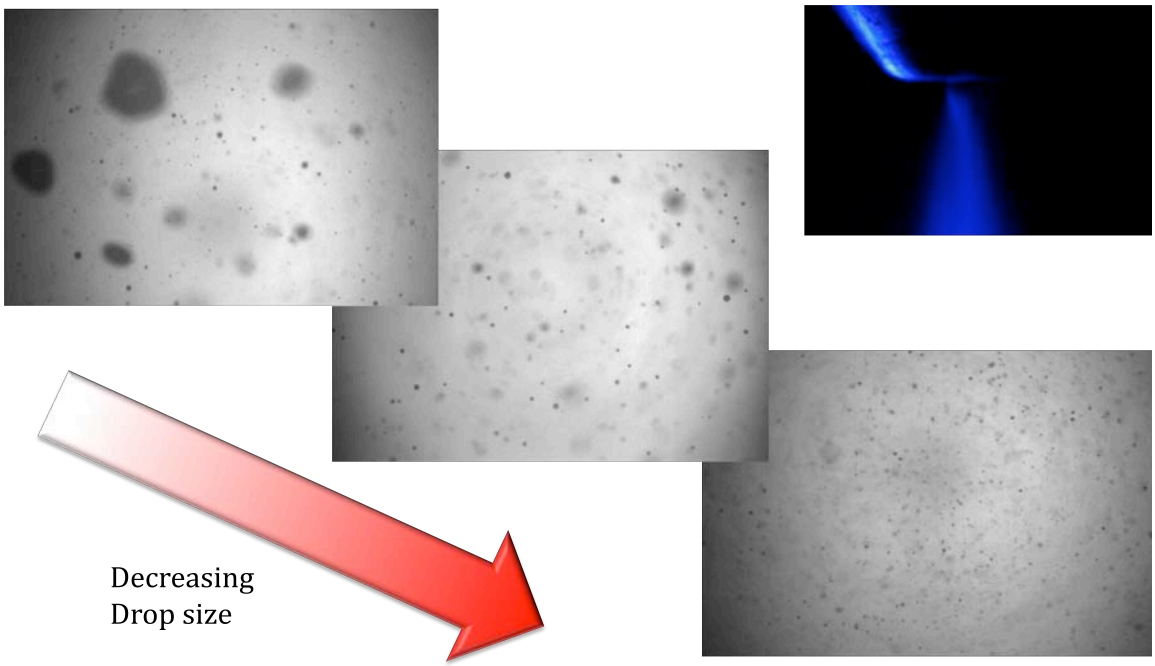

Figure 69: Changes in spray characteristics with spray pressure.

An experiment was designed and a second order model was fit to the resulting data to create a model to predict the LMD of a spray as a function of air pressure and fluid flow rate. A 3^k design was used (where k=2) with two replicates for a total of 18

readings. Three fluids were characterized: water, 2% solid content ink, and 4% solid content ink. The general form of the second order regression model used was [164]:

$$y = \beta_0 + \beta_1 x_1 + \beta_2 x_2 + \beta_3 x_1 x_2 + \beta_4 x_1^2 + \beta_5 x_2^2$$

The experimental design used is shown in Table 16. Actual data for the experiments is attached in appendix A.

Table 16: Experimental design for 3^2 droplet size (LMD) model.

Run	Flow Rate	Air Pressure
1	-	-
2	-	0
3	-	+
4	0	-
5	0	0
6	0	+
7	+	-
8	+	0
9	+	+

5.4.4.1 Water droplet size model

A 3^2 (three level, two factor) experiment was conducted to determine the LMD values of sprays produced by changing the flow rate and atomizing air pressure of the spraying nozzle. Table 17 shows the ANOVA table for the data that was fit to a linear regression model, using the least squares method. The fluid used in this experiment was water. The F-test, and p-statistic were used to identify significant variables and their interactions. The condition for these test were that, $F_o > F_{5,12} = 3.106$ (α=0.05) and $p < 0.05$ in order to be considered significant.

Table 17: ANOVA table for droplet size model with water.

Source	Degrees of Freedom	Sum of Squares	Mean Square	F_o	P
Flow rate	1.000	1556.800	1556.800	43.244	0.000
Air Pressure	1.000	8781.500	8781.500	243.931	0.000
Flowrate*Air Pressure	1.000	1651.400	1651.400	45.872	0.000
Flowrate^2	1.000	31.500	31.500	0.875	0.520
Pressure^2	1.000	214.500	214.500	5.958	0.005
Error	12.000	432.300	36.025		
Total	17.000	12668.000			

Based on the F-test and the p-statistic, certain variables were eliminated and the calculated model was

$$\underline{Water}$$

$$LMD = 87.1 + 0.106\,\dot{V} - 4.05\,P_a - 0.00325\,\dot{m}P_a + 0.0732\,P_a^2$$

Where

P_a = Pressure of atomizing air (psi)

$\dot{m}$ = Mass flow rate of fluid (mg/s)

In order to check the adequacy of the model, residual analysis was conducted, the results of which are shown in Figure 70. The normal probability plot shows a linear trend, residual vs. fits, resembles a horizontal band, the frequency plot resembles a normal distribution and there are no patterns in the residual vs. observation order plot. All these observations conclude that the model is adequate and the variables that have been identified are significant.

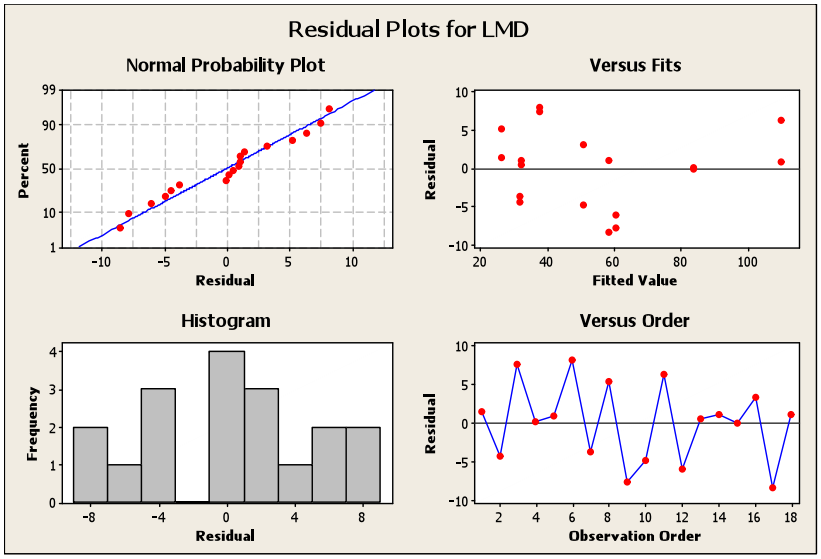

Figure 70: Residual plot for droplet size model with water.

5.4.4.2 Ink droplet size model: 2% SC

The previous experiment was repeated with 2% SC carbon black ink as the fluid. The ANOVA table for this experiment is presented in Table 18. The F-test and p-statistic were used to identify significant variables, which would satisfy the conditions $F_o > F_{5,12} = 3.106$ (α=0.05) and $p < 0.05$.

Table 18: ANOVA table for droplet size model with 2% SC Ink.

Source	Degrees of Freedom	Sum of Squares	Mean Square	F	P
Flowrate	1.000	1538.300	1538.300	16.612	0.000
Air Pressure	1.000	5056.500	5056.500	54.606	0.000
Flowrate*Air Pressure	1.000	331.200	331.200	3.577	0.030
Flowrate^2	1.000	0.600	0.600	0.006	0.990
Pressure^2	1.000	1.300	1.300	0.014	0.990
Error	12.000	1111.700	92.642		
Total	17.000	8039.600			

The regression model calculated is:

$$\underline{2\%\ Solid\ Content\ Carbon\ Ink}$$

$$LMD = 54.1 + 0.158\,\dot{V} - 1.62\,P_a - 0.00435\,\dot{m}P_a$$

Where

P_a = Pressure of atomizing air (psi)

$\dot{m}$= Mass flow rate of fluid (mg/s)

Results of a residual analysis conducted are shown in Figure 71. No anomalies are detected, and the model variables identified were considered significant.

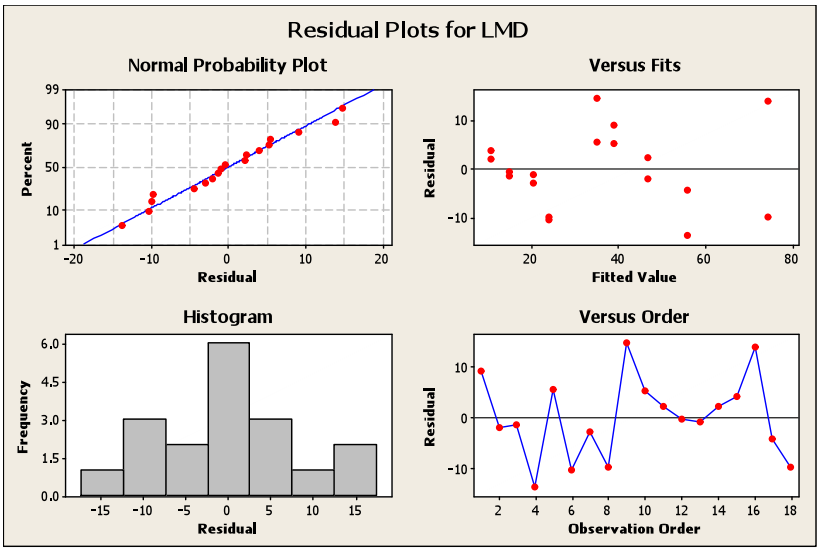

Figure 71: Residual plot for droplet size model with 2% ink.

Ink droplet size model: 4% SC

Similar to the previously tested fluids (Water and 2% SC ink), the same experiment was repeated with 4% SC ink. ANOVA results are shown in Table 19 and Figure 72 shows residual analysis performed to ascertain the quality of the fit.

Table 19: ANOVA table for droplet size model with 4% SC Ink.

Source	Degrees of Freedom	Sum of Squares	Mean Square	F	P
Flowrate	1.000	2784.700	2784.700	152.169	0.000
Air Pressure	1.000	3472.400	3472.400	189.749	0.000
Flowrate*Air Pressure	1.000	1483.100	1483.100	81.044	0.000
Flowrate^2	1.000	15.000	15.000	0.820	0.558
Pressure^2	1.000	62.900	62.900	3.437	0.036
Error	12.000	219.900	18.325		
Total	17.000	8038.000			

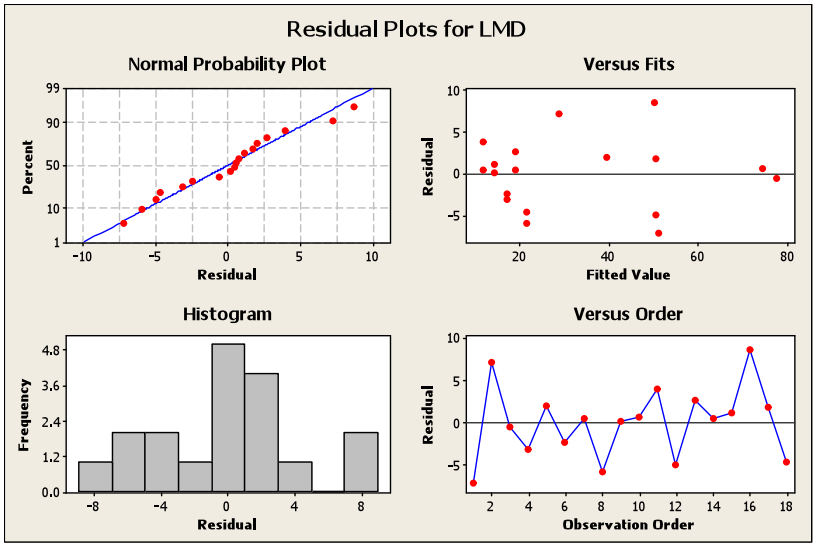

Figure 72: Residual plot for droplet size model with 4% ink.

The predicted model is:

$$\underline{4\%\ Solid\ Content\ Carbon\ Ink}$$

$$LMD = 9.44 + 0.314\,\dot{V} + 1.28\,P_a - 0.0092\,\dot{m}P_a - 0.001\,\dot{m}^2 - 0.0397\,P_a^2$$

Where

P_a = Pressure of atomizing air (psi)

$\dot{m}$ = Mass flow rate of fluid (mg/s)

Based on the residual analysis it can safely be concluded that the predicted model will provide an accurate representation of the physical processes.

5.4.5 Analysis of droplet size models

The predicted response of these models is visually depicted in Figure 73, where a three-dimensional plot is used to show the dependence of the length mean diameter on the two variables, air pressure and fluid flow rate. There are three surfaces shown in the plot. The top surface represents water, the middle represents a 2% solid content ink and the bottom surface represents a 4% solid content ink. A close correlation is clearly evident by comparing these three surfaces. As the viscosity of the fluid increases, the LMD values are lower for the same air pressure and fluid flow rate settings.

What this implies is that a fluid of higher viscosity produces smaller droplets. Upon cursory observation, this seems entirely incorrect, as a more viscous fluid should require more energy for atomization. The viscosity of a liquid has been noted to exert a significant influence on the average drop size of a spray, the size decreasing with decreasing viscosity [165]. But there is a key difference between the carbon inks and water. More than half of the ink is composed of isopropyl alcohol (IPA), which has a much lower boiling point than that of water. It can be reasoned that as the atomization process increases the surface area of the fluid, by creating thousands of tiny droplets, the rate at which the alcohol content is evaporating is increased tremendously and the droplet loses volume. So at the point at which the measurement is made, an ink droplet could be smaller than a water droplet produced at the same air pressure and flow rate settings.

Another contributing factor to the smaller drop sizes produced by ink is that IPA lowers the surface tension of water. The primary force resisting the drop formation process in a liquid is surface tension. As the surface tension of inks is lower, it could be

hypothesized that they will require less energy for atomization, or for the same energy have a higher degree of atomization, as shown in the model.

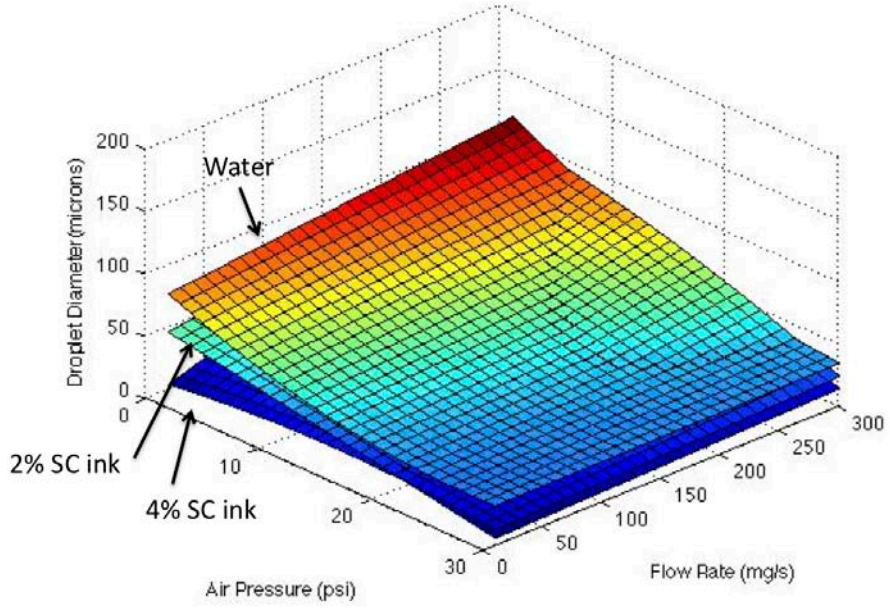

Figure 73: Change in LMD with air pressure and fluid flow rate.

Another observation is that increasing the air pressure decreases the droplet size. The same trend is observed across all the fluids, starting from water to 4% SC ink. This implies that air pressure is a key driver of droplet size, which in turn could possibly affect the electrode microstructure. This observation is consistent with what was expected, as a higher pressure would provide more energy for atomization, thereby producing finer droplets. Also it can be observed that as the flow rate is increased, while keeping the pressure constant, the drop size increases. We propose the following explanation: as the pressure is held constant, the atomizing energy remains the same, but the amount of liquid to be atomized per unit time increases; hence, less energy is transferred to the fluid on a mass basis, producing larger droplets.

The utility of these models for the spraying process of catalyst ink onto substrates during the fabrication of PEMFC and DMFC electrodes is that it allows for a clear identification of what droplet sizes can be expected, and how the spray can be made 'finer' or 'coarser'. What influence the spray size has on the electrode structure and its performance is discussed in detail in the next chapter.

5.5 CHAPTER SUMMARY

This chapter begins with a description of atomization process and atomizers in general, in order to justify the selection of a two fluid air-assist nozzle, which was used to deposit catalyst inks onto a substrate. It was shown that varying nozzle control parameters, specifically the fluid flow rate and atomizing air pressure, could produce sprays with different characteristics. In order to quantify and quantitatively differentiate between different sprays, a droplet size measuring apparatus, based on high-speed photography, was built. Using this apparatus, the nozzle performance was characterized with different fluids, and an empirical model fit to the data to predict its response under different operation conditions.

6. DMFC MEA fabrication, testing and optimization

It is important to fabricate and study DMFC MEAs in which the electrode has been fabricated by the spraying process. Such a study would allow for the optimization of key parameters that affect the spraying process in relation with the electrochemical performance of the electrode produced by this process.

6.1 INTRODUCTION

Previous chapters describe the function, components and types of MEAs in elaborate detail. This chapter focuses on describing the actual MEA fabrication process in a laboratory environment. The type of MEA that has been chosen for manufacture is a catalyst coated membrane (CCM) fabricated by the decal transfer method (DTM)[28, 43]. Although the CCM-DTM process involves an extra step, which is the transfer of electrodes from the decal substrate onto the ionomer membrane, it helps avoid the problem of membrane swelling, which happens when a wet coating is directly applied onto the ionomer membrane (typically Nafion)[37].

6.2 DMFC MEA FABRICATION

DMFC MEA fabrication by the decal transfer method consists of a few steps, which are: membrane preparation, electrode fabrication, electrode transfer, and finally the attachment of diffusion media on the 3 layer MEA produced so far, to form a 5 layer MEA. This chapter details the actual experimental procedures used, which will be used towards the development of the continuous MEA manufacturing process.

6.2.1 Membrane preparation

The ionomer membrane of choice for DMFC MEA fabrication is Nafion, which is a perfulorsulfonic acid/PTFE copolymer in the acid (H^+) form [15]. It is available in a variety of thicknesses and equivalent weights (EW). The EW is the weight of Nafion per mole of the sulfonic acid group (SO_3H). The naming scheme for Nafion is such that, for example in N117 membrane, the first two digits represent the EW, which in this case is 1100, and the last digit, 7 refers to the membrane thickness in mils.

Typically membrane preparation for MEA manufacture involves two steps. The first is cleaning the membrane to remove any unwanted substances and the second step is the re-protonation process, by which it is ensured that the membrane is in the acid (H^+) form. H^+ form refers to the sulfonic acid group in the ionomer membrane. Its presence is necessary for proton transfer between the two electrodes of a fuel cell. The cleaning process involves boiling the membrane in hydrogen peroxide for an hour and then boiling it in deionized water for an hour. The re-protonation process requires the boiling of the membrane in 0.5 M or 1 M sulfuric acid for one hour and then boiling in deionized water for one hour [166].

Some researchers convert the H^+ form membrane into Na^+, K^+ or TBA^+ form by treating with sodium hydroxide (NaOH), potassium hydroxide (KOH) or tetrabutylammonium hydroxide (TBAOH) for additional mechanical strength during the electrode fabrication process. If such a path is taken, the membrane in the MEA has to be re-protonated by boiling in sulphuric acid and then water as was described above [26, 29].

The membranes used in the experiments presented in this section were prepared by the first method, that is boiling in hydrogen peroxide for one hour, then boiling in

water for one hour, followed by boiling in 1M sulphuric acid for one hour and finally boiling in water for one hour.

6.2.2 Ink formulation

Catalyst ink is comprised of a the following components

- Catalyst, which can be supported or unsupported platinum and platinum ruthenium
- Binder, which is an ionomer (Nafion solution) in the case of thin film electrodes
- Solvents, typically water and alcohols (Isopropyl alcohol, Ethanol, Methanol)
- Additives, such as pore formers (Lithium carbonate, Ammonium carbonate)

In the case of PEMFC electrodes carbon-supported platinum catalyst (20% to 80% noble metal content) are preferred [26], whereas in the case of DMFC electrodes unsupported Pt-Ru is used for the anode and unsupported Pt is used on the cathode[18, 40, 43]. HiSPEC^{TM} 6000, platinum ruthenium black Pt:Ru 50:50 atomic wt %, procured from Alfa Aesar was used as the anode catalyst material, whereas platinum black (high surface area) also procured from Alfa Aesar was used as the cathode catalyst material.

As defined earlier, the solid content (SC %) of ink represents the amount of total solids in ink. Higher loadings can be deposited in a single layer, if inks with a higher solid content are used. Our experimentation revealed that for spraying, best results were obtained by preparing 4% SC inks. Thicker inks were prepared and sprayed, but they had

a tendency of clogging up the spray nozzle. All inks prepared and used for the experiments presented in this section have a 4% solid content.

An equal ratio (1:1) mixture of water and isopropyl alcohol (IPA) was used as a solvent in the ink. A 5% solution of Nafion was used as the binder. Typically ionomer content was kept at 10 wt% of the catalyst weight, for inks used in the preparation of both the anode and the cathode. A Nafion content optimization study was also conducted in which the Nafion amount was systematically changed to identify the optimal amount, results of which will be discussed in the coming sections.

6.2.3 Electrode fabrication

Electrode fabrication involves the application of catalyst ink onto a suitable substrate. For the DTM method, typically Teflon, fiberglass reinforced Teflon and Kapton films are the substrates of choice [26, 28, 29, 46]. Besides a requirement to withstand the temperature and mechanical environment of spraying and the subsequent step of hot pressing, which is necessary for the transfer of the electrode from the substrate to the membrane, the most important characteristic is the release properties of the substrate. Once the electrode is dried on the substrate it is hot pressed onto a Nafion membrane, and it must release the electrode to allow it to adhere onto the Membrane to form the MEA. All three substrates were examined and transfer tests were done, from which Kapton was selected as it consistently yielded complete transfers of the dried electrode onto the membrane.

Depending on the area of the electrode to be fabricated, suitably sized substrate tokens are cut out and their initial mass is recorded. After that they are affixed onto a vacuum table that is maintained at a constant temperature of 60 ºC [43]. A mask is affixed onto the vacuum plate, which has an area of the desired electrode size cut out of it. This allows for clean edges of the electrode, and ensures that the catalyst ink is only

deposited in the desired area. Also this area is important for the catalyst loading calculation.

Initially spraying was performed on the modular coating test bed with the two-fluid external mixing Nordson EFD-781S nozzle. It was considered advantageous that for the purpose of further experimentation and optimization, that the spraying module be extracted from the test bed and installed in its own chassis, which could be placed inside a fume hood. For this purpose a 2-axis a computer-controlled machine was constructed, as shown in Figure 74 with degrees of freedom in the x and y coordinate axis. This provided for a mounting platform for the nozzle and corresponding armature to allow for fine-tuning of the nozzles' aim and to adjust the working distance of the nozzle from the material. As shown in the figure, the spraying nozzle was positioned above a heated vacuum mounting plate. The nozzle was driven by a Nordson EFD ValveMate 8040 controller, which permitted for the triggering of the nozzle, when instructed by a host computer. The host computer controlled the motion of the nozzle head mounted on the X-Y table and synchronized it with the nozzle triggering at the desired locations. In this fashion the desired geometry of the electrode was sprayed onto the substrate.

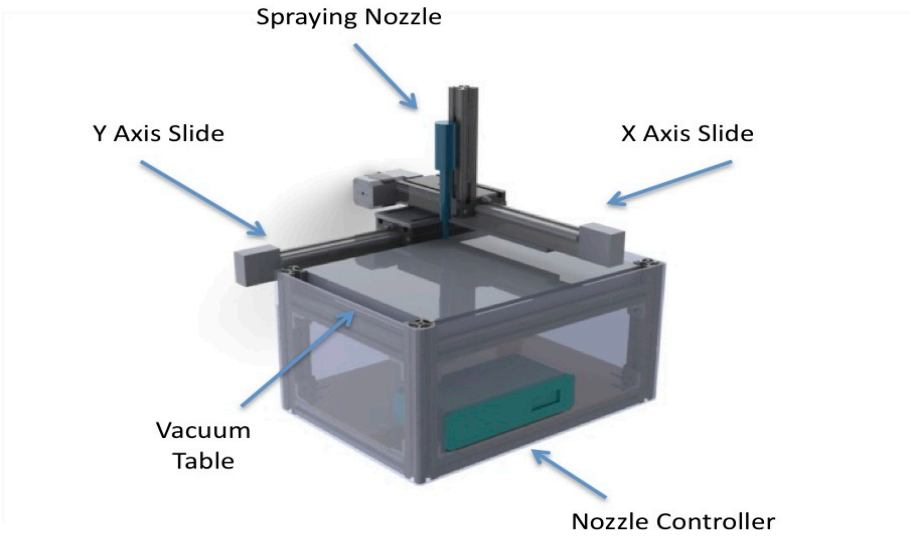

Figure 74: 2-axis spraying machine.

6.2.4 Electrode transfer

One of the important steps in the MEA fabrication process by the decal transfer process is the transfer of the dried electrode from the decal substrate onto the membrane to form the MEA. It requires the simultaneous application of heat and pressure onto the electrode. Typically temperatures ranging from 130 ºC to 210 ºC are employed in the transfer process with pressures ranging from 250-3500 psi and transfer time ranging from 180 s to 720 s [29, 76-82]. In this study a low-temperature, high-pressure route was taken, the transfer temperature was set at 130 ºC while the pressure used was 5000 psi for 180 s duration.

6.2.5 Diffusion media hot pressing

In the diffusion media transfer step, two appropriately sized pieces of diffusion media (ELAT LT-1400, ETEK) are affixed onto the 3-layer MEA formed with the assistance of temperature and pressure. A temperature of 120 ºC and a pressure of 1200 psi was used for this step for a 60 s duration as described in [167].

6.3 DMFC MEA TESTING

This section briefly describes the procedure and conditions used in testing the MEA's fabricated by the CCM-DTM method. A *Fuel Cell Technologies* test station was used, along with single cell 5 cm^2 hardware provided by the same company. A new MEA is first subjected to a 24 hr break-in period. The break-in procedure involved the following steps:

- Cell installation in single cell hardware (bolt torque set at 40 in-lb)
- Perform leak test
- Backpressure set at 20 psi
- Cell temperature set at 90 ºC
- Dry oxygen supplied to cathode at 250 SCCM
- 1M Methanol solution supplied to anode at 2 ml/min
- Cell maintained at 0.2 V for 24 Hrs

After the break-in period the cell is ready for further testing and data collection. Break-in and testing conditions are summarized in Table 20. These conditions were decided upon after extensive testing and evaluation, which are discussed in the proceeding sections.

Table 20: Break-in and testing conditions for 5cm^2 single cell DMFC MEA.

Parameter	Value
Temperature	
Cell Temperature	65 ºC/90 ºC
Anode humidity bottle temperature	24 ºC (no humidification required) / not used
Cathode humidity bottle temperature	24 ºC (no humidification required)
Anode line heater temperature	24 ºC / not used
Cathode line heater temperature	65 ºC
Flow rates	
Methanol	2 ml/min
Oxygen / Air	250 sccm
Back pressure	
Anode back pressure	n/a
Cathode back pressure	20 psi
Bolt Torque	40 in-lb
Seal thickness	20 mil
Seal material	Teflon coated fiber glass
VI Curve	Constant Current
Current step size	0.25 A
Delay b/w readings (scan rate)	180 s

Figure 75 shows the effect of backpressure on the performance of a 5cm^2 DMFC MEA, prepared by the CCM-DTM method. The goal of this experiment was to understand how the performance of MEAs created by the spraying process described in previous chapters is affected by changing the backpressure. This would allow for an approximate comparison of these results with those in literature results, if they were tested at different cathode gas backpressures, which is often the case. As expected the performance of the MEA increases with increasing cathode gas backpressure. Peak power (at 0.35 A/cm^2) increases from 95 mw/ cm^2 to 110 mw/ cm^2.

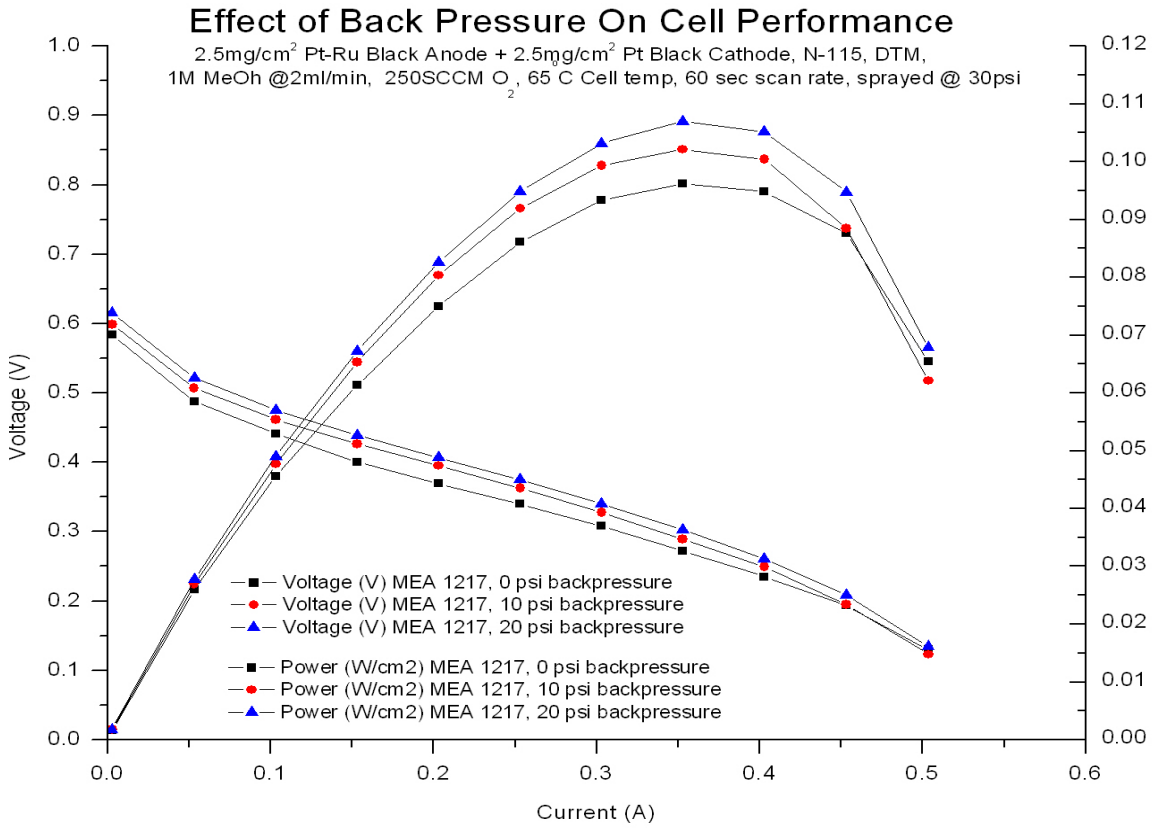

Figure 75: Effect of backpressure on cell performance.

Another important consideration during testing was to use humidified gas or dry gas. Initially humidified oxygen and air were used as is the norm in PEMFC testing, but a few anomalies were noted in the results obtained. For the same cell, operating at the same conditions, a slight variation was observed in VI curves run at different times. It was suspected that the diffusion media flooding had a part to play in these 'surges.'

In order to isolate these power surges, a test was run in which the cell current was slowly ramped up in steps of 0.5 A (0.1 A/cm$^{2)}$). Each step was allowed to stabilize for an hour in order to observe any fluctuation in the response, which was the cell voltage. Figure 76 shows how the cell voltage changes in these constant current steps. In the first 4.5 hrs, humidified oxygen was used and for the remainder of the test, dry oxygen was

used. As can be clearly seen in the humidified region, there are periodic surges in the voltage, which are consistent with the observations made earlier. These surges completely disappear when the cell is switched to dry oxygen. There is the presence of some noise in the high current density regions, but that is expected due to mass transport limitations at such high currents, that is the cell is not being supplied with reactants fast enough and the reaction products are not being removed fast enough.

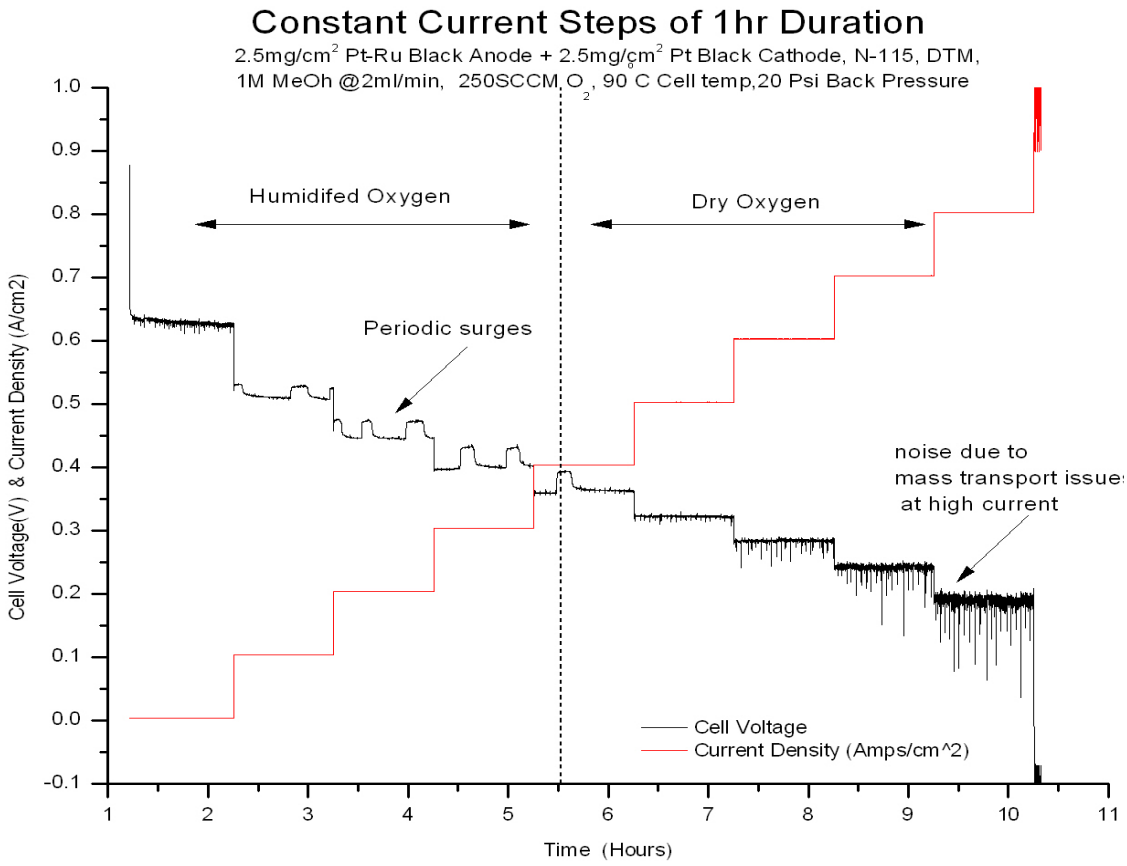

Figure 76: Dry vs. humidified oxygen test.

The next important parameter to be investigated for establishing a robust testing protocol was the current scan rate. To collect the performance data, the cell is connected

to a load bank, which holds either the voltage or current constant, and measures the response of the other variable. Typically constant current sweeps are conducted to generate a VI curve, and the voltage is measured as the response. This is due to the design of the load box itself, as most have circuitry to control current rather than voltage.

The two parameters that can be set, and which effect the VI curve generated are: the step size, which refers to the change in current per step, and the second parameter is the scan rate, which refers to the time delay between the tie when the step change is initiated and the time when the data reading is taken. A step size of 0.25 A was chose, as it provided sufficient detail in the VI curve.

Choosing the scan rate required further experimentation, the results of which are shown in Figure 77. It was important to allow for sufficient time for the transients to settle down and the voltage to achieve a steady state value for that particular current setting. As shown in the figure, five different scan rates were used, ranging from 1 minute to 1 hour. A faster scan rate would give a false reading, as the transients would not have settled down. On the basis of the results a 180 s interval between each data point measurement was selected.

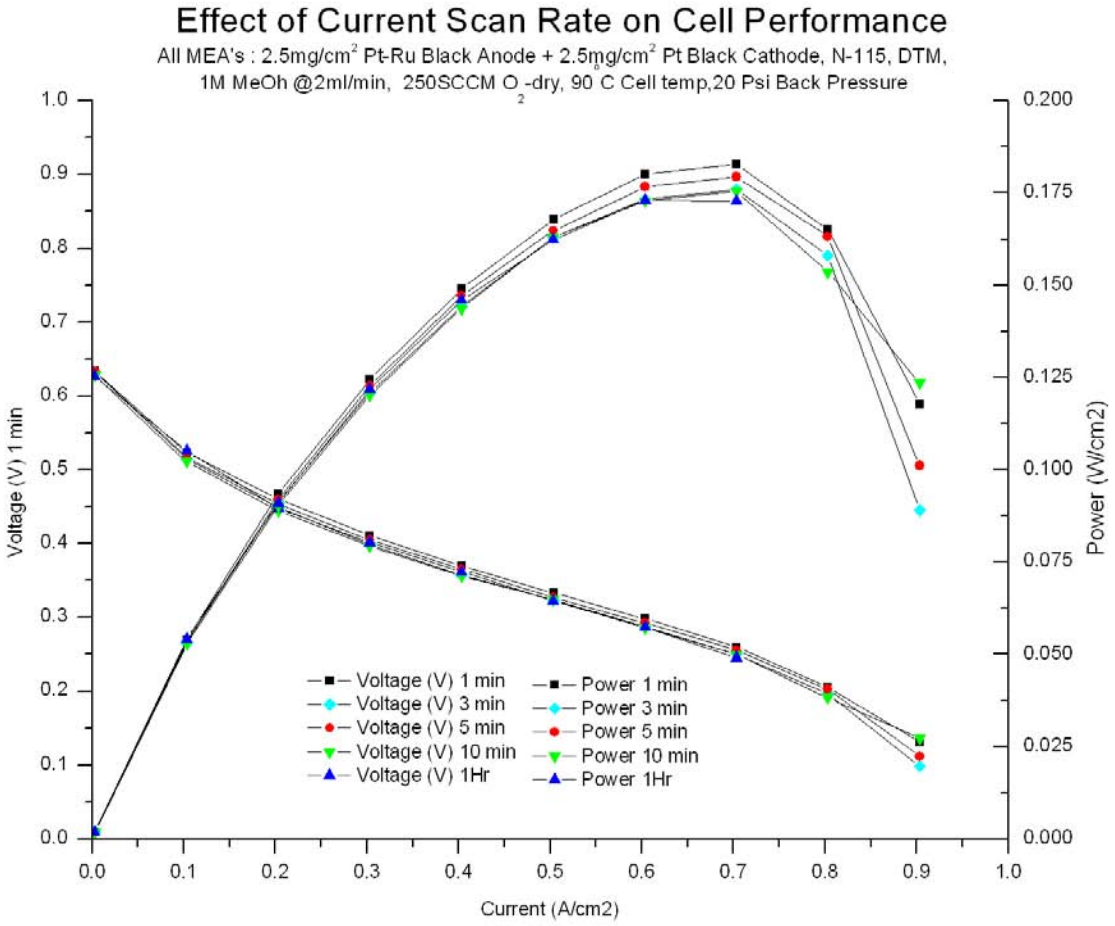

Figure 77: Effect of current scan rate during data collection.

6.4 MEA OPTIMIZATION

A MEA is fabricated by the assembly of electrodes onto an ionomer membrane. The most important sub-step in this overall process is the fabrication of the electrodes, which is achieved by the application of catalyst ink on to a substrate. Any optimization exercise should focus on the parameters of the ink application procedure and the catalyst ink composition. In this research study, a spraying process was selected to apply the catalyst ink onto the necessary substrate. Additionally it was identified that the atomizing air pressure supplied to the nozzle had a substantial effect on the spray produced, it affected the droplet size in the spray. It was considered important to identify the relation

between atomizing air pressure and the electrode microstructure, and the subsequent electrochemical performance of the electrode.

The second parameter considered for optimization is the Nafion content in the catalyst ink to be used. The amount of Nafion ionomer in the ink impacts the electrode microstructure, electronic and protonic conductivity between the catalyst particles, therefore it is important to examine it in detail.

6.4.1 Nafion content

Wilson et al[28]. used a ratio of 1:3 (33 wt%) for catalyst to Nafion content, but that was for supported catalyst. For unsupported catalyst Ren et al. [43] suggest a much lower Nafion content, 15 wt% for the anode and 7 wt% for the cathode. Reshetenko et al. [40], suggest a 12 wt% Nafion content for the anode and a 26 wt% Nafion content for the cathode. Song et al. [81] suggests a 15 wt% Nafion content for the anode where as a 10 wt% content for the cathode. Thomas et al. [70] identified an optimal Nafion content of 10 wt% for a DMFC cathode made from Pt-Black , for the anode they suggest that performance increases with decreasing Nafion content, and in some cases (due to presence of hydrous RuO_x) even eliminating the presence of Nafion in the anode is advantageous.

For this study five MEAs were prepared with different Nafion content. Both the anode and the cathode used had the same Nafion content. All electrodes used Pt: Ru black (1:1) as anode catalyst with a loading of 2.5 mg/cm^2, whereas Pt-black with a loading of 2.5 mg/cm^2 was used as the cathode catalyst. MEAs were sprayed at a pressure of 10psi and ink composition, decal transfer and GDL transfer settings used was as described in earlier sections. Cell break-in and data collection also followed the same settings and method as described earlier.

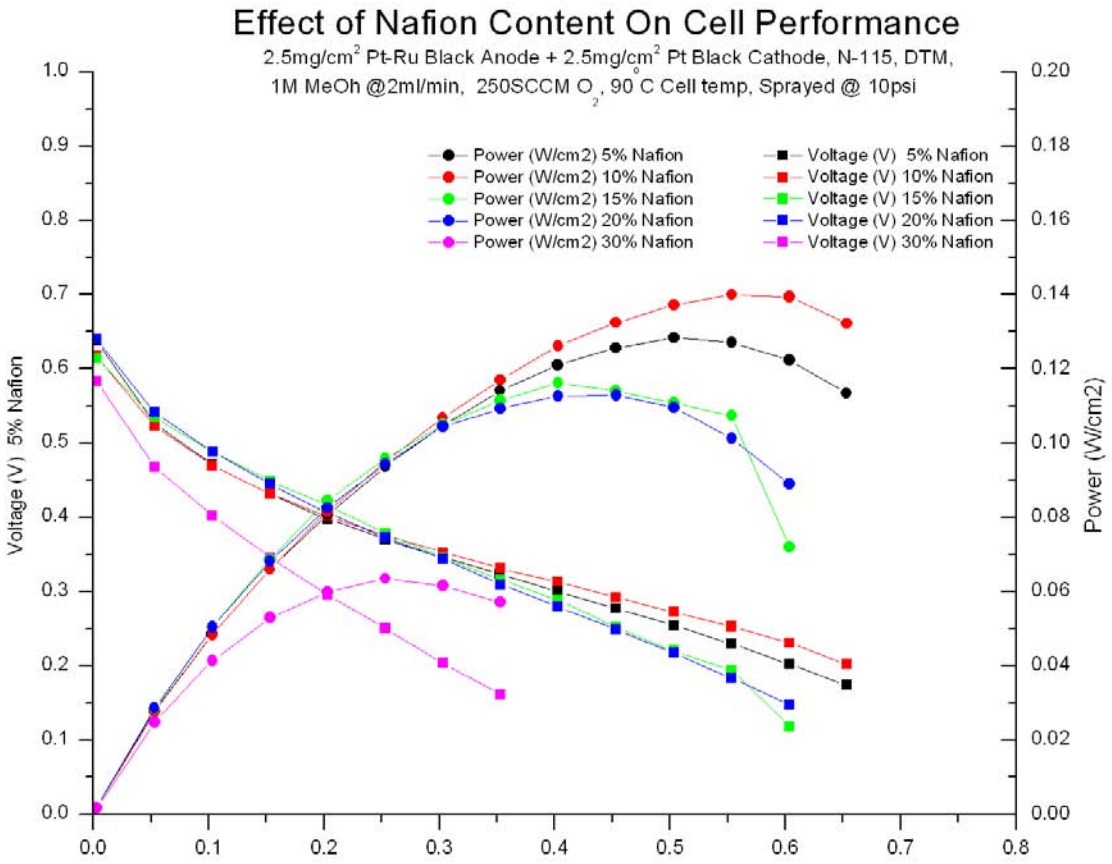

Figure 78: Effect of Nafion content on cell performance.

Figure 78 shows the results of this study when Nafion content was symmetrically changed, that is, both anode and cathode Nafion content had the same. The best overall performance achieved was by a Nafion content of 10%. It can be argued that lower Nafion content leads to thinner electrode layers [70], which allows for better mass transport. In comparison to unsupported catalyst, carbon supported catalyst used in PEM fuel cells thrive with higher Nafion contents, with values as high as 33 wt% being reported [28]. Supported catalyst have much bigger particle sizes, by virtue of the carbon supports used, (~40 nm) as compared to platinum blacks whose average sizes are around

2-3 nm. Too high a Nafion content would prevent good particle-to-particle contact, thereby drastically reducing electronic access to the interior region of the catalyst layer. Similarly, too thick a Nafion film surrounding a catalyst particle can prevent gas-phase access to the catalyst sites. Too little a Nafion content could potentially lead to catalyst sites that are not connected by the ionomer, which is necessary for protonic conduction to the membrane.

Figure 79, presents an alternate view of the same data, showing the power produced by these MEAs at 0.2V. As can be clearly identified as Nafion content is increased from 5 wt% to 10 wt% there is an increase in performance, and then there is a steady decline as the content increases to 30 wt% of Nafion content in the electrodes.

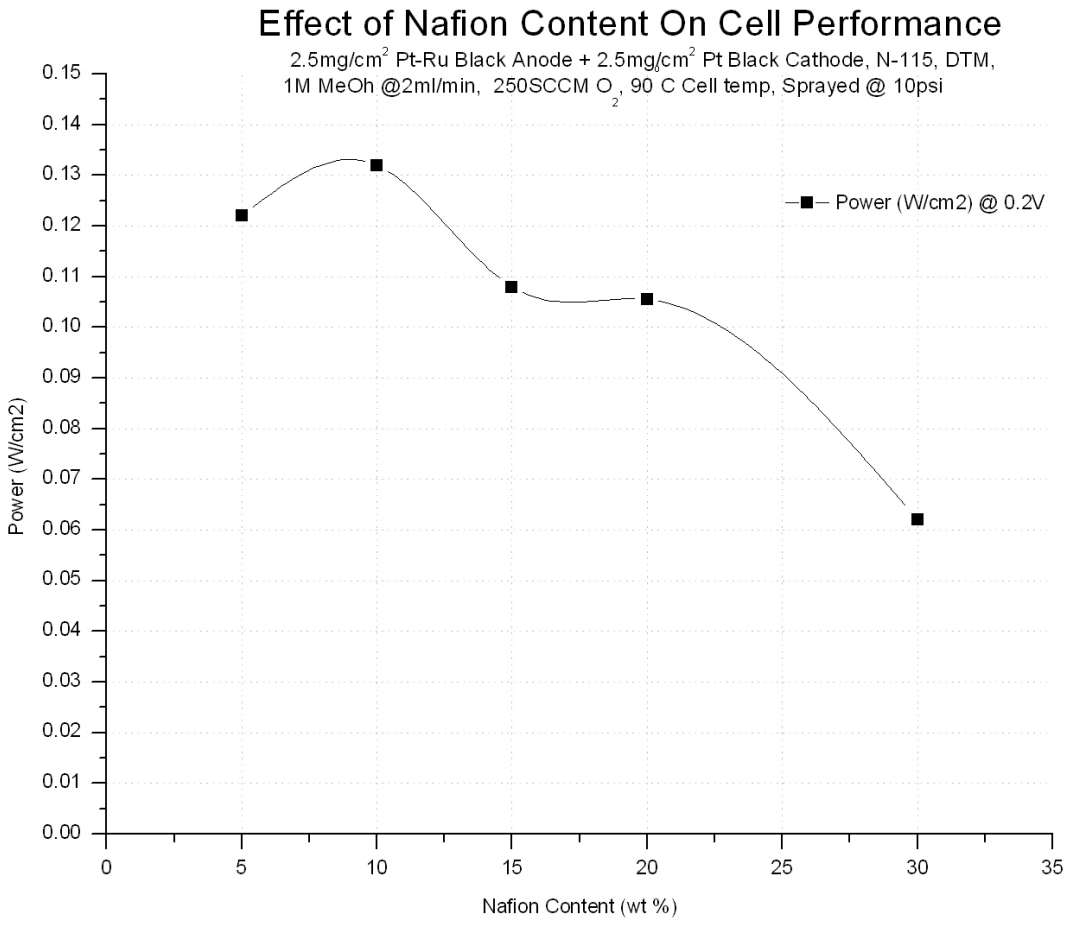

Figure 79: Power @ 0.2 V at different Nafion content.

The previous experiment involved a symmetrical Nafion loading between the anode and cathode. It was decided to isolate the anode performance with varying Nafion content. This was achieved by keeping the cathode Nafion content constant at 10 wt%, while varying the anode Nafion content from 5 wt% to 20 wt% in four equal increments. All electrodes fabricated used Pt: Ru black (1:1) as anode catalyst with a loading of 2.5 mg/cm^2, whereas Pt-black with a loading of 2.5 mg/cm^2 was used as the cathode catalyst. MEAS were sprayed at a pressure of 10 psi. Ink composition, decal transfer, GDL

transfer settings, break-in and data collection procedures used was as described in earlier sections.

Figure 80 shows the VI curves for four different Nafion contents in the anode, while Figure 81 represents the same data in a different manner. At lower current densities the performance of the four MEA's is very similar but at higher current densities, the MEA with 15 wt% Nafion performs better than the rest.

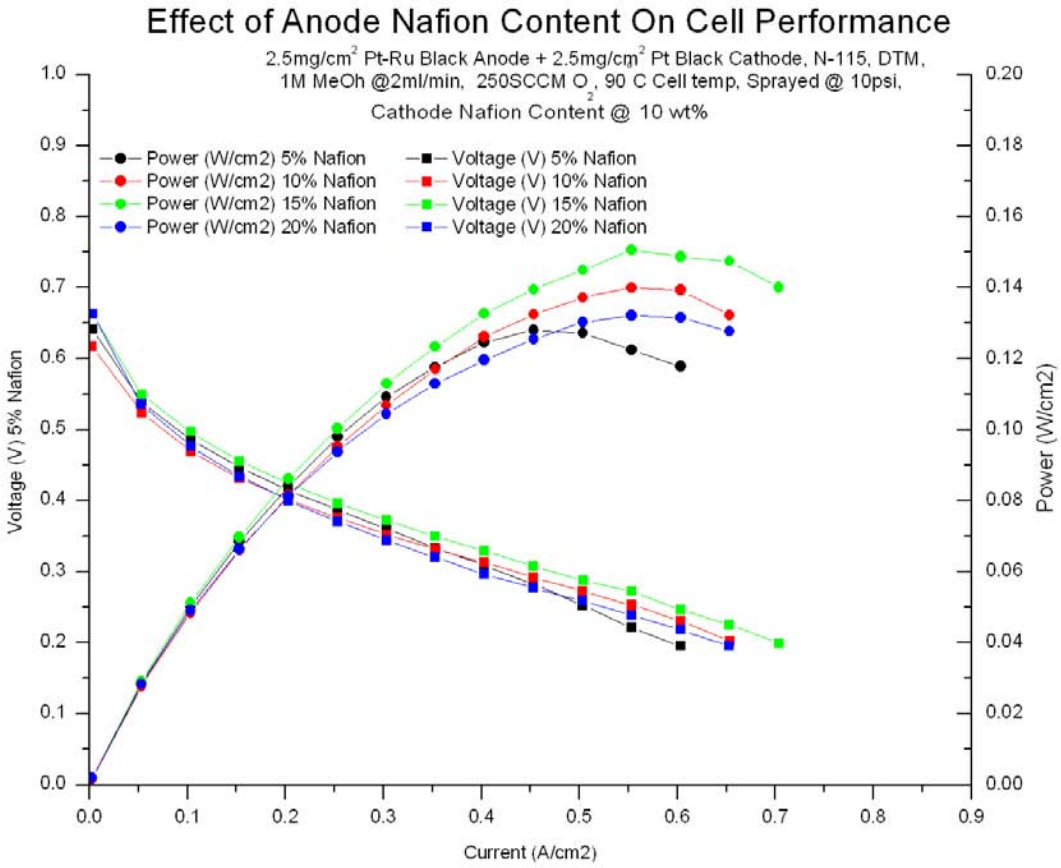

Figure 80: Effect of anode Nafion content on MEA performance.

It can be argued that the anode and cathode will have different Nafion content requirements because of a number of reasons. On the anode, a liquid fuel is fed to the electrode, whereas on the cathode a gas, air/oxygen is supplied. This would lead to

different mass transport scenarios. Additionally the very nature of the catalyst, and the catalyst inks formed is different. Pt-Ru black catalyst tends to form agglomerates during the ink making process, and is generally much more difficult to process that Pt-black ink. Evidence of this agglomeration is even apparent at the microstructure level, as shown in Figure 83, which shows SEM micrographs of the two different catalysts at different magnifications. As can be seen Pt-Ru black anode has an entirely different microstructure as compared to the Pt-Black cathode microstructure. Discrete clumps of catalyst and ionomer are visible in the anode, whereas the cathode has a much finer structure, with no evident clumping or agglomeration. As clear from Figure 81, a slight improvement in MEA performance can be obtained by using a 15 wt% Nafion content in the DMFC anode.

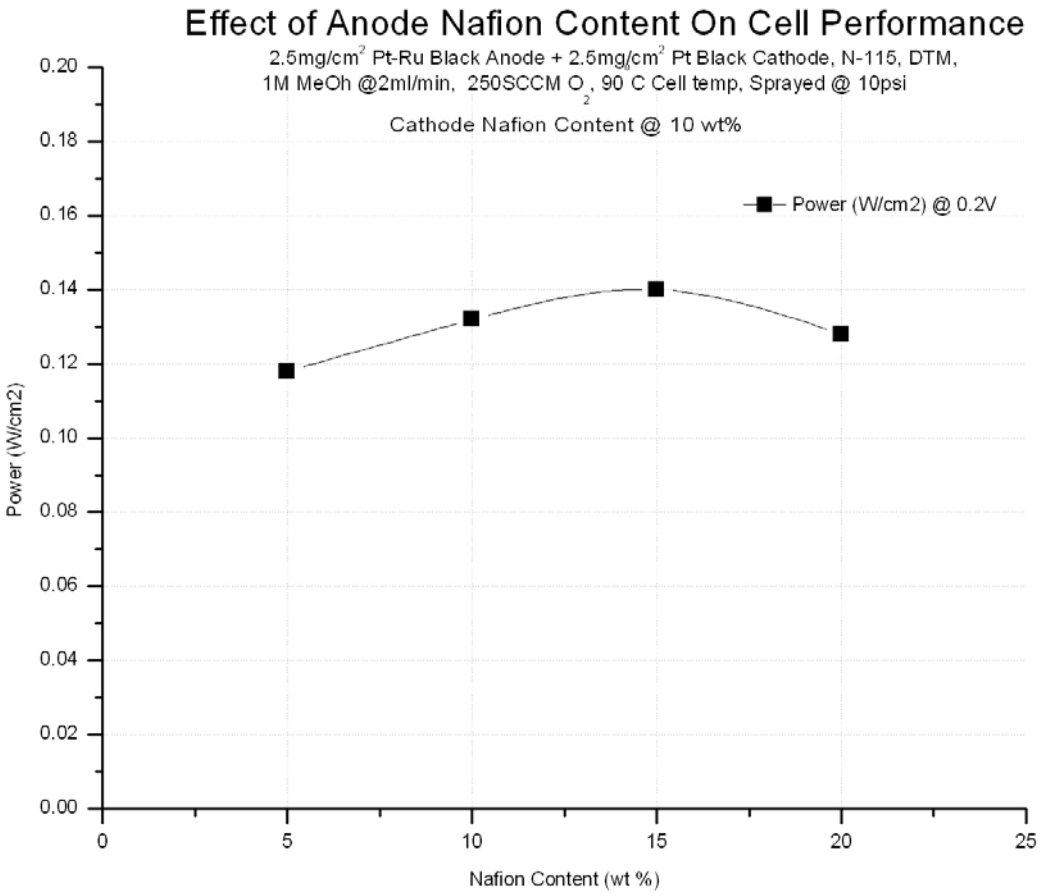

Figure 81: Power @ 0.2V at different anode Nafion content.

6.4.2 Spraying pressure/ Drop size

The second stage of the optimization process was to ascertain what is the optimal spraying pressure for the Nordson EFD-781S nozzle. The previous chapter characterized the spray produced by this nozzle at different pressures and flow rates. It was ascertained that higher pressures translated into smaller drop sizes. How do smaller drop sizes affect the microstructure of the electrode and how does that microstructure (if at all different) produced at the different pressures affect the overall MEA performance is the question that this section will answer.

The first step in investigating the effects of different catalyst ink drop sizes on the electrode microstructure was to observe electrode samples produced by these sprays in a SEM. Six samples were prepared, three anodes and three cathodes, sprayed at different pressures, which were mounted and observed in an electron microscope. Figure 82 shows the results of the SEM study. The anode microstructure is changing as the spray pressure changes, the pore distribution and sizes are clearly affected by the smaller drop sizes. Whereas there is little change observed on the cathode microstructure.

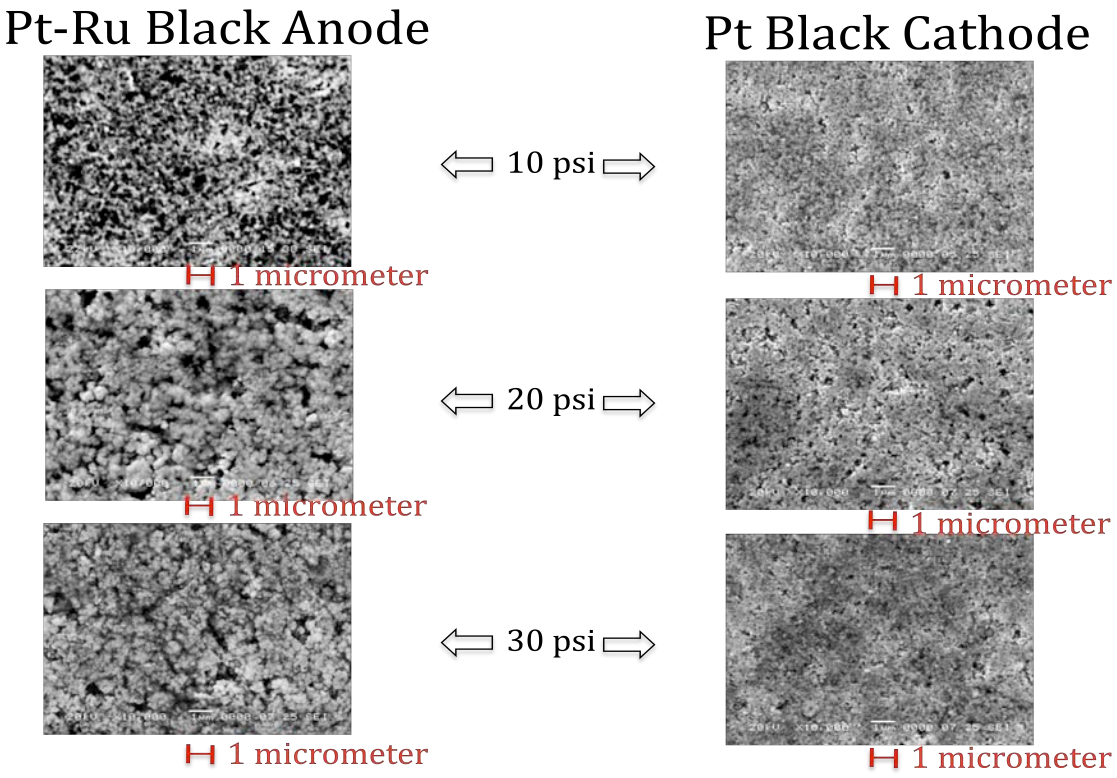

Figure 82: Electrode microstructures (at 10000x) produced by sprays at different atomizing air pressures.

In order to develop a better understanding of the microstructure produced at the 30psi atomizing air pressure, samples were studied at higher magnification, as shown in

Figure 83, which shows the same electrodes (anode and cathode, 30 psi) at three different magnifications. The anode clearly constitutes of clumps of catalyst and ionomer particles, in-between, which exists pores. The cathode has a much more refined 'spongy' appearance which does not appear to have changed with increasing atomizing air pressure. From these observations it is reasoned that smaller droplets produce a much more refined pore structure on the anode, which could potentially allow for better mass transport, electronic and protonic conductivity between the different catalyst sites.

Mass transport could potentially improve because smaller pores, which appear to have a much denser network, replace the larger pores visible in the 10 psi electrodes. Such a structure could potentially impact the CO_2 formation and removal process on the catalyst sites.

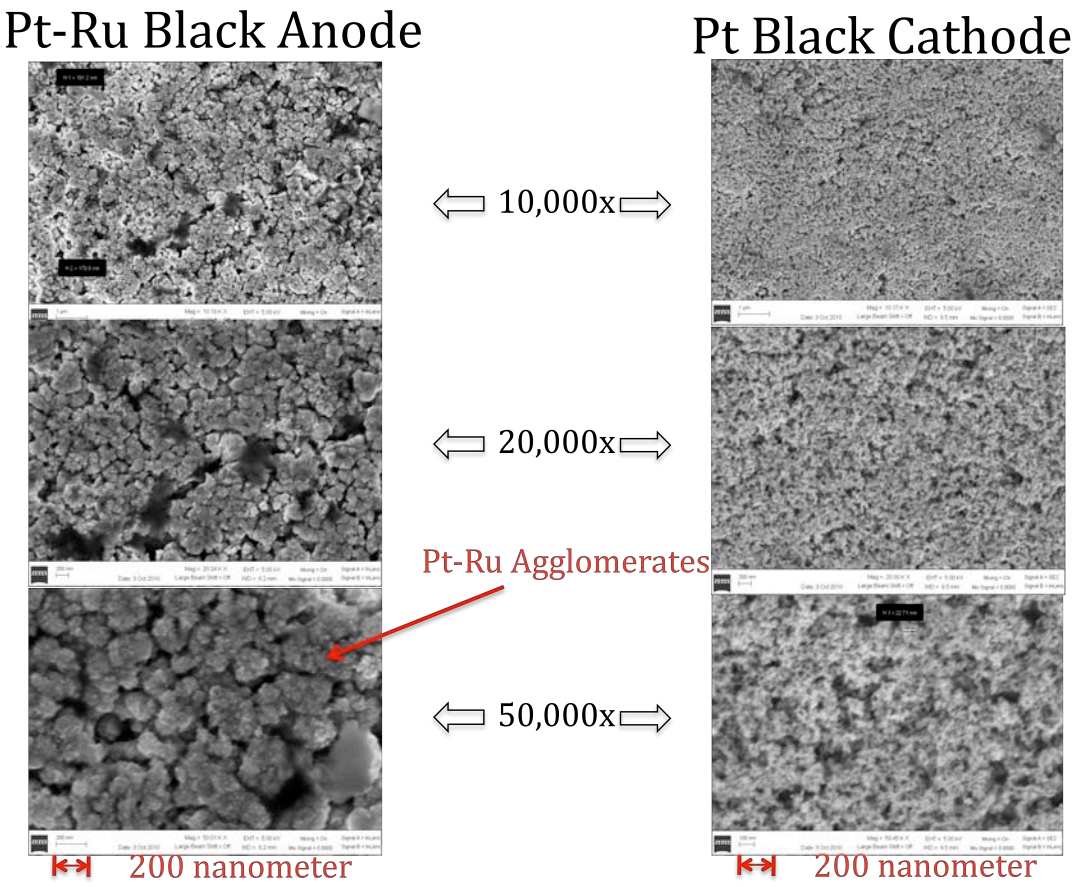

Figure 83: Electrode microstructure at different magnifications (sprayed @ 30 psi).

The next stage in the atomization air pressure optimization process was to see if this change in microstructure translated into any difference in MEA performance. In order to address this issue, MEAs were prepared with the method described previously. Anode and cathode loadings were maintained at 2.5 mg/cm^2 using Pt-Ru black and Pt-Black respectively. Nafion content was kept at 10 wt% in both the electrodes. 15 MEA's were prepared, 5 each at 10, 20 and 30 psi spray pressures. The purpose of testing 5 MEAs at each pressure and averaging them out was to show the repeatability of the MEA fabrication and ink formulation process. These MEAs represent two different batches of inks, sprayed at different times, but with the same process conditions.

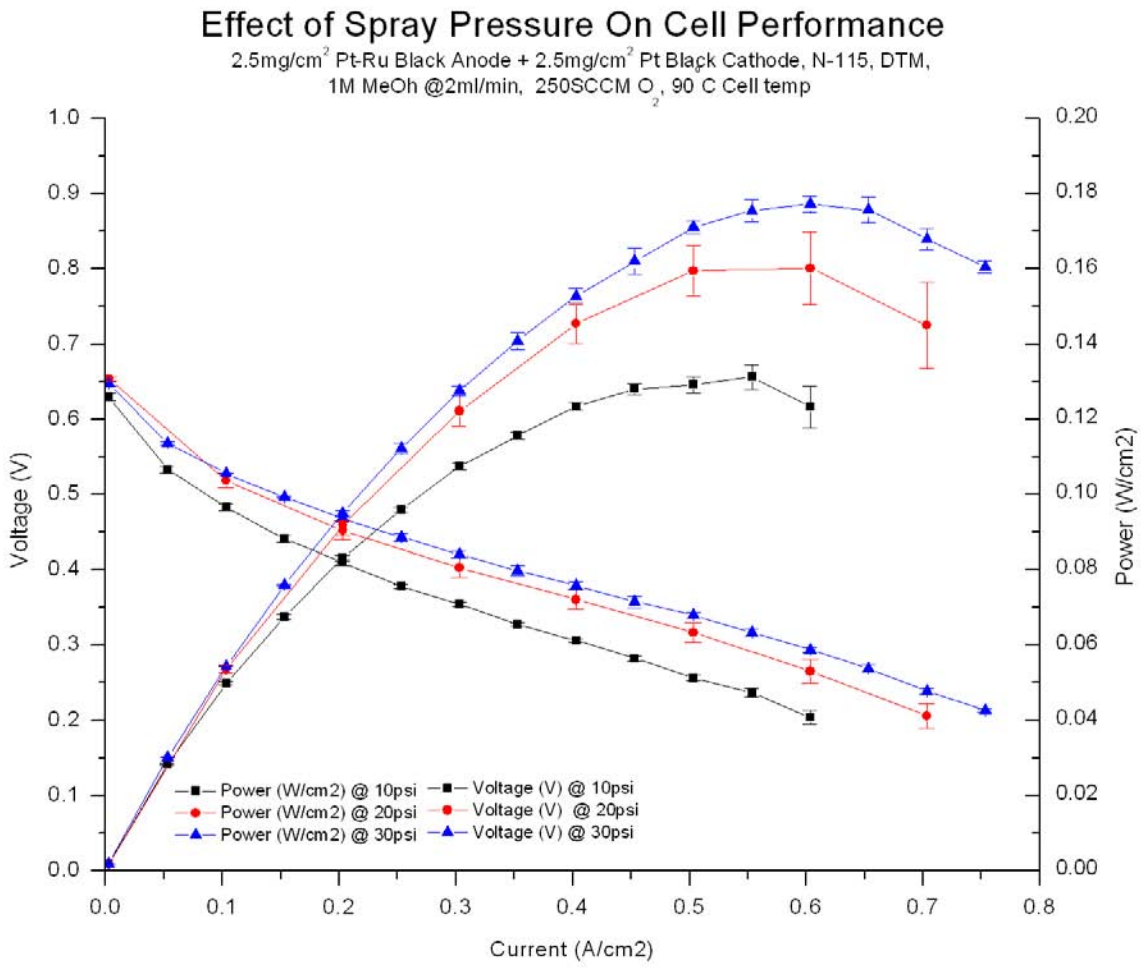

Figure 84: Effect of spray pressure on MEA performance.

Figure 84 shows the results of this study. As is clearly evident MEAs sprayed at 30psi far outperformed those prepared at lower pressures. As was suspected by studying the microstructure the refined pore network allows for a significant improvement in the overall MEA performance. This answers the questions that were posed earlier. There is a clear relation between drop size of the sprayed catalyst ink and microstructure in the electrode, which in turn affects the overall MEA performance. Higher atomizing air pressures produce smaller drops, which produce finer pores in the electrode, which improve the MEA electrochemical performance significantly.

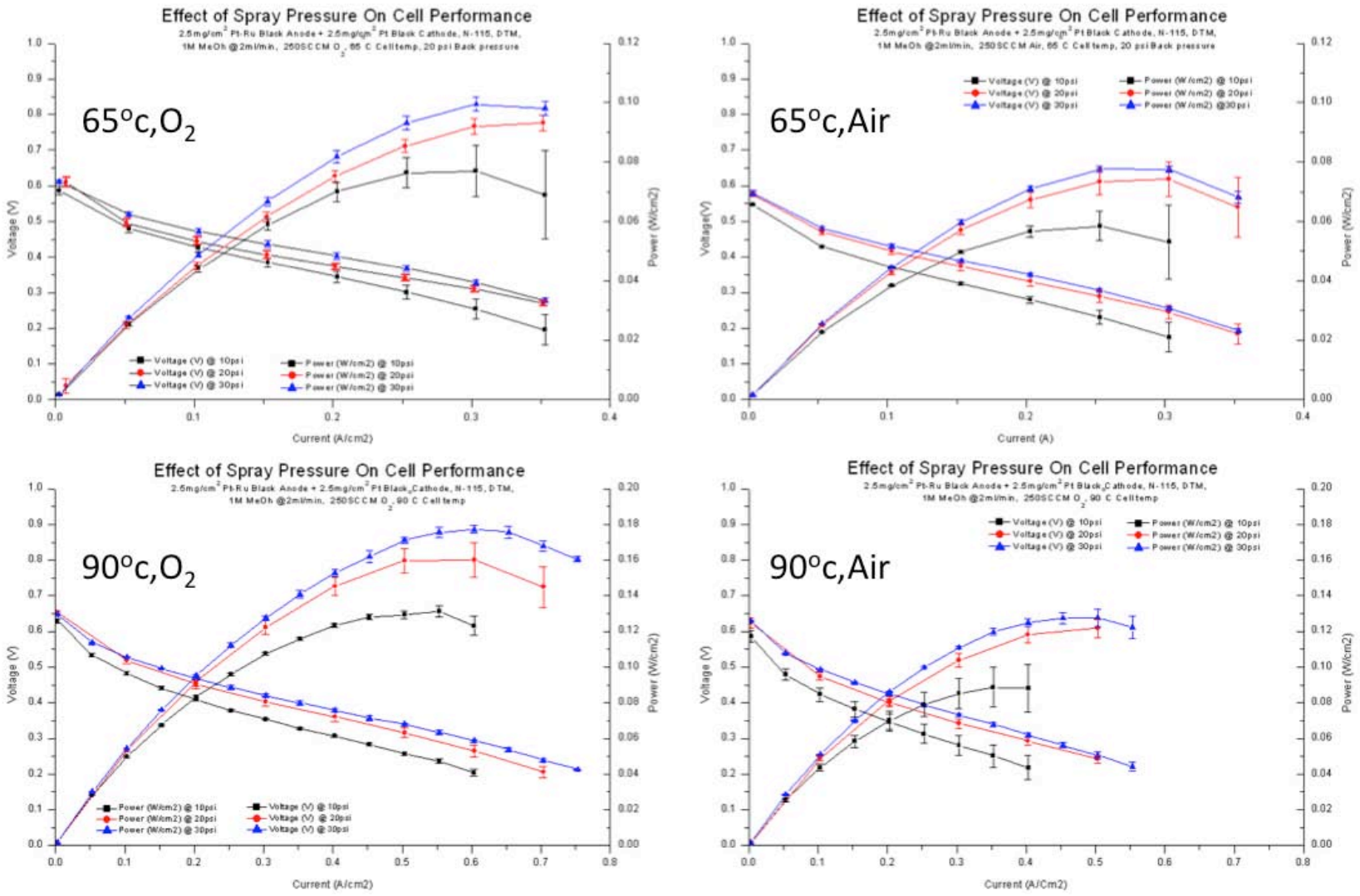

Figure 85: Effect of spray pressure on MEA performance taken at different temperatures, with air and oxygen.

Figure 85 shows the performance of the MEAs at different temperatures, with air and oxygen. As can be seen, the best performance is with oxygen at 90 ºC, with a peak power of around 180 mw/cm^2. The performance with air at 90 ºC decreases to around 130 mw/cm^2. MEA performances at 65 ºC behave similarly.

6.4.3 Catalyst utilization

Cyclic voltammetry was conducted to qualitatively identify any change in electrochemical surface area (ECSA) of DMFC anodes prepared at different atomizing air pressures. The anode was made the working electrode and cathode was the reference/counter electrode. Humidified Nitrogen was supplied to the anode, whereas humidified hydrogen was supplied to the cathode (both at 150 sccm). The potential of the working electrode was swept at a rate of 50 mV/s. While it is difficult to determine precise readings of the surface areas in these MEAs, it is possible to note the general trend, as the area under the curve generally corresponds to a higher ECSA. Results of the analyses are shown in Figure 86, from which it can be ascertained that there is a definite increase in ECSA as the atomizing air pressure is increased. As the test were conducted to deliver the same total loading in each case, the data suggests better connectivity and higher utilization of the deposited catalysts. This supports the results observed previously.

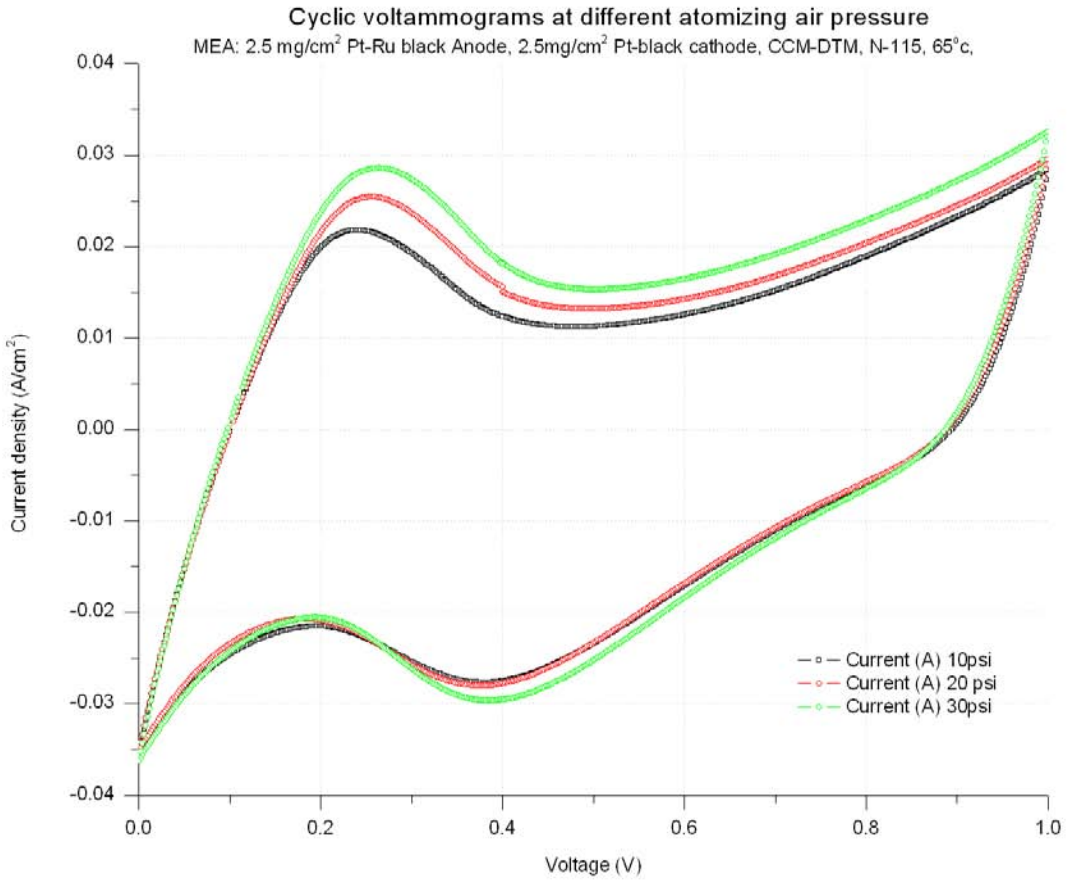

Figure 86: Cyclic voltammograms of MEAs prepared at different atomizing air pressures.

6.4.4 Catalyst loading

Another study was conducted to investigate the effect of the anode catalyst loading on MEA performance. The intention behind this study was to see that does the structure produced by spraying offer any advantage in terms of catalyst utilization. For this purpose three MEAs were prepared with loadings, 1 mg/cm^2, 2.5 mg/cm^2, and 4 mg/cm^2 of Pt-Ru black catalyst, with a 10 wt% Nafion content. The cathode was kept constant with a loading of 2.5 mg/cm^2 Pt black, 10 wt % Nafion. All electrodes were sprayed at 10psi pressure.

Figure 87 shows the results of this study. An anode catalyst loading of 2.5 mg/cm2 offers the best performance. What is surprising is the performance of the MEA with 4 mg/cm^2 anode catalysts loading. Figure 88 offers an alternate view of the same data, showing the power density of the three MEAs at 0.2 V. The MEA with 4 mg/cm^2 anode loading performs slightly lower than the one at 2.5 mg/cm^2. This drop in performance could be attributed to the increase in electrode thickness, which is known to adversely effect mass transport.

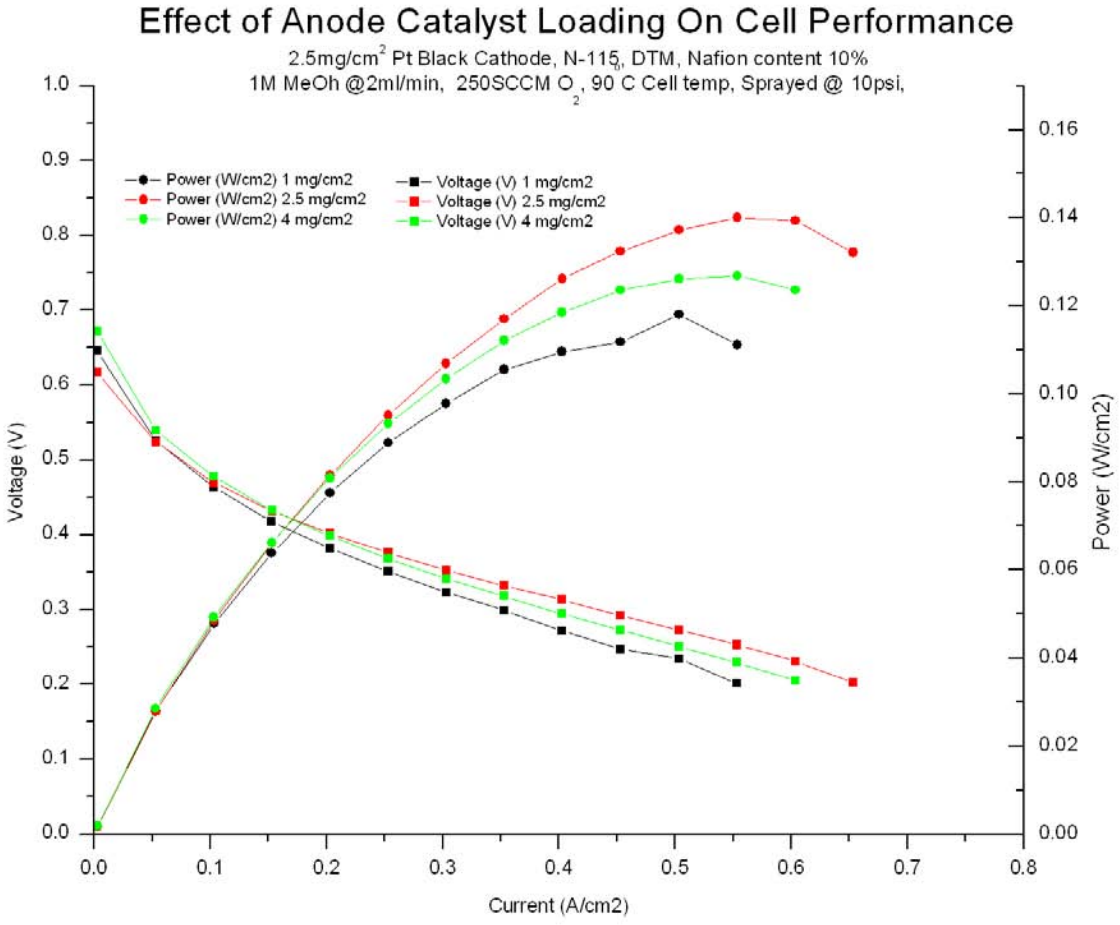

Figure 87: Effect of anode catalyst loading on MEA performance.

Another interesting observation that can be made for Figure 88 is the difference between the performance of the electrode with loading of 2.5 mg/cm^2 and that with a loading of 1 mg/cm^2. A difference of 1.5 mg/cm^2 in catalyst loading produces a difference of a mere 20 mw/cm^2, which is quite surprising. This would imply that the anode is not that sensitive to catalyst loading, whereas the cathode of a DMFC fuel cell, where the oxygen reduction reaction is taking place could potentially be more responsive to changes in catalyst loading.

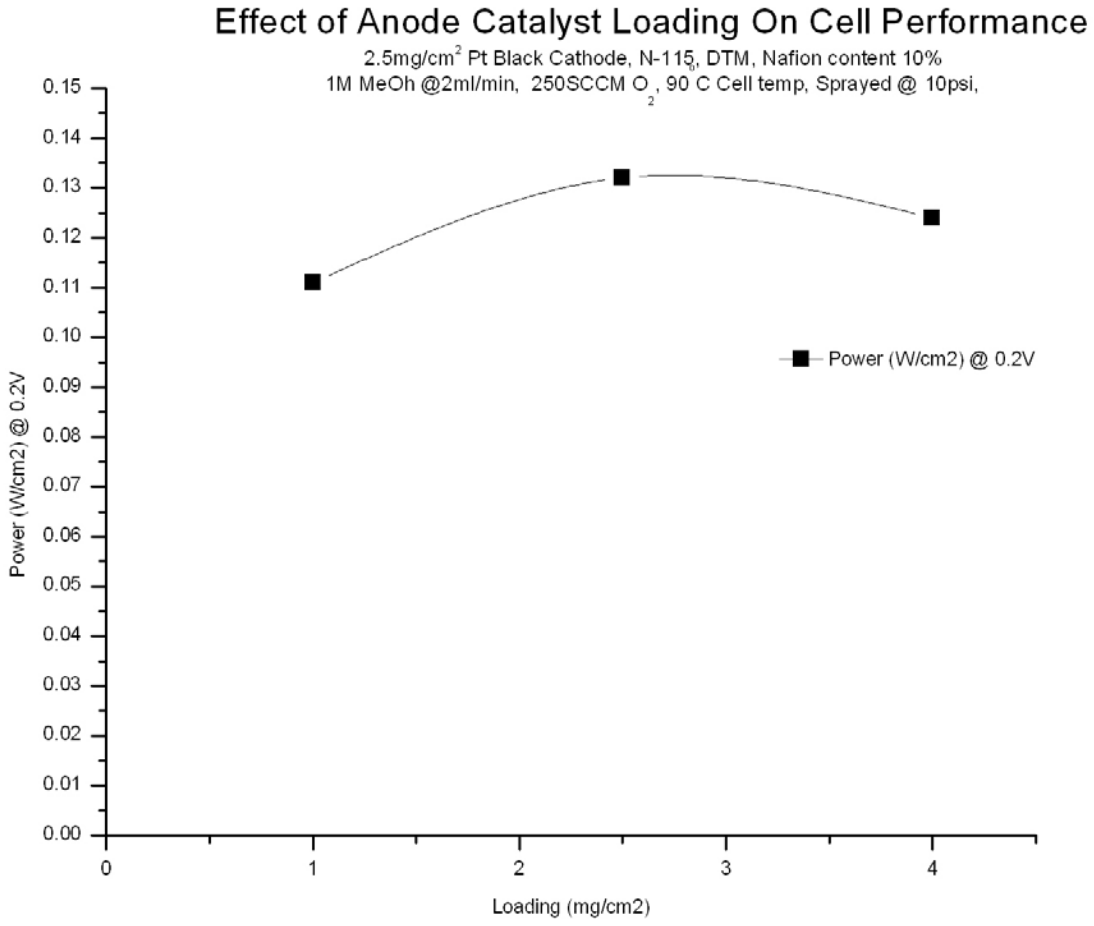

Figure 88: Power at 0.2V with different anode catalyst loadings.

6.5 PERFORMANCE COMPARISONS WITH COMMERCIAL MEAS

In order to gauge the performance of MEAs produced by the spraying process, commercially available MEAs were procured from www.fuelcellstore.com and tested. Figure 89 shows the result of this comparison. Both MEAs perform similarly in the kinetic and ohmic regions, at lower current densities but the commercial MEA suffers from significant losses due to mass transport issues at higher current densities. The interesting fact about this comparison is that the in-house prepared MEA has a catalyst loading of 2.5 mg/cm^2 on both electrodes, whereas the MEA from fuelcellstore.com has a catalyst loading of 4.0 mg/cm^2 on both electrodes. Another difference that exists in this comparison is that, the commercial MEA uses N117 membrane, while the in-house MEA uses N115.

What can be ascertained from this comparison is that despite the significant difference in catalyst loading, both MEAs have similar activation and ohmic losses in the low current density regions. This indicates better performance of the in-house manufactured MEAs. At higher currents the lower performance of the commercial MEA could be attributed to mass transport losses caused by the diffusion media.

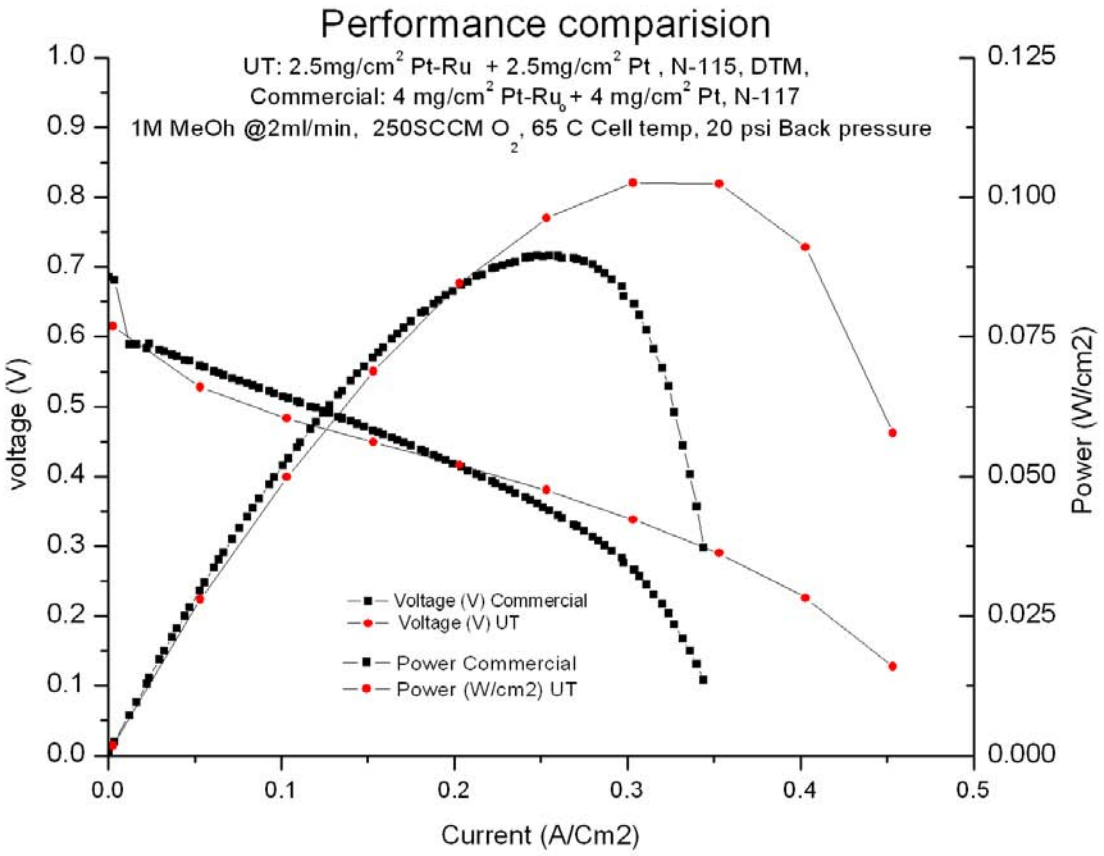

Figure 89: Comparison with MEA from fuelcellstore.com.

A second comparison was done with publicly available data for a mass produced DMFC MEA (12D-W) manufactured by E-Tek. The results of this comparison are shown in Figure 90. The E-Tek MEA performs significantly better than the in-house MEA, but this was expected due to the fact that the E-Tek MEA has twice the catalyst loading, 5 mg/cm^2 on each electrode as compared to 2.5mg/cm^2 of the MEA manufactured in-house.

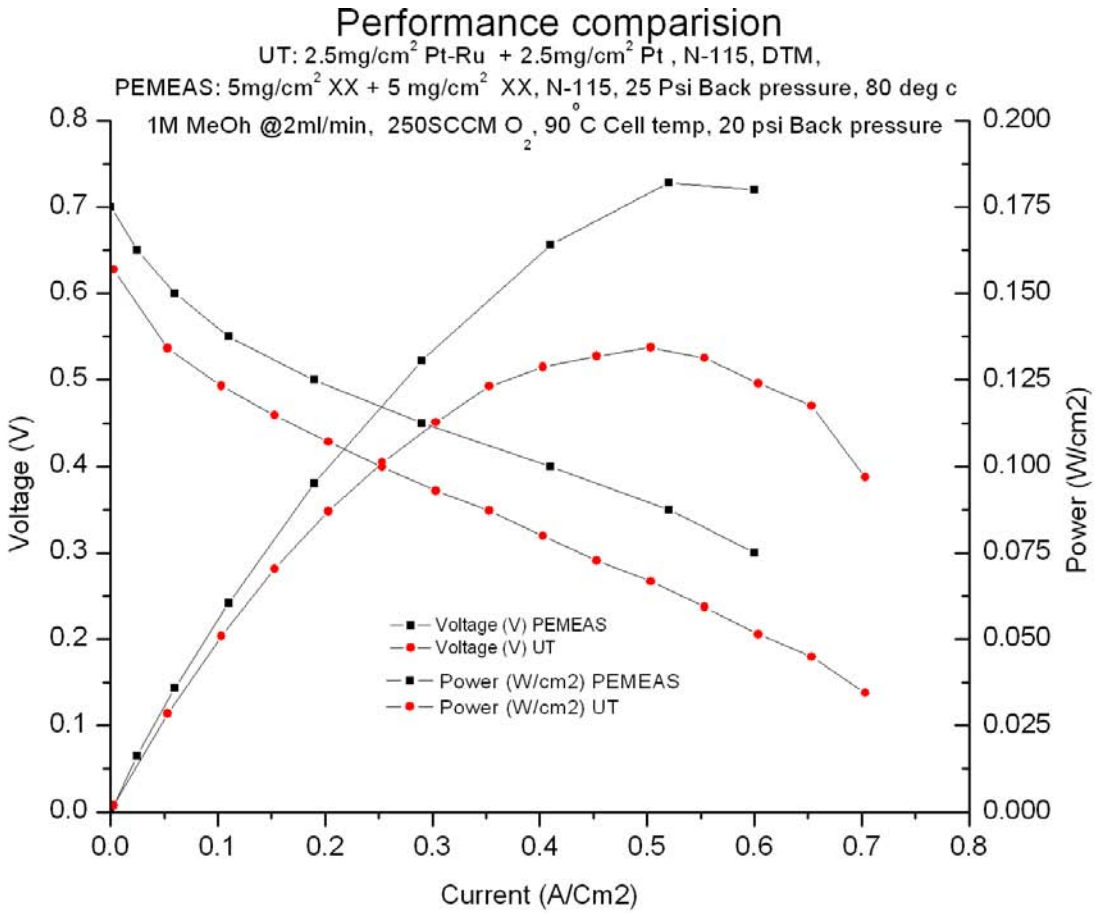

Figure 90: Comparison with E-Tek 12D-W DMFC MEA.

In order to negate the effects of the difference in catalyst loadings, the same data is presented differently by normalizing it with the catalyst loading of the MEA. Figure 91 shows the comparison data from the fuelcellstore.com MEA. Note that the bottom axis has different units (A/mg). The in-house prepared MEA shows much better performance per milligram of catalyst.

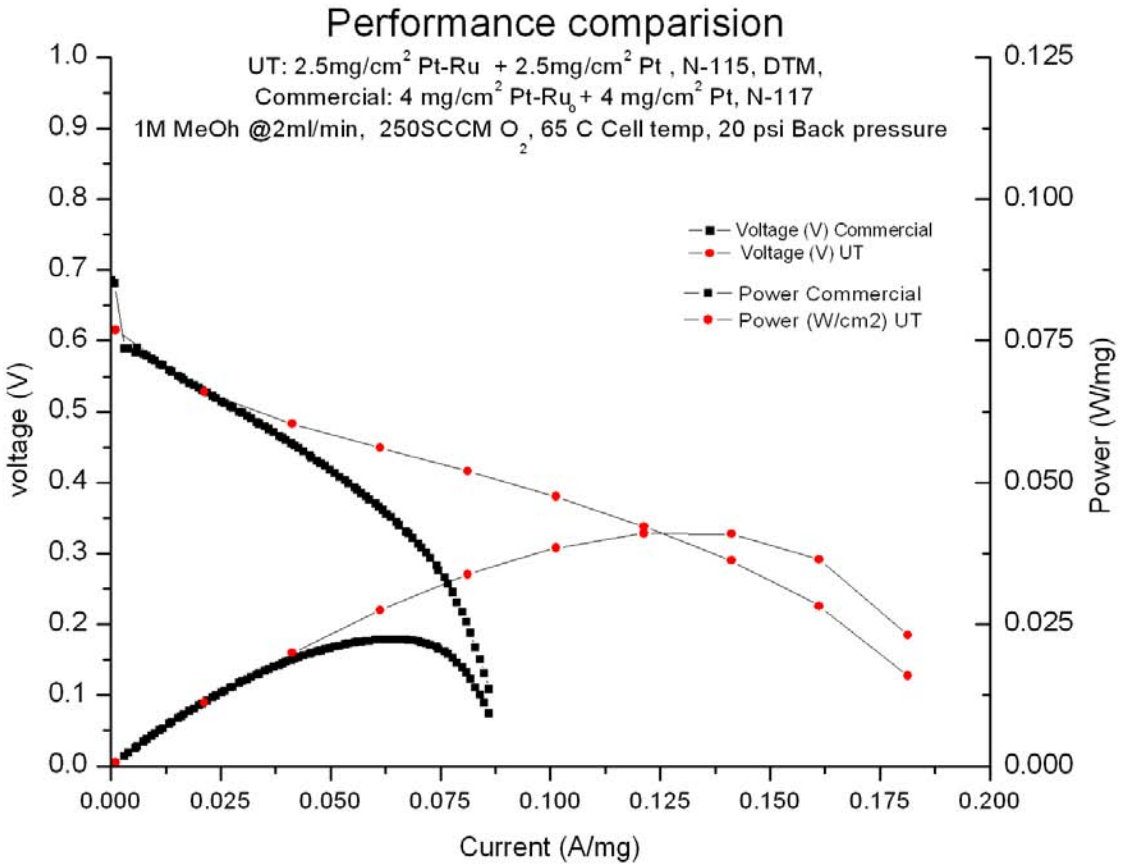

Figure 91: Comparison with MEA from fuelcellstore.com normalized with catalyst loading.

Figure 92 shows a similar comparison with the E-Tek MEA. From this plot it can be ascertained that the in-house MEA delivers more performance per milligram of catalyst.

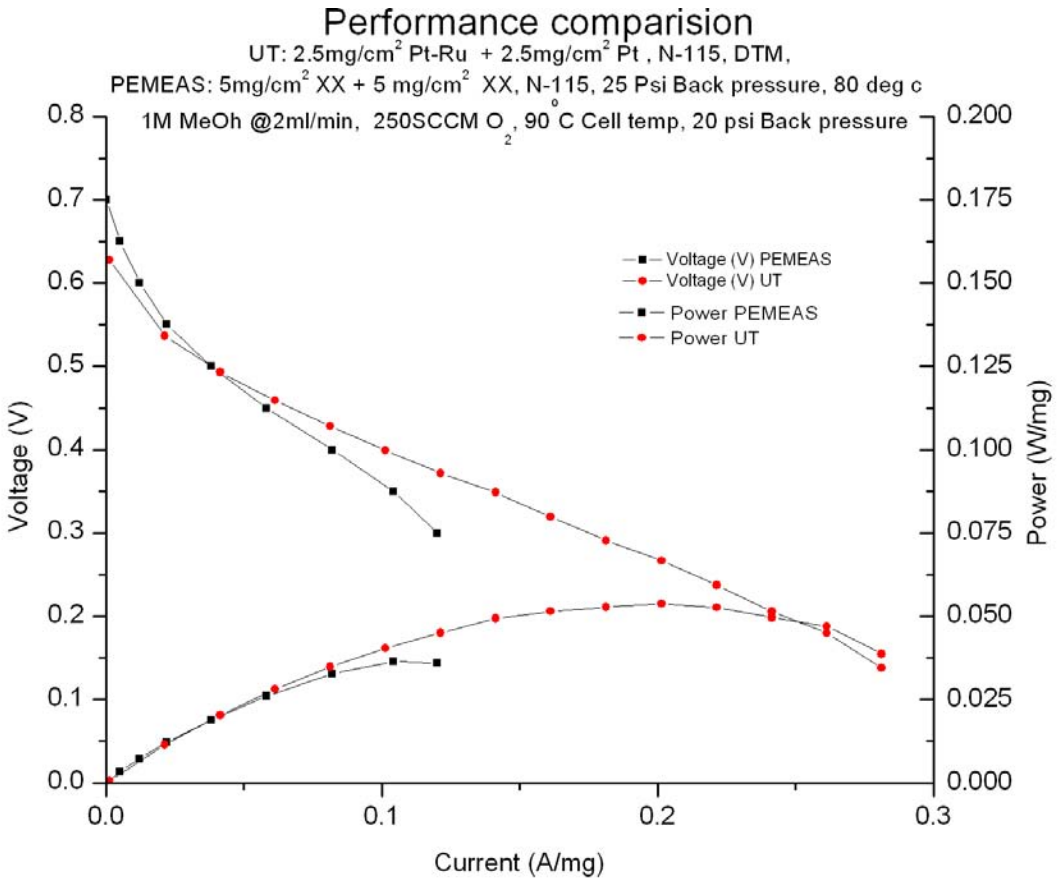

Figure 92: Comparison with E-Tek 12D-W DMFC MEA normalized with catalyst loading.

6.6 CHAPTER SUMMARY

In this chapter, the fabrication procedures for MEAs in a discrete fashion are described in detail. MEAs were fabricated in discrete quantities rather than in a continuous mode so that optimal process parameters and catalyst ink compositions could be explored. In future these results would be applied to the continuous DMFC MEA manufacturing process under development.

In order to test the fabricated MEAs a rigorous testing protocol was also defined. Two parameters were identified for optimization, the atomizing air pressure in the spraying nozzle and the ionomer content in the catalyst ink used. A clear correlation

exists between the atomizing air pressure and the drop size. It was shown that smaller drop sizes produced by increasing the atomizing air pressure affected the anode microstructure, which in turn refined the pore distribution. This microstructure performed significantly better in the single cell tests performed. Additionally the Nafion content was systematically changed and its influence studied in detail. The continuous manufacturing process under development will utilize these results for MEA fabrication.

This chapter concludes with a comparison of in-house fabricated MEAs by the spraying process with performance data of commercial MEAs. The in-house prepared MEAs perform well against these MEAs and offer more performance per milligram of catalyst.

7. Conclusions and future work

We have developed and characterized a manufacturing process to create a membrane electrode assembly (MEA) for the direct methanol fuel cell. A roll-to-roll manufacturing process was chosen for its compatibility with the requirements for making the overall process continuous. The manufacturing requirements thereby impose constraints on the following elements of the fuel cell: architecture of the three-layered assembly; geometry of the membrane (bulk availability in roll form); and composition of the electrode components (nanometer sized catalyst particles and soluble ionomer), which are constituted into ink. A literature review revealed the advantage of pursuing a decal-transfer method (DTM) approach to fabricating the MEA, which essentially reduced the problem to the selection of an appropriate catalyst ink coating process for electrode fabrication, and a subsequent electrode transfer process for MEA assembly.

From an initial lot of seven candidate coating processes, two were selected for further evaluation and successfully prototyped on a custom-built coating test bed. On the basis of coating tests performed, spraying was the method selected as the final process.

The spraying process was then characterized by analyzing the spray produced by various nozzle control parameters. The characteristic of interest was the length mean diameter (LMD) of the spray, which is an average of the drop sizes in a spray distribution. This LMD value was used to characterize a spray distribution with a single numerical value, by which to compare different sprays. Parameters that were varied included the atomizing air pressure of the two-fluid, external mixing, air assist nozzle, and the flow rate of the catalyst ink. A high-speed photography apparatus was used to take pictures of the drops in the spray; hundreds of such images were captured and

processed by automatic software to measure the droplet size distribution of the spray, from which LMD values were calculated.

A two-factor, three-level experiment was designed to develop an empirical model of the LMD value of sprays produced at different fluid flow rates and atomizing pressures. It was concluded that droplet sizes are strongly dependent on atomizing air pressures. The intention behind the development of this droplet sizing apparatus and the subsequent calculation of an empirical model was to quantify the spray characteristics, so that the electrodes produced by different sprays could be compared.

The final stage of this research involved the study and optimization of MEAs produced by spraying at different atomizing air pressures and ink compositions. Atomizing air pressures were studied to determine the effect of droplet size on finished electrode microstructure. Catalyst inks of various compositions were studied to find the optimal ionomer content for a DMFC electrode fabricated by spraying.

7.1 VALIDATION OF HYPOTHESIS

The hypothesis presented at the beginning of this research effort was that the design and fabrication of the electrode is influenced by the material composition of the catalyst ink, and the method of catalyst ink deposition.

From the results presented in this dissertation, it can be ascertained that the composition of the catalyst ink does, indeed, affect the performance of the electrode. Inks of different ionomer contents were used to fabricate MEAs and a clear correlation between ionomer content and MEA performance has been demonstrated. Additionally, the microstructure and electrochemical surface area of the electrode is shown to vary with the atomizing air pressure, which shows the influence of the deposition mechanism on the

electrode performance. This supports the notion that the method of catalyst ink deposition affects the electrode structure and performance.

7.2 CONTRIBUTIONS

Original contributions of this research effort are summarized in the following sections.

7.2.1 Manufacturing of electrodes

Key contributions have been made to the manufacturing science of membrane electrode assemblies. First, the spraying process has been studied in detail, and the influence of atomizing air pressure on the microstructure and performance of DMFC electrodes has been identified. Secondly, Nafion content for DMFC electrodes has been studied, and an optimal content of Nafion for DMFC electrodes has been proposed. Key process control parameters for MEA manufacture by spraying have been identified and an MEA testing procedure has been defined.

7.2.2 Modular coating test bed

A modular test bed for the study of a variety of coating processes was designed and fabricated. This test bed was used to study the following processes: tape casting, slot die coating, air assist spraying, drop jet printing, and ultrasonic atomization spraying. It provides for a flexible platform, which can accept multiple coating modules, dryer orientations, and substrate widths and types.

7.3 FUTURE WORK

A few interesting research avenues have been identified as an outcome of this research, and some avenues of development have begun in earnest. We summarize proposed development activities and preliminary work that has been completed already.

7.3.1 Application of electrode spraying technique to a continuous manufacturing process

These electrodes layers produced in the spraying operation must be transferred onto a continuous web of ionomer membrane to form a three-layer catalyst-coated membrane (CCM). This transfer process requires registering, alignment, and positioning of these electrodes with relation to the membrane, and a transfer of the electrodes on to the membrane by the simultaneous application of heat and pressure on the decal substrate.

7.3.1.1 Substrate web movement and catalyst ink spraying

If electrodes are to deposited on the decal transfer substrate, the substrate can either move intermittently, in a semi-batch process, or with constant velocity. This choice defines the requirements of the down stream modules: the spraying section and the electrode transfer section.

The choice between intermittent or continuous web motion affects the spraying module path length and the masking mechanism. A constant velocity motion of the web could potentially be faster overall, but this could lead to longer process path lengths in the spraying section, necessitated by the fact that more nozzles would be needed to achieve the required loadings. If an intermittent motion was used then the same number of nozzles could apply multiple coats on the substrate during the duration the web is stationary under them.

The second concern is the masking mechanism that has to be used to produce clean edges of the electrode. Due to the nature of the spraying process, if the catalyst layer is not to extend to the edge of the MEA, the process will require a mask, which can then be removed to reveal the area onto which the coating has been sprayed. For continuous web motion, a mask in the form of a film with cutouts can be attached to the

web itself so that it can travel with the web during the multiple spray coats, and then be peeled off, once spraying is completed. For an intermittent motion of the web, this masking could be attained by using a fixed template which is lowered onto the substrate when it stops under the nozzles, after which the spray is distributed, followed by a step in which the template is retracted, allowing the web to continue its motion until the next stop cycle.

The deciding factor in this choice would be the electrode transfer step, in which the two electrodes on either side of the membrane are pressed onto the ionomer and transferred due to the action of heat and pressure. Further experimentation would conclusively determine if continuous transfer is possible. In the absence of this information, an intermittent motion of the continuous web of decal substrate is preferred.

In order to achieve the catalyst loadings required by a DMFC fuel cell, multiple layers of catalyst ink would be applied to incrementally build up the catalyst loading. In a continuous process this could be achieved by banks of nozzles, which would each apply a coat of ink onto the portion of substrate underneath it.

Multiple nozzles would be aligned and positioned on top of the web as shown in Figure 93. The spacing of these nozzles is determined by the distance the web moves during each cycle, so that upon each step of the web, the electrode would be positioned under the next nozzle. The number of nozzles required would be determined by the loading of catalyst required.

When the web would be stationary under a nozzle, a template (with cutouts for the electrode area) would be lowered onto the web, aligned with the electrodes and spraying would be initiated. The entire web bank would have to move back and forth to apply uniform layers onto the electrode. This process would continue till the web is ready

to move again, the duration determined by the amount of time required for the hot press step.

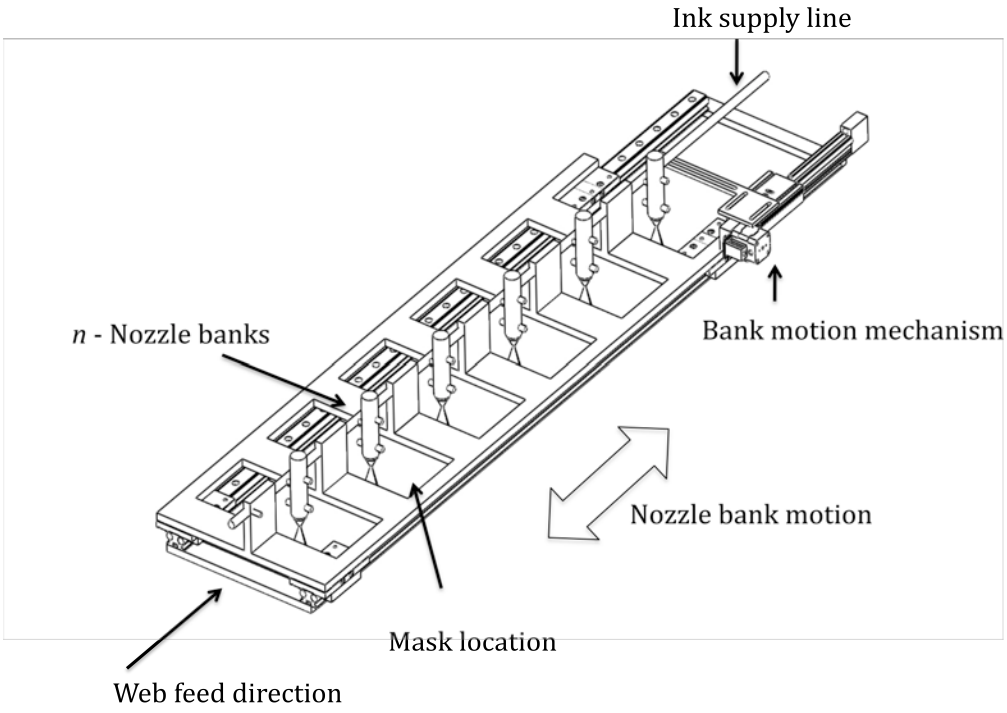

Figure 93: Nozzle bank concept.

Different coating geometries can be sprayed onto the substrate as shown in Figure 94 With split patch coating geometry, a single web of substrate is used, which would be slit and manipulated during downstream processes to produce the desired orientation of electrodes, with the ionomer membrane in between. Details of this web slitting and manipulation are discussed in the following sections.

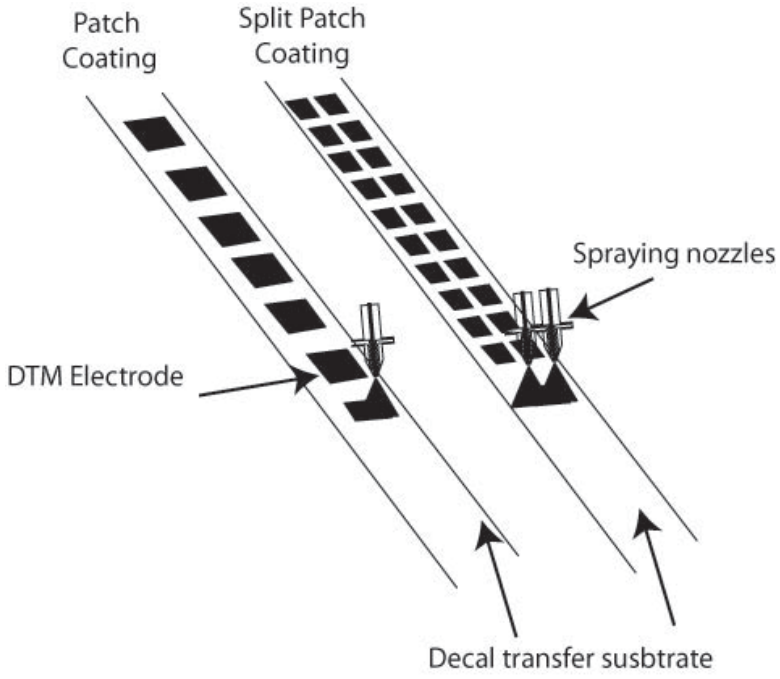

Figure 94: Coating geometries.

7.3.1.2 Electrode thickness monitoring and control

In the electrode fabrication by the spraying process, it is important to control and quantify the electrode thickness to ensure that the desired catalyst loading of the electrode is achieved. Both of these parameters are linked to measuring the electrode thickness in the traverse and the web feed direction of the process. Adequate measurement capability must be built into the relevant sections of the continuous manufacturing process.

7.3.1.3 Web manipulation apparatus

Continuous DTM-type MEA manufacture involves the convergence of three web substrates: one web of the ionomer membrane, which is flanked on either side by a web onto which the electrode is cast. These webs are hot pressed together to form MEAs. If the anode and cathode electrodes were fabricated on respectively separate webs, it would require the construction of either two separate coating paths in the machine, which would

merge in the assembly stage, or alternatively, electrodes could be coated on separate webs in a coating machine, stored, and subsequently assembled on a separate machine.

We propose and present a prototype for a technique, which eliminates the need for a second coating path and substrate. Pairs of electrodes are cast onto the same web of substrate in two separate rows. This substrate is then split and manipulated into a suitable orientation by the proposed mechanisms for the hot pressing stage, in which the electrodes are transferred onto the membrane to form an MEA. The concept for this web splitting and manipulation was embodied in two apparata, which were designed, prototyped, and successfully tested.

In the split patch coating concept two rows of electrode are sprayed onto a single continuous substrate. For the electrode transfer step these electrodes have to be positioned on either side of a ionomer membrane, which would require that this substrate be split into two separate substrate, and turned to face each other, with the electrodes being on the inside surfaces of the web, as depicted in Figure 95

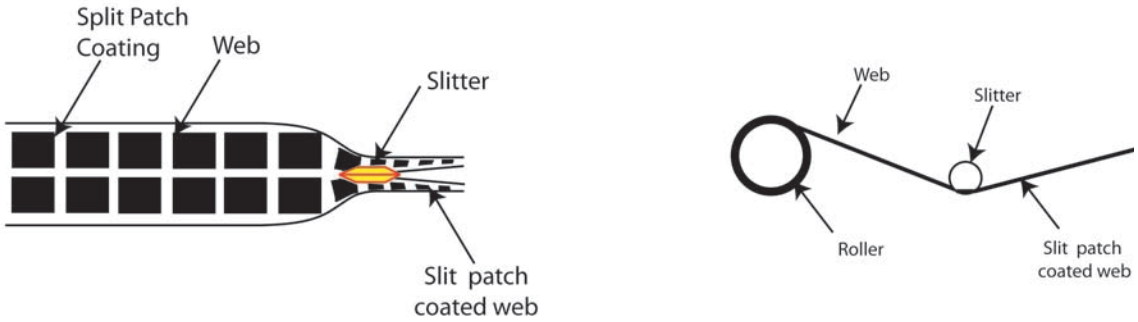

Figure 95: Split patch coating concept.

To achieve this manipulation and alignment two concepts are presented. The first is the 'Twister' concept as shown in Figure 96, which shows an actual SLS prototype constructed to demonstrate this concept.

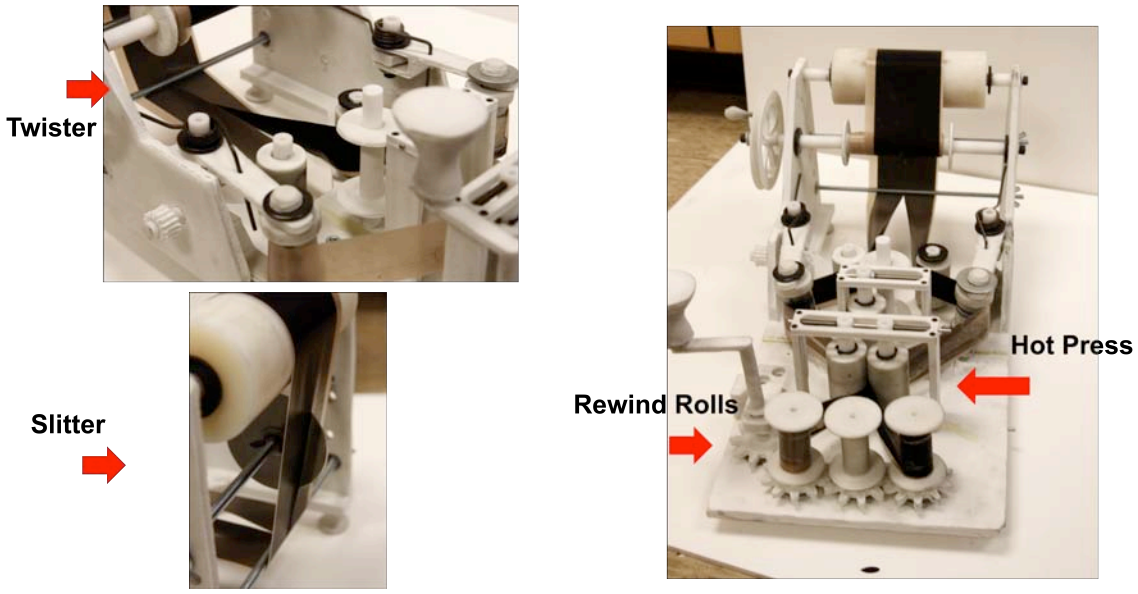

Figure 96: Web manipulation, twister concept.

In this concept first the web is slit into two streams by a rotating blade, after which these two horizontally aligned webs are passed around vertical rollers, which causes them to twist midway. The distance between the point where the web is horizontal and the vertical rollers control the rate at which the web 'twists'. Once vertical the two webs are threaded through the necessary rollers till they reach the rewind rollers. In the prototype shown, the web passes through two rolls, which simulates the hot press step. Turning the rewind rollers pulls the web of the supply spool.

In the second concept, called the offset three-bar concept, a spool of single coated material is first slit as shown in Figure 97, after which one of the webs is allowed to

continue its motion, while the other is passed over three bars. The first bar allows the web to turn at a 45° angle; the second one positions it so that it is aligned with the next bar, which again turns the web by 45°. What is achieved by these two rotations is that the web is flipped over, so that now it is positioned over the other web, which was allowed to pass through with out any manipulation

Figure 97: Web manipulation, offset three bar concept.

In summary what both concepts achieve is they take a single web with coatings on it, break it into two, and manipulate them so that the end up parallel to each other with the coated sided on the inside, facing each other. A web with split patch electrode coatings if subjected to such an exercise would result in the proper orientation for the two electrodes on either side of an ionomer membrane.

7.3.1.4 Continuous electrode transfer

A continuous transfer process in which heated rolls apply the requisite heat and pressure for electrode transfer onto a continuously moving web can easily replace laboratory bench-scale intermittent operation. Such an apparatus should be designed, prototyped and tested.

We propose a concept as shown in Figure 98, in which three webs are aligned between rollers. If the electrodes are not continuous, it is important to synchronize the webs containing the electrodes so that they perfectly overlap each other on either side of the membrane. Once aligned, the web is positioned between two heated platens, and stopped (due to the intermittent motion). In this proposed configuration, the platens clamp together, applying the required pressure and raising the temperature to the required value for the transfer process. The duration of this step will dictate the intermittent motion of the entire web of substrate. After the set interval of time the web is allowed to move forward, where subsequently the decal transfer substrates are peeled of and a three layer MEA is revealed, on a continuous web of ionomer, which can be wound on a spool or cut into discrete pieces.

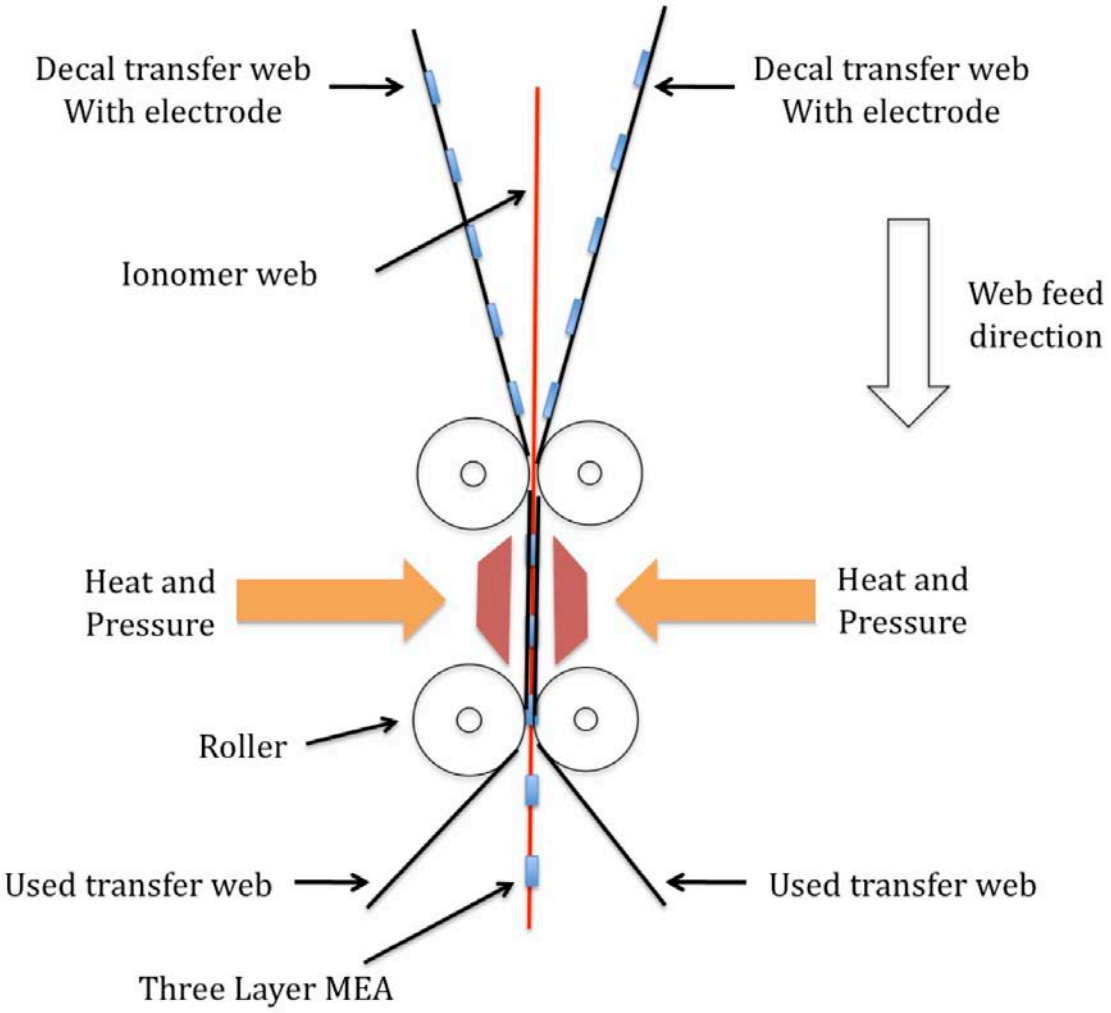

Figure 98: Electrode transfer process.

7.3.1.5 Overall layout

On the basis of the concepts produced for individual sections of the manufacturing process, a layout for the overall concept is proposed, as shown in Figure 99. As identified on the diagram a spool of decal transfer material is unwound, tensioned and then positioned under the spraying section, where two rows of patch-coated electrodes are produced. From here the substrate proceeds onto a slitting assembly, which

divides these two rows as shown. One of these slit web is allowed to proceed as is, while the other is passed through a turning assembly (for which two concepts were presented). By the manipulation of this assembly the web is turned around so that now the two slit webs face each other, with the coated electrodes on the inside. A spool of ionomer web is inserted and threaded in between the electrode carrying webs; all three are pulled through an electrode transfer section, depicted by two rollers. At the end a continuous web with electrodes on either side, as required for a CCM MEA is produced.

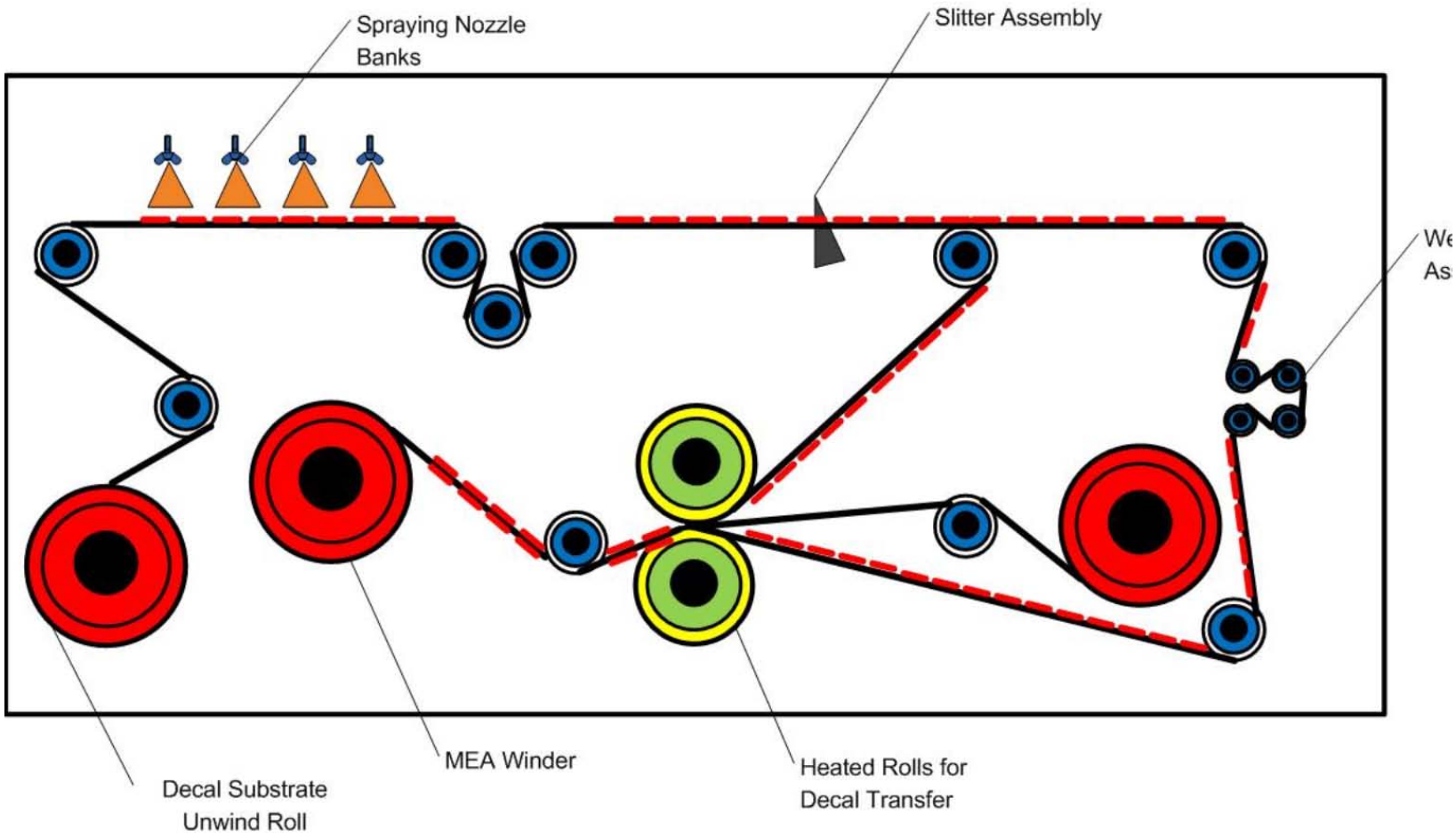

Figure 99: Overall continuous MEA manufacturing process concept.

7.3.2 Ink formulation

Inks made from Pt:Ru or Pt catalyst (catalyst blacks) are prone to forming clumps. These clumps of catalyst and ionomer particles cause blockages in the nozzle orifice during spraying. Additionally, SEM images of the DMFC anode reveal catalyst particle agglomerates, which can potentially lead to low utilization of the deposited catalysts. Furthermore, if higher solid content inks could be tailored for use in the spraying process, fewer coats would be needed to achieve the loading required by the DMFC electrodes. Another concern is that catalyst particles in an ink are prone to settling. This poses challenges in the design of an ink delivery mechanism, as well as ink processing and handling. Electrode porosity is also a characteristic that warrants further investigation. An in-depth study on pore-forming additives could potentially benefit the electrode structure. In a DTM type MEA, transfer properties of an electrode from the decal substrate to the ionomer membrane could potentially be improved by the addition of release agents. This could significantly alter the processing time, temperature and pressure requirements of the transfer stage.

In light of these considerations, we propose a significant research contribution to new ink chemistries and formulation procedures. This effort would require the identification of suitable additives to address the challenges of agglomeration, clumping, suspension stabilization, electrode porosity, release properties, etc., while remaining benign to the charge-transfer and mass transport processes in the electrode.

Additionally, ink formulation procedures could include different mixing and filtration stages to remove larger particles that can congest the passages in a spray nozzle, and allow for the formulation of higher solid content inks.

Appendix A:

Nozzle flow rate model

Table 21: Experimental design and results for the nozzle flow rate model.

Fluid Pressure	Area	Air Pressure	Flow Rate
-	+	-	0.662
-	+	-	0.669
-	-	+	0.219
-	+	+	0.677
-	-	+	0.216
+	+	+	1.14
+	+	+	1.133
+	+	-	1.13
-	-	-	0.214
-	+	-	0.685
+	-	+	0.408
-	-	-	0.215
+	+	-	1.127
+	-	+	0.411
+	+	+	1.14
+	-	-	0.403
-	+	+	0.687
-	-	-	0.218
-	+	-	0.685
-	+	+	0.688
-	+	+	0.684
+	+	-	1.126
+	-	-	0.404
-	-	+	0.22
-	-	-	0.217
-	-	+	0.214
+	+	+	1.147
+	+	-	1.141
+	-	+	0.409
+	-	+	0.407
+	-	-	0.401
+	-	-	0.398

Droplet size model: Water

Table 22: Experimental design and results for droplet model with water.

Flow Rate	Pressure	LMD
+	+	27.5
-	+	27.4
-	0	45.31
0	-	84.1
+	-	111
-	0	45.96
-	+	28.1
+	+	31.4
+	0	53
0	0	45.8
+	-	116.4
+	0	54.7
0	+	32.7
-	-	59.52
0	-	83.9
0	0	53.9
-	-	50
0	+	33.2

Droplet size model: 2% Ink

Table 23: Experimental design and results for droplet size model with 2% SC ink.

Flow Rate	Pressure	LMD
-	-	48
+	0	44.7
0	+	13.65
0	-	42.2
0	0	40.5
-	0	13.8
+	+	17.4
+	-	64.44
0	0	49.76
-	-	44.11
-	+	12.7
0	+	14.63
+	+	19.41
+	0	49.1
-	+	14.63
+	-	88.4
0	-	51.6
-	0	14.37

Droplet size model: 4% Ink

Table 24: Experimental design and results for droplet size model with 4% ink.

Flow Rate	Pressure	LMD
+	0	43.94
0	0	36
+	-	76.9
0	+	14
0	0	41.6
0	+	14.68
-	+	12.4
-	0	15.5
+	+	14.5
+	-	75.14
-	+	15.88
0	-	45.4
-	-	21.8
-	-	19.64
+	+	15.44
+	0	58.96
0	-	52.15
-	0	16.76

References

1. A. S. Aricòa, S.S. and V. Antonuccia, *DMFCs: From Fundamental Aspects to Technology Development*. Fuel Cells, 2001.
2. Carrette, L., K.A. Friedrich, and U. Stimming, *Fuel Cells - Fundamentals and Applications*. Fuel Cells, 2001. **1**(1): p. 5-39.
3. Fuller, T.F. and M.L. Perry, *A historical perspective of fuel cell technology in the 20th century*. Journal of The Electrochemical Society, 2002. **149**(7).
4. Acres, G.J.K., *Recent advances in fuel cell technology and its applications*. Journal of Power Sources, 2001. **100**(1-2): p. 60-66.
5. Meyers, J.P. and H.L. Maynard, *Design considerations for miniaturized PEM fuel cells*. Journal of Power Sources, 2002. **109**(1): p. 76-88.
6. Zhao, T.S., W.W. Yang, R. Chen, and Q.X. Wu, *Towards operating direct methanol fuel cells with highly concentrated fuel*. Journal of Power Sources, 2010. **195**(11): p. 3451-3462.
7. Srinivasan, S., *Fuel Cells: From Fundamentals to Applications*. 2006: Springer.
8. Lee, k.S. and Y.S. Kim, *Method of manufacturing 5-layer MEA having improved electrical conductivity*. 2010: US.
9. Wheeler, D. and G. Sverdrup, *2007 Status of Manufacturing: Polymer Electrolyte membrane (PEM) Fuel Cells*. 2007.
10. Cindrella, L., A.M. Kannan, J.F. Lin, K. Saminathan, Y. Ho, C.W. Lin, and J. Wertz, *Gas diffusion layer for proton exchange membrane fuel cells--A review*. Journal of Power Sources, 2009. **194**(1): p. 146-160.
11. Wilde, P.M., M. Mandle, M. Murata, and N. Berg, *Structural and physical properties of GDL and GDL/BPP combinations and their influence on PEMFC performance*. Fuel Cells, 2004. **4**(Compendex): p. 180-184.
12. Litster, S. and G. McLean, *PEM fuel cell electrodes*. Journal of Power Sources, 2004. **130**(1-2): p. 61-76.
13. DeLuca, N. and Y. Elabd, *Polymer electrolyte membranes for the direct methanol fuel cell: a review*. Journal of Polymer Science Part B: Polymer Physics, 2006. **44**(16): p. 2201-2225.
14. *Cost Analyses of Fuel Cell Stack/Systems*. 2008 11/11/2010]; Available from: http://www.hydrogen.energy.gov/pdfs/progress07/v_a_5_lasher.pdf.
15. *Dupont Nafion PFSA Membranes*. 11/05/2010]; Available from: http://www2.dupont.com/FuelCells/en_US/assets/downloads/dfc101.pdf.
16. Rajendran, R., *Polymer electrolyte membrane technology for fuel cells*. MRS bulletin, 2005. **30**: p. 587.
17. Ravikumar, M. and A. Shukla, *Effect of Methanol Crossover in a Liquid-FeedPolymer-Electrolyte Direct Methanol Fuel Cell*. Journal of The Electrochemical Society, 1996. **143**(8): p. 2601-2606.

18. Ren, X., P. Zelenay, S. Thomas, J. Davey, and S. Gottesfeld, *Recent advances in direct methanol fuel cells at Los Alamos National Laboratory*. Journal of Power Sources, 2000. **86**(1-2): p. 111-116.
19. Ren, X., T. Springer, T. Zawodzinski, and S. Gottesfeld, *Methanol transport through nation membranes. Electro-osmotic drag effects on potential step measurements*. Journal of The Electrochemical Society, 2000. **147**: p. 466.
20. Heinzel, A. and V.M. Barragan, *Review of the state-of-the-art of the methanol crossover in direct methanol fuel cells*. Journal of Power Sources, 1999. **84**(1): p. 70-74.
21. Passalacqua, E., G. Squadrito, F. Lufrano, A. Patti, and L. Giorgi, *Effects of the Diffusion Layer Characteristics on the Performance of Polymer Electrolyte Fuel Cell Electrodes*. Journal of Applied Electrochemistry, 2001. **31**(4): p. 449-454.
22. Giorgi, L., E. Antolini, A. Pozio, and E. Passalacqua, *Influence of the PTFE content in the diffusion layer of low-Pt loading electrodes for polymer electrolyte fuel cells*. Electrochimica Acta, 1998. **43**(24): p. 3675-3680.
23. Ge, J., A. Higier, and H. Liu, *Effect of gas diffusion layer compression on PEM fuel cell performance*. Journal of Power Sources, 2006. **159**(Compendex): p. 922-927.
24. Yim, S.-D., B.-J. Kim, Y.-J. Sohn, Y.-G. Yoon, G.-G. Park, W.-Y. Lee, C.-S. Kim, and Y.C. Kim, *The influence of stack clamping pressure on the performance of PEM fuel cell stack*. Current Applied Physics, 2010. **10**(2, Supplement 1): p. S59-S61.
25. Paganin, V.A., E.A. Ticianelli, and E.R. Gonzalez, *Development and electrochemical studies of gas diffusion electrodes for polymer electrolyte fuel cells*. Journal of Applied Electrochemistry, 1996. **26**(3): p. 297-304.
26. Wilson, M., J. Valerio, and S. Gottesfeld, *Low platinum loading electrodes for polymer electrolyte fuel cells fabricated using thermoplastic ionomers*. Electrochimica Acta, 1995. **40**(3): p. 355-363.
27. Wilson, M.S., *Membrane catalyst layer for fuel cells*. 1993(5211984).
28. Wilson, M. and S. Gottesfeld, *Thin-film catalyst layers for polymer electrolyte fuel cell electrodes*. Journal of Applied Electrochemistry, 1992. **22**(1): p. 1-7.
29. Cho, J.H., J.M. Kim, J. Prabhuram, S.Y. Hwang, D.J. Ahn, H.Y. Ha, and S.-K. Kim, *Fabrication and evaluation of membrane electrode assemblies by low-temperature decal methods for direct methanol fuel cells*. Journal of Power Sources, 2009. **187**(2): p. 378-386.
30. Niedrach, L.W., *Electrode Structure and Fuel Cell incorporating the same*. US.Patent 3297484, 1967.
31. Niedrach, L.W. and H.R. Alford, *Polytetrafluroethylene coated and bonded cell structures*. US.Patent 3432355, 1969.
32. Chun, Y.-G., C.-S. Kim, D.-H. Peck, and D.-R. Shin, *Performance of a polymer electrolyte membrane fuel cell with thin film catalyst electrodes*. Journal of Power Sources, 1998. **71**(1-2): p. 174-178.

33. Raistrick, I.D., *Electrode assembly for use in solid polymer electrolyte fuel cells*. US.Patent 4876115, 1989.
34. Srinivasan, S., E.A. Ticianelli, C.R. Derouin, and A. Redondo, *Advances in solid polymer electrolyte fuel cell technology with low platinum loading electrodes*. Journal of Power Sources, 1987. **22**(3-4): p. 359 - 375.
35. Ticianelli, E.A., C.R. Derouin, A. Redondo, and S. Srinivasan, *Methods to advance technology of proton exchange membrane fuel cells*. Journal of The Electrochemical Society, 1988. **135**(9): p. 2209 - 2214.
36. Ticianelli, E.A., C.R. Derouin, and S. Srinivasan, *Localization of platinum in low catalyst loading electrodes to attain high power densities in SPE fuel cells*. Journal of Electroanalytical Chemistry and Interfacial Electrochemistry, 1988. **251**(2): p. 275 - 295.
37. Wilson, M.S. and S. Gottesfeld, *High Performance Catalyzed Membranes of Ultra-low Pt Loadings for Polymer Electrolyte Fuel Cells*. Journal of The Electrochemical Society, 1992. **139**: p. L28.
38. Wilson, M.S., J.A. Valerio, and S. Gottesfeld, *Low platinum loading electrodes for polymer electrolyte fuel cells fabricated using thermoplastic ionomers*. Electrochimica Acta, 1995. **40**(3): p. 355-363.
39. Ren, X., M.S. Wilson, and S. Gottesfeld, *High performance direct methanol polymer electrolyte fuel cells*. Journal of The Electrochemical Society, 1996. **143**(1): p. 12-15 -.
40. Reshetenko, T.V., H.-T. Kim, U. Krewer, and H.-J. Kweon, *The effect of the anode loading and method of MEA fabrication on DMFC performance*. Fuel Cells, 2007. **7**(3): p. 238 - 245.
41. Ballard, *AvCarb Carbon Fiber Products*.
42. Zelenay, P.D.J.R.X.G.S.T.S.C., *Catalyst inks and method of application for direct methanol fuel cells*. 2004(6696382).
43. Ren, X., M.S. Wilson, and S. Gottesfeld, *High performance direct methanol polymer electrolyte fuel cells*. Journal of The Electrochemical Society, 1996. **143**(Compendex): p. L12-L15.
44. Jung, H.-Y., K.-Y. Cho, K.A. Sung, W.-K. Kim, and J.-K. Park, *The effect of sulfonated poly(ether ether ketone) as an electrode binder for direct methanol fuel cell (DMFC)*. Journal of Power Sources, 2006. **163**(1 SPEC ISS): p. 56 - 59.
45. Chen, C.Y., P. Yang, Y.S. Lee, and K.F. Lin, *Fabrication of electrocatalyst layers for direct methanol fuel cells*. Journal of Power Sources, 2005. **141**(1): p. 24 - 29.
46. Bender, G., T.A. Zawodzinski, and A.P. Saab, *Fabrication of high precision PEFC membrane electrode assemblies*. Journal of Power Sources, 2003. **124**(1): p. 114-117.
47. Lim, C. and C.Y. Wang, *Development of high-power electrodes for a liquid-feed direct methanol fuel cell*. Journal of Power Sources, 2003. **113**(1): p. 145 - 150.
48. Gulzow, E., M. Schulze, N. Wagner, T. Kaz, R. Reissner, G. Steinhilber, and A. Schneider, *Dry layer preparation and characterisation of polymer electrolyte fuel cell components*. Journal of Power Sources, 2000. **86**(1-2): p. 352-362.

49. Gulzow, E., R. Reissner, S. Weisshaar, and T. Kaz, *Progress in DMFC Development Using the Dry Spraying Preparation Technique*. Fuel Cells, 2003. **3**(1-2): p. 48 - 51.
50. Manco, J.C.C.N.J.T.F., *Method of making an electrode for a membrane electrode assembly and method of making the membrane electrode assembly*. 2006(7153802).
51. Schonert, M., K. Jakoby, C. Schlumbohm, A. Glusen, J. Mergel, and D. Stolten, *Manufacture of robust catalyst layers for the DMFC*. Fuel Cells, 2004. **4**(3): p. 175 - 179.
52. Witham, C.K., W. Chun, T.I. Valdez, and S.R. Narayanan, *Performance of direct methanol fuel cells with sputter-deposited anode catalyst layers*. Electrochemical and Solid-State Letters, 2000. **3**(11): p. 497 - 500.
53. OíHayre, R., S.J. Lee, S.W. Cha, and F.B. Prinz, *A sharp peak in the performance of sputtered platinum fuel cells at ultra-low platinum loading*. Journal of Power Sources, 2002. **109**(2): p. 483-493.
54. Haug, A.T., R.E. White, J.W. Weidner, W. Huang, S. Shi, T. Stoner, and N. Rana, *Increasing Proton Exchange Membrane Fuel Cell Catalyst Effectiveness Through Sputter Deposition*. Journal of The Electrochemical Society, 2002. **149**: p. A280.
55. Frey, T., K.A. Friedrich, L. Jorissen, and J. Garche, *Preparation of direct methanol fuel cells by defined multilayer structures*. Journal of The Electrochemical Society, 2005. **152**(3): p. 545-551 -.
56. Wan, N., Z. Mao, C. Wang, and G. Wang, *Performance of an integrated composite membrane electrode assembly in DMFC*. Journal of Power Sources, 2007. **163**(2): p. 725 - 730.
57. Kim, J.-r., *Membrane and electrode assembly, production method of the same and fuel cell employing the same*. 2007(7232624).
58. O'Brien, W.G., *Continuous production of catalyst coated membranes*. 2008(7316794).
59. Oh, I.-W., H. Ha, H. Yong, Seong-Ahn, S.-Y. Ahn, Y.-C. Lee, T.W. Lim, K.C. Lee, S.W. Kim, and J.H. Lee, *Method of preparing membrane-electrode-gasket assemblies for polymer electrolyte fuel cells*. 2006(7056612).
60. Chang, H., *Method for fabricating membrane-electrode assembly and fuel cell adopting the membrane-electrode assembly*. 2004(6749892).
61. Dearnaley, G.A.J.H., *Catalytic coatings and fuel cell electrodes and membrane electrode assemblies made therefrom*. 2007(7303834).
62. Debe, M.K., J.M. Larson, W.V. Balsimo, A.J. Steinbach, and R.J. Ziegler, *Membrane electrode assemblies*. 2002(6432571).
63. Parsonage, E.E. and M.K. Debe, *Nanostructured electrode membranes*. 1994(5338430).
64. Preischl, C., P. Hedrich, and A. Hahn, *Continuous method for manufacturing a Laminated electrolyte and electrode assembly*. 2001(6291091).
65. Tabata, K., F. Fujibayashi, and M. Aimu, *Membrane-electrode-assembly with solid polymer electrolyte*. 2004(6723464).

66. Tani, M., H. Shinkai, K. Kohyama, I. Tanaka, Y. Hama, and J. Yano, *Method for producing membrane-electrode structure and polymer electrolyte fuel cell*. 2007(7306876).
67. Tanuma, T., *Membrane-electrode assembly for polymer electrolyte fuel cell, and process for its production*. 2007(7157176).
68. Uchida, M., J. Niikura, H. Gyoten, Y. Takebe, K. Hatoh, M. Hosaka, T. Kanbara, A. Mukoyama, H. Shimoda, and S. Kinoshita, *Method for producing film electrode jointed product and method for producing solid polymer type fuel cell*. 2005(6855178).
69. Wittpahl, S., M.R. Vogt, K.-a. Starz, and J. Köhler, *Method for the production of membrane electrode assemblies for fuel cells*. 2006(7141270).
70. Thomas, S.C., X. Ren, and S. Gottesfeld, *Influence of Ionomer Content in Catalyst Layers on Direct Methanol Fuel Cell Performance*. Journal of The Electrochemical Society, 1999. **146**(12): p. 4354 - 4359.
71. Sister, V.G., V.N. Fateev, and D.A. Bokach, *Effect of the fuel electrode composition and structure on the performance of the direct methanol fuel cell*. Russian Journal of Electrochemistry, 2007. **43**(9): p. 1097 - 1100.
72. Zhang, J., G.-P. Yin, Z.-B. Wang, Q.-Z. Lai, and K.-D. Cai, *Effects of hot pressing conditions on the performances of MEAs for direct methanol fuel cells*. Journal of Power Sources, 2007. **165**(1): p. 73 - 81.
73. Song, C. and P.G. Pickup, *Effect of hot pressing on the performance of direct methanol fuel cells*. Journal of Applied Electrochemistry, 2004. **34**(10): p. 1065 - 1070.
74. Chen, C.Y. and C.S. Tsao, *Characterization of electrode structures and the related performance of direct methanol fuel cells*. International Journal of Hydrogen Energy, 2006. **31**(3): p. 391 - 398.
75. Tucker, M.C., M. Odgaard, P.B. Lund, S. Yde-Andersen, and J.O. Thomas, *The pore structure of direct methanol fuel cell electrodes*. Journal of The Electrochemical Society, 2005. **152**(9): p. 1844-1850 -.
76. Jeon, S., J. Lee, G.M. Rios, H.-J. Kim, S.-Y. Lee, E. Cho, T.-H. Lim, and J. Hyun Jang. *Effect of ionomer content and relative humidity on polymer electrolyte membrane fuel cell (PEMFC) performance of membrane-electrode assemblies (MEAs) prepared by decal transfer method*. 2010. Langford Lane, Kidlington, Oxford, OX5 1GB, United Kingdom: Elsevier Ltd.
77. Krishnan, N.N., J. Prabhuram, Y.T. Hong, H.J. Kim, K. Yoon, H.Y. Ha, T.H. Lim, and S.K. Kim, *Fabrication of MEA with hydrocarbon based membranes using low temperature decal method for DMFC*. International Journal of Hydrogen Energy, 2010. **35**(Compendex): p. 5647-5655.
78. Liu, P., G.-P. Yin, E.-D. Wang, J. Zhang, and Z.-B. Wang, *Influence of hot-pressing temperature on physical and electrochemical performance of catalyst coated membranes for direct methanol fuel cells*. Journal of Applied Electrochemistry, 2009. **39**(Compendex): p. 859-866.

79. Park, H.-S., Y.-H. Cho, Y.-H. Cho, I.-S. Park, N. Jung, M. Ahn, and Y.-E. Sung, *Modified decal method and its related study of microporous layer in PEM fuel cells*. Journal of The Electrochemical Society, 2008. **155**(Compendex): p. B455-B460.
80. Saha, M.S., D.K. Paul, B.A. Peppley, and K. Karan, *Fabrication of catalyst-coated membrane by modified decal transfer technique*. Electrochemistry Communications, 2010. **12**(Compendex): p. 410-413.
81. Song, S.Q., Z.X. Liang, W.J. Zhou, G.Q. Sun, Q. Xin, V. Stergiopoulos, and P. Tsiakaras, *Direct methanol fuel cells: The effect of electrode fabrication procedure on MEAs structural properties and cell performance*. Journal of Power Sources, 2005. **145**(Compendex): p. 495-501.
82. Wei, Z., S. Wang, B. Yi, J. Liu, L. Chen, W. Zhou, W. Li, and Q. Xin. *Influence of electrode structure on the performance of a direct methanol fuel cell*. in *7th Grove Fuel Cell Symposium, Grove VII, September 11, 2001 - September 13, 2001*. 2002. London, United kingdom: Elsevier.
83. Kundu, S., M. Fowler, L. Simon, and S. Grot, *Morphological features (defects) in fuel cell membrane electrode assemblies*. Journal of Power Sources, 2006. **157**(2): p. 650-656.
84. Lindermeir, A., G. Rosenthal, U. Kunz, and U. Hoffmann, *Improvement of MEAs for direct-methanol fuel cells by tuned layer preparation and coating technology*. Fuel Cells, 2004. **4**(1-2): p. 78 - 85.
85. Tawfik, H., Y. Hung, and D. Mahajan, *Metal bipolar plates for PEM fuel cell--A review*. Journal of Power Sources, 2007. **163**(2): p. 755-767.
86. Tsuchiya, H. and O. Kobayashi, *Mass production cost of PEM fuel cell by learning curve*. International Journal of Hydrogen Energy, 2004. **29**(10): p. 985-990.
87. Mehta, V. and J.S. Cooper, *Review and analysis of PEM fuel cell design and manufacturing*. Journal of Power Sources, 2003. **114**(1): p. 32-53.
88. Fly, G.W.B.B.K., *Fuel cell with convoluted MEA*. 2003(6663994).
89. Kuo, J. and C. Chen, *A novel Nylon-6-S316L fiber compound material for injection molded PEM fuel cell bipolar plates*. Journal of Power Sources, 2006. **162**(1): p. 207-214.
90. Hermann, A., T. Chaudhuri, and P. Spagnol, *Bipolar plates for PEM fuel cells: A review*. International Journal of Hydrogen Energy, 2005. **30**(12): p. 1297-1302.
91. Lawrance, R., *Low cost bipolar current collector-separator for electrochemical cells*. 1980, Google Patents.
92. Balko, E. and R. Lawrance, *Carbon fiber reinforced fluorocarbon-graphite bipolar current collector-separator*. 1982, Google Patents.
93. Huang, J., D.G. Baird, and J.E. McGrath, *Development of fuel cell bipolar plates from graphite filled wet-lay thermoplastic composite materials*. Journal of Power Sources, 2005. **150**: p. 110-119.

94. Maheshwari, P.H., R.B. Mathur, and T.L. Dhami, *Fabrication of high strength and a low weight composite bipolar plate for fuel cell applications*. Journal of Power Sources, 2007. **173**: p. 394-403.
95. Busick, D.N. and M.S. Wilson, *Low-cost composite materials for PEFC bipolar plates*. Fuel Cells Bulletin, 1999. **2**(5): p. 6 - 8.
96. Besmann, T.M., J.W. Klett, J.J.J. Henry, and E. Lara-Curzio, *Carbon/carbon composite bipolar plate for proton exchange membrane fuel cells*. Journal of The Electrochemical Society, 2000. **147**(11): p. 4083 - 4086.
97. Busick, D. and M. Wilson, *Development of composite materials for PEFC bipolar plates*. Materials Research Society Symposium - Proceedings, 2000. **575**: p. 247 - 251.
98. Middelman, E., W. Kout, B. Vogelaar, J. Lenssen, and E. de Waal, *Bipolar plates for PEM fuel cells*. Journal of Power Sources, 2003. **118**: p. 44-46.
99. Kuan, H.-C., C.-C.M. Ma, K.H. Chen, and S.-M. Chen, *Preparation, electrical, mechanical and thermal properties of composite bipolar plate for a fuel cell*. Journal of Power Sources, 2004. **134**: p. 7-17.
100. Heo, S.I., K.S. Oh, J.C. Yun, S.H. Jung, Y.C. Yang, and K.S. Han, *Development of preform moulding technique using expanded graphite for proton exchange membrane fuel cell bipolar plates*. Journal of Power Sources, 2007. **171**: p. 396-403.
101. Wilson, M.S. and D.N. Busick, *Composite bipolar plate for electrochemical cells*. US Patent 624867, 2001.
102. Bin, Z., M. Bingchu, S. Chunhui, and Y. Runzhang, *Study on the electrical and mechanical properties of polyvinylidene fluroide/titanium silicon carbide composite bipolar plates*. Journal of Power Sources, 2006. **161**: p. 997-1001.
103. Blunk, R., M.H.A. Elhamid, D. Lisi, and Y. Mikhail, *Polymeric composite bipolar plates for vehicle applications*. Journal of Power Sources, 2006. **156**: p. 151-157.
104. Chunhui, S., P. Mu, W. Qiong, and Y. Runzhang, *Performance of an aluminate cement /graphite conductive composite bipolar plate*. Journal of Power Sources, 2006. **159**: p. 1078-1083.
105. Cunningham, B.D. and D.G. Baird, *Development of bipolar plates for fuel cells from graphite filled wet-lay material and a compatible thermoplastic laminate skin layer*. Journal of Power Sources, 2007. **168**: p. 418-425.
106. Cunningham, B.D., J. Huang, and D.G. Baird, *Development of bipolar plates for fuel cells from graphite filled wet-lay material and a thermoplastic laminate skin layer*. Journal of Power Sources, 2007. **165**: p. 764-773.
107. Du, L. and S.C. Jana, *Highly conductive epoxy/graphite composites for bipolar plates in proton exchange membrane fuel cells*. Journal of Power Sources, 2007. **172**: p. 734-741.
108. Dweiri, R. and J. Sahari, *Electrical properties of carbon-based polypropylene composites for bipolar plates in polymer electrolyte membrane fuel cell (PEMFC)*. Journal of Power Sources, 2007. **171**: p. 424-432.

109. Davies, D.P., P.L. Adcock, M. Turpin, and S.J. Rowen, *Stainless steel as a bipolar plate material for solid polymer fuel cells*. Journal of Power Sources, 2000. **86**: p. 237-242.
110. Davies, D., P. Adcock, M. Turpin, and S. Rowen, *Bipolar plate materials for solid polymer fuel cells*. Journal of Applied Electrochemistry, 2000. **30**(1): p. 101-105.
111. Wind, J., R. Sp√§h, W. Kaiser, and G. B√∂hm, *Metallic bipolar plates for PEM fuel cells*. Journal of Power Sources, 2002. **105**: p. 256-260.
112. Wang, H., M.A. Sweikart, and J.A. Turner, *Stainless steel as bipolar plate material for polymer electrolyte membrane fuel cells*. Journal of Power Sources, 2003. **115**: p. 243-251.
113. Wang, H., M.P. Brady, G. Teeter, and J.A. Turner, *Thermally nitrided stainless steels for polymer electrolyte membrane fuel cell bipolar plates: Part 1: Model Ni-50Cr and austenitic 349(TM) alloys*. Journal of Power Sources, 2004. **138**: p. 86-93.
114. Wang, H. and J.A. Turner, *Ferritic stainless steels as bipolar plate material for polymer electrolyte membrane fuel cells*. Journal of Power Sources, 2004. **128**: p. 193-200.
115. Wang, H., M.P. Brady, K.L. More, H.M.M. III, and J.A. Turner, *Thermally nitrided stainless steels for polymer electrolyte membrane fuel cell bipolar plates: Part 2: Beneficial modification of passive layer on AISI446*. Journal of Power Sources, 2004. **138**: p. 79-85.
116. Lee, S.-J., C.-H. Huang, J.-J. Lai, and Y.-P. Chen, *Corrosion-resistant component for PEM fuel cells*. Journal of Power Sources, 2004. **131**: p. 162-168.
117. Lee, S.-J., J.-J. Lai, and C.-H. Huang, *Stainless steel bipolar plates*. Journal of Power Sources, 2005. **145**: p. 362-368.
118. Padhy, B.R. and R.G. Reddy, *Performance of DMFC with SS 316 bipolar/end plates*. Journal of Power Sources, 2006. **153**(1): p. 125 - 129.
119. Fleury, E., J. Jayaraj, Y.C. Kim, H.K. Seok, K.Y. Kim, and K.B. Kim, *Fe-based amorphous alloys as bipolar plates for PEM fuel cell*. Journal of Power Sources, 2006. **159**: p. 34-37.
120. Jin, S., E. Ghali, and A.T. Morales, *Corrosion behavior of 316L stainless steel and Zr75Ti25 bulk amorphous alloy in simulated PEMFC anode environment in a solution containing 12.5 ppm H2SO4 + 1.8 ppm HF at 25 and 80 ¬∞C*. Journal of Power Sources, 2006. **162**: p. 294-301.
121. Chung, C.-Y., S.-K. Chen, P.-J. Chiu, M.-H. Chang, T.-T. Hung, and T.-H. Ko, *Carbon film-coated 304 stainless steel as PEMFC bipolar plate*. Journal of Power Sources, 2008. **176**: p. 276-281.
122. Feng, K., Y. Shen, J. Mai, D. Liu, and X. Cai, *An investigation into nickel implanted 316L stainless steel as a bipolar plate for PEM fuel cell*. Journal of Power Sources, 2008.

123. Ren, Y.J. and C.L. Zeng, *Corrosion protection of 304 stainless steel bipolar plates using TiC films produced by high-energy micro-arc alloying process*. Journal of Power Sources, 2007. **171**: p. 778-782.
124. Fukutsuka, T., T. Yamaguchi, S.-I. Miyano, Y. Matsuo, Y. Sugie, and Z. Ogumi, *Carbon-coated stainless steel as PEFC bipolar plate material*. Journal of Power Sources, 2007. **174**: p. 199-205.
125. El-Enin, S.A.A., O.E. Abdel-Salam, H. El-Abd, and A.M. Amin, *New electroplated aluminum bipolar plate for PEM fuel cell*. Journal of Power Sources, 2008. **177**: p. 131-136.
126. Padhy, B.R. and R.G. Reddy, *Performance of DMFC with TiN coated aluminum bipolar/end plates*. ECS Transactions, 2005. **V1**(n8): p. 2292 -.
127. Fu, Y., M. Hou, G. Lin, J. Hou, Z. Shao, and B. Yi, *Coated 316L stainless steel with CrxN film as bipolar plate for PEMFC prepared by pulsed bias arc ion plating*. Journal of Power Sources, 2008. **176**: p. 282-286.
128. Brady, M.P., B. Yang, H. Wang, J.A. Turner, K.L. More, M. Wilson, and F. Garzon, *The formation of protective nitride surfaces for PEM fuel cell metallic bipolar plates*. JOM, 2006. **58**(8): p. 50 - 57.
129. Garcia, M.A.L. and M.A. Smit, *Study of electrodeposited polypyrrole coatings for the corrosion protection of stainless steel bipolar plates for the PEM fuel cell*. Journal of Power Sources, 2006. **158**: p. 397-402.
130. Joseph, S., J.C. McClure, P.J. Sebastian, J. Moreira, and E. Valenzuela, *Polyaniline and polypyrrole coatings on aluminum for PEM fuel cell bipolar plates*. Journal of Power Sources, 2008. **177**: p. 161-166.
131. Wang, Y. and D.O. Northwood, *An investigation into polypyrrole-coated 316L stainless steel as a bipolar plate material for PEM fuel cells*. Journal of Power Sources, 2006. **163**: p. 500-508.
132. Tian, R.J., J.C. Sun, and L. Wang, *Effect of plasma nitriding on behavior of austenitic stainless steel 304L bipolar plate in proton exchange membrane fuel cell*. Journal of Power Sources, 2007. **163**: p. 719-724.
133. Wang, Y. and D.O. Northwood, *An investigation into the effects of a nano-thick gold interlayer on polypyrrole coatings on 316L stainless steel for the bipolar plates of PEM fuel cells*. Journal of Power Sources, 2008. **175**: p. 40-48.
134. Wang, Y. and D.O. Northwood, *An investigation into TiN-coated 316L stainless steel as a bipolar plate material for PEM fuel cells*. Journal of Power Sources, 2007. **165**: p. 293-298.
135. Wang, H., J.A. Turner, X. Li, and R. Bhattacharya, *SnO2:F coated austenite stainless steels for PEM fuel cell bipolar plates*. Journal of Power Sources, 2007. **171**: p. 567-574.
136. Wang, H. and J.A. Turner, *SnO2:F coated ferritic stainless steels for PEM fuel cell bipolar plates*. Journal of Power Sources, 2007. **170**: p. 387-394.
137. Wang, S.-H., J. Peng, and W.-B. Lui, *Surface modification and development of titanium bipolar plates for PEM fuel cells*. Journal of Power Sources, 2006. **160**: p. 485-489.

138. Satas, D., *Coatings Technology Handbook*. 1991, New York: Marcek Dekker, Inc.
139. *What is Flexography?* 10/25/2010]; Available from: http://www.phoenixchallenge.org/PCWeb/PCPages/Reading%20Assignments/FP&P%20Core%20%28B%29%20V1%20pgs%203-12.pdf.
140. *"The Yasui Seiki Micro Gravure coating method"*. 10/25/2010]; Available from: http://www.yasui.com/2004/MicroGravure.pdf.
141. Sinha, J., S. Lasher, Y. Yang, and P. Kopf. *Direct Hydrogen PEMFC Manufacturing Cost Estimation for Automotive Applications*. 2008; Available from: http://www1.eere.energy.gov/hydrogenandfuelcells/pdfs/fctt_pemfc_cost_review_0908.pdf.
142. DeMarinis, M., E.S. De Castro, and K. Shaikh, *Structure and methods of manufacture for fas diffusion electrodes and electrode components*. 2000, De Nora S.p.A., Italy.
143. *Mayer Rod, Meter Bar, Adhesive Coating*. 10/24/2010]; Available from: http://www.holoeast.com/machines/coating/adhesive-coating-Meyer-Bar.html.
144. *Slot Die Basics*. 10/26/2010]; Available from: http://www.yasui.com/2004/slotdie.htm.
145. Coatema. *Slot Die System*. 13/11/2010]; Available from: http://www.coatema.de/eng/lab_solutions/modular_coating/slot_die_system.php.
146. Nasr, G.G., A.J. Yule, and L. Bendig, *Industrial Sprays and Atomization*. 2002: Springer.
147. Lefebvre, A.H., *Atomization and Sprays*. 1989: CRC Press.
148. Bayvel, L. and Z. Orzechowski, *Liquid Atomization*. 1993: Taylor & Francis.
149. Manuelli, A., *Influences of Printing Techniques on the Electrical Performances of Conjugated Polymers for Organic Transistors*. 2006, University of Chemnitz.
150. Blayo, A. and B. Pineaux. *Printing processes and their potential for RFID printing*. 2005: ACM.
151. *Flexographic Printing*. 10/24/2010]; Available from: http://www.imerys-paper.com/pdf/Flexographic-Printing.pdf.
152. *Printing techniques are a total package: digital plates, better dot formation, more versatile inks and other improvements help make packaging better and cheaper*. 10/24/2010]; Available from: http://findarticles.com/p/articles/mi_m0UQX/is_4_68/ai_n6030785/?tag=content;col1.
153. Krebs, F.C., *Fabrication and processing of polymer solar cells: A review of printing and coating techniques*. Solar Energy Materials and Solar Cells, 2009. **93**(4): p. 394-412.
154. Otto, K. and K.L. Wood, *Product Design: techniques in Reverse Engineering and New Product Development*. 2001, NJ: Prentice Hall.

155. Pahl, G. and W. Beitz, *Engineering design. A systematic approach (KM Wallace, L. Blessing & F. Bauert, Trans. 2 nd, enlarged and updated ed.)*. 1977, London: Springer.
156. Liu, H., *Science and Engineering of Droplets*. 2000: William Andrew.
157. Martin, S., P.L. Garcia-Ybarra, and J.L. Castillo, *Electrospray deposition of catalyst layers with ultra-low Pt loadings for PEM fuel cells cathodes*. Journal of Power Sources, 2010. **195**(9): p. 2443-2449.
158. Jaworek, A. and A.T. Sobczyk, *Electrospraying route to nanotechnology: An overview*. Journal of Electrostatics, 2008. **66**(3-4): p. 197-219.
159. *Nordson-EFD-781S-Data-Sheet*. 11/02/2010]; Available from: http://www.nordson.com/en-us/divisions/efd/Literature/Brochures-Data-Sheets/Valve-Systems/Valves/Nordson-EFD-781S-Data-Sheet.pdf.
160. Jiang, Y., H.Y. Jeon, L. Tian, and L.E. Bode, *Measuring particle size distribution using LED-illumination*. International Journal of Multiphase Flow, 2010. **36**(3): p. 193-201.
161. Dodge, L.G., *Comparison of performance of drop-sizing instruments*. Appl. Opt., 1987. **26**(7): p. 1328-1341.
162. Myers, R.H. and D.C. Montgomery, *Response Surface Methodology: process and product optimization using designed experiments*. 2008, Hoboken, New Jersey: John Wiley & Sons, Inc.
163. Koraishy, B.M., D. Morter, S. Solomon, B. McDonald, J.P. Meyers, and K. Wood, *Manufacturing of Direct Methanol Fuel Cell Electrodes by Spraying*. ECS Transactions, 2010. **33**(1): p. 1997-2010.
164. Montgomery, D.C., *Design and Analysis of Experiments*. 2001: John Wiley & Sons, Inc.
165. Lavernia, E.J. and Y. Wu, *Spray Atomization and Deposition*. 1996: Wiley.
166. Ren, X., T. Springer, and S. Gottesfeld, *Water and methanol uptakes in Nafion membranes and membrane effects on direct methanol cell performance*. Journal of The Electrochemical Society, 2000. **147**: p. 92.
167. Park, I.-S., W. Li, and A. Manthiram, *Fabrication of catalyst-coated membrane-electrode assemblies by doctor blade method and their performance in fuel cells*. Journal of Power Sources, 2010. **195**(Compendex): p. 7078-7082.

Vita

Babar Masood Koraishy was born in Karachi, Pakistan on September 3, 1977, the son of Masood and Kishwar Koraishy. He graduated from DHA Degree College in 1995, and obtained a Bachelor of Science in Mechanical Engineering from the Ghulam Ishaq Khan Institute of Technology (GIKI), Pakistan in 2000. He attended the graduate school at the University of Southern California (USC) in 2000 and received a Master of Science in Manufacturing Engineering from USC in 2002.

Permanent address: 78 Darulaman Society, Karachi, Pakistan -74800

Permanent email address: bkoraishy@gmail.com

This dissertation was typed by the author.